Identification of biomarkers of metastatic disease in uveal melanoma using proteomic analyses

Thesis submitted in accordance with the requirements of the University of Liverpool for the degree of Doctor in Philosophy

Martina Angi

June 2015

To Mario, the wind beneath my wings

Acknowledgments

First and foremost, I would like to acknowledge my primary supervisor, Prof. Sarah Coupland, for encouraging me to undergo a PhD and for supporting me in this long journey. I am truly grateful to Dr Helen Kalirai for being the person I could always turn to, for a word of advice on cell culture as much as on parenting skills. I would also like to acknowledge Prof. Bertil Damato for being an inspiration and a mentor; and Dr Sarah Lake and Dr Joseph Slupsky for their precious advice. I would like to thank Dawn, Haleh, Fidan and Fatima for becoming my family away from home, and the other members of the LOORG for the fruitful discussions and lovely cakes.

I would like to acknowledge Prof. Heinrich Heimann and the clinical team at LOOC, especially Sisters Hebbar, Johnston, Hachuela and Kaye, for their admirable dedication to UM patients and for their invaluable support to clinical research. I would also like to thank the members of staff in St Paul's theatre and Simon Biddolph and Anna Ikin in Pathology for their precious help in sample collection.

I am grateful to Dr Rosalind Jenkins who guided my first steps in the mysterious word of proteomics, and to Dr Deb Simpsons and Prof. Rob Beynon for showing me its beauty.

I am truly grateful to my parents for always supporting and believing in me, and to my sister Giulia for always being there for me. I am also very grateful to my husband Mario for the sacrifice of being apart in these years, and to Lucia and Ferdinando for having given a completely different meaning to our life.

Finally, I would like to gratefully acknowledge Cancer Research UK for funding the Clinical Research Training Fellowship that lead to this PhD.

Abstract

Uveal melanoma (UM) is the most common intraocular malignancy in adults. Despite successful ocular treatment, about 50% of patients succumb to metastatic dissemination, which occurs haematogenously and mainly affects the liver. On the basis of clinical, histopathological and genetic features of the primary tumour it is possible to predict if the individual patient is at high risk (HR) or low risk (LR) of developing metastases. However, the mechanisms responsible for the development of metastatic disease in UM are still largely unknown; therefore no adjuvant treatment is currently offered to HR patients to prevent development of fatal disease. As the time to discovery of clinically detectable metastases can range from months to decades, a secreted biomarker(s) that could be routinely tested in blood is much needed. The scope of the work presented in this thesis was to use proteomics as a tool to identify potential novel, UM-specific biomarkers. Moreover, the proteomic data acquired would complement genomic and transcriptomic information already generated by the Liverpool Ocular Oncology Research Group, with the ultimate aim of increasing our understanding of UM development and dissemination. The aim of Chapter 2's project was to compare the proteome of UM tissue samples at HR versus LR of developing metastatic disease using isobaric tags for relative and absolute quantitation (iTRAQ) labelling and mass spectrometry (MS). The quantification of proteins in our samples, proteomic analysis and further validation by immunohistochemistry has led to the identification of two novel prognostic and potentially therapeutic target, S100A6 and the tumour suppressor PDCD4. In Chapter 3 we focused on proteins released in the conditioned medium (secretome) of short-term cultures of HR and LR UM cells, as well as normal melanocytes. Using a label-free quantitative proteomic approach, almost 2000 proteins were identified and quantified, with more than 30% of these identified as secreted and/or previously described in exosomes. Using these data, an 18-protein signature able to discriminate between HR and LR UM was identified. Further validation will be necessary in secretome samples and in the peripheral blood of UM patients, but this has the potential of being translated into a clinically useful assay to detect early development of metastatic disease. As reported in Chapter 4, we also conducted a pilot clinical study on circulating tumour cells (CTC) in UM, using the CellSearch® platform with the novel melanoma kit to enumerate CTC in the peripheral blood of UM patients at LR, HR or with overt metastatic disease. CTC were detected in metastatic and HR tumours and were not present in LR UM, however, the number of CTC detected varied widely, calling into question the clinical value of using this platform in UM patients. The research detailed in Chapter 5 had a direct clinical value, as it addressed the procedures undertaken during the acquisition and processing of prognostic biopsies from UM tumours treated conservatively. The modifications introduced led to a significant improvement of the success rate of such prognostic biopsies for risk stratification, which is essential for clinical management, follow-up and research purposes.

In conclusion, the work conducted throughout this PhD has provided further insight into the molecular characteristics that can differentiate between HR and LR UM, identifying novel potential biomarkers that will need validation in the clinical setting.

Table of contents

List of abbreviations

2-DE	Two dimensional gel electrophoresis
6pG	Polysomy 6p (6p gain)
8qG	Polysomy 8q (8q gain)
AJCC	American Joint Committee on Cancer
amu	Atomic mass unit
BAP1	BRCA1 associated protein-1
BBS	Balanced salt solution
BSA	Bovine serum albumine
CGH	Comparative genome hybridisation
CTC	Circulating tumour cells
CXCR4	Chemokine receptor type 4
D3	Disomy 3
DAPI	4',6-diamidino-2-phenylindole
DIGE	Difference gel electrophoresis
DMEM	Dulbecco's modified Eagle's medium
DTT	Dithiothreitol
EDTA	Ethylenediaminetetraacetic acid
ELISA	Enzyme-linked immunosorbent assay
EOE	Extraocular extension
FBS	Foetal bovine serum
FDR	False discovery rate
FFPE	Formalin fixed paraffin embedded
FISH	Fluorescence in situ hybridisation
FNAB	Fine-needle aspiration biopsies
GFP	Green fluorescent protein
H&E	Haematoxylin and eosin
HR	High risk
HRP	Horseradish peroxidase

IHC	Immunohistochemistry
LBD	Largest basal diameter
LC	Liquid chromatography
LOOC	Liverpool Ocular Oncology Centre
LOORG	Liverpool Ocular Oncology Research Group
LR	Low risk
LUMPO	Liverpool Uveal Melanoma Prognostic Online
M3	Monosomy 3
MCSP	Melanoma-associated chondroitin sulphate proteoglycan
mins	Minutes
MLPA	Multiplex ligation-dependent probe amplification
MMTS	Methyl methanethiosulfonate
MRI	Magnetic Resonance Imaging
MS	Mass Spectrometry
MSA	Microsatellite analysis
mTOR	Mammalian target of rapamycin
OOB	Ocular Oncology Biobank
PAGE	Polyacrylamide gel electrophoresis
PAS	Periodic acid schiff
PBR	Proton beam radiotherapy
PBS	Phosphate buffered saline
PCR	Polymerase chain reaction
ROC	Receiver operating characteristic
RPE	Retinal Pigment Epithelium
RPMI	Roswell Park Memorial Institute
RT	Room temperature
s	Seconds
SDS	Sodium dodecyl sulphate
SFM	Serum free medium
SILAC	Stable isotope labelling by amino acids in cell cultures
SNP	Single nucleotide polymorphism

SRB	Sulforhodamine-B
TAM	Tumour associated macrophages
TCA	Trichloroacetic acid
TCEP	Tris(2-carboxyethyl)phosphine
TEAB	Triethylammonium bicarbonate
TFA	Trifluoracetic acid
TMA	Tissue microarray
UM	Uveal melanoma
WB	Western blot
αMEM	Minimum Essential Medium, alpha modification

List of publications

- **Angi M**, Versluis M, Kalirai H. Culturing Uveal Melanoma Cells. Ocul Oncol Pathol 2015;1:126-132
- Damato B, **Angi M**, Coupland SE, Heimann H, Groenewald C. Miscellaneous Uveal Biopsy Techniques in *Clinical Ophthalmic Oncology*, ed. Springer-Verlag 2014 (book chapter)
- Grixti A, **Angi M**, Damato BE, Jmor F, Konstantinidis L, Groenewald C, Heimann H. Vitreoretinal surgery for complications of choroidal tumor biopsy. Ophthalmology. 2014;121(12):2482-8
- **Angi M**, Kalirai H, Coupland SE, Damato BE, Semeraro F, Romano MR. Proteomic analyses of the vitreous humour. Mediators Inflamm. 2012;2012:148039

Manuscripts in preparation:

- Angi M, Kalirai H, Simpson D, Lane B, Damato BE, Madigan M, Beynon R, Coupland SE. Proteomic analysis of the secretome from primary uveal melanoma cells in culture reveals a distinctive signature discriminating between tumours at high versus low risk of metastatic disease.
- Angi M, Kalirai H, Taktak A, Groenewald C, Laguardia M, Staunton M, Heimann H, Damato BE, Coupland S. Prognostic biopsies in uveal melanoma.
- Angi M, Kalirai H, Damato BE, Jenkins R, Kitteringham N, Coupland SE. Proteomic analysis of uveal melanoma reveals potential therapeutic targets.

List of poster and oral presentations

- 15.2014 Oral presentation at the 2015 Roy Mapstone Research Prize,

  Department of Eye and Vision Science, University of Liverpool, UK.

  Quantitative proteomic analysis of uveal melanoma reveals potential therapeutic targets

  Winner of the third prize for best presentation

- 06.2013 Oral presentation at the XIV Annual Meeting of the Italian Society of

  Vitreoretinal Surgery (GIVRE). Turin, Italy.

  Prognostic biopsies in uveal melanoma

  Winner of the best paper prize and travel grant

- 05.2013 Poster presentation at the Association for Research in Vision and

  Ophthalmology (ARVO) annual meeting. Seattle, USA.

  Detection of circulating tumour cells in uveal melanoma using the CellSearch® system

  Travel grant awarded by the British Association for Cancer Research

Recipient of the 1st Gregg Stracks Award for Emerging Leaders in Ocular Melanoma

- 02.2013 Oral presentation at the 42nd Ophthalmic Oncology Group (OOG)

  Spring Meeting. Ivalo, Finland.

  Prognostic biopsy of choroidal melanoma

- 10.2012 Invited oral presentation at the European association for Vision and

  Eye Research (EVER) Annual Meeting. Nice, France.

  Serum biomarkers of metastatic disease: current practice and future perspectives

- 05.2012 Poster presentation at the Liverpool CRUK Centre Research Day,

  University of Liverpool, UK.

  Optimization of culture conditions for the analysis of the secretome of primary uveal melanoma cells

  Commended as best poster

- 05.2012 Poster presentation at the Association for Research in Vision and

  Ophthalmology (ARVO) annual meeting. Fort Lauderdale, USA

  Optimization of culture conditions for the analysis of the secretome of primary uveal melanoma cells

  Travel grant awarded by the University of Liverpool

- 09.2012 Oral presentation at the 12th Euretina Annual Meeting. Milan, Italy

  Detection of a novel inhibitory isoform of VEGF in the vitreous humour of uveal melanoma patients

- 03.2012 Poster presentation at the 40th Ophthalmic Oncology Group (OOG)

  Spring Meeting. Paris, France

  VEGFxxx and VEGFxxxb levels in the vitreous of uveal melanoma patients

- 10.2011 Oral presentation at the European association for Vision and Eye

  Research (EVER) Annual Meeting. Crete, Greece

  Genetic and histological heterogeneity in uveal melanoma: a peculiar case.

  Travel grant awarded by the University of Liverpool

Chapter 1

General introduction

1.1 Uveal melanoma

1.1.1 Incidence and risk factors

Uveal melanoma (UM) is the most common primary intraocular malignancy in adults.[1] The average incidence is 5-7 cases per million individuals per year in Europe, ranging from 4.3 to 10.9 wordwide.[2, 3] UM most commonly affects faired-skinned, grey/blue eyed Caucasians, where it is eight times more common than among African blacks, and three times more common than amongst Asians.[4]

UM has been reported in patients of all ages, but only 1% of cases occur in younger patients under the age of eighteen.[5] The incidence increases with age, climbing to more than 20 cases per million individuals per year by the age of 70.[2] Males and females are affected in equal numbers.

UM typically occurs sporadically, but it is known in association with oculo-dermal melanocytosis,[6] familial atypical mole and melanoma (FAM-M) syndrome,[7] neurofibromatosis type 1 (NF1),[8] and Li-Fraumeni syndrome.[9] The occurrence of familial UM has been reported but it is exceptionally rare, comprising only 0.6 % of all UM patients.[10]

Recently, germline mutations in the BRCA1 associated protein-1 (BAP1) gene have been identified to be responsible for a cancer predisposition syndrome associated with UM, malignant mesothelioma, meningioma and lung adenocarcinoma development.[11] In particular, a BAP1 germline inactivating mutation has been identified in a family affected by familial melanoma.[12] On the basis of this finding, the authors advocate screening and counselling of families with such a mutation, even in absence of other cancers. Germline BAP1 mutations have also been

investigated in a particular subset of young patients (14 cases, age ranging from 3 months to 29 years) affected by UM, but only one of them tested positive.[13]

The aetiology of UM remains unclear. Ultraviolet radiation has been proposed as a possible environmental cause and a number of epidemiological studies (summarised here[14]) have been performed, however there is still no definite evidence for it.

1.1.2 Anatomical considerations and clinical features

UM is a neoplasm thought to arise from the uncontrolled proliferation of melanocytes of the uveal tract, which is the vascularised middle layer of the eye, between the sclera and the retina. The name uvea (uva = grape in Latin) derives from the resemblance of this vascularised and pigmented layer to a black grape, noted by early anatomists when removing the outer scleral layer.[15] The uveal tract is composed of three parts: the choroid, the ciliary body and the iris. (Figure 1.1)

1.1.2.1 Choroidal melanoma

Ninety percent of UM cases arise in the choroid,[16] which is the largest and most posterior component of the uveal tract. It is composed of three interconnected layers of blood vessels of decreasing size, interspersed with scarce connective tissue and dendritic melanocytes containing melanin granules. The inner surface of the choroid, formed by a network of fenestrated tiny vessels called choriocapillaris, rests directly beneath a specialised layer of connective tissue called Bruch's membrane, which separates the choroid from the inner layer of the eye, the retina. Initially, choroidal melanomas are restricted by Bruch's membrane and therefore assume a "dome shaped" appearance, often associated with exudative retinal

detachment and deposits of lipofuscin. If they break through Bruch's membrane, the choroidal melanomas may take on a "collar-stud" or "mushroom" appearance, which is a pathognomonic clinical feature of this disease. Depending on the size and location of the tumour, choroidal melanomas can present symptomatically with visual loss, photopsia or floaters. In 30% of cases UM is completely asymptomatic and detected by chance on routine examination.[17]

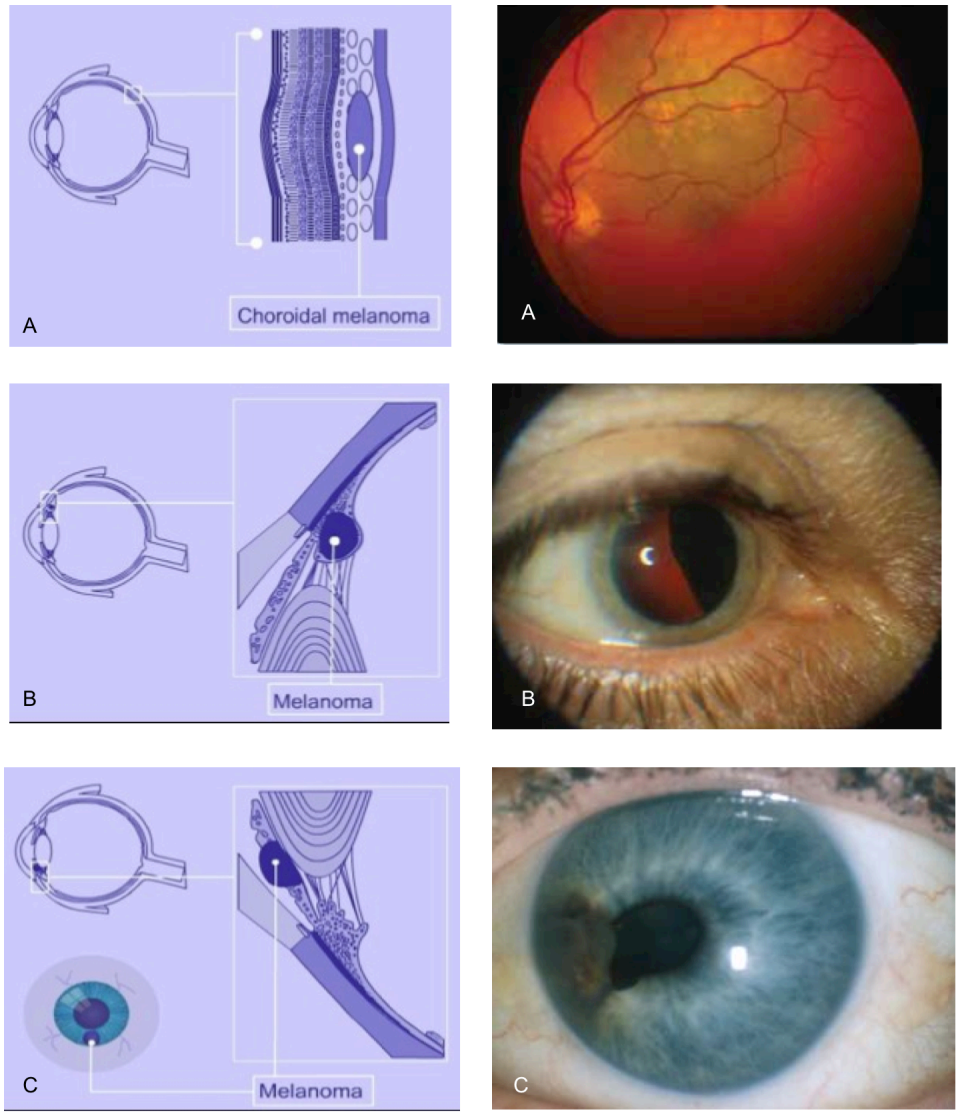

Figure 1.1 Anatomical location and clinical appearance of UM. A) Choroidal melanoma; B) Ciliary body melanoma; C) Iris melanoma. *(Courtesy of Prof. B. Damato)*

1.1.2.2 Ciliary body melanoma

The choroid continues anteriorly with the ciliary body, which is a circular structure composed of the pars plana, posteriorly, and the pars plicata, anteriorly. The pars plicata contains the ciliary muscles and the ciliary processes. The ciliary muscles are responsible for changing the shape of the lens providing accommodation of vision. The ciliary processes are finger-like projections lined by the ciliary epithelium, which produces of the aqueous humour, the fluid that fills the eye.

UM develops in the ciliary body in five percent of cases.[16] These are the most challenging to diagnose because of difficulties in visualising the area during routine ophthalmological examination. Patients can present with unilateral cataract, raised intraocular pressure, dilated episcleral vessels in the corresponding sector of the eye, but visual symptoms do not usually occur until the lesion is so large as to cause a visual field defect.

1.1.2.3 Iris melanoma

The iris is the most anterior part of the uveal tract. It is a thin, varyingly pigmented diaphragm, which can contract or dilate to change the intensity of light entering the eye.

Iris melanomas are usually small, pigmented, vascularised nodular lesions, with an indolent clinical course. Because of the anterior location, iris melanomas may be detected by the patient externally, and therefore be promptly diagnosed in most cases. A rare, more aggressive variant is diffuse iris melanoma, which is often associated with glaucoma and has an increased prevalence of metastatic disease.

1.1.3 Diagnosis and treatment

The diagnosis of UM relies on clinical examination (slit lamp examination and ophthalmoscopy) and ocular ultrasonography. Traditionally, UM have been subdivided according to their largest basal diameter (LBD) and thickness into small, medium or large. Small melanomas have a LBD > 5 mm with a thickness of 1-2.5 mm; medium tumours have a LBD ≤ 16 mm with a thickness of 2.5-10 mm; large melanomas have a LBD > 16 mm and/or a thickness > 10 mm.[18] More recently, this anatomical classification has been updated to new evidence-based categories that provide basis for staging UM as part of the tumour, node, metastasis (TNM) system used in all cancer types. The "T" categories define the anatomic extent of primary UM and take into consideration not only the LBD and thickness, but also the presence of extraocular extension (EOE) and/or ciliary body involvement.[19,20]

Large to medium-sized UM are reliably diagnosed clinically, with an accuracy of 99.5%.[18] Small melanomas are more difficult to differentiate from choroidal naevi. Shields et al. have devised the mnemonic "TFSOM", which stands for "to find small ocular melanomas", to identify indicators of potential malignancy: tumour 'Thickness' of more than 2 mm, subretinal 'Fluid', visual 'Symptoms', 'Orange' pigment, and location of the tumour 'Margin' within 3 mm of the optic disc.[21] Each of the risk characteristics roughly doubles the likelihood of growth so that the risk for malignant transformation is about 30 times higher when all five characteristics are present.[22] Additional risk factors are a low internal acoustic reflectivity on ultrasound, the absence of a halo around the tumour and the absence of drusen over its surface.[23]

Optical coherence tomography and fundus autofluorescence imaging are becoming part of routine examination as they are non-invasive diagnostic tools that help in identifying subretinal fluid, drusen and orange pigment, as well as in measuring the thickness of thin choroidal tumours.[24] On the contrary, invasive diagnostic tools that require intravenous injection of dye, such as fluorescein angiography and indocyanine green angiography, are performed only rarely to help the differential diagnosis with infective and inflammatory chorioretinal diseases or vascular tumours.[25]

The differential diagnosis of UM includes several conditions, the most common being choroidal naevus, eccentric disciform, congenital hypertrophy of the retinal pigment epithelium, systemic metastases to the choroid, and circumscribed choroidal haemangioma.[26] In case of diagnostic uncertainty, a choroidal biopsy is performed.

1.1.3.1 Treatment of primary UM

The management of UM depends on tumour size and location, associated ocular co-morbidities, visual acuity status of each eye, and patient wishes. The treatment options include various types of radiotherapy, surgical excision, or phototherapy, as detailed below.

The most widely employed treatment for posterior UM is radiotherapy, in particular brachytherapy using a radioactive plaque, with Ruthenium-106 and Iodine-125 being the most commonly used isotopes, in Europe and the USA, respectively.[27] The overall tumour control rate is approximately 90% at 5 years and treatment failure is associated with greater size and posterior extension of the

tumour.[28] Local recurrence rate is significantly reduced for smaller tumours, being only 3% at 7 years.[29] Radiation-induced complications, such as radiation retinopathy, exudative retinal detachment, radiation maculopathy, neovascular glaucoma, can occur and eventually lead to secondary enucleation in 12-17% of cases, depending on the isotope and dose of radiation used.[30, 31]

In selected centres, it is possible to treat UM with proton beam radiotherapy (PBR), which delivers a very precise focused beam of radiation to the region of the tumour from an external source, sparing the surrounding tissues.[32] It can be modulated to treat UM of any size and location, including iris melanoma.[33] To ensure the precise delivery of the radiation beam, the patient is postured in a fixed position and the eye is monitored with x-ray to visualise the tantalum markers. These are small inert metal buttons that are sutured to the sclera overlying the tumour prior to the PBR.[34] Tumour control is excellent, but visual loss almost inevitably occurs if either the optic nerve or the macula are in the field of radiation.[35]

A more widely available alternative source of radiation that can be used to treat UM is fractionated stereotactic radiotherapy, which can be performed using a gammaknife, a cyberknife or a linear accelerator.[36] The rate of local control is similar to that of brachytherapy; however there is a higher incidence of radiation-related complications, in particular neovascular glaucoma, leading to secondary enucleation.[37]

Following any source of irradiation, large UM are at risk of developing “toxic tumour syndrome”, which manifests as exudative retinal detachment, rubeosis and neovascular glaucoma and can ultimately lead to loss of the eye.[38] Surgical removal

of the ischemic irradiated tumour is an effective way to deal with such complications.[39]

The surgical removal of a primary or irradiated tumour can be performed ab externo using a partial lamellar sclerouvectomy technique commonly known as local resection,[40] or ab interno using a 25G cutter to "hoover" the choroidal tumour through the retina, known as endoresection.[41] Adjunctive brachytherapy is being routinely applied after resections of primary tumours to improve local control.[42] With these techniques, it is possible to preserve the eye, and in some cases useful vision, also for UM that would not have been suitably treated with radiotherapy.[43]

Enucleation, which is the removal of the eye globe, has been the standard treatment for UM in the past, as it was considered the safest way to treat it. The Collaborative Ocular Melanoma Study (COMS) group conducted a large, multicentre, randomised trial in the USA comparing enucleation, with conservative treatment using radioactive plaque brachytherapy.[44] No difference in survival was seen, therefore enucleation is currently being reserved for advanced UM that are larger than 18mm in LBD or thicker than 10 mm, that involve the optic nerve or cause severe ocular complications such as total retinal detachment or neovascular glaucoma. The volume of the globe is replaced by an orbital implant; the extraocular muscles are sutured to it to ensure postoperative ocular motility, and a customised prosthesis designed to match the fellow eye is clipped under the eyelid to provide pleasing cosmetic appearance.

Phototherapy for UM includes photodynamic therapy and transpupillary thermotherapy. Photodynamic therapy requires the intravenous injection of the photosensitiser verteporfin, which circulates in the choroid and is activated with by

laser shone over the tumour.[45] The success in local tumour control is inconsistent, although some small amelanotic choroidal melanomas regress completely; therefore it is not a preferred choice of treatment for UM, but rather for circumscribed choroidal haemangioma and vascular tumours.[46] Transpupillary thermotherapy uses an infrared laser to disrupt the metabolic activity of the tumour cells by increasing their temperature for about 1 minute, without any contrast agent being necessary.[47] After initial enthusiasm for this minimally invasive treatment option, concerns have been raised on its efficacy.[48] A recent paper reporting the results for 391 patients has shown a recurrence rate of up to 42%, and hence concluded that this technique should only be reserved for small choroidal melanoma with no more than two risk factors such as lipofuscin, subretinal fluid, acoustic hollowness, etc.[49]

1.1.4 Metastatic dissemination of UM

In medicine, the aim of treating cancer is to cure patients and, if not possible, to prolong the survival of the patient. For UM patients, it is still not known whether ocular treatment influences survival, and if so, in whom.[50] Indeed, approximately 50% of UM patients develop metastatic disease despite successful treatment of the primary tumour.[1]

Due to the lack of lymphatic vessels in the eye, metastatic dissemination of UM occurs via the bloodstream, while local spread to surrounding tissues is rare as long as the conjunctiva is not infiltrated transclerally.[51] Circulating tumour cells (CTC) have indeed been detected in the peripheral blood of UM patients at all stages of the disease.[52] As detailed in Chapter 4, we also investigated the clinical value of CTC

detection in UM patients using a novel platform (CellSearch® by Veridex) that had been approved for clinical use in other cancer types.

The liver is the main target organ of metastatic UM dissemination, being involved in up to 90% of UM patients with metastatic disease, while other potential sites are lung, bone and skin, but almost exclusively after liver invasion.[53] This marked hepatic tropism suggests that there must be something peculiar about the liver ("soil") in terms of metastatic niche development for UM cells ("seeds"). It is indeed by examining UM patients that the Austrian Ophthalmologist Ernst Fuchs first described in 1882 the 'predisposition' of an organ to be the recipient of specific growths,[54] inspiring Paget's well known seed and soil theory of metastasis.[55]

More recently, Logan et al.[56] provided experimental evidence for this in UM by injecting green fluorescent protein (GFP)-labelled 92.1 cells into the tail vein of nude mice and showing their dissemination via skin-flap and epifluorescence microscopy. Post-injection, cells were present in multiple organs; however after two weeks they survived exclusively in the liver, where they persisted as single metastatic seeds for the whole duration of the experiment (42 days). There is further experimental evidence from a murine xenograft model that, once in the liver, individual melanoma cells can give rise to micrometastases, which have the capacity to remain dormant, as avascular small aggregates of cells in the G0 phase of the cell cycle.[57] By evaluating histological and immunohistochemical findings of post-mortem livers from 10 metastatic UM patients, Grossniklaus has demonstrated the presence of such dormant micrometastases in humans.[58] Based on size, Grossniklaus categorised UM metastases into three stages, showing that avascular stage 1 (≤50 μm in diameter) metastases progress through stage 2 to

larger stage 3 (>500 µm in diameter) tumours, becoming vascularized and mitotically active during this process. How and why such progression occurs has not yet been clarified. The innate immune system is known to play an important role, with natural killer cells residing in the liver eliminating UM cells on one side,[59] and polarised tumour associated macrophages (TAM) creating a favourable microenvironment on the other.[60]

On the basis of tumour doubling times and mathematical modelling published by Eskelin et al.[61], it has been suggested that metastatic spread commences years before the primary ocular tumour is large enough to be detected clinically, hence occult micrometastatic disease may already be present in UM patients at the time of ocular treatment. Interestingly, however, only 1-2% of UM patients are found to have detectable metastatic disease at the time of diagnosis of the primary ocular tumour.[62] Indeed, liver metastases are typically detected 1-3 years following the ocular treatment. Moreover, there have been reports of metastatic disease developing 10, 20 and even 40 years later. The reason for such latency is not fully understood yet, but tumour dormancy is indeed a very challenging and fascinating topic that is being investigated by scientists in the field of UM.[63]

For the clinicians, the rationale behind early detection and treatment of UM is the hope that ocular treatment may prolong life, even once metastatic spread has commenced, by stopping the shedding of tumour cells into the bloodstream and therefore limiting the metastatic burden.[64, 65]

1.1.5 Personalised prognostication in UM

Although 50% of UM patients develop metastatic disease, the risk of developing metastatic disease for a given patient is not 50%. Over the years, a number of clinical, histopathological and more recently genetic features of the ocular tumour have been identified as being significantly correlated with the development of systemic disease. It is now therefore possible to estimate the survival probability for the individual patient by examining a tissue sample at the time of ocular treatment.

1.1.5.1 Clinical and histopathological features

The size of UM at the time of diagnosis has been long known as an important clinical prognostic factor for development of metastatic disease, with larger tumours having a more aggressive behaviour. Other negative clinical features are the presence of extraocular extension and an anterior location with ciliary body involvement. A recent collaborative study on 7731 patients has demonstrated that the "T" category defined according to the 7th edition of the American Joint Committee on Cancer (AJCC) classification, which takes into consideration of all the above elements, predicts prognosis. In particular, the risk for metastasis and death increased 2-fold with each increasing melanoma category from T1 to T4.[66]

Histopathological assessment of haematoxylin and eosin (H&E) staining allows the identification of the prevalent melanoma cell type in the sample, categorised as spindle, epithelioid and mixed based on the modified Callender classification.[67] The mortality is greater if the tumour contains epithelioid cells, which have abundant cytoplasm, are polygonal in size and are poorly cohesive, as opposed to spindle

cells, which have a fusiform configuration and form interweaving fascicles of parallel oriented cells. However, melanoma cells constitute a continuous biological spectrum, thus there can be a degree of subjectivity in determining cell category.

Other histopathological features commonly used for assessing the malignant potential of UM are the number of mitotic figures and the presence of closed loops. The number of mitotic figures in 40 high power fields indicates the proliferation rate of the tumour, hence the higher the figure the worse the prognosis. As detecting mitotic figures in H&E stained slides can be tedious and time consuming, we have previously demonstrated that this can be facilitated by immunohistochemical staining using the mitosis-specific marker Phospho-Histone H3 Ser10 (PHH3).[68] The presence of extracellular matrix Periodic Acid Schiff (PAS) positive closed loops, which are vasculogenic mimicry patterns, is another feature associated with death from metastatic melanoma.[69]

Other histopathological features have been identified as having a prognostic value but are less commonly assessed in routine clinical practice: mean diameter of ten largest nucleoli,[70] presence of tumour infiltrating lymphocytes,[71] degree of pigmentation and necrosis.

1.1.5.2 Genetic features

The majority of UM contain non-random gross chromosomal aberrations on either the short arm (p) or the long arm (q) of chromosomes 1, 3, 6 and 8, which can be used as prognostic markers.

A variety of genetic techniques are being used for prognostication in UM. These vary from lower resolution techniques such as fluorescence in situ hybridization

(FISH) and microsatellite analysis (MSA), to high resolution microarray based techniques, such as comparative genome hybridisation (CGH) and single nucleotide polymorphism (SNP) analysis. In Liverpool, the preferred technique at present is multiplex ligation-dependent probe amplification (MLPA), which allows the relative quantification of multiple loci on chromosomes 1p, 3, 6 and 8 in a single reaction, making it an affordable and accurate screening assay. When the amount of DNA extracted from the sample is insufficient for MLPA, chromosome 3 status is assessed by MSA. Please refer to Chapter 5 for more details.

The most important chromosomal abnormality in UM is the loss of one copy of chromosome 3, monosomy 3 (M3), which is associated with a reduction in the 5-year survival probability from approximately 100% to less than 50%, as first reported by Prescher et al. in 1996.[72]

Polysomy 8q (8q gain – 8qG) is also strongly linked with a poor prognosis.[73] Our group has recently analysed chromosomal data from 602 UM tested with MLPA, and demonstrated that M3 or 8qG have a similar impact on survival, when occurring in isolation. In combination, M3 and 8qG reduce the 5-year cumulative survival rate to 30%.[74]

Deletion of chromosome 1p occurs in approximately in 30% of UM. When occurring together with M3 the disease-free survival time in shorter.[75]

In contrast to chromosomal aberrations associated with a poor prognosis, the presence of polysomy 6p (6p gain, 6pG) is frequently found in disomy 3 (D3) tumours and is associated with prolonged survival.[73] Based on this observation, it has been suggested a “protective” effect of 6pG, however no single gene that may justify this benign tumour biology has been identified to date. Furthermore, 6pG

has been observed in a small proportion of M3 cases and is additionally found together with 8qG in D3 tumours,[76] therefore, no conclusive clinical implications can be drawn as yet.

1.1.5.3 The Liverpool Uveal Melanoma Prognostic Online (LUMPO) tool

Liverpool was the first specialist centre to combine the clinical, histomorphological and genetic features discussed above to provide a personalised prognostic curve for each UM patient based on a clinically validated mathematical algorithm. This software is freely available as the LUMPO tool (www.ocularmelanomaonline.org).[77] A recent Google Analysis of the tool demonstrated that over the last 2 years, there have been 1133 hits from 552 users in 291 cities around the globe.

The parameters included are: gender and age of the patient; tumour LBD and thickness; ciliary body involvement; extraocular extension; cell type; presence of PAS-positive connective tissue loops; mitotic rate; chromosome 3 status. A personalized survival curve is generated indicating the patient's survival probability at 10 years as compared to healthy population matched for age and sex (Figure 1.2).

The data is interpreted by a Consultant Ophthalmologist, who classifies the patient as at high risk (HR) or at low risk (LR) of developing metastatic disease. HR patients are referred to a Medical Oncologist specialized in UM for intense follow-up screening with 6-monthly liver MRI and serological liver function tests, whereas LR patients are reassured and discharged to their referring ophthalmologist.[78] A small proportion of patients have ambiguous or incomplete results and is therefore

clustered as “indeterminate”. Systemic screening is performed at patient’s discretion in such rare cases.

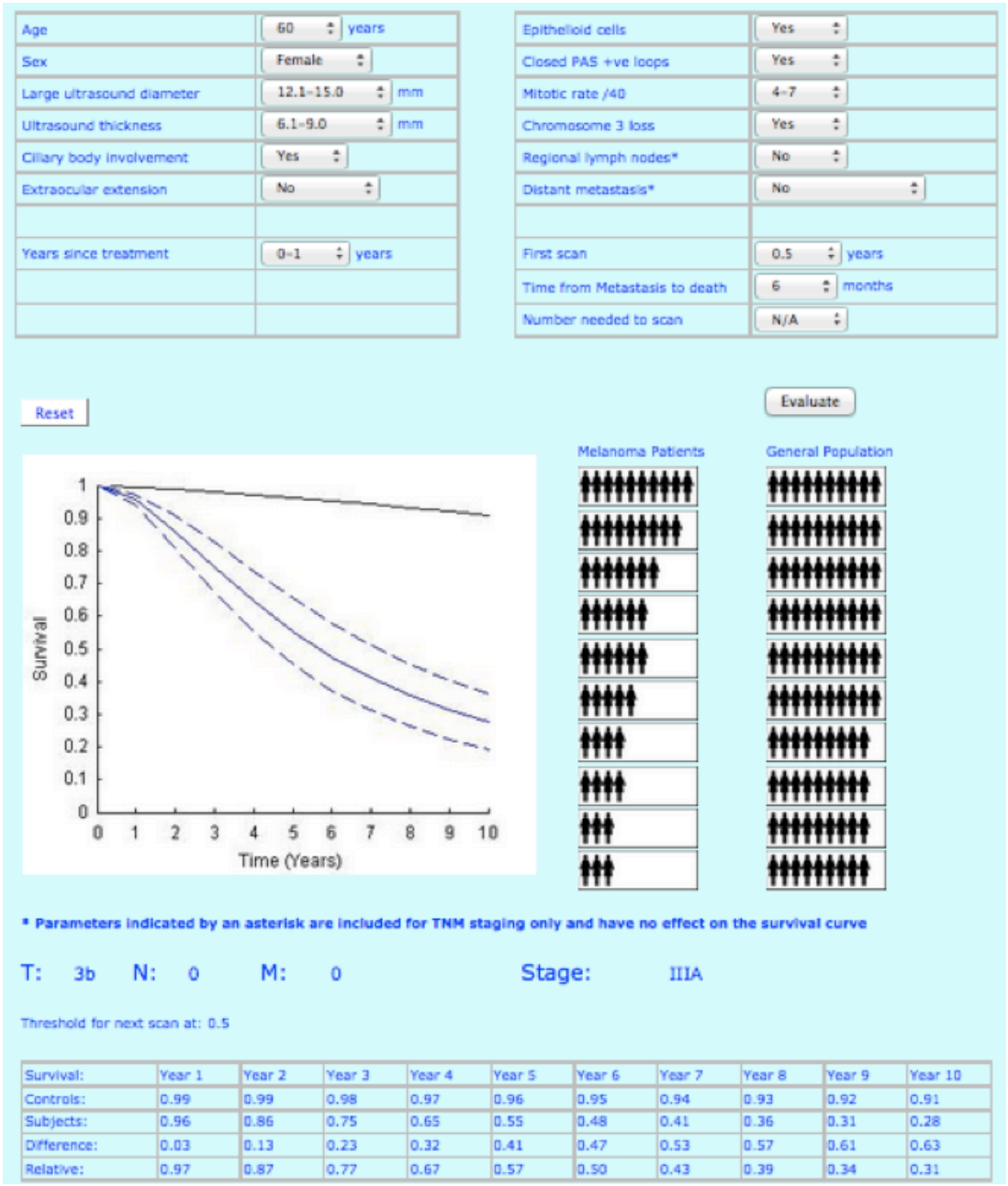

Figure 1.2 Example of a personalised survival curve indicating HR of developing metastatic disease. This 60-year-old woman with a cilio-choroidal melanoma containing epithelioid cells with M3 has a 60% greater chance to be dead in ten-year time as compared to sex and age-matched population. The continuous black line at the top of the graph refers to the normal population; the patient’s line is the blue continuous one. The dash line indicates the confidence interval. The pictograph on the right hand side is provided to facilitate the explanation of the results to the patients.

1.1.5.4 Gene expression profiling (GEP)

GEP is a high-throughput tool capable of simultaneous quantitative detection of a large number of genes in a single experiment. It is most commonly done using cDNA microarrays and fluorescent-based detection.[79] GEP has been used as an alternative approach for metastatic risk stratification in UM patients. Onken *et al.*[80] examined the expression profile of 35 untreated UM using high-density oligonucleotide arrays and performed unsupervised analyses that clustered them into two groups, named class 1 and class 2. They then performed supervised techniques to identify genes that discriminated the tumour classes. (Figure 1.3 A)

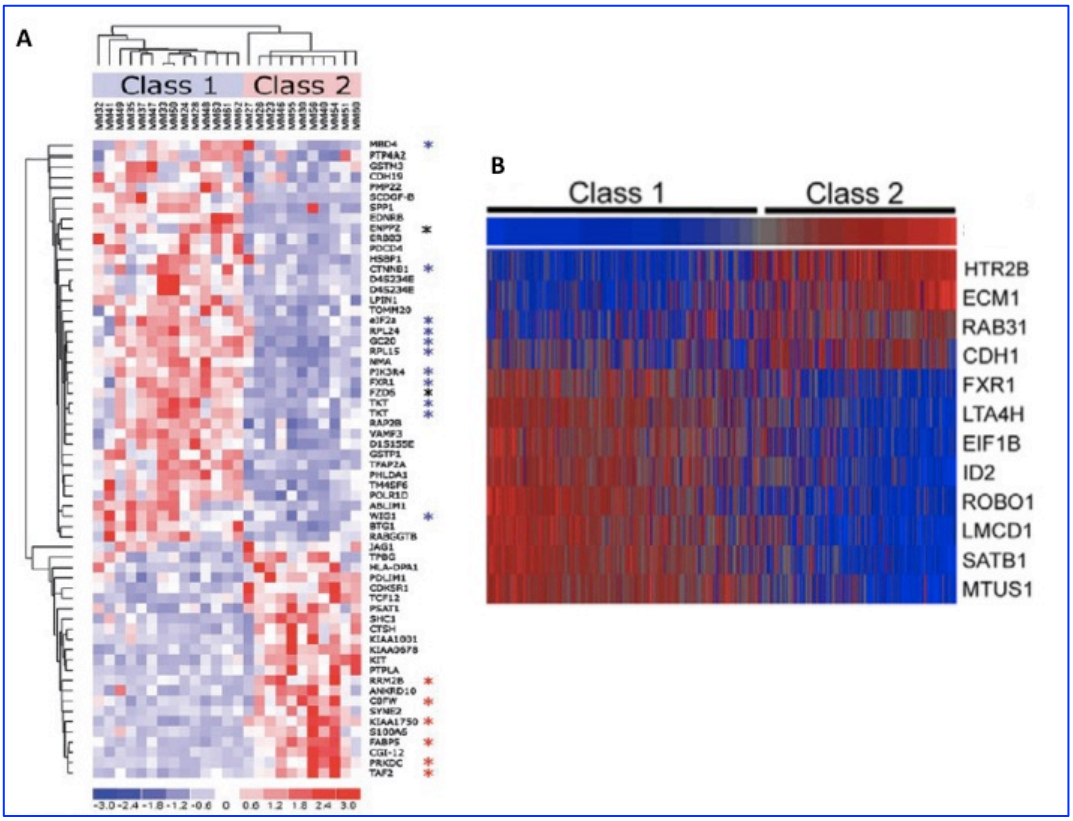

Figure 1.3 A) Hierarchical clustering heatmap of 62 discriminating genes from the original GEP analysis of 25 UM.[80] Class 1 (low-grade) and class 2 (high-grade) tumours are indicated. Blue asterisks indicate chromosome 3 genes that are down-regulated in class 2, red asterisks indicate chromosome 8q genes that are up-regulated in class 2, and black asterisks indicate chromosome 8q genes that are down-regulated in class 2. **B)** Heatmap showing normalised expression of the 12 discriminating genes chosen for the clinical assay.[81]

By correlating the molecular findings with the clinical data of the tumour and patient outcomes, class 1 was defined as low risk for metastatic disease, while class 2 as high risk. These data have since been used to develop a commercially available assay comprising 12 discriminating genes (listed in Figure 1.3 B) and 3 control genes (DecisionDx-UM; Castle Biosciences, Friendswood, Texas, USA).[81]

Based on recent observations that some Class 1 patients, considered to have low metastatic risk, developed metastases, the DecisionDx-UM assay now has an additional discriminatory category, Class 1B, for UMs with an 'intermediate' metastatic risk.

Whether GEP or DNA-based chromosomal analyses are more accurate in determining a UM patient's risk of developing metastasis is still being debated and clearly depends on the sensitivity of the technique used to determine chromosome 3 status. Estimates of the percentage of UM that are currently not accurately stratified by molecular testing vary from 5-25% of tumours.[82]

The advantages and limitations of both approaches and the clinical implications are discussed further in Chapter 5.

1.1.6 Detection and treatment of metastatic UM

Despite the advances in chemotherapy, radiotherapy, and surgical treatment for metastatic UM, the 5-year relative survival rate has not improved over the last three decades.[83-86] The median survival from the time of the development of metastatic disease is 2 to 12 months and 1-year survival is only 10-15%.[87]

Patients typically die from liver failure because of parenchymal invasion of disseminated disease or toxicity from chemotherapeutic agents.[87] In recent years, a number of targeted systemic therapies, immunotherapies and loco-regional treatments have shown promising results in preclinical settings and are currently being investigated in clinical trials across the world.[88]

So far, however, the best results in terms of survival have been seen in those patients with localised liver disease, who have been diagnosed early enough to be eligible for surgical removal by liver resection.[78, 89, 90] Likewise, the earlier detection of metastatic disease may potentially increase the effectiveness of already existing therapies.

1.1.6.1 Conventional screening tools for metastatic UM

The mainstream of systemic surveillance is based on liver imaging. Ultrasound is a cheap, non-invasive methodology that is widely available. However, it is operator-dependent, non-specific (hence leading to a number of incidental false-positive findings), and difficult to perform in patients with elevated body mass index. In Liverpool, we have been offering liver MRI to HR UM patients, and this allowed for pre-symptomatic detection of liver disease in 92% of patients.[78] However, MRI has

a significant cost and therefore it cannot be proposed as life-long monitoring system for all UM patients.

Liver-function tests are also routinely used to detect asymptomatic liver metastasis. In UM patients they have high specificity (90-96%) but a very low sensitivity (27%) as they are markers of liver damage, released when a significant portion of the organ has been invaded by cancer cells.[91] On the other hand, they may be also be influenced by other factors that elevate liver functions, such as the use of cholesterol-lowering agents.[92]

1.1.6.2 Other blood biomarkers

Based on the experience in cutaneous melanoma patients, a number of proteins with high specificity for cells of the melanoma lineage have also been tested as potential blood biomarkers for metastatic disease in UM patients. (Table 1.1)

Melanoma inhibitory activity (MIA) is an integrin ligand normally expressed in cartilage and aberrantly produced by melanoma and, to a lesser degree, by other cancer cells. It is implicated in metastasis through interaction with the components of the extracellular matrix.[93] MIA has been the first and the most widely melanoma-specific blood biomarker to be investigated in UM.[94] It is expressed in primary and metastatic UM tumours.[92, 95]

S100B, a member of a family of calcium-binding proteins, is expressed by a variety of cells and is implicated in the aberrant proliferation and differentiation that characterise tumours.[96] In contrast to cutaneous melanoma, where S100B is used for early detection of relapse/metastasis,[97] in UM patients S100B serum con-

centration is not of prognostic value and does not correlate with other prognostic factors.[98]

Osteopontin (OPN) is a component of the noncollagenous bone matrix, associated with aggressive tumour behaviour and metastases in other cancers.[99] Increased levels of OPN described have been described in metastatic UM, up to 6-months prior to clinically detectable liver disease.[100]

However, none of these markers alone has clinical value as a prognostic marker in UM. Moreover, clinical value was assessed for the most part by comparing serum levels of the protein of interest with clinical and pathological surrogate predictors, and not actual survival. They may have utility in monitoring patient status, as elevation on serial samples usually indicated the presence of metastatic disease. However, these same markers can also rise in presence of other conditions, such as autoimmune conditions and liver alcohol disease. They are therefore being implemented in addition but not as substitute for routine liver function tests in some ocular oncology centres, and do not represent the standard of care.[101,102]

Table 1.1 Serum proteins investigated as potential biomarkers of metastatic disease in UM

Authors (year)	Marker	Study type	Patients (n)			Comment
			UM	MUM	ctrl	
Schaller et al. (2002)	MIA	Case-control Prospective (8 months)	131	8 at diagnosis; 3 at f-up	-	Increased levels in the 3 pts who developed metastases
Missotten et al. (2003)	S100B	Prospective (60 months)	64	20 at f-up	58	No significant difference between pts and controls
Reininger et al. (2005)	MIA	Case-control Prospective (18 months)	293	12 at diagnosis; 8 at f-up	-	Increased levels in the 8/20 pts who developed metastases
Kakdkol et al. (2006)	OPN	Case-control	37	15	30	Increased levels in metastatic pts
Reininger et al. (2007)	OPN	Case-control	19	8	8	Increased levels in metastatic pts
Missotten et al. (2007)	MIA S100B	Case-control	104	30	50	Elevated in MUM pts: S100B in 62%, MIA in 52%, LDH in 62%
Barak V et al. (2007)	MIA, OPN S100B	Case-control	38	44 (8 before/after metastases)	18	91% AUC for 3 markers combined
Haritoglou et al. (2009)	MIA, OPN	Case-control	18	14	-	Increased levels in metastatic pts
Barak V et al. (2011)	MIA, OPN S100B, TPS	Case-control (sequential samples over 4 years)	43	32	53	Lead time for predicting metastases: S100B 18-24 months, OPN 12-18 months
Suesskind D et al. (2011)	GDF-15	Case-control	170	18	18	Increased levels in metastatic pts

1.1.7 The need for novel biomarkers

As detailed above, enormous progress has been made in the treatment of primary UM and in our ability to identify those patients at HR of developing metastatic disease. However, the time to discovery of clinically detectable metastases can range from months to decades and assessment of primary tissue cannot be used to monitor tumour dissemination or response to (a potential) adjuvant therapy. Novel biomarkers of UM metastasis are much needed. As UM disseminates haematogenously, blood biomarkers would be ideal because they could be assessed serially in a minimally invasive way.

Proteins are the ideal biomarkers, as they can be easily assessed with a number of non-expensive, antibody-based techniques that are already available in most pathology laboratories. The most widely used clinical biomarkers for monitoring of metastatic relapse in other cancer types are indeed proteins: prostate-specific antigen, carcino-embryonic antigen, alpha-feto-protein, etc.[103]

As melanoma-specific proteins derived from studies in cutaneous melanoma have not proven successful for UM patients, the aims of the studies described in this thesis were to investigate and compare the entire complement of proteins present in UM samples at HR versus LR of developing metastatic disease in search for novel biomarkers for clinical use.

1.2 Proteomics

Proteomics is the large-scale study of the entire complement of proteins, the so-called proteome, present in a cell, tissue, biofluid or organism in any given state.[104] It can be used to investigate the abundance, activity, modification and interaction of proteins in a given tissue.

1.2.1 Proteomics workflow

The proteomic workflow involves a multi-step process, which includes: sample acquisition, digestion into peptides, fractionation of the peptide mixture (or pre-fractionation of the proteins, depending on the technique chosen), and protein identification by mass spectrometry (MS) and data analysis. The various methods differ in their requirements for sample preparation, the extent and the level of sample fractionation (proteins or peptides), the type of MS and the data processing tool used.[105] Because proteomes are very complex mixtures, a number of techniques have been employed to extract them prior to analysis. (Figure 1.4)

Protein fractionation is often referred to as “top-down proteomics”. The most common techniques for this purpose are affinity chromatography for protein depletion and gel electrophoresis for protein separation.

Peptide fractionation is used in “bottom-up proteomics” where the entire proteome is digested into peptides, which are then fractionated and identified by MS. This approach is gel-free and is thought to introduce less bias into a biological sample, hence it is most frequently used in quantitative protein expression profiling. Column chromatography plays a major role in this phase.

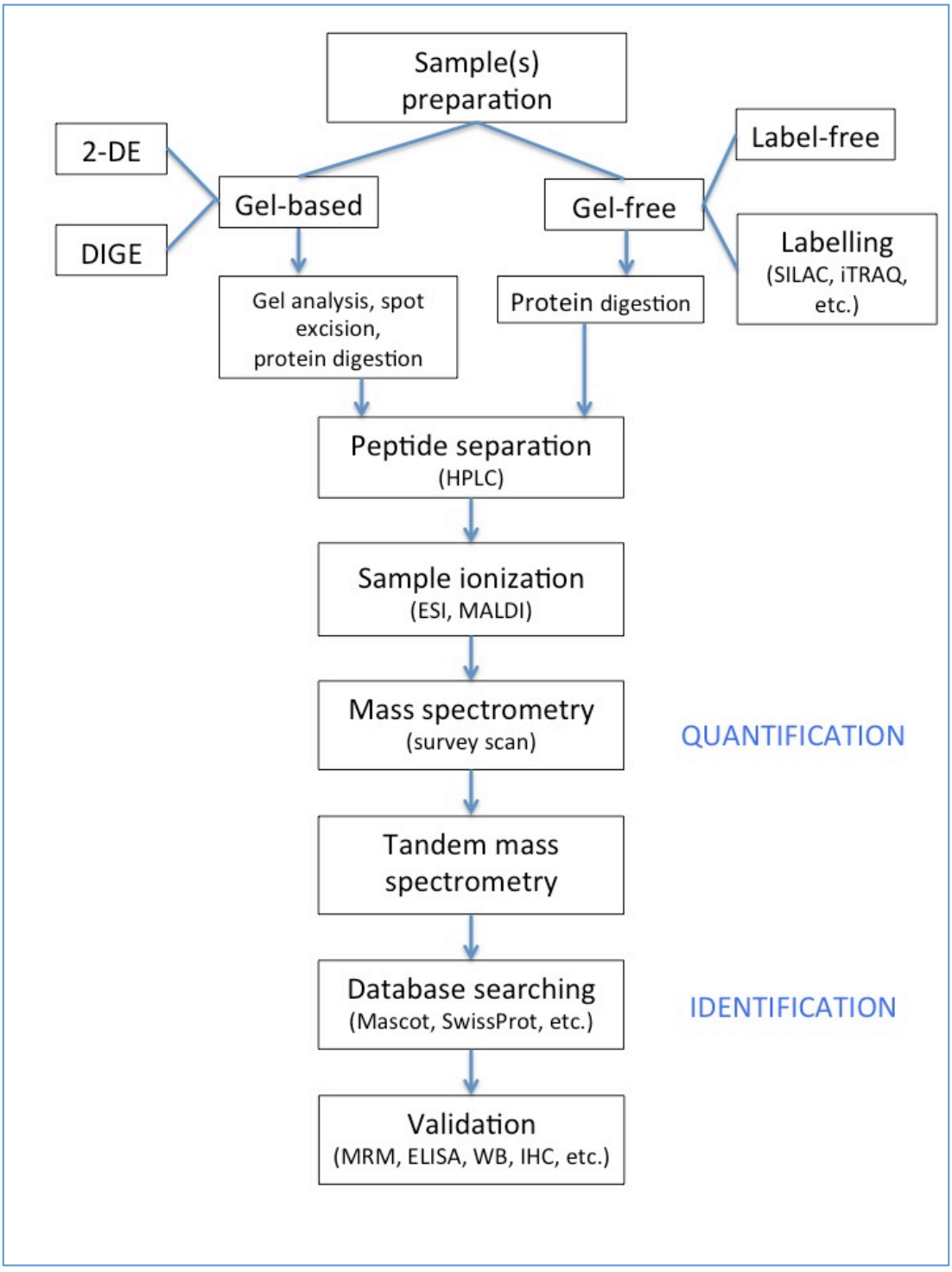

Figure 1.4 Workflow and techniques of discovery proteomics.

All techniques and abbreviations are explained in the text of this chapter.

1.2.1.1 Protein separation by gel electrophoresis

Sodium dodecyl sulphate – polyacrylamide gel electrophoresis (SDS-PAGE) separates proteins according to their electrophoretic mobility. The sample is first denatured with a buffer containing SDS, which charges each protein with a negative charge, identical per unit mass, so that the electrophoretic run leads to fractionation based solely on size. Depending on gel size and resolution, SDS-PAGE enables separation of proteins into about 10-50 fractions, which are recovered by excision and digested into peptides for sequencing by MS.

For separation of complex protein mixtures with a higher resolution, SDS-PAGE has been combined with isoelectric focusing (IEF), which separates proteins based on isoelectric points. This is called two-dimensional (2D) gel electrophoresis, (2-DE) and has been used for several decades in proteomics. The use of immobilised pH gradient strips for IEF is an improved technique that allows resolution of hundreds of denatured proteins in a single 2-DE gel.[106] After electrophoresis, the proteins in the gel are stained for visualisation, quantification and comparison. The various detection methods (radioactivity, dyes, fluorescence, and silver) as well as the data analysis issues that must be taken into account when quantitative comparative analysis of 2D gels is performed have been critically reviewed in a recent work.[107]

2-DE has been the pre-fractionation technique of choice in the majority of proteomic studies on UM conducted to date.[108-112] The stain and detection software used evolved over time, moving from Coomassie brilliant blue (CBB) for global protein detection to fluorescent dyes with higher sensitivity and dynamic range, such as SYPRO Ruby protein stain. Relative quantification of protein expression levels between samples was estimated based on the assumption that the optical

density of the spots (OD%) had to be proportional to the protein concentration. Differences in apparent protein expression levels between the UM samples were considered potentially significant when matched spots exhibited at least a two- fold difference in their averaged OD%.

A more reproducible method of relative protein quantitation from two or more samples is 2D fluorescence difference gel electrophoresis (DIGE), a version of 2D-PAGE where the proteins of each sample are labelled with a different fluorophore prior to electrophoresis.[113] Gels are scanned at wavelengths unique to each fluorescent label and the images are analysed for differences in protein patterns, such as spot density or mass shift. As DIGE is extremely sensitive, however, the amount of proteins present in the spots to be excised is sometime not sufficient for downstream MS analysis, hence limiting the capability for protein identification.

1.2.1.2 Protein identification

MS is the key analytical technique in proteomics for the identification and, increasingly, for the quantification of proteins. The principle of MS is to measure the mass (m) to charge (z) ratio of ions in the gas phase, hence the peptides need to be first transferred into the gas phase and ionised.

The two relevant techniques for ionization are matrix assisted laser desorption/ionization (MALDI)[114] and electrospray ionization (ESI).[115] For MALDI, the analyte is dissolved and co-crystallised with a matrix on a probe surface, which is then irradiated by UV laser pulses. The laser evaporates and converts the analyte into gas phase at the ion source. The ionised analyte is then separated by the time-of-flight (TOF) analyzer, most commonly employed in MALDI-MS. The m/z value of

peptides is measured by recording the time required for ions to travel over a fixed distance inside the mass analyser. In ESI, the peptide mixture is dissolved in a liquid solvent system instead of the matrix. Highly charged analyte droplets from a fine spray outlet are ionised at atmospheric pressure in the presence of a strong electric field, to generate a series of charged gas-phase ions. The charged ions are then emitted and focused into the high-vacuum region of the mass analyser, which records the various charge states of the molecule separated according to their m/z ratios. There are a number of mass analysers in addition to the above-described TOF: e.g. quadrupole, ion trap, orbitrap, and fourier transform cyclotron ion resonance (FT-ICR). Each one works differently, having their own strengths and weaknesses and can be used alone or in combination.[116]

The mass spectra can be directly compared with protein databases for matching the molecular weights using appropriated scoring algorithm (peptide mass fingerprinting).[117] This technique, however, is limited by the database (as it should contain prior information on the protein for matching) and by the complexity of the protein mixture (as it becomes difficult to select the right peptide mass from a lot of peaks).[118] Tandem mass spectrometry (MS/MS) involves two consecutive steps: peptide mass determination and generation of partial amino acid sequence information for a particular peptide based on further fragmentation. The m/z values of the fragments are then recorded in the tandem mass spectrum. Tandem MS can be done by two separate analysers (e.g. TOF-TOF) or inside the same mass analyser (e.g. ion trap).

To enhance detection of proteins from very complex mixtures, frequently used platforms are the LC-MS/MS instruments, where ion-pair reversed chromatography

or nano high performance liquid chromatography (HPLC) is used prior to tandem MS.[119] Advances in LC-MS/MS have greatly improved the dynamic range and sensitivity for analysis of complex protein mixtures.[120] Large-scale proteome profiling has been verified for different organisms, as well as mammalian tissues and cell lines by using multi-dimensional LC-MS/MS.[121]

1.2.1.3 Gel-free quantitative proteomics

Quantitative proteomics allows for accurate measurements of quantitative differences between two analytes, for example healthy and disease, and has therefore been largely applied for biomarker discovery.[122] There are two main methods: incorporation of metabolic or chemical labels, and label-free analysis of MS/MS spectra.

Metabolic labelling requires incorporation into the cell of specific amino acids with "heavy" isotypes (such as ^{13}C and ^{15}N), which can then be distinguished from their "light" (normal) counterpart by MS, and quantified. This technique, named Stable Isotope Labelling by Amino acids in Cell cultures (SILAC), reflects the immediate metabolic state of the cells and is regarded as an extremely accurate proteomic technique.[123] However, it requires that cells be grown in special culture media for five to ten passages to ensure complete incorporation of labels, and it is therefore only suitable for use in stable cell lines.

Chemical labelling is, on the other hand, suitable for use in all types of analytes, as it relies on biochemical reactions to bind specific "tags" to peptides post sample processing. Isobaric Tag for Relative and Absolute Quantification (iTRAQ) is the most widely used technique for biological samples, as it allows for parallel

identification and quantification of peptides from up to 8 different samples in the same MS run. As detailed in Chapter 2, iTRAQ was used to compare the protein profile of 20 primary UM specimens at HR or LR of developing metastatic disease.

Complex sample preparation, need for greater sample concentration, and incomplete labelling are potential limitations of label-based quantification, therefore label-free proteomic techniques have been developed based on the use of technologically advanced MS and bioinformatic platforms.[124] Approaches of label-free quantitative proteomics can be divided into two different quantification strategies. In the *spectral-counting* approach, peptide and protein abundances can be estimated based on the number of acquired peptide spectrum matches. This quantification method has been widely used but remains controversial, as it relies on a simple counting of acquired MS/MS spectra, rather than on measuring physical data. In the *ion-intensity*-based approach, the changes of peptide abundances are determined by measuring and comparing the chromatographic peak areas of the corresponding peptides. The areas of chromatographic peaks have been shown to correlate linearly in a wide range with the protein abundance, which makes their measurement feasible for quantitative studies.[125]

iTRAQ and label-free approaches have been compared by Patel et al.[126] to characterise the proteome of a bacterium, showing good agreement, with respect to protein identification and relative quantification. The label-free experiment did, however, have advantages in terms of sample requirement, sample preparation and instrumental time requirements. Sample requirement and preparation are very important when looking at low protein abundance, such as for secretome analysis. As discussed in Chapter 3, an ion-intensity-based label-free proteomic workflow

was successfully developed to analyse the secretome of short term primary UM cells in culture.

1.2.1.4 Data analysis

Protein identification traditionally relies on complex algorithms that match the information contained in mass spectra against a database of theoretical or previously identified spectra. Label-free technologies have been made possible thanks to the development of sophisticated software for peptide identification. Algorithms, however, can generate both false-positive and false-negative assignments, which are influenced by the stringency of spectra to sequence criteria. Discerning a true match from a false match is critical in proteomic data analysis. Discussing this, however, is behind the scope of this thesis. The most common tools for MS/MS based peptide identification and data analysis have been comprehensively reviewed elsewhere.[127]

1.2.1.5 Validation

Because of the complexity of the proteomic workflow and data analysis, many argue that it is essential to validate the identified candidate proteins using independent techniques, such as Western Blot or ELISA. Using an antibody-dependent method of validation, however, relies on extensive optimisation of the methodology, and can produce false negatives (e.g. related to poor antibody-antigen binding). For this reason, targeted proteomics techniques have been developed, that are highly sensitive, specific and high throughput. Selected reaction monitoring (SRM) and multiple reaction monitoring (MRM) are MS-based

technologies that can detect low-abundance molecules in complex mixtures by only recording the ions of interest corresponding to preselected proteins.[128]

In summary, proteomics offers a number of powerful tools to investigate similarities and peculiarities of biological samples, potentially leading to the identification of specific proteins that could be used as clinical biomarker. Experiments need to be carefully designed and the most suitable proteomic approach chosen by taking into consideration the complexity of the tissue of interest, the amount and concentration of proteins it contains, the degree of biological variability, etc.[105] Moreover, potential biomarkers then need to be validated in a large cohort of independent clinical samples, making discovery proteomic just the first step of a long path towards clinical benefit for patients.

1.2.2 Previous proteomics studies in UM

Proteomic technologies have been largely used to study different ocular structures and diseases (as comprehensively reviewed here by Jay and Gillies[129]). UM has been extensively investigated at the DNA and RNA level; however, only a limited number of proteomics studies have been published to date (Table 1.2).

The first paper was published in 2003 by Missotten et al.[130] who compared the MS of aqueous humour from 24 UM patients with 24 controls using a strong anion exchange surface protein chip array and surface-enhanced laser desorption ionization (SELDI) TOF MS. A large number of samples, especially among the controls, could not be assessed because of low protein content. Nevertheless, two proteins were identified that could distinguish between UM and control eyes in

89% of cases. Although this study has not been translated clinically (the two proteins have yet to be named), it suggested that proteomic evaluation could be relevant to find diagnostic markers for UM patients.

In 2005, Pardo et al. performed the first global proteome analysis of UM.[108] Using 2-DE and LC-MS/MS with a quadrupole TOF they were able to identify 683 proteins from a primary UM cell culture (UM-A). Sixty-nine (18%) of the 683 proteins had been previously described in cancer-related processes, such as invasion and metastasis, oncogenesis, drug resistance, invasion, etc. Interestingly, the melanoma-associated antigen MUC18, which has been recently used to characterise CTC in UM patients (as discussed in Chapter 4), was amongst the proteins detected in this original work.

The following year, the same group published a follow-up study where they focused on the characterisation of the invasion phenotype of UM tumour cells.[109] By performing differential 2-DE, they compared the proteome of primary UM-A cells versus that of its derived, highly invasive, cell line UM-A >7. New nuclear proteins were identified in the invasive cell line, such as BRCA-1 and high mobility group protein HMG-1. The authors validated by Western Blot a selection of novel proteins in 5 different UM cell lines, showing a possible correlation of MUC18 and HMG-1 expression with UM invasiveness. They also showed the overexpression of the oncoprotein DJ-1, which had also been identified in their previous study, but was shown here to be secreted. Moreover, they indicated DJ-1 as a potential serum biomarker of UM. A later study from the same group has indeed shown that elevated serum levels of DJ-1 are associated with risks factor for malignant transformation of choroidal naevi.[133]

Pardo et al. were also the first to perform proteomic analysis on the secretome of UM cell lines, identifying cathepsin D, syntenin and gp100 as potential biomarkers in UM.[110] As discussed in Chapter 3, these studies formed the basis for the development of our work on UM secretome.

In 2006, Zuidervaart et al.[111] performed differential proteomic analyses of UM cell lines by 2-DE and MALDI-TOF/TOF. They compared Mel270, which is a primary UM cell line, with two cell lines derived from liver metastases in the same patient (OMM 1.3 and OMM 1.5). They could identify only 24 differentially expressed proteins, but amongst these were a number of novel proteins expressed only by the metastatic cell lines, such as heat-shock αβ-crystallin, cofilin, and heat shock protein 27 (HSP27). Interestingly, differential proteomic analysis of primary UM tissues performed by our group has also identified HSP27 as differentially expressed between tumours at a HR versus LR of developing metastatic disease.[112] Please refer to Chapter 2 for further details on this study, as it posed the basis for the current proteomic analysis of UM tissue samples described in that chapter.

More recently, proteomic analyses of nine primary UM tumour samples from patients who developed metastatic disease versus 16 primary UM tumour samples from patients who did not develop metastatic disease, with a minimum of 7 years follow-up was performed using 2D DIGE.[137] Fourteen protein spots were identified as being differentially expressed, and those proteins were then identified by LC-MS/MS. Nine proteins were upregulated and four downregulated in primary UM tissue from patients who developed metastasis. IHC validation on a small cohort of FFPE UM samples showed correlation with the 2D DIGE results for two of these proteins: fatty acid-binding protein 3 (FABP3) and trioseposphate isomerase (TPI1).

Their functional role was tested by siRNA knockdown in the 92.1 UM cell line, which caused reduction in invasion and migration. In a recent review article published by the same group,[138] the authors mention unpublished results from a label-free LC-MS/MS analysis of eight primary UM tumour samples from patients who developed metastatic disease versus eight primary UM tumour samples from patients who did not. Interestingly, FABP3, TPI1 and HSP27 were also identified as being differentially expressed here, in keeping with previous studies.

Finally, two independent studies published in 2013 used SILAC and LC-MS/MS to study the change in protein expression following irradiation in the 92.1 UM cell line.[139, 140] Their aim, however, was to develop novel insight to enhance the sensitivity of primary UM cells to radiotherapy, which is outside the scope this thesis, therefore these will not be discussed here.

Table 1.2 Summary of previous proteomic studies in UM

Authors (year)	Samples	Proteomics technique	Main findings
Missotten *et al.* (2003)	Aqueous humour from 24 UM patients and 24 healthy controls	SELDI-TOF-MS	Two proteins discriminating between UM and control eyes
Pardo *et al.* (2005)	Primary UM cell culture (UM-A)	2-DE LC-MS/MS	683 proteins identified, 96% of which novel in UM
Pardo *et al.* (2006)	UM-A versus its derived aggressive cell line (UM-A>7)	Differential 2-DE LC-MS/MS	HMG-1 and MUC18 in aggressive UM. DJ-1 as potential serum marker
Zuidervaart *et al.* (2006)	Primary (Mel270) versus metastatic (OMM 1.3, OMM 1.5) UM cell lines	Differential 2-DE LC-MS/MS	24 differentially expressed proteins. Upregulation of HSP-27, aB-crystallin and cofilin in metastatic cell lines
Pardo *et al.* (2007)	Secretome of 5 UM cell lines (UM-A, SP6.5, UW-1, 92.1, OCM-1); serum from 11 UM patients and 8 controls	PAGE LC-MS/MS of secretomes; Differential 2-DE LC-MS/MS of depleted sera	Secretome analysis as promising tool for biomarker discovery in UM. Syntenin, Cathepsin D, and gp100 as potential candidates
Coupland *et al.* (2010)	UM tissue: 3 D3 versus 4 M3	Differential 2-DE LC-MS/MS	Downregulation of HSP-27 in M3 UM
Linge *et al.* (2012)	UM tissue: 16 non-metastasising versus 9 metastasising	2D-DIGE LC-MS/MS	Upregulation of FABP3 and TPI1 in metastasising primary UM
Wang *et al.* (2013)	UM Cell line (92.1) after 15 h and 48 h of 10 Gy radiation versus non-irradiated	SILAC 2D-LC-MS/MS	Radiation-induced down-regulation of cell cycle- and immunity-related proteins
Yang *et al.* (2013)	UM Cell line (92.1) after 15 h of 10 Gy radiation versus non-irradiated	SILAC 2D-LC-MS/MS	Changes in metabolism and signal transduction protein pathways in irradiated UM
Ramasamy et al. (2014)	UM tissue: 8 non-metastasising versus 8 metastasising	Label-free LC-MS/MS	Upregulation of DJ-1, syntenin-1, TPI1, FABP3, PHB2, PFKM, and downregulation of HSP-27 in metastasising primary UM

Adapted in part from Ramasamy et al.[138]

1.3 Scope and outline of this thesis

The aims of this thesis were to identify novel biomarkers for the early detection of metastatic disease in UM patients and to generate proteomics data to increase the understanding of the biology of this disease.

The objectives of this work were:

- To perform comparative quantitative proteomic analyses of primary UM tissues with different metastatic risk
- To perform comparative quantitative proteomic analyses of the conditioned medium (secretome) from primary UM cells and normal choroidal melanocytes in short-term culture
- To investigate the role of CTC as an alternative biomarker for early detection of metastatic disease in UM patients

The aims and objectives are described in further details below, alongside a brief explanation of the content of each chapter of this thesis.

In Chapter 2 we compared the protein profile of primary UM tissue samples from patients at HR versus LR of developing metastatic disease using iTRAQ labelling and MS. A selection of differentially expressed proteins was then validated by IHC in an independent cohort of FFPE samples. To enhance our chance to identify secreted proteins, we performed quantitative label-free MS to compare the secretome from short-term primary UM cells in culture, as well as normal melanocytes. Bioinformatic analysis was then applied to identify a panel a proteins that could

differentiate between patients at HR versus LR of developing metastatic disease, as detailed in Chapter 3.

Simultaneously, we investigated CTC as an alternative biomarker of metastatic disease in UM patients. In collaboration with the Paterson Institute in Manchester (now the Manchester CRUK Institute), we conducted a pilot study to assess the value of the CellSearch® platform for CTC detection in patients with primary and metastatic UM. As discussed in Chapter 4, we also investigated the expression of the antigens used for CTC capture and detection in UM cell lines grown in different conditions.

While conducting the above-mentioned study, we realised that some prognostic UM biopsies were unsuccessful, despite great efforts of the surgical and pathology teams, but obviously to the disappointment of the patient. We therefore performed a large audit, reviewing the whole biopsy process (from surgical technique, to sample handling and processing). As a consequence, a change in practice was adopted, with a successful increase in the success rate. This is described in Chapter 5.

Finally, in Chapter 6 we summarise the main findings and limitations of this work, and present future research perspectives deriving from it.

Chapter 2

Quantitative proteomic analysis of uveal melanoma tumour tissue

2.1 Introduction

During the last decade, enormous progress has been made in our understanding of the molecular features of UM thanks to numerous genomic and transcriptomic studies.[141] Such studies have identified characteristic DNA copy number alterations and mutations, and RNA expression profiles that strongly correlated with prognosis, but the search for tumour biomarkers and therapeutic targets is still at a preliminary stage. Proteomics is a complementary technique to genetic analyses that has been heralded as a novel tool for identifying new and specific biomarkers in many cancer types.[142] In UM, only a limited number of studies (reviewed in Chapter 1) have been published to date using proteomics technologies and the large majority of these have been performed on cells in culture.[108-112, 130, 137, 139, 140, 143]

The first proteomic analysis of UM tissue was published by our group comparing the protein expression profile of frozen UM samples, three with D3 and four with M3, as determined by FISH analysis.[112] The samples were subjected to high-resolution, two-dimensional (2D) gel electrophoresis for protein fractionation, followed by silver staining and densitometric image analysis. Four well-separated and clearly focused protein spots showing at least 1.5 fold change in expression between the two metastatic risk groups were excised and subjected to in-gel digestion. Nine proteins were identified by nano-LC-MS/MS, three of which could be detected by Western Blot: vimentin, HSP-27 and pyruvate dehydrogenase β. Immunohistochemical studies on an independent cohort of 41 formalin-fixed paraffin embedded (FFPE) UM specimens demonstrated a statistically significant

association between chromosome 3 loss and downregulation of HSP-27, raising the possibility of using such immunohistochemical staining as a surrogate prognostic indicator where genetic analyses were not possible. The clinical usefulness of the immunohistochemical assessment of HSP-27 protein expression has been validated in a further study on a larger series, showing that a low HSP-27 expression correlated with monosomy 3 and with increased predicted mortality. When assessed together with other clinical and pathological variables, the HSP-27 score was found to enhance estimation of survival probability.[144] HSP-27 immunohistochemistry is routinely used in our ocular pathology service.

These encouraging results constituted the basis of this study, to pursue the chase for biomarkers of metastatic disease in UM patients using more advanced discovery proteomics techniques on a larger number of samples. It is indeed known that proteomics results depend largely on the quality of the samples and on the proteomic methodologies used.[104, 145] For example, 2D-gel-based fractionation techniques can introduce quantitative bias into a biological sample, as large proteins and integral membrane proteins are difficult to display on 2D gels because they become insoluble at pH values close to their isoelectric points and precipitate out, while co-migration of multiple proteins poses problems for spot boundary.[146] Other problems include consistency when quantifying lower intensity proteins, which is limited by the sensitivity of the stain and of the sample acquisition device, as well as by the amount of sample that can be loaded onto gels without compromising spot resolution.[147] We therefore decided to adopt a "shotgun proteomics" approach, where the entire proteome is digested into peptides that are subsequently fractionated and identified by MS.

2.1.1 iTRAQ

To be able to quantify the relative abundance of the same peptide in different samples, we applied the isobaric tags for relative and absolute quantification (iTRAQ) labelling method, which had been successfully used in the discovery of biomarkers from a variety of clinical specimens, including plasma.[148-151]

The iTRAQ method allows for the differential labelling of peptides from up to eight different biological samples. The labels consist of three elements: a peptide reactive group, which binds to the N-terminal of peptides; a balance group, which compensates for the difference in mass of the labels; and a reporter group of variable mass.[152] (Figure 2.1) Prior to iTRAQ labelling, the samples are denatured and digested into peptides. The labelled peptides from each sample are then mixed, separated using 2D-liquid chromatography and analysed by tandem MS. Because of the isobaric nature of these reagents, the same peptide from each sample appears as a single peak in the MS spectrum. Upon collision-induced dissociation, the iTRAQ-tagged peptides fragment to release reporter ions. The peak areas of the reporter ions are used to assess relative abundance of peptides and consequently the proteins from which they are derived.[153] (Figure 2.2)

Relative quantification is possible across large patient cohorts by creating a pooled standard control, which is analysed in every run and against which all samples are then compared.

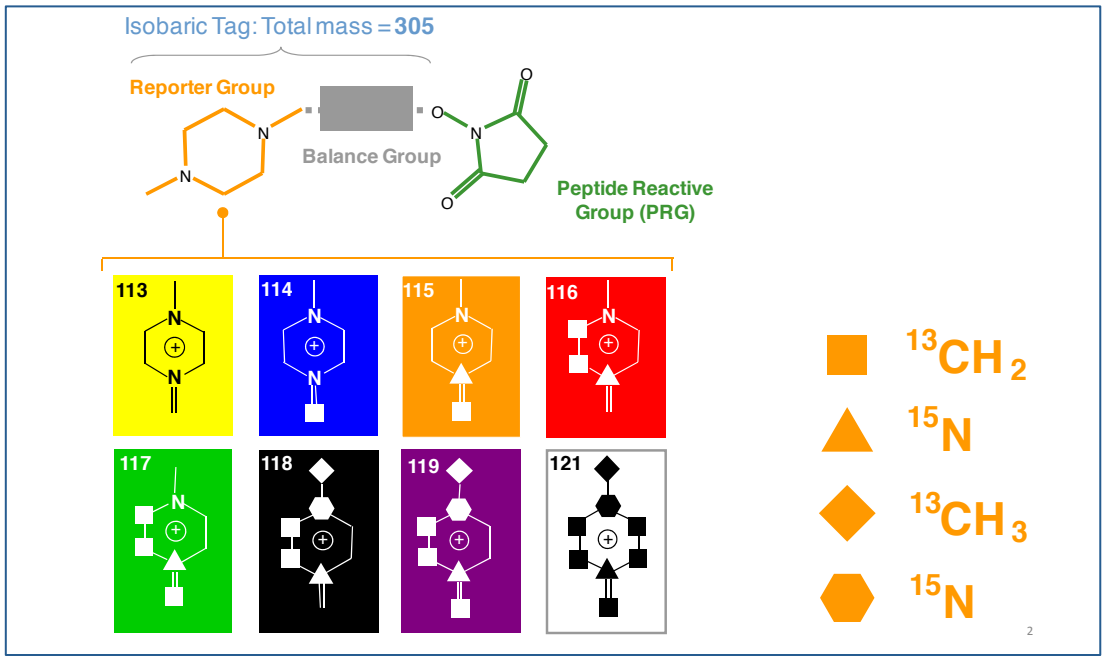

Figure 2.1 iTRAQ 8-plex reagent structure *(Courtesy of Dr C. Lane, AB Sciex)*

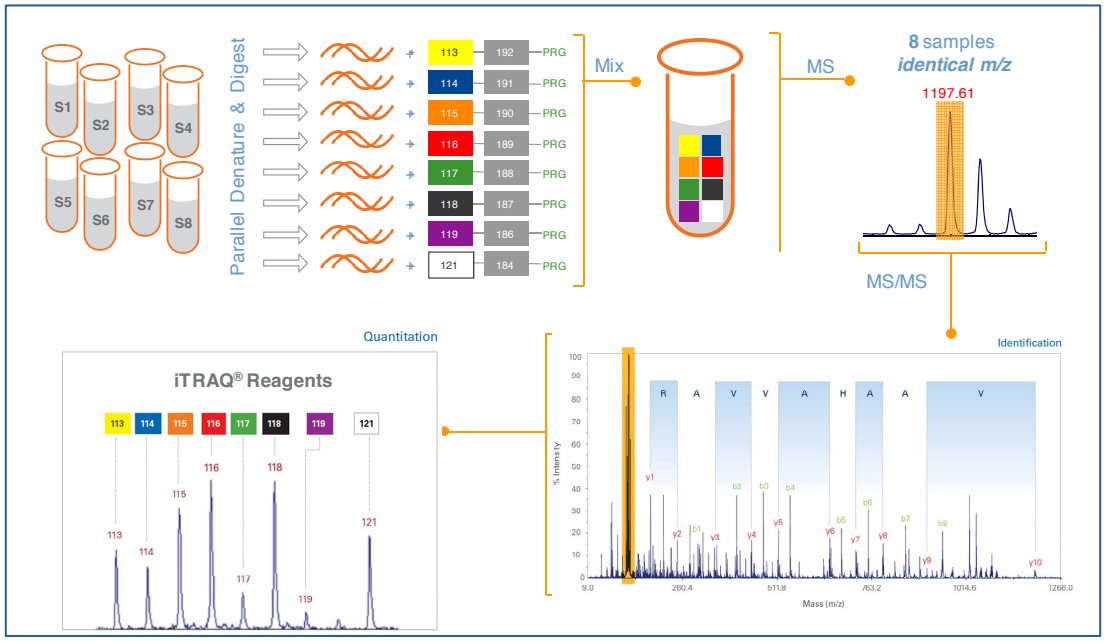

Figure 2.2 iTRAQ workflow *(Courtesy of Dr C. Lane, AB Sciex)*

2.2 Methods

2.2.1 Sample preparation

2.2.1.1 Selection of samples

Snap-frozen UM tumour tissues of different weights (17 µg, 30 µg and 50 µg) were obtained from the Liverpool Ocular Oncology Biobank (OOB) following approvals from the local and national ethics committees (NRES Ref No. 11/NW/0568). Preliminary experiments were conducted to determine the optimal weight of the frozen sample necessary to obtain a good spread of proteins following digestion, iTRAQ labelling and MS analysis. Following determination of the optimal sample weight (50 µg), a prospective collection of fresh-frozen samples was commenced from March 2011 from those patients undergoing enucleation or transcleral local resection as their primary treatment for UM. Twenty samples were used for the final iTRAQ analysis: 10 were from patients at HR of developing metastatic disease, and 10 from patients at LR. The risk category was determined on the basis of the clinical, histopathological and genetic characteristics, as explained in detail in Chapter 1.

Snap-frozen non-involved choroid was also obtained from fresh enucleated globes, to be used as a normal reference in the proteomic experiments. This was harvested from a macro- and microscopically unaffected area distant from the tumour. The genetic profile of the non-involved choroid harvested from eyes harbouring a M3 UM was analysed by MLPA to verify the absence of such alteration and substantiate its use as a normal reference sample.

1.5.1.2 Protein extraction and quantification

Unless otherwise state, all the reagents were supplied by Sigma (Sigma-Aldrich, Dorset, UK).

A maximum of four samples were thawed at the one time and kept on ice to minimise protein degradation. 200 µl of iTRAQ-compatible lysis buffer (0.5M triethylammonium bicarbonate (TEAB)/0.1% sodium dodecyl sulphate (SDS)) were added to the tissue, which was mechanically masticated using a blunt probe. The sample was then re-frozen in dry ice and allowed to defrost at room temperature (RT). Samples were further broken down by ultrasonication for ~ 10 seconds (s) using a Tekmar TM50 Sonic Disruptor with the output set at 45%. If the sample was not yet completely dissolved, 100 µl of buffer was added and ultrasonication repeated. Samples were then centrifuged at 14,000 rpm (~10,000 x G; 5415 C centrifuge, Eppendorf, Hamburg, Germany) for 20 minutes (mins) at 4°C, and the supernatant collected, transferred to a fresh Eppendorf tube and stored at -80°C until required.

The protein concentration of the samples was calculated using the method of Bradford.[154] To generate a standard curve, a range of known concentrations were made by diluting bovine serum albumin (BSA) in iTRAQ buffer to final concentrations of 2, 1.4, 1.0, 0.8, 0.4, 0.2 and 0.1 mg/ml, and placed in triplicate in a 96 well plate. Serial dilutions of each sample were made at concentrations of 1:5, 1:10, 1:20, 1:40, and placed in triplicate in the same 96 well plate. 250 µl of Bradford reagent (Bio-Rad Laboratories Ltd., Hertfordshire, UK) was added to each well, and the samples mixed thoroughly by repeat pipetting. Colour densitometry

was measured using a plate reader (Multiskan FC, Thermo Scientific) at an absorbance of 570 nm. Protein concentration within the samples was calculated by comparison with the standard curve.

2.2.2 iTRAQ labelling

The iTRAQ labelling procedure was undertaken according to the manufacturer's instructions (AB Sciex, Framingham, MA). 100 µg of protein was prepared in a volume of 20 µl of the iTRAQ-compatible lysis buffer. 2 µl of tris(2-carboxyethyl)phosphine (TCEP) reducing agent was added, the sample was vortexed and then incubated at 60 °C for one hour. Cysteine sulfhydryls were blocked by addition of 1 µl of methyl methanethiosulfonate (MMTS), the sample was vortexed, and then incubated at RT for 10 mins. Proteins were digested by addition of 10 µl of reconstituted porcine trypsin (Promega UK, Southampton, Hants, UK) and incubated at 37 °C overnight (12−16 hours). Individual iTRAQ reagents were reconstituted by the addition of 50 µl of isopropanol, vortexed, then added to individual sample tubes and incubated at RT for 2 hours. The labelled proteins were then combined, and the final volume was made up to 5 ml using cation exchange buffer A (10 mM potassium dihydrogen phosphate (KH2PO4)/25% acetonitrile (ACN) pH < 3). The pH was adjusted to between pH 2 and pH 3 by addition of concentrated phosphoric acid where necessary.

2.2.2.1 Creation of reference pool

Eight-plex iTRAQ is restricted by the number of available labelling reagents to 8 different samples per run. To overcome this limitation, we created a reference pool of normal choroid that was analysed in each run and used as common denominator

to calculate relative quantitation. The pool was formed from 22 snap-frozen normal choroid samples from 19 eyes, homogenised together as detailed above. Protein concentration was calculated using a Bradford assay. This mix was then aliquoted, and stored at -80°C until required. For each iTRAQ run, an aliquot was removed from the freezer, brought to room temperature and vortexed for 5 mins. An adequate amount of reference pool protein was removed and combined with 10 µl of lysis buffer, to give a final concentration of 100 µg of reference pool protein in 20 µl, and labelled with one of the isobaric tags.

2.2.2.2 Allocation of samples to iTRAQ experiment labelling

Samples were randomly allocated to each 8-plex run. Eight cards labelled 113, 114, 115, 116, 117, 118, 119 and 121 were placed in a sealed bag. Patient samples and reference pool were allocated to a specific label on the morning of the labelling part of the experiment by picking a numbered card from the bag.

2.2.3 MS analysis

2.2.3.1 Cation Exchange

Sample clean-up and pre-fractionation was performed using strong cation-exchange chromatography. A Polysulfoethyl A Column (PolyLC, Columbia, MD) 5 µm of 200 mm length × 2.1 mm inner diameter, 200 Å pore size, on a Agilent 1100 quaternary HPLC unit (Agilent Technologies, Santa Clara, CA), at a flow-rate of 300 µl / min was used. Peptides were eluted using a gradient of 0−15% B (10 mM KH2PO4/25% ACN/ 1M KCl pH < 3) in 45 mins and 15-50% B in 15 mins at a flow rate of 1ml/min. A total of 40 2-mins fractions were collected and dried in a vacuum

concentrator (Eppendorf Speedvac). They were desalted using a macroporous C18 high-recovery reversed phase column (4.6 x 50 mm, Agilent Technologies) installed on a Vision workstation (AB Sciex UK Ltd, Cheshire, UK) before being dried once more.

2.2.3.2 Mass spectrometry

The peptides were resuspended in 40 µl 0.1% formic acid just prior to LC-MS/MS analysis. Samples were delivered into a Triple TOF 5600 mass spectrometer (AB Sciex) by automated in-line reversed phase liquid chromatography, using an Eksigent NanoUltra cHiPLC System mounted with microfluidic trap and analytical column (15 cm × 75 µm) packed with ChromXP C18-CL 3µm. A NanoSpray III source was fitted with a 10 µm inner diameter PicoTip emitter (New Objective). Samples loaded onto the trap were washed with 2% ACN / 0.1% formic acid for 10 mins at 2µl / min before switching in-line with the analytical column. A gradient of 2-50% (v/v) ACN / 0.1 % formic acid over 90 mins was applied to the column at a flow rate of 300 nl / min. The mass spectrometer was set to perform data acquisition in positive ion mode, with survey scans of 250 ms, and with an MS/MS accumulation time of 100 ms for the 25 most intense ions (total cycle time 2.5 s). A threshold for triggering of MS/MS of 100 counts per second was used, together with dynamic exclusion for 12 s and rolling collision energy, adjusted for the use of iTRAQ reagent in the Analyst method. Information-dependent acquisition was powered by Analyst TF 1.5.1 software, using mass ranges of 400–1600 atomic mass unit (amu) in MS and 100–1400 amu in MS/MS. The instrument was automatically calibrated after every fifth sample using a beta-galactosidase digest.[155]

2.2.3.3 Protein identification and quantitation

Protein identification was carried out using ProteinPilot software (version 4.2; AB Sciex). The search was performed against the Uniprot Swiss-Prot database (release 23/01/12) using the Paragon algorithm. The search parameters allowed MMTS-modification of cysteine residues and biological modifications predefined in the software. Only those proteins identified with at least 95% confidence were taken into account. False discovery rate (FDR) was calculated as the percentage of decoy proteins identified against the total protein identification database. Decoy proteins were defined by searching against a reverse database, and the maximum acceptable FDR value was set at 1%. Relative protein quantification from iTRAQ labelling used code written in the statistical program R, as previously described.[149]

2.2.4 Data analysis

All tumour samples were quantified relative to normal choroid. Supervised and unsupervised hierarchical cluster analyses were performed using the statistical program R. Outlier analysis based on box plots of fold changes was calculated using the median absolute deviation (MAD) technique to identify commonly up- and down-regulated protein expression. Data was log2 transformed and the Z-score for each protein was calculated using the formula:

$$Z = 0.6745*(x(i)-xm)/MAD$$

where x(i) is the 'ith' observation and 'xm' is the median of the sample.

Outliers (Z >2 or <-2) represent proteins that are differentially expressed in each tumour sample.

Among these, proteins with known functions in tumour development/progression and shown to be differentially expressed between HR and LR UM samples were manually identified. A selection of these was validated in FFPE tissues by immunohistochemistry (IHC).

2.2.5 Immunohistochemical analysis

All products used for IHC were supplied from Dako (Dako UK Lts, Cambridgeshire, UK) unless otherwise specified. The same protocol was used for both whole tissue section and TMA slides.

2.2.5.1 Selection of samples

For all antibodies, initial optimisation experiments were conducted on a panel of FFPE slides of normal tissues (kidney, skin, testes, colon) known to express the protein of interest in order to define the antibody concentration to be used.

4 µm tumour sections from the corresponding FFPE blocks of the 20 UM (10 HR and 10 LR) used in the iTRAQ analysis underwent IHC using the optimised staining conditions, in order to validate proteomics findings.

To verify the clinical relevance of those proteins showing differential expression between HR and LR samples, IHC was performed on slides from a TMA containing tumour tissues (3 cores per tumour) from 74 primary UM patients with complete clinical information, including at least 7 years of follow-up.

2.2.5.2 Antigen Retrieval

Prior to IHC staining, all slides underwent de-paraffinisation, rehydration and heat-induced epitope retrieval using the pre-treatment module for tissue specimens (PT

Link, Dako). Once the module was pre-heated to 65°C, the slides were placed in a rack and incubated in a PT link tank containing 1.5 litres of high pH retrieval solution (Target Retrieval Solution, pH9.0) for 20 mins at 97°C. The sections were allowed to cool in the PT Link for approximately 50 mins until it reached a temperature of 65°C. The slide rack was then removed from the tank and immediately dipped into a container of 1X EnvisionTM Flex Wash Buffer (Tris buffered saline containing Tween-20, pH 7.6) at RT and left for 5 mins.

2.2.5.3 Staining

IHC staining was performed using the Dako Autostainer, which is an automated slide processing system designed to automate manual staining methods. All the reagents were part of the EnVision™ FLEX, High pH kit, which is a high-sensitivity visualization system intended for use in IHC together with the autostainer. It is a dual link system where the signal from the primary antibody (mouse or rabbit) is amplified by adding a species-specific detection reagent consisting of a dextran backbone to which horseradish peroxidases (HRP) are bound coupled with secondary antibody molecules. The reaction is then visualised through the addition of a chromogenic substrate that reacts with HRP in the presence of peroxide. For this work we used AEC (3-amino-9-ethylcarbazole), which forms a red end-colour, rather than the classic DAB (3,3'-diaminobenzidine tetrahydrochloride), which forms a brown-coloured product, as the red staining is more easily detected in pigmented tumours.

Following a wash in distilled water, the slides were counterstained in freshly filtered haematoxylin (VWR International, Leicestershire, UK) for 30 s and microscopically

examined to assess the staining intensity. Haematoxylin stained nuclei were blued using Scott's Tap Water for 30 s to allow contrast with the red chromogen end products. Slides were mounted using aqueous mounting medium (Merk, Millipore UK Limited, Hertfordshire, UK).

Details of the primary antibodies used can be seen in Table 2.1. A positive and a negative control slide for each antibody were stained alongside the tumour slides.

Table 2.1 Antibodies used for IHC validation of selected proteins identified by iTRAQ analysis

Antibody	Supplier	Species	Type	Conc (µg/mL)	Dilution	Control
Nesprin 2	Abcam Ab	Mouse	IgG2b	500	1:250	Skin
PDCD4	Abcam Ab	Mouse	IgG1	200	1:400	Testes
S100A6	Santa Cruz	Mouse	IgG1	200	1:250	Testes

2.2.5.4 Scoring

Scoring of the stained slides was performed by two independent observers and consisted of assessing the presence/absence of the stain and its cellular localisation within the tumour tissue. The three antibodies used showed different localisation: perinuclear, cytoplasmic, and both nuclear and cytoplasmic.

The percentage of tumour cells showing perinuclear, cytoplasmic or nuclear staining was determined in four categories, and the intensity of the staining was also assessed (Table 2.2). The final score for each slide was calculated by multiplying these two values, i.e. percentage tumour positivity and intensity. For one antibody showing both nuclear and cytoplasmic staining, the final value was calculated by adding the total cytoplasmic and nuclear scores. In the TMA slides, three independent cores are present to represent each sample. An average score

for both cytoplasmic and nuclear staining was calculated from the different cores present on the TMA to determine the final result. If more than one core was missing or not assessable the sample was dismissed from the final analysis.

Table 2.2 IHC scoring criteria

Intensity of staining in the cytoplasm*	1	weak
	2	moderate
	3	strong
% of cells showing cytoplasmic* staining	0	none
	1	1-25%
	2	26-50%
	3	51-75%
	4	76-100%
Intensity of staining in the nucleus	0	absent
	1	present
% of cells showing nuclear staining	0	none
	1	1-15%
	2	16-30%
	3	31-60%
	4	61-100%

* Perinuclear staining was scored in the same way as cytoplasmic staining

2.2.5.5 Statistics

Correlations were drawn between the staining results of the TMA slides and the clinical, histopathological and genetic data of the corresponding tumours, as well as the clinical information about the patients, including survival at the end of the follow-up time, using the statistics software SPSS (Version 21).

2.3 Results

2.3.1 Characteristics of tumour and choroid samples

Twenty primary UM tumours (10 HR and 10 LR) were analysed following iTRAQ labelling. The clinical, histopathological and genetic characteristics of the samples, used to determine the risk categories, are shown in Table 2.3. During the three-year follow-up period, six out of 10 patients defined as HR developed subsequent metastases in the liver, whereas all 10 LR cases were disease free at this time. This is in line with the predictions made by the prognostication algorithm (please refer to Chapter 1 for further details).

As described above, non-involved choroid was harvested from 19 eyes, enucleated because of UM. Meticulous care was taken when collecting the specimens to ensure that they were from a macro- and microscopically disease-free area. The weight of these samples ranged from 7µg to 35µg, therefore a large number of samples had to be pooled in order to achieve a concentration of at least 5 mg/ml of extracted proteins following homogenization.

Where the choroid sample was large enough, part of it was used for DNA extraction and MLPA analysis, to compare the genetic profile of what was considered normal tissue to that of the tumour in the eye. This was possible in six cases, all of which showed a normal profile for the chromosomes tested, in contrast to the tumours, as shown in Table 2.4.

Table 2.3 Clinical, histopathological and genetic characteristics of the UM tumours used for iTRAQ analysis

Sample No.	Age	Sex	LBD	HT	CB	EOE	Cell type	Loops	Mitosis	Risk	Genetic
S042-11	65	F	20.5	11.4	N	N	SPIN	N	2	LR	3N, 8N
S061-11	39	M	19.6	12.9	N	N	SPIN	N	3	HR*	3L, 8G
S067-11	62	F	17.2	10.7	Y	N	SPIN	N	9	HR*	3L, 8G
S159-11	22	M	15.9	8.5	N	N	MIX	Y	12	LR	3N, 8G
S165-11	73	F	20.8	15.4	N	N	MIX	N	4	HR*	3L, 8G
S166-11	53	F	17.8	12.9	Y	N	MIX	Y	21	HR*	3L, 8G
S196-11	71	F	14.5	6.8	N	N	SPIN	N	7	LR	3N, 8G
S228-11	48	F	17.1	15.3	N	N	EPI	Y	17	HR*	3L, 8G
S065-12	74	F	20.3	11.2	N	N	MIX	Y	10	HR*	3L, 8G
S070-12	57	M	16.7	7.3	N	N	SPIN	Y	4	LR	3N, 8N
S113-12	58	M	17.9	10.7	N	N	MIX	Y	5	LR	3N, 8N
S116-12	59	F	16.8	5.2	Y	N	SPIN	Y	7	HR	3L, 8G
S124-12	74	F	16.2	7.2	N	N	SPIN	N	6	LR	3N, 8N
S140-12	69	M	17.6	11	N	Y	MIX	N	5	HR	3L, 8G
S147-12	62	M	16.3	8.6	N	N	MIX	Y	5	LR	3N, 8G
S163-12	46	M	16.4	5.9	N	N	SPIN	N	8	LR	3N, 8G
S194-12	42	M	12.7	11.6	N	N	MIX	N	3	LR	3N, 8N
S195-12	77	F	14.7	5.7	N	N	EPI	N	7	HR	3L, 8G
S197-12	71	F	13.6	8	N	N	MIX	Y	6	HR	3L, 8U
S204-12	48	M	12.7	10.5	N	N	SPIN	N	3	LR	3N, 8N
S216-12	47	M	17.9	14.4	Y	N	MIX	Y	5	HR	3L, 8U

*F: female; M: male; Y: yes; N: no; LBD: largest basal diameter; HT: tumour thickness; CB: ciliary body involvement; EOE: extraocular extension; Cell type: spindle, mixed, epithelioid; HR: high risk; LR: low risk of developing metastases; genetic (chromosomal alteration determined by MLPA): N-normal, L-loss, G-gain, U-unclassified. *Indicates patients who have developed metastatic disease during the follow-up period.*

Sample no.	*Tumour MLPA*	*Choroid MLPA*
S018-11	*3L, 8N*	*3N, 8N*
S029-11	*3L, 8U*	*3N, 8N*
S040-11	*3L, 8G*	*3N, 8N*
S082-11	*3L, 8G*	*3N, 8N*
S172-11	*3L, 8G*	*3N, 8N*
S027-12	*3L, 8N*	*3N, 8N*

Table 2.4 MLPA analysis of matched choroid and tumour samples from the same eye, showing lack of chromosomal alterations in the normal choroid for chromosomes 3 and 8.

Legend: L: loss; N: normal; G: gain; U: unclassified.

2.3.2 iTRAQ results

2.3.3 Protein identification

The samples were analysed in three non-consecutive MS runs performed between June and October 2012. Each run included a mixture of high- and low- risk samples as well as one aliquot from the choroid pool, which remained constant (Table 2.5).

Table 2.5 Allocation of samples to different MS runs

Run no.	iTRAQ label	Sample	Patient ID	Risk
A	113	1	S065-12	HR
A	114	2	S042-11	LR
A	115	3	S166-11	HR
A	116	4	S159-11	LR
A	117	5A	S067-11	HR
A	118	5B	S067-11	HR
A	119	6	S196-11	LR
A	121	Ch	Choroid pool	Normal
B	115	7	S147-12	LR
B	121	8	S124-12	LR
B	119	10	S165-11	HR
B	114	11	S070-12	LR
B	118	12	S061-11	HR
B	113	13	S228-11	HR
B	117	14	S194-12	LR
B	116	Ch	Choroid pool	Normal
C	118	15	S195-12	HR
C	114	16	S197-12	HR
C	117	17	S216-12	HR
C	113	18	S116-12	HR
C	121	19	S113-12	LR
C	115	20	S163-12	LR
C	116	21	S204-12	LR
C	119	Ch	Choroid pool	Normal

Overall, 3022 unique proteins were identified: 1896 (63%) were common to all runs, while 2428 (80%) were detected in at least two runs. The number of identified proteins differed among runs, with run 'A' being optimal in terms of quantity and

quality (based on number of peptides) of identified proteins. Details for each run, including: protein ID, accession number, number of peptides identified with at least 95% confidence and percentage of sequence coverage can be seen in Appendix 1.

2.3.3.1 Protein quantification

Relative quantification based on the iTRAQ labelling was calculated using the pooled choroid sample as a denominator in all cases, as this sample was present in all runs.

Unsupervised hierarchical clustering (UHC) of the samples in Run A showed a nice separation between high- (T1, T3, T5, with 5A and 5B being technical replicates) and low- (T2, T4, T6) risk samples. This would remain true whether using as common denominator a tumour sample (in this case, T5B), or the normal choroid pool (Figure 2.3).

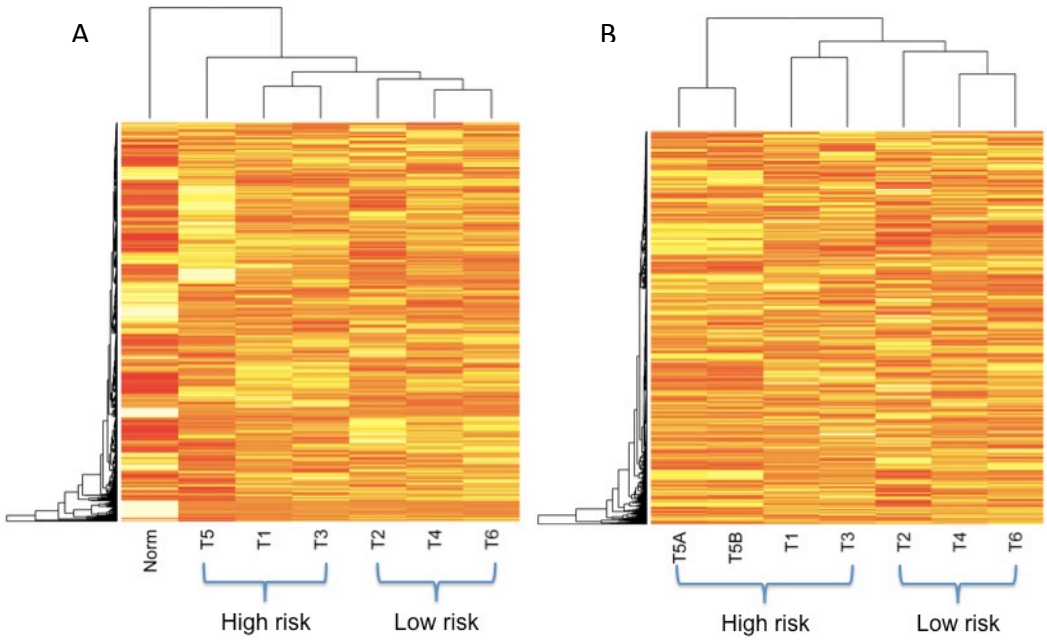

Figure 2.3 Unsupervised hierarchical clustering of samples in Run A, showing a nice separation between risk categories when using a tumour sample (T5B) as common denominator (A), as well as when using the choroid pool (norm) as denominator (B).

However, the quality and quantity of proteins quantified progressively decreased with runs. Moreover, using the choroid pool as common reference could no longer distinguish the low- and high- risk samples upon UHC, whereas this would remain true when using a tumour sample as common denominator (Figure 2.4).

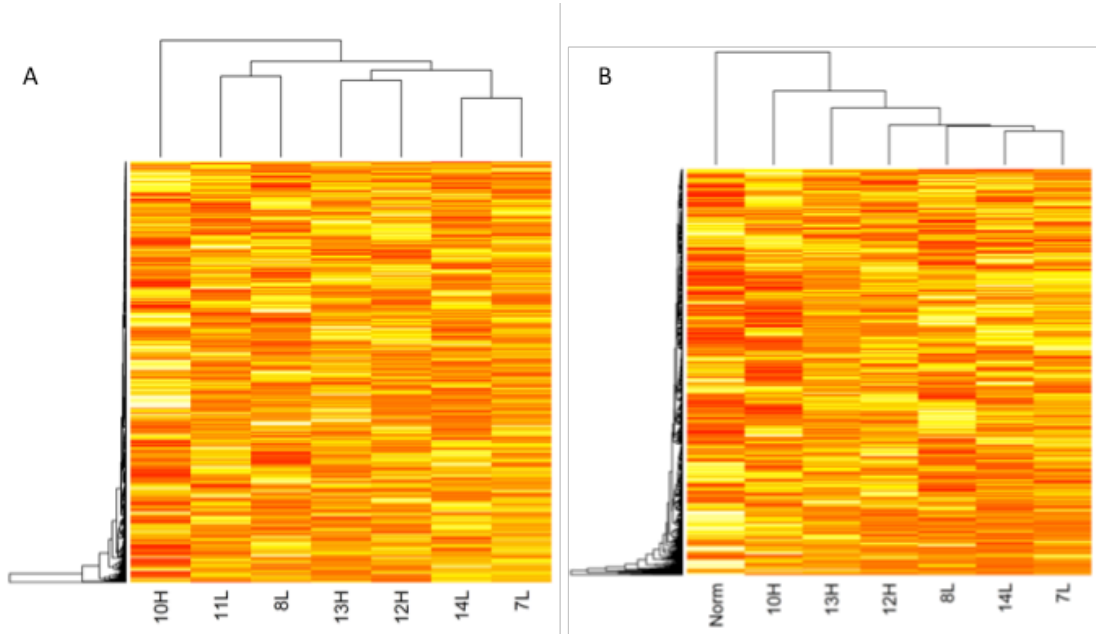

Figure 2.4 Unsupervised hierarchical clustering of samples in Run B, showing a nice separation between risk categories when using a tumour sample (11L) as common denominator (B), but now when using the choroid pool (A). *L: low-risk, H: high-risk; norm: choroid pool.*

This indicates that the most likely source of problem was the choroid pool. Indeed, the protein concentration of the pooled stock, which should have remained stable, did change over time (Table 2.6). This could be due to protein degradation and may explain the deterioration of the iTRAQ results.

Table 2.6 Protein concentration (assessed by Bradford assay) of the choroid pool at different time points

Date	mg/mL
18.06.2012	5.64
11.09.2012	5.99
03.10.2012	7.53
16.10.2012	6.99

However, the choroid pool was the only sample in common between runs, so we still used it as a common denominator to perform a cumulative analysis of the 10 HR versus 10 LR samples. When merged, 821 unique proteins were quantified in all three runs. Data were scaled to adjust for protein loading differences between runs before performing cluster analysis, but nevertheless UHC only separated the samples into run (not HR vs LR).

2.3.3.2 Selection of relevant proteins

iTRAQ Run 'A' was identified as the optimal run both in terms of the internal control and the identification/quantification of proteins and was used to select proteins for further validation. A median expression value (using the normal choroid as the denominator) was calculated for the three HR samples and the three LR samples. For sample S067-11, which was run in duplicate, the average of the values was used.

All 1960 unique accessions were subsequently ranked according to the median value for HR (from lowest to highest), highlighting those with differing median values between HR and LR tumours (n=81). These proteins were manually examined in the complete spreadsheet containing the merged data from all three the iTRAQ runs: of the 81 selected proteins, 16 showed difference in expression between HR and LR across most samples. These are detailed in Table 2.7.

Table 2.7 List of proteins showing differential expression between HR and LR tumours

Expression	Accession	Name	Gene
LR >HR	P61225	Ras-related protein Rap-2b	RAP2B
LR >HR	P07108	Acyl-CoA-binding protein	DBI
LR >HR	Q96N67	Dedicator of cytokinesis protein 7	DOCK7
LR >HR	P42356	Phosphatidylinositol 4-kinase alpha	PI4KA
LR >HR	Q9H008	Phospholysine phosphohistidine inorganic pyrophosphate phosphatase	LHPP
LR >HR	Q8NBS9	Thioredoxin domain-containing protein 5	TXNDC5
LR >HR	P37840	Alpha-synuclein	SNCA
LR >HR	P50453	Serpin B9	SERPINB9
LR >HR	P11216	Glycogen phosphorylase, brain form	PYGB
LR >HR	Q96RF0	Sorting nexin-18	SNX18
LR >HR	Q53EL6	Programmed cell death protein 4	PDCD4
LR >HR	Q09666	Neuroblast differentiation-associated protein AHNAK	AHNAK
HR >LR	P06865	Beta-hexosaminidase subunit alpha	HEXA
HR >LR	P06703	Protein S100-A6	S100A6
HR >LR	Q15155	Nodal modulator 1	NOMO1
HR >LR	Q8WXH0	Nesprin-2	SYNE2

After studying their function, localization and potential role in cancer using UniProtKB and Genecard, three proteins were selected for further IHC validation: nesprin 2, S100 A6 and programmed cell death protein 4 (PDCD4). The first two proteins showed a relatively higher abundance in the HR samples, whereas PDCD4 was more abundant in the LR samples. Detailed values are shown in Appendix 2.

2.3.4 Protein expression in tissue sections

Matched FFPE slides were available for all 20 tumours used in the iTRAQ experiments; however in one case (S165-11) the residual tumour was mainly necrotic, hence the IHC staining could not be assessed. In all other cases, IHC confirmed the presence of the proteins in the tissues and their different levels of expression between the HR and LR samples (Appendix 2).

Nesprin was expressed on the perinuclear membrane, S100A6 in the cytoplasm, and PDCD4 in the nucleus and/or cytoplasm. Nesprin expression showed a high degree of heterogeneity across the tissue section, such that positive tumour cells were limited to one region of the tumour (generally the edge), while protein expression was not detected in the rest of the tumour section (Figure 2.5). For this reason, assessing Nesprin expression in small TMA cores would be not representative, as the positive-staining areas could be over- or under-represented; hence only PDCD4 and S100A6 were selected for further clinical validation in the TMA.

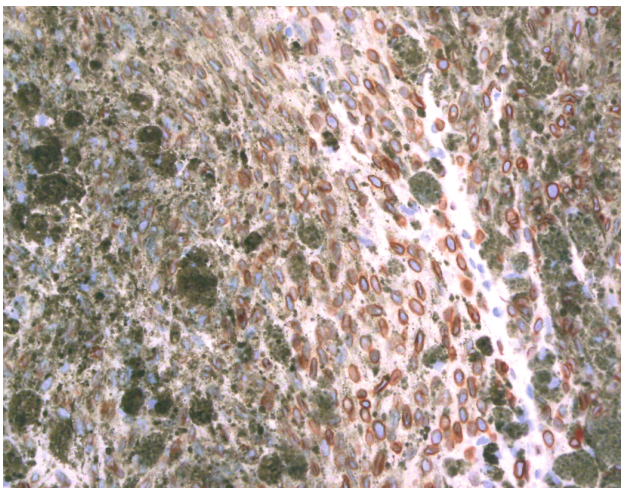

Figure 2.5 Immunohistochemical staining of Nesprin 2 in a pigmented UM specimen (20x). The protein of interest is expressed on the perinuclear membrane of UM cells, visible as red circles around the blue nuclei. The large dark brown cells are melanomacrophages.

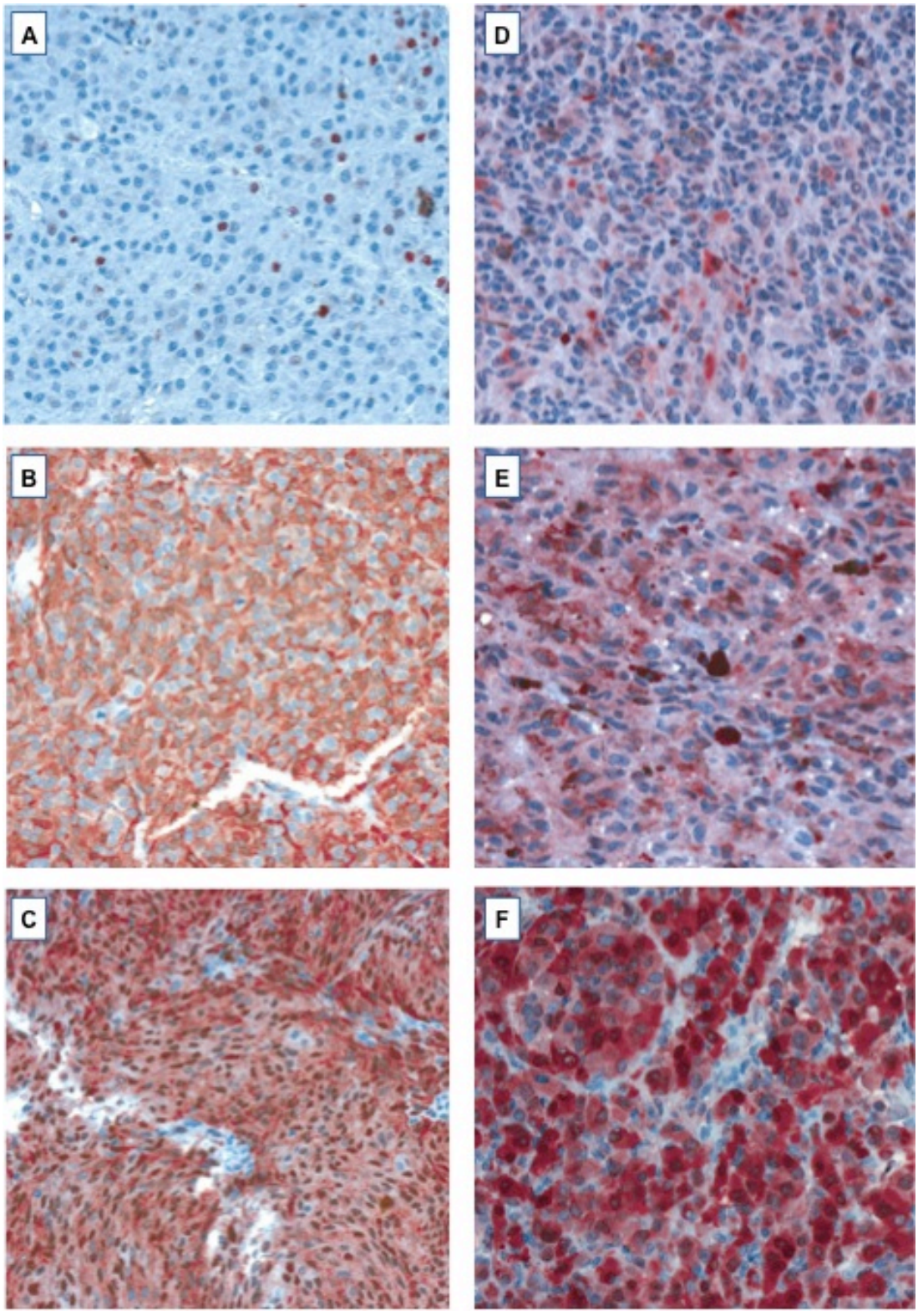

Figure 2.6 Immunohistochemical staining for PDCD4 (right) and S100A6 (left) proteins in UM TMA. A) PDCD4 is expressed in the nucleus but not in the cytoplasm; B) PDCD4 is expressed in the cytoplasm but not in the nucleus; C) positive PDCD4 expression both in the nucleus and in the cytoplasm. S100A6 is strictly cytoplasmic, but its expression has been defined as: D) weak; E) moderate; F) strong. (Image magnification 20x and 40x)

2.3.5 Validation of PDCD4 and S100A6 expression in an independent cohort of primary UM tissues

The TMA comprised UM from 42 males and 32 females, with a mean age at diagnosis of 62 years (median, 61yrs; range, 39-89yrs). The tumours had a mean largest basal diameter of 16.7 mm (median, 17.0 mm; range, 8.8-23.6mm). Histological examination previously performed on full tumour sections as part of the routine diagnostic work-up, identified epithelioid cells in 42 tumours. Closed PAS positive loops were found in 48 UM, and the mitotic count exceeded 5 per 40 high power fields in 23 tumours. Genetic analysis of all UM examined by MLPA classified 44 of these tumours as D3, and 29 as M3. In one patient, the chromosome 3 status was not known. Follow-up information was available for 72 patients at the close of study, in June 2014: 40 patients were still alive; 28 had died of metastatic melanoma; and four had died of other causes. After excluding these four patients, the mean survival time was 6.7 years (median 7.0 years; range 0.4-14.0 years).

2.3.5.1 Expression of PDCD4

PDCD4 protein expression was assessable in 67/74 tumours because some cores were missing or damaged. PDCD4 staining was localised to the cytoplasm and nucleus of tumour cells in 62/67 (92%) and 25/67 (37%) of primary UM cases, respectively (Figure 2.6 A,B,C). For all cases in the TMA, the staining score in the individual cores of each case did not differ by more than 10%, indicating no significant heterogeneity in the presence or absence of PDCD4 protein expression across any individual tumour. Nuclear expression of PDCD4 protein was found in the presence of cytoplasmic PDCD4 staining in 23/25 (92%) cases, with the

hypothesis being that PDCD4 protein dynamically shuttles in and out of the nucleus from the cytoplasm.[156] Thus Receiver Operating Characteristic (ROC) analysis was performed on the PDCD4 cytoplasmic staining data only. ROC curve analysis identified an optimal threshold for PDCD4 staining scores, of ≤4, giving a sensitivity of 79% and specificity of 70%. For all further statistical analyses, PDCD4 cytoplasmic protein expression ≤4 was considered as negative and all other values as positive.

2.3.5.2 Expression of S100A6

S100A6 protein expression was assessable in 68/74 tumours because some cores were missing or damaged. S100A6 staining was localised to the cytoplasm of tumour cells in 42/68 (62%) cases of primary UM (Figure 2.6 D,E;F). For all cases in the TMA, the staining score in the individual cores of each case did not differ by more than 10%, indicating no significant heterogeneity in the presence or absence of S100A6 protein expression across any individual tumour. ROC curve analysis identified an optimal threshold for S100A6 staining scores of ≤1, giving a sensitivity of 79% and specificity of 55%. For all further statistical analyses, S100A6 protein expression ≤1 was considered as negative and all other values as positive.

2.3.5.3 Correlation of protein expression with clinicopathological and genetic features of metastatic risk

Univariate analysis of all cases demonstrated that the presence of S100A6 protein expression was strongly associated with clinicopathological and genetic features of increased metastatic risk, namely: increased age at primary management (p=0.010); presence of PAS+ closed connective tissue loops (p=0.088); presence of epithelioid

cells (p=0.004); a high mitotic count (p=0.028); and monosomy 3 (p=0.002). Importantly, an absence of PDCD4 protein expression was also associated with the following clinicopathological and genetic features of increased metastatic risk: increased age at primary management (p=0.032); a high mitotic count (p=0.054); and monosomy 3 (p=0.014) (Table 2.8).

Table 2.8 Association of S100A6 and PDCD4 protein expression with clinical, pathological and genetic risk factors in UM

Variable	S100A6 negative	S100A6 positive	p value	PDCD4 negative	PDCD4 positive	p value
Age (years)						
Mean	57.6	65.1	**0.010**	69.5	61.0	**0.032**
Gender						
Female	10 (31%)	22 (69%)	0.160	5 (16%)	27 (84%)	0.678
Male	20 (48%)	22 (52%)		5 (12%)	36 (88%)	
LBD (mm)						
Mean	16.2	17.1	0.224	17.8	16.5	0.245
Height (mm)						
Mean	9.4	9.0	0.591	9.4	9.2	0.834
Epithelioid cells						
Yes	11 (26%)	31 (74%)	**0.004**	6 (15%)	35 (85%)	0.796
No	19 (59%)	13 (41%)		4 (12%)	28 (88%)	
Closed loops						
Yes	16 (33%)	32 (67%)	**0.088**	7 (15%)	40 (85%)	0.695
No	14 (54%)	12 (46%)		3 (11%)	23 (89%)	
Mitotic count						
Mean	3.7	7.1	**0.028**	10.6	5.0	**0.054**
Monosomy 3						
Yes	5 (17%)	24 (83%)	**0.002**	8 (29%)	20 (71%)	**0.014**
No	25 (57%)	19 (43%)		2 (4%)	42 (96%)	
Not available	0	1		0	1	

Statistically significant associations are highlighted in bold (p<0.05, not corrected for multiple testing).

2.3.5.4 S100A6 and PDCD4 as prognostic factors of metastatic disease

Kaplan-Meier survival analysis showed that patients whose primary UM expressed S100A6 had a significantly shorter survival time than those patients whose primary tumour was classified as negative for S100A6 staining (Log Rank, p=0.006). (Figure 2.7)

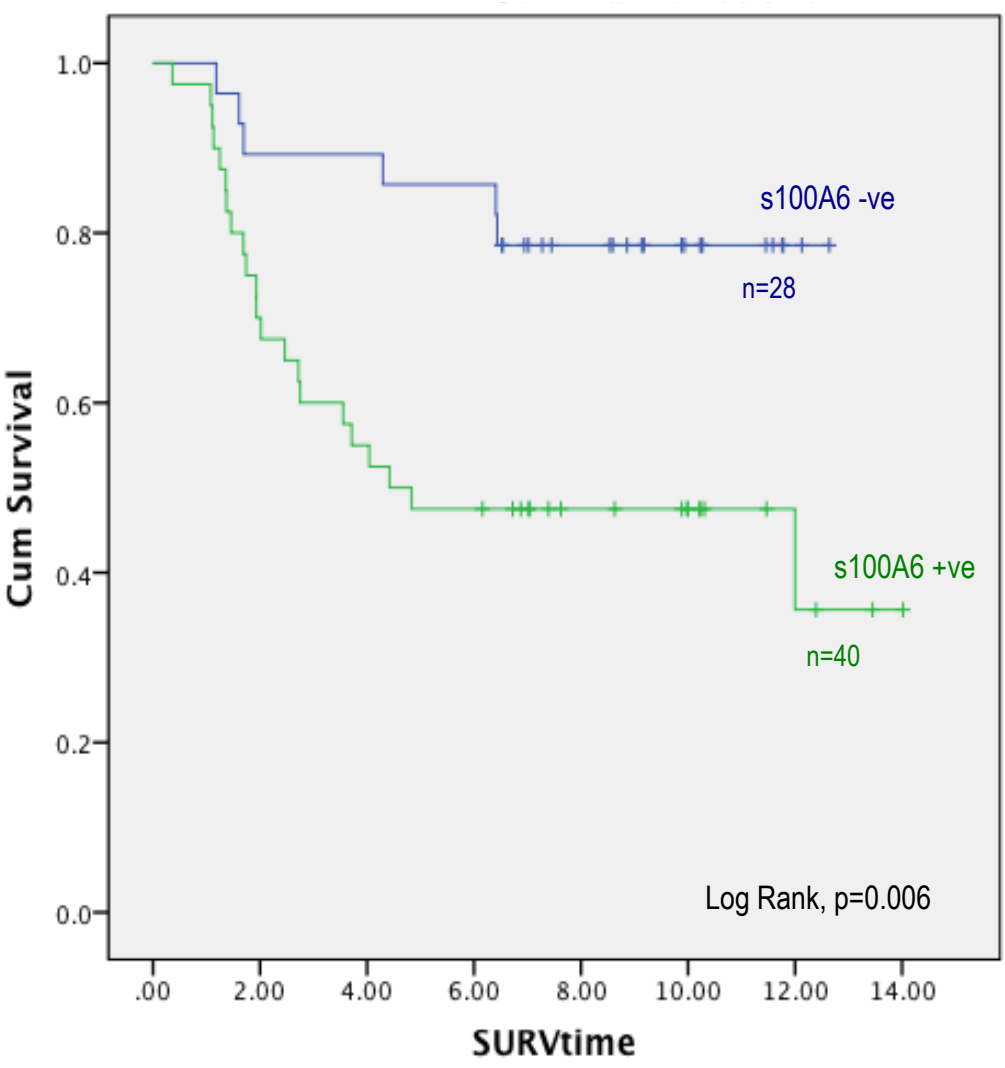

Figure 2.7 Kaplan-Meier survival analysis showing a significantly shorter survival time for UM expressing S100A6. Survival time is expressed in years from diagnosis of primary tumour

Conversely, patients whose primary UM was classified as positive for PDCD4 expression had a significantly longer survival time than those patients whose primary UM was classified as negative for PDCD4 expression (Log Rank, p=0.001). (Figure 2.8)

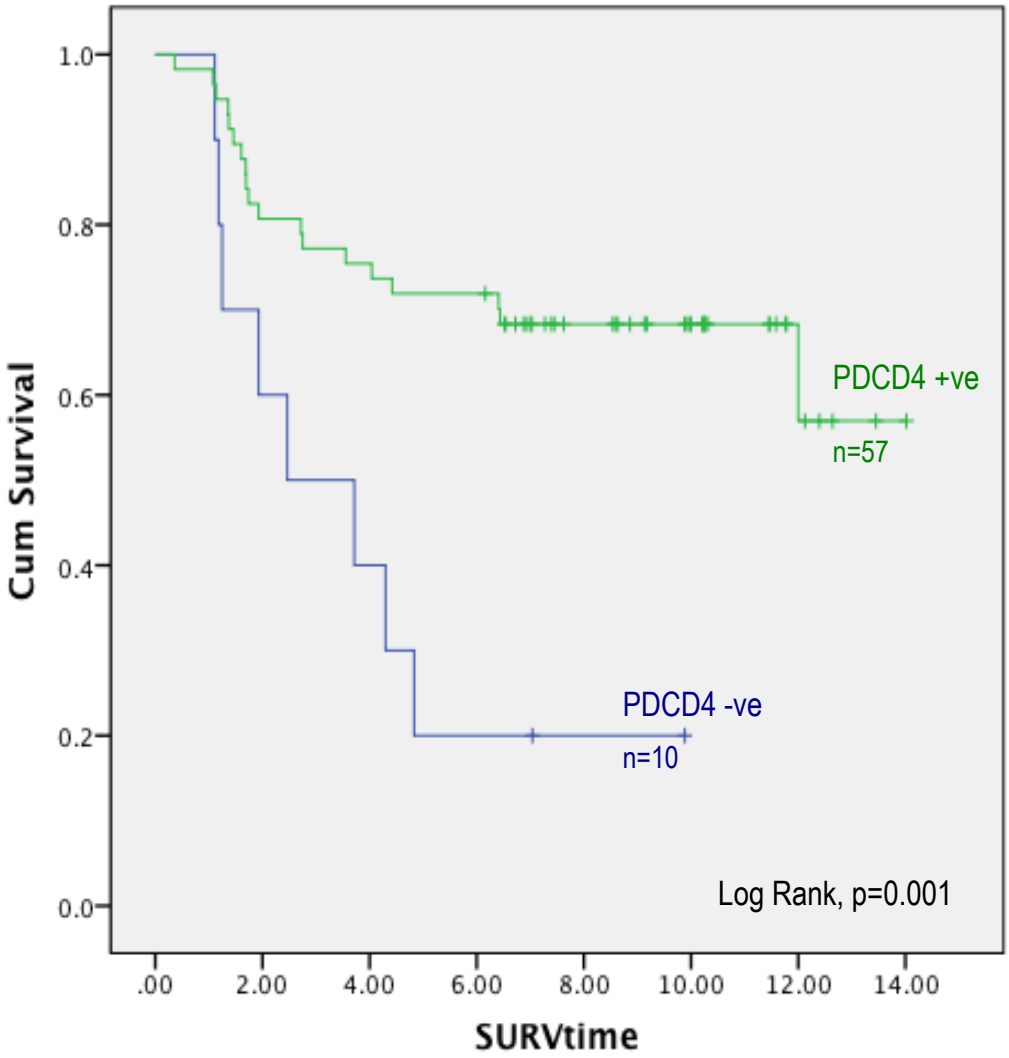

Figure 2.8 Kaplan-Meier survival analysis showing a significantly shorter survival time for UM not expressing PDCD4.

A combined analysis for expression of PDCD4 and S100A6 in the same tumours showed that those patients whose primary UM expressed PDCD4 but not S100A6 achieved the longest survival time (Figure 2.9). The Mantel-Cox test for overall

comparisons showed a significant difference (p=0.001) in survival distributions for the different combinations of PDCD4/S100A6 expression.

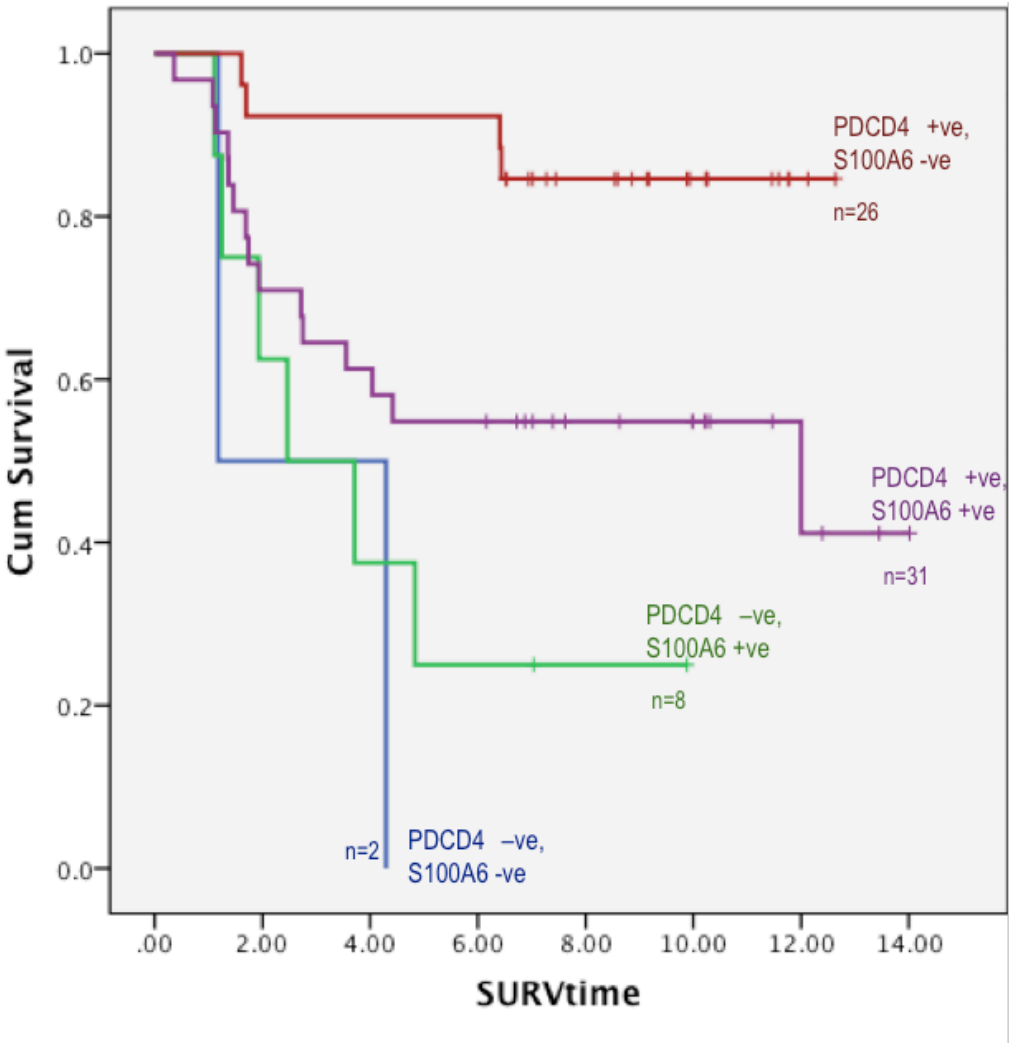

Figure 2.9 Combined Kaplan-Meier survival analysis for PDCD4 and S100A6, showing the best survival for UM expressing PDCD4 in absence of S100A6.

2.4 Discussion

By performing comparative proteomic analysis of a cohort of HR versus LR UM, we have identified a number of differentially expressed proteins, two of which have been further validated and shown to be of prognostic value.

The main limitation of this work is the lack of reproducibility between iTRAQ experiments, which did not allow us to merge the data from the different runs and perform the solid data mining analyses that had been planned. The most likely explanation for this are the technical difficulties encountered during sample preparation. Extracting proteins from small UM tissues samples has proven difficult; therefore we applied a quite "aggressive" method, based on mechanical as well as chemical denaturation. On retrospective, this may have caused nuclear disruption with DNA precipitation as well. Such contamination is likely to have affected the quality of the protein determination, hence all downstream analyses. In particular, iTRAQ labelling requires a precise peptide to label ratio, hence it is likely that some peptides loaded in the MS were not labelled properly. Moreover, the protein load in each MS run may have been different, hence the impossibility to reliably merge the runs. Another technical aspect that may have affected the quality of the experiments is that the protein lysates have been prepared and then stored for over a year without protease inhibitors before being analysed in the MS.

Despite these limitations, however, we managed to identify and validate two promising proteins, S100A6 and PDCD4. Interestingly, these two had been previously identified in UM by gene expression profiling. In the original study by Onken et al.,[80] these two factors were among the 62 genes that discriminated

between class 1 and class 2 tumours. The mRNA expression levels were concordant with our proteomic finding: PDCD4 is overexpressed in class 1 (LR) tumours, while S100A6 is overexpressed in class 2 (HR) ones. The authors, however, subsequently selected only 15 of the 62 genes to limit the size of the assay and develop it for clinical use,[157] and neither S100A6 nor PDCD4 were among these. S100A6, but not PDCD4, have been previously reported in the global proteomic analysis of UM cells.[108]

Our IHC study in an independent cohort of UM samples with long follow-up has shown the prognostic value of these proteins, which had not previously been described in UM.

2.4.1 S100A6

S100A6, also known as calcyclin, is a member of the S100 calcium-binding protein family. This is a multi-gene family clustering on chromosome 1q21, comprising at least 20 known members, each coded by a different gene.[158] It is well documented that S100 proteins have a broad range of intracellular and extracellular functions. These have been implicated in establishing the metastatic phenotypes of various cancers types, including UM.[159] It has long been known that the vast majority of UM express some members of the S100 family, which can be determined by IHC staining using a rabbit polyclonal antibody which binds all isoforms.[160] However, further studies with isoform-specific monoclonal antibodies showed marked differences between particular isoform expression.[161-163] In particular, Van Ginkel et al.[162] performed western blot analysis and immunofluorescence microscopy on a panel of cells, namely: normal choroidal melanocytes, a primary UM sample, the

OCM-1 (spindle) and OCM-3 (epithelioid) UM cell lines and the M7 cutaneous melanoma cell line. They compared the expression level of seven calcium-binding proteins, and concluded that S100A6 was more highly expressed in UM than normal melanocytes, and hence may correlate with the malignant properties of the tumour. No further studies to validate these findings have been published to date.

Given that cutaneous melanoma cells are known to secrete a soluble form of S100,[164] Cochran et al.[165] investigated the levels of S100 protein in ocular fluids, but found the quantification to be of limited use as a diagnostic tool in UM patients. Studies in cutaneous melanoma patients, on the contrary, have shown that serum levels of S100β correlate with clinical stage, prognosis and survival, making it a valuable biomarker.[97] As discussed in Chapter 1, serum levels of S100β are also of some value in UM patients.[102]

However, the question arising from our current discovery is whether the marker that should be investigated in UM patients is not rather S100A6, given that it can also be detected in the serum, as recently demonstrated in gastric cancer.[166]

2.4.2 PDCD4

Programmed cell death 4 was originally identified as an inhibitor of tumour promoter-induced neoplastic transformation in a murine model.[167] Its loss or down-regulation has subsequently been described to correlate with tumour progression and prognosis in a number of human cancers, including lung,[168] renal,[169] breast,[170] colorectal,[171] and ovarian carcinoma.[172] Loss of PDCD4 causes more aggressive tumour behaviour through increased proliferation, cell motility and invasion, resistance to apoptosis, and resistance to chemotherapeutic agents.[173] Therefore,

there has been great interest in targeting molecular pathways that cause PDCD4 depletion and in identifying small molecules that would act to stabilize PDCD4 in cancer cells.[174] PDCD4 is regulated by multiple mechanisms at the different levels, including proteosomal degradation,[175] mRNA decay and translational suppression mediated by microRNAs (in particular miR-21),[176] as well as promoter methylation-dependent suppression of transcription.[177] A main player in PDCD4 repression is mammalian target of rapamycin (mTOR), which has long been known to cause proteasomal degradation via the S6K1 pathway,[178] but which has also very recently been identified as being responsible for transcriptional repression in lung cancer cells.[179] This is very interesting for UM, where the mTOR pathway is known to be activated in most cell lines independent of AKT signalling and is becoming a novel therapeutic target.[180]

To date, there are no studies on the role of PDCD4 in UM, whereas there are some encouraging data in cutaneous melanoma. Wang et al.[181] established clones of the human melanoma cell line B16 with expression of different PDCD4 fragments, providing "direct evidence for an essential role of the PDCD4 in melanoma". Indeed, upregulation of PDCD4 expression in the cell line (by transfection of cDNA) resulted in decreased proliferation, increased apoptosis and diminished migration. Furthermore, they provided evidence that PDCD4 could inhibit mobility of these cells by down-regulating the expression of the chemokine receptor CXCR4.[181] This protein is also of interest in UM: please refer to Chapter 4.

A recent study examined the expression of PDCD4 by western blot in 23 cell lines derived from metastatic lesions of stage IV cutaneous melanoma patients and detected variable levels of the protein. PDCD4 expression was completely absent in

25% of the cell lines.[182] The authors then tested the effect of treating these cells with mTOR, PI3K and MEK 1/2 inhibitors, concluding that although PDCD4 loss is not a common event in melanoma, it can be reversed by treatment with inhibitors of AKT signalling. Therefore, PDCD4 up-regulation might be contributing to the anti-tumour effect of AKT pathway inhibitors, which are also being investigated as therapeutic tools for metastatic UM patients.[88]

PDCD4 regulation by the MAPK pathway via members of the p90 ribosomal S6 kinase (RSK) family of proteins has also been described recently in melanoma cells.[183] This study demonstrated that RSK inhibitors promote PDCD4 stability in melanoma cells, suggesting that this could be exploited in other cancers characterized by the hyperactivation of the MAPK pathway. This is of particular relevance for UM, where GNAQ/11 mutations cause constitutive activation of the MAPK pathway in the vast majority of patients.[184]

In summary, although there have been some issues with the quantification of proteins in our samples, proteomic analysis and IHC validation of UM tumour tissue from HR and LR samples has led to the identification of two novel prognostic and potentially therapeutic targets. We plan to assess these two proteins further: S100A6 as prognostic biomarker in the peripheral blood of UM patients, and PDCD4 as potential therapeutic target. In particular, we will assess the expression of PDCD4 by IHC in a TMA of metastatic UM, and by Western Blot in a variety of well-phenotyped cell lines derived from primary and metastatic UM. Our lab has recently acquired a panel of newly characterised UM cell lines that show mTOR pathway activation independent of AKT signalling and whose viability can be

inhibited with the mTOR inhibitor Everolimus:[180] these will be the ideal tool to study the relationship between PDCD4/SK61/PDCD4 in UM.

In conclusion, proteomic analysis of UM tissues has been instrumental to the identification of potentially very interesting proteins that have not yet been fully investigated in UM, opening new avenues for collaborative research. Unfortunately, the issues encountered with the iTRAQ labelling and samples degradation has precluded the possibility to merge all the data and perform a systems biology analysis of the large dataset from all the tumours. Moreover, although S100A6 will be investigated a serum biomarker, it is reasonable to speculate that a number of potentially interesting secreted proteins could not be detected in the tumour tissue. To overcome these limitations, we have then performed label-free comparative proteomic analysis of the secretome from HR versus LR UM cells in short-term cultures, as detailed in the next chapter.

Chapter 3

Quantitative proteomic analysis of the secretome from cultured primary uveal melanoma cells

3.1 Introduction

Cancer biomarkers provide diagnostic, prognostic and therapeutic information and are of increasing importance for early detection of disseminated disease.[101] Cancer proteomics is a rapidly expanding field, which has increasing potential in biomarker discovery.[185] Blood is a logical choice for biomarker application as its constituents change rapidly in response to pathological states, and its sampling is easy and comparatively less invasive. Accordingly, plasma and serum have been the major targets of proteomic studies aimed at identifying potential cancer biomarkers.[186] However, these studies have faced major technical limitations, due to the fact that blood is a very complex fluid, comprising an enormous diversity of proteins with a high dynamic range of concentrations. Essentially, a few high-abundance proteins, such as albumin and immunoglobulins, make the detection of low-abundance proteins extremely difficult, mainly because the disease-specific biomarkers are at low concentrations. A number of depletion techniques have been developed to remove the more abundant proteins for proteomic analysis; however it is a labour-intensive process that may also indiscriminately remove the desired proteins by nonspecific binding.[187] As a result, additional methods for cancer biomarker discovery are being explored, such as analysing other accessible biological fluids, and, in particular, the secretome.

The term “secretome” was originally introduced in a genome-wide study of secreted proteins in bacteria.[188] It is now commonly used to describe the total proteins that are released by cells, tissues or organisms through different secretion mechanisms, including classical secretion, non-classical secretion and secretion via

microvesicles.[189] It can also be broadly used to indicate the conditioned medium of cells in culture, which contains proteins that are secreted, shed from the cell surface and intracellular proteins released due to apoptosis, lysis or necrosis.[190] Because the limited complexity of such samples enhances identification of less abundant, disease-specific proteins, secretome profiling of cancer cell lines is seen as promising strategy for cancer biomarker discovery.[191]

A pioneer study by Pardo et al. successfully characterised the secretome of a panel of UM cell lines (SP6.5, UW-1, 92.1, OCM-1) and one short-term primary UM culture (UM-A) by 2DE and MS, and further validated the presence of two candidate biomarkers (gp100 and cathepsin D) in UM patients' sera.[110] Interestingly, the authors pointed out that the variety and diversity of the proteins identified in the short-term primary UM culture (UM-A) was much greater than in the cell lines. Since the above-mentioned publication, great progress has been made in MS-based analysis of clinical tissues and biofluids, with the identification and quantification of thousands of proteins now becoming increasingly routine.[192]

Secretome analysis, however, does face analytical challenges that interfere with the search for true secreted tumour biomarkers. In particular, it is important to optimise experimental conditions, in order to minimise the contamination of serum proteins in the conditioned medium.[193] However, at the same time, it is also as important to monitor cell viability during secretome production if using 'serum starvation'.[194]

Based on the points above, the present study examined the secretome (conditioned media) of a panel of heterogeneous primary UM cells in short-term culture, using a nanoLC-MS/MS-based label-free quantitative proteomics approach,

which had previously been used for colorectal cancer samples.[185] The aims of this study were to increase our understanding of the metastatic process in UM and possibly to identify a secreted biomarker of metastatic disease for these patients. To achieve this, a comparative analysis of secretome samples from UM patients at HR versus LR of developing metastatic disease, as well as normal choroidal melanocytes from post-mortem human eyes was performed.

3.2 Methods

3.2.1 Establishment of primary UM cell cultures

3.2.1.1 Choice of culture medium

UM cells are notably hard to culture, and even when they do adhere to the bottom of the flask, they grow slowly, with a doubling time of several days. Since it was our intention to preserve the unique features and the heterogeneity of cells in short-term for secretome production, a culture medium was selected that favoured enhanced plating efficiency and proliferation. Three media were compared (all cell culture media, unless otherwise indicated, were supplied by Gibco, Life Technologies, Paisley, UK):

i) "Standard" or Roswell Park Memorial Institute (RPMI) 1640-based: RPMI with 10% foetal bovine serum (FBS), antibiotics (penicillin 50 IU/ml, streptomycin 500 µg/ml), and 200 mM L-Glutamine. This is the medium most commonly used to culture uveal melanoma cell lines.

ii) "Basal" or DMEM-based: 1:1 Dulbecco's modified Eagle's medium (DMEM) high glucose and Ham's F12, 1 x B27 supplement, 20 ng/ml epidermal growth factor (EGF), 1% FBS, plus antibiotics and L-Glutamine as above.

iii) "Primary" or αMEM-based: 1:1 Minimum Essential Medium, alpha modification (αMEM) and Quantum 3-21, (PAA Laboratories Ltd, UK), 10% FBS, plus antibiotics and L-Glutamine as above. This is a very rich medium, as the Quantum 3-21 was developed as a substitute for amniotic liquid to culture amniotic villi for antenatal screening.

Cells from two primary tumours (one M3, one D3) and two cell lines (Mel270 and OMM 2.5) were seeded at a density of 5000 cells/well in a 96-well plate, in each of the three different media. Cell number was assessed at day 0, 2, 5 and 7 using the sulforhodamine-B (SRB; Sigma) method with 0.4% SRB dye.[195] This colourimetric assay relies on the ability of the SRB dye to bind in a stoichiometric manner to basic amino-acid residues of cells that have been fixed by trichloroacetic acid (TCA). The dye dissociates under basic conditions, and the intensity of the colour, which is proportional to the cell mass, can be assessed with a plate reader. As there is a linear relationship between the absorbance reading and the cell number, this technique allows assessing and comparing the number of cells in the different plates.

At various time points the medium was removed from the 96 well plate and the cells were fixed with 100µl 10% TCA (Sigma) for 1 hour at 4°C. The plates were then washed with distilled water and allowed to air dry. 100µl 0.4% SRB in 1% acetic acid was then added to each well of the plate and incubated for 1 hour at RT. Unbound SRB was removed by rinsing the plate in 1% acetic acid prior to solubilising the bound dye with 10mM Tris base solution. Absorbance readings were made at 570nm on a microplate reader (ELx 800, BioTek) and the background absorbance measured at 650nm subtracted from these values. All data were analysed in Excel.

To corroborate the findings and for their use in the experiments described within this chapter, this same experiment was repeated with three UM primary samples.

3.2.1.2 Samples

Following approvals from the local and national ethics committees (NRES Ref No. 11/NW/0568), fresh UM specimens were acquired via the LOOB from patients undergoing enucleation or transcleral local resection as their primary treatment for UM. Clinical, histopathological and genetic information for each sample were available for each specimen, so that the risk category for developing metastatic disease could be determined, as explained in Chapter 1.

3.2.1.3 Isolation and culture of primary UM cells

A small sample of fresh UM tissue (approximately 3 mm^3, depending on the size of the tumour) was collected within an hour of surgical removal, and placed in RPMI containing antibiotics. All subsequent procedures were performed under sterile conditions in a Class II Biological Safety Cabinet. A single cell suspension was obtained by finely mincing the sample with a sterile scalpel blade, and then subsequently digesting the clumps with 5 ml of type I collagenase (Sigma) at 37°C for approximately 1 hour, with occasional agitation of the solution. The presence of single cells was assessed by examining a 10 µl aliquot on the haemocytometer. When digestion was considered complete, FBS was added to a concentration of 10%. The single cells in the solution were then recovered by gentle centrifugation (1800 rpm for 2 minutes) and re-suspended in primary medium. The cells were counted under the haemocytometer and seeded into two T75 vented tissue culture flasks (Falcon, VWR international, Leicestershire, UK) at a density of $1.5x10^6$ cells in 10 ml of medium. The flasks were kept at 37°C in a humidified 95% air, 5% CO^2 incubator and grown to approximately 75-80% confluence.

3.2.2 Characterisation of cells in culture

Particular attention was paid to document the characteristics of each primary UM cell culture, and to determine its similarity with the original tumour, so that results from downstream analyses could be related to its clinical features. Data were recorded in a template designed ad hoc to summarise all the available information from the original tumour, as well as tracking the processing of the cultured cells. Observations of the characteristics of each culture used for production of secretome were also recorded in a systematic manner using a template.

3.2.2.1 Cellular morphology

The morphology of the cells in culture was observed using an inverted microscope and documented by digital images. Primary UM cells can grow as a monolayer of spindle cells creating a neural-like network or as a carpet of more epithelioid-like cells. Occasionally, clumps or small spheres of cells formed, which were then spontaneously shed into the culture medium. These different phenotypes are not mutually exclusive as they reflected the variety of UM cells in the primary tissue. The degree of pigmentation was also variable and can be best appreciated in bright field microscopy. The presence of other cells, classified as fibroblasts or mesenchymal -like cells was also recorded. Both overgrowth by fibroblasts or suspicion of infection were strict exclusion criteria for collection of the secretome.

3.2.2.2 Immunofluorescence

From each primary UM, cells were also seeded at 50,000 cells/well in two 8-well glass chamber slides (Fisher Scientific, UK) and grown to 70-80% confluence before being fixed with 3.7% formaldehyde in phosphate buffered saline (PBS) for 10 mins.

This was performed in order to determine the proportion and characteristics of UM cells in the culture, using a panel of antibodies known to characterise the melanocytic lineage, as previously shown in UM cell lines (Table 3.1).[196] In order to allow for the detection of nuclear antigens, permeabilisation was performed with 0.2% Triton X-100 for 5 mins at RT, followed rinsing in PBS. Blocking was achieved by incubating the cells with 10% normal goat serum in PBS containing 1% BSA for 1 hour at RT. Incubation with primary antibodies was performed overnight at 4°C, followed by appropriate rinsing in PBS before addition of the appropriate secondary antibody: goat anti-rabbit Alexa Fluor® 555 or goat anti-mouse Alexa Fluor® 488 (both from Molecular Probes, Life Technologies, Paisley, UK). Slides were incubated for 1 hour at RT in the dark, and subsequently rinsed in PBS. Finally, Vectashield (Vector Laboratories, Peterborough, UK) mounting medium with DAPI (4',6-diamidino-2-phenylindole) was applied to counterstain the nuclei, prevent photobleaching and drying of the slide under the coverslip.

Table 3.1 Details of the antibodies used to characterise primary UM cells in short-term cultures

Antibody	Full name	Species	Isotype	Dilution	Supplier
HMB45	Melanocyte lineage-specific antigen	Mouse	IgG_1k	1:200	Dako
Ki67	Ki67	Mouse	IgG_1k	1:200	Leica
MelanA	Melan-A / MART1	Mouse	IgG_1k	1:100	Dako
MITF	Microphthalmia Transcription Factor	Mouse	IgG_1k	1:100	Dako
S100P	S100 calcium binding protein	Rabbit	Polyclonal	1:400	Dako
VIM	Vimentin	Mouse	IgG_2a	1:200	Dako

3.2.2.3 Genetic profiling of cells in culture

Following incubation of the cells in serum-free medium (SFM) for secretome production (see below), primary UM cells were harvested and split into two cell pellets: one cell pellet was stored for further protein analyses, the other was lysed in 180µl of ATL buffer (Qiagen) and stored at -20°C for DNA extraction. When all cultures had been completed, samples were retrieved and DNA was extracted and quantified. Depending on the DNA concentration obtained, either MSA or MLPA was performed, and compared to the genetic profile of the primary UM specimen. All of the above-mentioned procedures were performed following the same protocols used for clinical samples.[197] Please refer to Chapter 5 for further details on these techniques.

3.2.3 Establishment of choroidal melanocytes in culture

3.2.3.1 Samples

Human choroidal melanocytes were isolated from post-mortem eyes with a delay of less of 8 hours, obtained with consent from the Lions New South Wales (NSW) Eye Bank, by our collaborator Dr Michele Madigan in Sydney, Australia. The study was performed according to the Declaration of Helsinki and with approval from the University of Sydney Human Research Ethics Committee.

3.2.3.2 Isolation and culture of human choroidal melanocytes

All chemicals, unless otherwise indicated, where supplied by Sigma Chemical Co., St. Louis, MO (USA). Melanocytes were isolated and grown as previously described[198] with minor modifications. Briefly, the anterior segment and the

vitreous were removed. The retina was gently separated from the *ora serrata*, and then cut at the optic nerve head and removed from the eyecup, leaving the retinal pigment epithelium (RPE) and underlying choroid and sclera. The eyecup was filled with warm 0.25% trypsin / 0.1% EDTA (ethylene-diamine-tetra-acetic acid) in PBS, and incubated at 37°C for 45 minutes, then the RPE removed by gentle pipetting. The eyecup was rinsed with warm PBS several times and the choroid finally removed from the underlying sclera, being careful to avoid the optic nerve head tissue. The choroid was then dissected into pieces approximately 5mm x 5mm, further rinsed in PBS, then incubated overnight (approximately 18 hours) in 0.25% trypsin / 0.1% EDTA at 4°C with gentle shaking.

Following this, the choroid pieces were incubated for 60 minutes at 37°C, and then 10 ml warm Ham's F12 / 10% FBS medium was added. Cells were collected by centrifugation (290 x g for 5 minutes at 20°C) and plated into a 6 well plate. The choroid pieces were then further incubated in two changes of 1.2 U/ml dispase II and 0.5mg/ml collagenase at 37°C for 1 hour, after which cells were collected by centrifugation (290 x g for 5 mins at 20°C) and plated into subsequent wells of the 6 well plate.

Isolated cells were maintained at 37°C and 5% CO_2 and initially washed with warm PBS at 3 to 4 days after plating to remove unattached cells. Cells were then grown for a further 2 weeks in melanocyte growth medium (MGM), with growth medium changes twice weekly. The MGM was composed of: Ham's F12 supplemented with 10% heat inactivated FBS, 2 mM L-glutamine, 50 IU/ml penicillin/50 µg/ml streptomycin and 10 ng/ml cholera toxin, 100 nM PMA (phorbol 12-myristate 13-acetate) and 0.1 mM isobutylmethylxanthine (IBMX).

Cells were detached using 0.25% trypsin/0.1% EDTA for 2 mins and centrifuged (163 x g for 5 mins at 20°C), resuspended in MGM and subcultured in 35mm dishes, 25 cm2 flasks or in 8-well chamber slides for immunocytochemistry (see below). Passage 1–3 melanocytes were used for all experiments. Cells were maintained in a humidified incubator at 37°C and 5% CO^2.

3.2.3.3 Characterisation by immunocytochemistry

Immunostaining was performed on primary melanocytes as follows. Sterile glass coverslips or 8-well chamber slides were seeded with 2.5 to 3 × 10^4 cells in MGM and incubated at 37°C for 3 to 5 days. Cells in chamber slides were fixed in 2% paraformaldehyde in PBS (pH 7.4) for 20 minutes at RT, then rinsed in PBS and blocked in 5% BSA for 30 mins to reduce non-specific binding.

Primary antibodies (all from Thermo Fisher Scientific Australia Pty Ltd, Scoresby Vic) used to assess the melanocyte cultures included Mel Ab-3 (HMB45+HMB50) Tyrosinase (T311), TRYP1 (TA99), MART-1 Ab-3, gp-100 and vimentin.

Cells were incubated with primary antibodies overnight at 4°C, rinsed in PBS three times, followed by incubation in the appropriate species-specific Alexa-488 conjugated secondary antibody (1:1000, Molecular Probes, USA) for 1 h at RT. Cells were then further rinsed in PBS, nuclei stained with either DAPI (1:10,000) or propidium iodide (1:10,000) for 5 mins, then rinsed, and finally chamber slide wells removed and the slide cover-slipped in glycerol and sealed with nail varnish. Cells were viewed with an Olympus DP70 fluorescence microscope (Olympus, Japan) or a Zeiss LSM510 confocal microscope. Immunofluorescence images were collected with either Olympus DP70 Manager Software or Zeiss ZEN software.

3.2.4 Secretome sample preparation and collection

Secretome analysis is usually performed by incubating cells in SFM, in order to avoid contamination and any masking of secreted proteins by serum proteins from the cell culture media.[199] Moreover, the cell monolayer requires rinsing to ensure removal of adherent serum proteins prior to incubation in SFM.[193] Please note that from this point onwards, SFM indicates phenol-red free αMEM (Gibco), without any other supplement.

Preliminary optimization experiments (Appendix 3) demonstrated that the most effective way to remove albumin and other serum proteins from UM cells in culture was to follow the protocol originally developed for glioblastoma cells.[200] Briefly, the cell monolayer was gently rinsed three times with 10 ml of PBS, incubated with 10 ml of SFM for 1 hour, and rinsed once again with fresh SFM. Cells were subsequently incubated with 8 ml of SFM for 48 hours, and the conditioned medium at the end of the incubation period was defined as the secretome.

3.2.4.1 Secretome collection

At the end of the incubation period, the secretome from both T75 flasks of the same patient was pooled into a 30 ml universal tube, and gently centrifuged at 1660 rpm x 5 mins at 4°C to pellet any floating cells. The supernatant was aliquoted in 1 ml units and stored at -80°C.

3.2.4.2 Cell viability assay

The cell monolayer was rinsed with Hanks's Balanced Salt Solution without calcium and magnesium (Gibco), covered with 3 ml of non-enzymatic cell dissociation solution (Sigma) and incubated at 37°C for 5-10 mins. When the cells had detached,

they were collected in the same universal tube used previously, so that adherent and non-adherent cells were combined and viability assessed by Trypan Blue exclusion test.[201] Trypan blue dye in PBS (10 µl of 0.4% w/v) was mixed with 10 µl of cell suspension and observed under the microscope. Cell viability was expressed as the ratio of total viable cells to the sum of total viable and dead (i.e. blue) cells.

The residual cell suspension was split into two and centrifuged at 2000g x 10 mins: one part was used for DNA extraction as explained above, the rest was stored 'dry' at -80°C.

The same protocol was adopted for secretome production from choroidal melanocytes in culture, with a difference only in the volume of medium used, as these cells were cultured in 35 mm dishes. The final volume of secretome for each sample was 1.4 ml, which was aliquoted (700 µl per vial) and stored at -80°C until further analysis.

The cell monolayer was harvested as described above, cell viability was also tested by Trypan blue, and the whole cell pellet was stored for future protein analysis (i.e., no DNA extraction was performed).

3.2.5 Secretome analysis

3.2.5.1 Protein quantification and digestion

All proteomic analyses were conducted only once the prospective collection of all secretome samples had been completed.

Protein concentration was determined for all UM secretome samples using a Bradford assay reagent (Pierce Coomassie Plus, Thermo Scientific) as previously described in Chapter 2. Samples were diluted two-and four-fold and after the

addition of reagent, samples were read at 595 nm in a plate reader (Multiskan FC, Thermo Scientific) and protein amounts interpolated from a BSA standard curve. For each sample, a volume equivalent to 15 µg/ml was added to a low bind microfuge tube containing 10 µl of StrataClean resin (Agilent Technologies Ltd, Oxfordshire, UK) (B1). Samples were vortexed for 1 min, centrifuged at 2000 rpm for 2 mins, and the supernatant aspirated and transferred to a second tube containing 10 µl of beads (B2). After vortexing for 1 min, the beads and sample were transferred to the first tube containing B1 and the sample centrifuged and the supernatant discarded. The beads were washed twice with 1 ml of 25 mM ammonium bicarbonate (hereafter termed 'ambic') (not pH adjusted). For on-bead digestion, the beads were re-suspended in 80 µl of 25 mM ambic and 5 µl of 1% (w/v) Rapigest (Waters Limited, Hertfordshire, UK) in 100 mM ambic. The samples were heated at 80°C for 10 mins. Samples were reduced by the addition of 5 µl of dithiothreitol (DTT, 9.2 mg/ml in 25 mM ambic) and heated at 60°C for 10 mins. Following cooling, 5 µl of iodoacetamide (33 mg/ml in 25 mM ambic) was added and the samples incubated at RT for 30 mins in the dark. Trypsin (Porcine trypsin sequencing grade, Sigma) (1µg) was added and the sample was incubated at 37°C overnight on a rotary mixer.

The digests were acidified by the addition of 1 µl of trifluoracetic acid (TFA) and incubated at 37°C for 45 mins. Samples were then centrifuged at 17,000 x g for 30 mins and supernatants transferred to 0.5 ml low-binding tubes. Samples were centrifuged for a further 30 mins and 10 µl transferred to total recovery vials for LC-MS analysis. The pre and post-acidification digest were analysed by SDS-PAGE to check for the absence of protein and hence complete digestion.

3.2.5.2 Liquid chromatography

All peptide separations were carried out using an Ultimate 3000 Nano LC system (Dionex, Thermo Fisher Scientific). For each analysis the sample was loaded onto a trap column (Acclaim PepMap 100, 2 cm x 75 µm inner diameter, C18, 3 µm, 100Å) at 5 ml/min with an aqueous solution containing 0.1% (v/v) TFA and 2% (v/v) acetonitrile. After 3 mins, the trap column was set on-line with an analytical column (Easy-Spray PepMap® RSLC 15 cm x 75 µm inner diameter, C18, 2 µm, 100Å) (Dionex). Peptide elution was performed by applying a mixture of solvents A and B. Solvent A was HPLC grade water with 0.1% (v/v) formic acid, and solvent B was HPLC grade acetonitrile 80% (v/v) with 0.1% (v/v) formic. Separations were performed by applying a linear gradient of 3.8% to 50% solvent B over 95 min at 300 nl/min followed by a washing step (5 mins at 99% solvent B) and an equilibration step (15 mins at 3.8% solvent B). 2 µl of each sample was injected.

3.2.5.3 Mass spectrometry analyses on a Quadrupole-Orbitrap instrument

The Q ExactiveTM (Thermo Fisher) instrument was operated in the 'data dependent mode' to automatically switch between full scan MS and MS/MS acquisition. Survey full scan MS spectra (m/z 300-2000) were acquired in the Orbitrap with 70,000 resolution (m/z 200) after accumulation of ions to $1x10^6$ target value based on predictive automatic gain control (AGC) values from the previous full scan. Dynamic exclusion was set to 20 s. The 10 most intense multiply charged ions ($z \geq 2$) were sequentially isolated and fragmented in the octopole collision cell by 'higher energy collisional dissociation' (HCD) with a fixed injection time of 100 ms and 17,500x

resolution. Typical MS conditions were as follows: spray voltage, 1.9kV, no sheath and auxillary gas flow; heated capillary temperature, 275°C; normalised HCD collision energy 30%. The MS/MS ion selection threshold was set to 1 x 104 counts. A 2Da isolation width was set.

3.2.5.4 Database search and protein identification

Raw data files were uploaded into Proteome Discoverer 1.3 and searched against the human UniProt database using the Mascot search engine (version 2.4.1). A precursor ion tolerance of 10 ppm and a fragment ion tolerance of 0.01 Da were used with carbamidomethyl cysteine set as a fixed modification and oxidation of methionine as a variable modification. The FDR against a decoy database was 1-5%.

The data set was analysed using Progenesis® 4.1 (Nonlinear Dynamics Limited, Newcastle upon Tyne, UK) label-free quantification software, where detection and quantification of all peptide ions is followed by expression analysis and identification of the proteins from which they originate. Protein abundance is calculated from the sum of all unique normalised peptide ion abundances for a specific protein on each run. Alignment and co-detection of features means the same number of identified peptides is quantified on all runs so that it is possible to compare the sum of ion abundances between groups. The top 5 MS/MS spectra were exported from the Progenesis® software as a Mascot generic file (mgf) and used for peptide identification using the above settings. The search results were adjusted to a FDR of 1% and imported into Progenesis®. When comparing different groups (i.e. normal versus tumour, or HR versus LR), a protein was defined as differentially expressed if the fold change was at least 2, with Anova set at $p \leq 0.01$.

3.2.6 Bioinformatics

3.2.6.1 Prediction of secreted proteins

To determine how many of the proteins identified in our secretome were actually secreted, we used a combination of bioinformatics tools, which are freely available online, and which have been validated for prediction of secreted proteins.[202]

In particular, we used SignalP 4.0 to estimate the presence of secretory signal peptide sequences (classical secretion pathway),[203] SecretomeP to deduce non-signal peptide-triggered protein secretion (non-classical secretion),[204] and the transmembrane Hidden Markov model (TMHMM) to predict transmembrane helices.[205]

3.2.6.2 Identification of protein signature discriminating between HR and LR

Expression analysis and hierarchical clustering of peptide MS intensity data from Progenesis® was performed in Partek® Genomics Suite® 6.6 (Partek Incorporated, Missouri, USA) following data normalisation using the open-source statistical package R (version 3.1.0). Peptides with identification confidence FDR values less than 1% were selected. MS intensity data were 'floored' to 0.001 before a Shapiro-Wilks normality test was applied to log2 transformed data. Those peptides with log normal distribution were retained and these were filtered to retain peptides with coefficient of variation <10% and interquartile range exceeding 0.5 across patients.

With the aim of identifying a protein signature that would discriminate between HR and LR, we selected only those secretome samples with a well-defined genetic

profile. Hierarchical clustering of differentially expressed log transformed peptide intensity data was performed over both peptides and patients using the Euclidean distance and average linkage in both cases. Clustered peptide intensity values were visualised by shifting the column mean to zero with standard deviation scaled to one.

3.2.7 Validation of putative biomarkers by quantitative Western Blot

MS-derived data have previously required validation by another technique, to confirm the presence of the protein of interest in the sample. Typically, this would have been performed with an antibody-based assay, such as ELISA or Western Blotting. We are of the opinion that with modern MS and associated identification software, this is no longer necessary. It is recognised, however, that label-free protein quantification performed by Progenesis® software remains a relative quantification, and therefore a low abundance protein may be difficult to be correctly quantified in the original sample. MS-based techniques for absolute quantification are available[206] and have shown promising results in secretome studies,[207] but they are expensive and time consuming. Simple Western™ is a gel-free, blot-free, automated capillary immunoassay system recently developed by ProteinSimple® (Santa Clara, CA, USA), which has been successfully used for absolute quantitation.[208]

We used the Wes system of Simple Western™, where up to 25 samples could be run simultaneously, and followed the manufacturer's instructions. In brief, undiluted secretome samples and recombinant protein were mixed with the master mix to a final concentration of 1:1 sample buffer to fluorescent molecular weight

markers, and 40 mM DTT, and subsequently heated at 95°C for 5 minutes. The samples, blocking reagent, primary antibodies, HRP-conjugated secondary antibodies, chemiluminescent substrate, and separation and stacking matrices were also dispensed to designated wells in the plate. After plate loading, the separation electrophoresis and immunodetection steps took place in the fully automated capillary system. Results were analysed using the Compass software (ProteinSimple®).

Using the Wes system we verified the concentration in the secretome samples of β-2 microglobulin (B2M), a putative secreted protein, which had been identified as overexpressed in the secretome of our HR samples by label-free proteomics. Both the antibody (rabbit monoclonal), as well as the corresponding human full-length recombinant protein, were purchased from Abcam (Cambridge, UK). Optimization experiments were conducted testing different concentrations of the primary antibody (1:25 to 1:400), using the recombinant protein at 1ng/µl as a positive control. The working concentration was ultimately set at 1:50.

3.3 Results

3.3.1 Primary culture of UM cells

3.3.1.1 Choice of culture medium

The results of the SRB proliferation assays are shown in Figure 3.1. The growth of Mel270 and Omm2.5 cell lines (top) was not influenced by culture medium. D3 primary UM cells (bottom left) did not grow in the short-term culture, irrespective of the medium used. In contrast, M3 primary UM cells (bottom right) showed the greatest increase in cell number over time in αMEM-based "primary" medium. Three further experiments using primary UM cells confirmed that the primary promoted proliferation of the cells in culture. This was evident even with light microscopy, as shown in Figure 3.2.

The primary medium was therefore used for all subsequent short-term cultures of isolated primary UM cells.

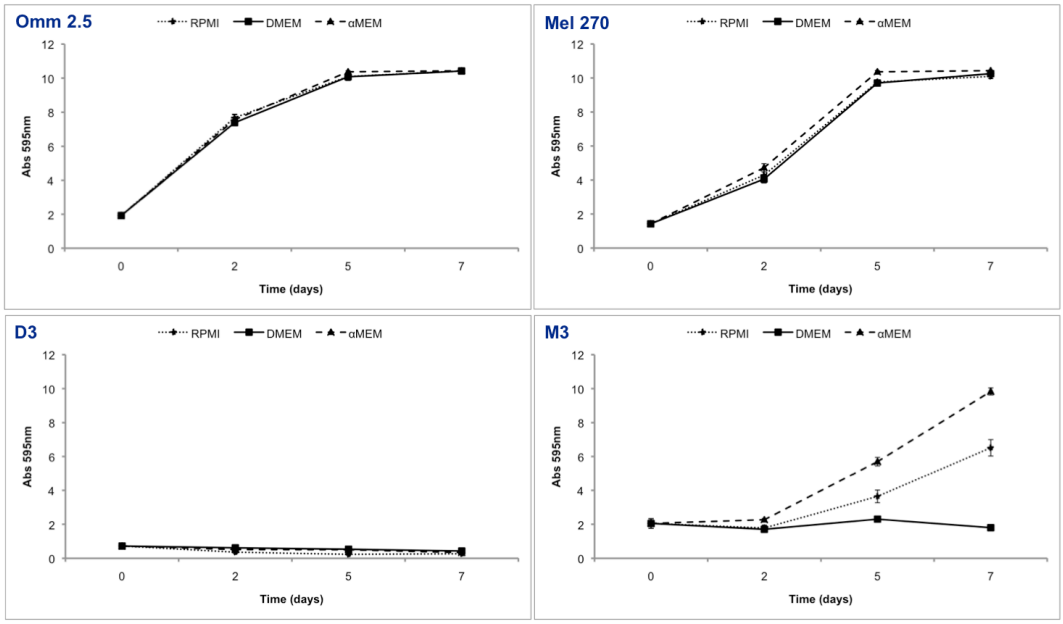

Figure 3.1 Assessment of cell proliferation in different media using sulforhodamine-B.

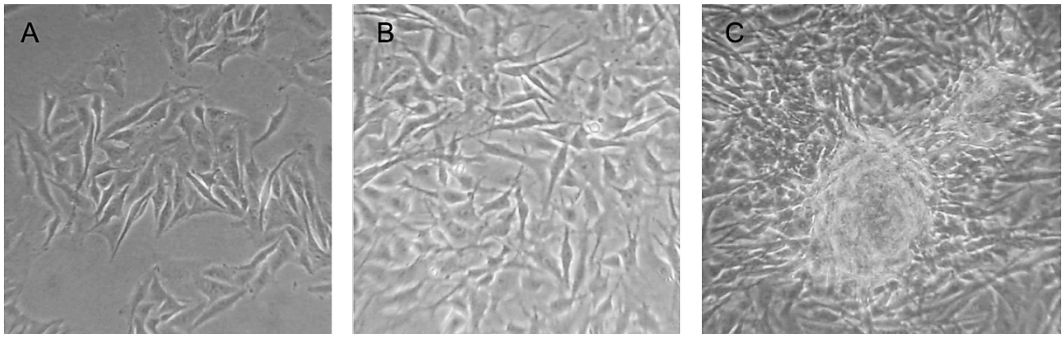

Figure 3.2 Light microscopy images of the same primary tumour (S171-10) grown for 5 days in three different media: A) RPMI-based; B) DMEM-based; C) αMEM-based. (40x magnification)

3.3.1.2 Clinical samples

Between May and December 2012, 32 UM samples were placed into culture: 21 (66%) successfully proliferated in vitro and were used for the preparation of secretome. The clinical, histopathological and genetic characteristics of the successfully cultured UM are shown in Table 3.2. Within 18 months follow-up time, 4/15 HR (27%) patients developed metastatic disease.

Of note, only 5/21 (24%) cultures were established from LR tumours. The reasons for this are discussed in detail below in the Discussion.

Three of the 21 samples were used for assay optimisation, hence a final cohort of 18 samples (14 HR, 4 LR) were included in the MS analysis.

Table 3.2 Clinical, histopathological and genetic characteristics of the UM tumours successfully grown in culture and used for secretome production.

Sample No.	Age	Sex	LBD	HT	CB	EOE	Cell type	Loops	Mitosis	Risk	Genetic
S116-12	59	F	15.7	5.2	N	N	SPIN	Y	7	HR	3L, 8G
S117-12°	43	M	11.3	3	N	N	SPIN	Y	4	HR	3L, 8G
S140-12	58	M	17.6	11	N	Y	MIX	N	5	HR	3L, 8G
S147-12	61	M	16.3	8.6	N	N	MIX	Y	5	LR	3N, 8G
S174-12	81	F	19.8	2.5	N	Y	MIX	Y	5	HR*	3L§
S175-12	64	F	17.4	6.5	N	N	SPIN	N	3	LR	3N§
S194-12	41	M	12.7	11.6	N	N	MIX	N	3	LR	3N, 8N
S195-12	77	F	14.7	5.7	N	N	EPI	N	7	HR*	3L, 8G
S197-12	71	F	13.6	8	N	N	MIX	Y	6	HR	3L, 8G
S216-12	46	M	19.9	14.4	N	N	MIX	Y	5	HR	3L, 8U
S220-12	80	F	18.2	12.5	N	Y	MIX	N	1	HR	3L, 8G
S221-12	51	M	16.2	14.8	Y	N	SPIN	Y	4	LR	3N, 8N
S223-12	67	M	18.7	12.2	Y	N	MIX	N	2	HR*	3L, 8G
S231-12°	71	M	13	7.5	N	N	MIX	Y	1	LR	3U, 8N
S235-12°	77	F	15.8	8.2	Y	N	SPIN	Y	3	HR	3L, 8G
S236-12	71	M	15.1	18.3	Y	N	MIX	Y	18	HR	3L, 8G
S248-12	50	M	17.9	11.5	N	N	SPIN	N	4	LR	3U, 8N
S265-12	76	F	15.4	7.8	N	N	SPIN	N	7	HR	3L, 8G
S281-12	71	M	13	5.9	N	Y	MIX	N	4	HR*	3L, 8G
S282-12	65	M	19.2	16.8	Y	N	MIX	Y	1	HR	3L, 8G
S285-12	77	F	15.2	8.9	N	N	MIX	N	4	HR	3L, 8G

LBD: largest basal diameter; HT: tumour thickness; CB: ciliary body involvement; EOE: extraocular extension; cell type: spindle, mixed, epithelioid; HR: high risk; LR: low risk of developing metastases; genetic (chromosomal alteration determined by MLPA, or MSA if marked with §): N-normal, L-loss, G-gain, U-undetermined.

** indicates development of metastatic disease.*

§ indicates samples used for optimisation but not included in the final MS analysis.

3.3.1.3 Characterization of UM cell cultures

Morphological examination under light microscopy showed clear differences between UM cells derived from the HR and LR tumours. UM cells from HR tumours

had a higher plating efficiency and commenced proliferation more readily than UM cells derived from LR tumours. Cells would often create neural-like networks or clumps (as shown in Figure 3.2C). The predominant cellular phenotype was plump spindle, but foci of epithelioid cells did develop in a limited number of cultures. Overall, UM cells derived from HR tumours were highly heterogeneous in culture; however, a common feature was their relatively rapid proliferation. In contrast, UM cells from LR tumours would often fail to adhere and survive, and when they did 'sit down', the cells grew slowly. The morphology was typically spindle, and was relatively similar between cell cultures. Immunofluorescence staining highlighted such differences, as shown in Figures 3.3 and Figure 3.4.

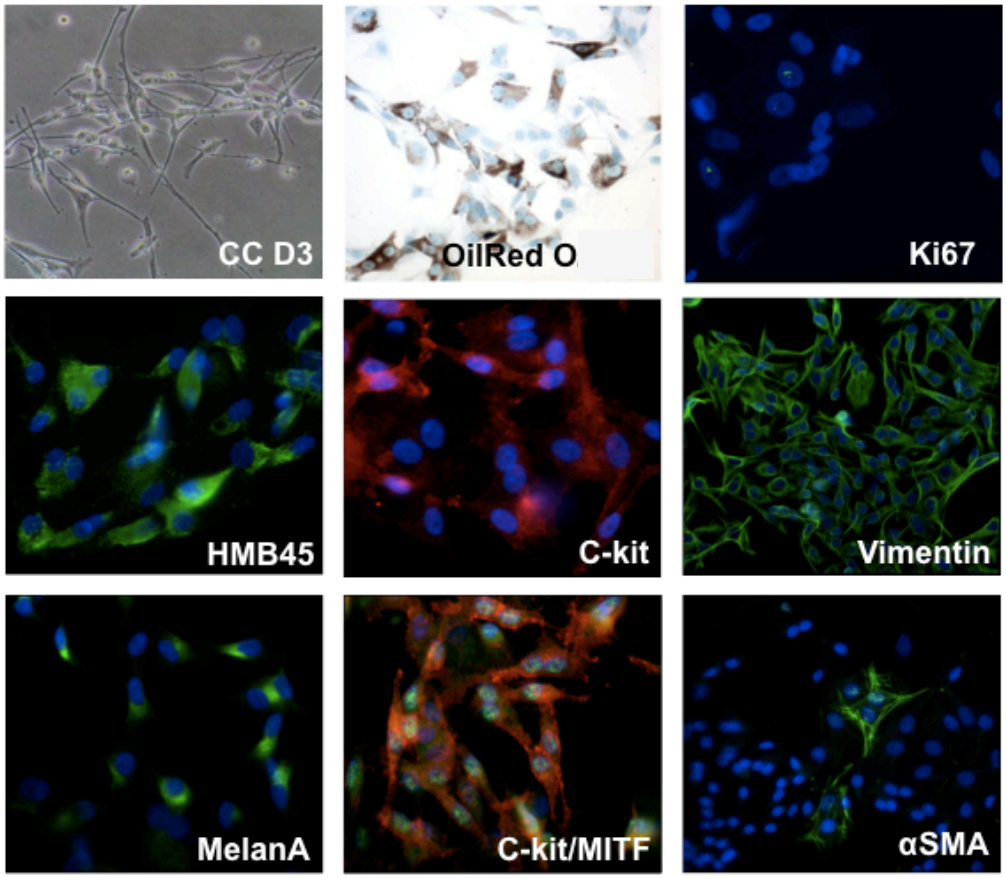

Figure 3.3 Cultured cells (CC) from a D3 UM, showing low proliferative capacity in culture (Ki67), high expression of melanoma specific antigens (HMB45, MelanA, Vimentin, MITF), small number of cells positive for the myofibroblast marker αSMA, but no positive staining for Oil Red O. Please note that the red fluorochrome is C-Kit while the green nuclear fluorochrome is MITF in the combined slide.

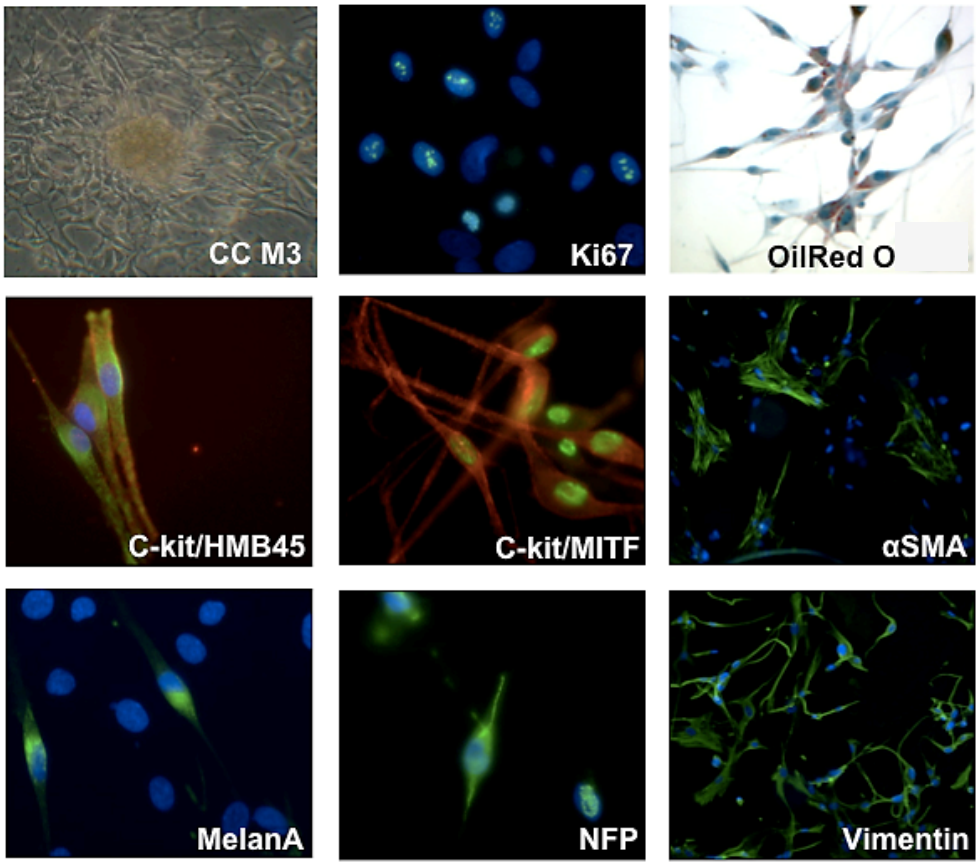

Figure 3.4 Cultured cells (CC) from a M3 UM, showing high proliferative capacity in culture (Ki67), expression of melanoma specific antigens (HMB45, MelanA, Vimentin, MITF), large number of cells positive for the myofibroblast marker αSMA and positive staining for Oil Red O. Please note that the red fluorochrome is C-Kit while the green nuclear fluorochrome is MITF in the combined slide.

3.3.1.4 Genetic profile of cultured cells as compared to original UM

DNA was successfully extracted and quantified from 16/18 cultures used for secretome analysis, as two vials were misplaced. The amount of purified DNA was >100 ng in 12/16 cases, which were analysed by MLPA, while the remaining four with <100 ng DNA were analysed by MSA. The metastatic risk classification of the patient was concordant with the data obtained from the short term cultures of the primary UM cells in all but two cases (shown in Table 3.3).

Table 3.3 Comparison between genetic profile / risk category of the original UM sample and that of the cells grown in culture (passage 0).

Culture name	Patient's Risk	Date of DNA collection	DNA analysed?	Test type	Result	Notes
S116-12	HR	22.06.2012	Yes	MLPA	HR	
S140-12	HR	22.06.2012	Yes	MLPA	HR	
S147-12	LR	20.06.2012	Yes	MLPA	LR	
S174-12	HR	08.08.2012	No	none	N/A	No DNA,§
S175-12	LR	10.08.2012	Yes	MLPA	LR	
S194-12	LR	31.08.2012	Yes	MLPA	LR	
S195-12	HR	30.08.2012	Yes	MLPA	HR	
S197-12	HR	02.09.2012	Yes	MSA	HR	
S216-12	HR	10.10.2012	Yes	MLPA	LR	M3 became D3,§
S220-12	HR	10.10.2012	Yes	MLPA	HR	
S221-12	LR	17.10.2012	No	none	N/A	No DNA
S223-12	HR	26.10.2012	Yes	MSA	HR	
S236-12	HR	02.11.2012	Yes	MLPA	HR	§
S248-12	U	08.11.2012	Yes	MLPA	LR	Unclassifiable, §
S265-12	HR	30.11.2012	Yes	MLPA	HR	
S281-12	HR	12.12.2012	Yes	MSA	HR	
S282-12	HR	12.12.2012	Yes	MSA	HR	
S285-12	HR	20.12.2012	Yes	MLPA	HR	

LR: low risk of developing metastatic disease; HR: high risk; U: undetermined; MLPA: multiplex ligation-dependent probe amplification; MSA: microsatellite analysis; M3: monosomy of chromosome 3; D3: disomy 3.
§: sample excluded from HR vs LR differential analysis

3.3.2 Culture of normal uveal melanocytes

3.3.2.1 Characterisation of choroidal melanocytes in culture

Five healthy post-mortem eyes were used for harvesting choroidal melanocytes.

The clinical details of the donors are shown in Table 3.4.

Table 3.4 Clinical features of the donor eyes used for culture of choroidal melanocytes

Sample No.	Age	Sex	Cause of death	Other history
10055	63	F	Renal cancer	Thyroid disease, hypercholesterolemia, atherosclerosis
10057	39	M	Cardiac arrest	Nil
10135	52	M	Pancreatic cancer	Non-insulin dependent diabetes
10205	55	M	Cardiac arrest	Nil
13635	17	M	Motor vehicle accident	Nil

F: female; M: male

Uveal melanocytes in culture show mainly spindle morphology, with evident pigmentation due to melanin granules in the cytoplasm. Incubation in SFM for 48 hours did not alter the morphological appearance of the cells, nor caused a significant increase of cell death, as judged by Trypan blue. (Figure 3.5).

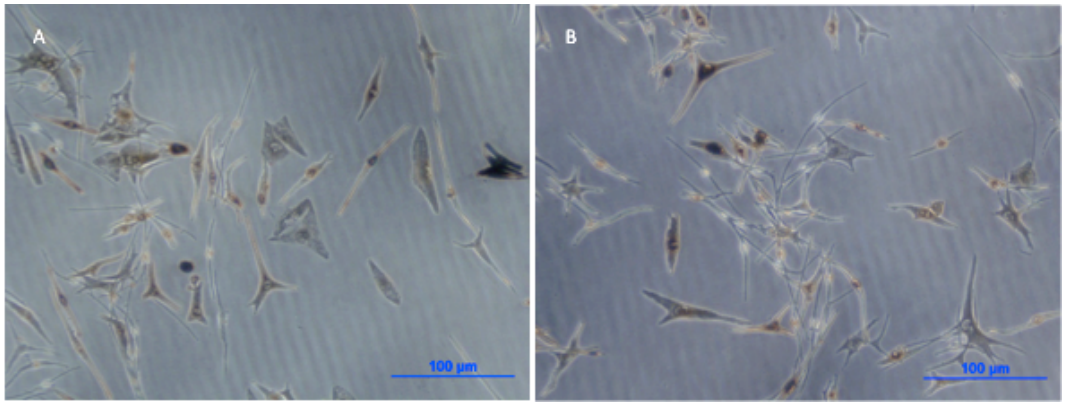

Figure 3.5 Light microscopy appearance of choroidal melanocytes in culture. A) In normal culture medium; B) after 48 hours in serum free medium. *(Courtesy Dr M. Madigan).*

As shown in Figure 3.6, the uveal melanocytes expressed the classical markers of the melanocytic lineage, i.e. MART-1 / MelanA, HMB45 and gp100. They also expressed the proteins tyrosinase and tyrosinase-related protein 1 (TYRP1), which are specific to melanin synthesis.

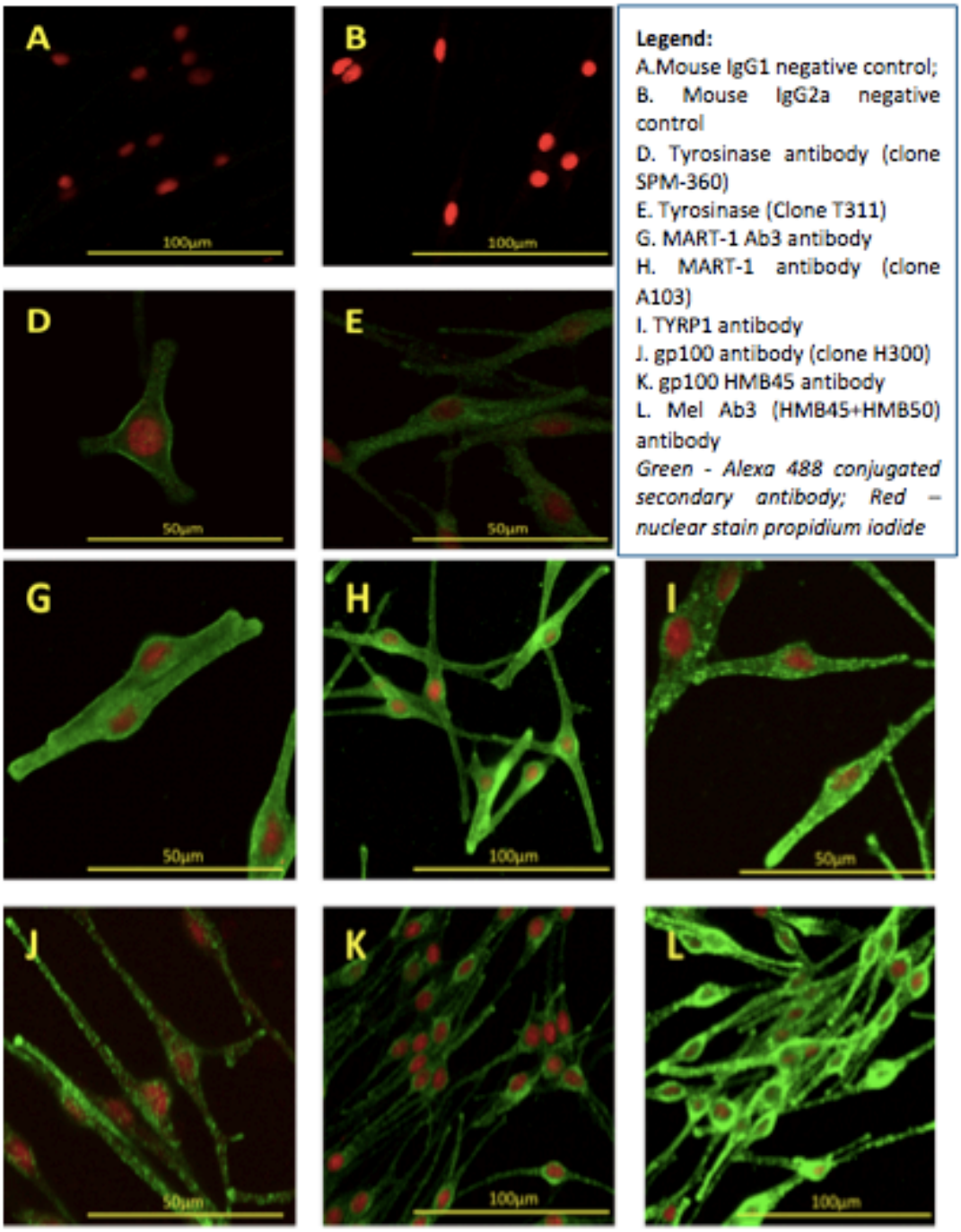

Figure 3.6 Immunophenotypical characterisation of cultured choroidal melanocytes, showing expression of the classic melanocytic proteins. (*Courtesy Drs R Zhu and M. Madigan).*

3.3.3 Secretome profiling by LC-MS/MS

Eighteen UM (4 LR and 14 HR) and 5 normal (N) samples were analysed in consecutive MS runs, interspaced by inter-sample blanks. A total of 1917 non-redundant proteins were identified using the above-described criteria and a 1% FDR. Among these, 1857 proteins were quantified in all three subgroups. There was a clear distinction in the proteome profile of N versus UM secretomes, with 947 proteins being differentially expressed with a fold change ≥2 (Figure 3.7).

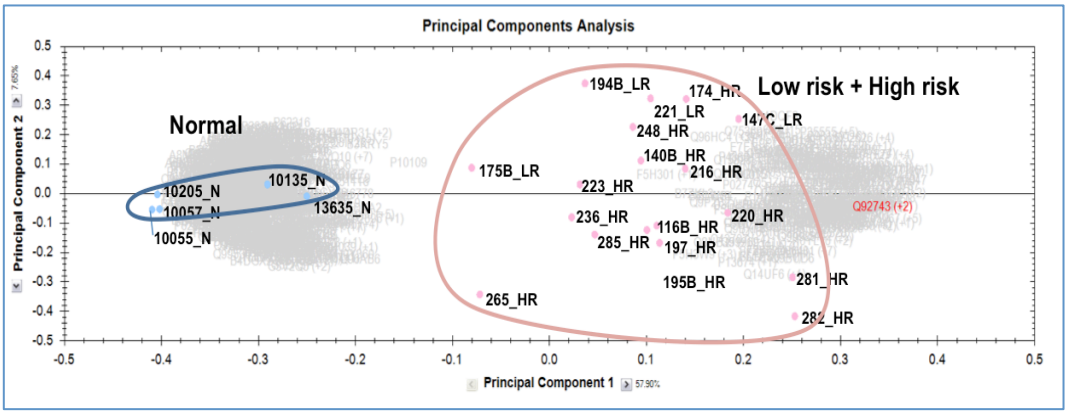

Figure 3.7 Principal component analysis (PCA) showing the segregation of 947 differentially expressed proteins between normal versus tumour secretome (Anova p≤0.01, Max-fold ≥2).

When analyzing only the UM secretomes, 67 proteins were identified as differentially expressed ≥2 fold between the HR and LR samples. (Figure 3.8)

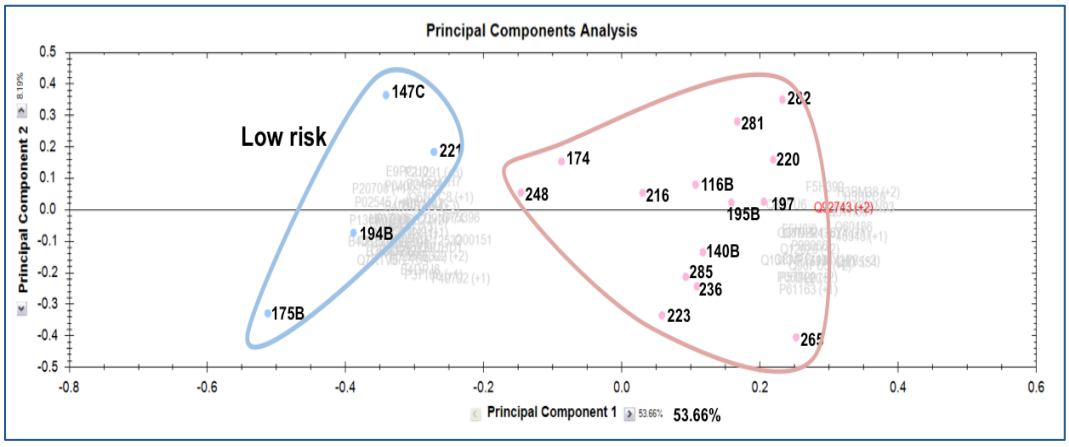

Figure 3.8 PCA showing the segregation of 67 differentially expressed proteins between LR versus HR UM secretome (Anova p≤0.01, Max-fold ≥2)

3.3.4 Prediction of secreted proteins

The secretory routes of the identified proteins were predicted based on their protein sequences. The SignalP program predicted that 341 (out of 1857, 18%) proteins were released through the classical secretion pathway (SignalP probability ≥0.8). 244 proteins (13%) were predicted to be secreted via non-classical secretion pathways (SecretomeP score ≥0.5). Among the proteins that could not be categorized into either secretion pathway, 42 (2%) were predicted to have transmembrane helixes and thus could be released via membrane shedding (TMHMM PredHel ≤1). Taken together, these results predict that 627 (34%) of the identified proteins in the SFM were likely to have been secreted.

3.3.4.1 Exosomal proteins

The list of proteins identified in the secretome of normal choroidal melanocytes and UM cells was cross-referenced with the online database of exosomal proteins (www.exocarta.org), and 554/1857 (30%) were identified as having been previously reported in exosomes. Of the 554 exosomal proteins, 108 were upregulated ≥2 fold with a p value ≤0.05 in UM versus normal melanocytes, while 190 were downregulated ≥2 fold with a p value ≤0.05 in UM versus N.

3.3.5 Protein signature discriminating between HR and LR

To identify proteins that could be investigated in the serum of UM patients as biomarkers for the early detection of metastatic disease, we selected a subset of 10 out of the 14 HR samples to compare with the four LR samples. Four samples were excluded for the following reasons: lack of post-culture DNA profiling due to

missing vial (S174-12); change of genetic profile in culture as compared to primary tumour (S216-12); unclassified chromosome 3 profile of the primary tumour (S248-12); abnormal MS peaks, making quantification unreliable (S236-12).

An analysis of the MS data from these 14 samples was performed with Progenesis®, leading to the quantification of 1577 proteins. The Shapiro-Wilk test of normality showed that 88.8% of these proteins could be considered as normally distributed once log-transformed (log2). Further to log2 transformation, normalization and ANOVA filtering at a FDR=1%, 842 proteins were used for downstream statistical analyses using the Partek® software. Figure 3.9 clearly illustrates the segregation between LR (to the left) and HR samples on principal component analysis (PCA). Interestingly, all LR samples mapped closely, whereas within the HR samples a wider distribution was observed, in line with the varied phenotypical appearances noticed in vitro and the known increased biological heterogeneity of HR UM in vivo. Noticeably, the clearly defined outlier in the HR group (S281-12, red polyhedral intersecting the X-axis) corresponds to the secretome from the only patient in this series with manifest metastatic disease.

Unsupervised two-way hierarchical clustering was performed according to Pearson similarity and Ward's linkage method, and the resulting plot can be seen in Figure 3.10. A signature of 18 proteins that discriminated between HR (top) and LR (bottom) samples was identified. It is again interesting to note the close mapping for these proteins of the LR samples as compared with the HR profile.

Details of the identified proteins are given in Appendix 4.

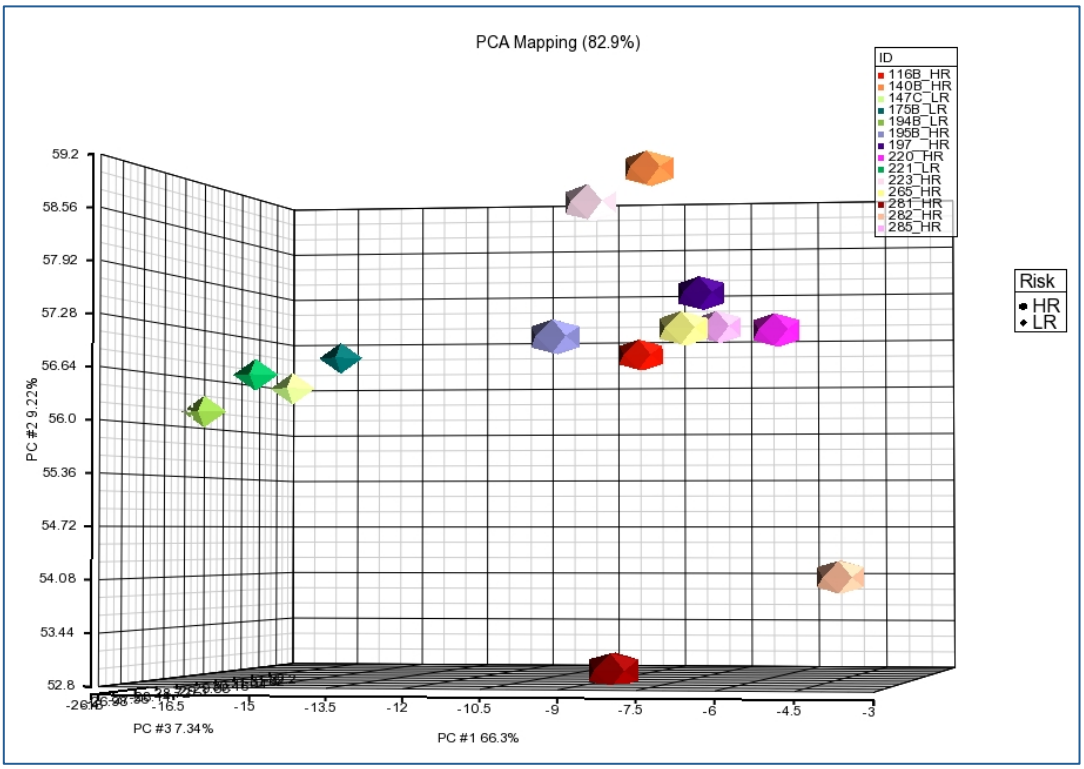

Figure 3.9 Principal component analysis (PCA) map for the first three eigenvectors, representing the percent variation accounted by each principal component. A clear segregation can be appreciated between LR and HR samples and the overall PCA mapping (82.9%) is excellent.

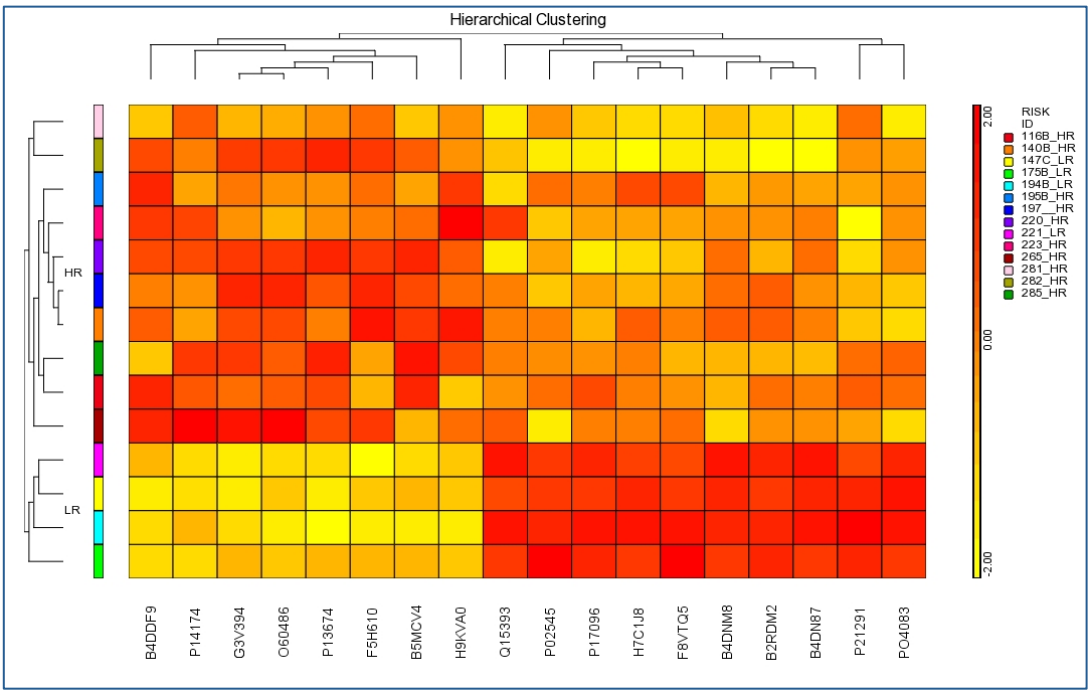

Figure 3.10 Hierarchical clustering shows an 18 protein signature that discriminated between HR and LR secretome samples. Samples are shown in the rows (colour-coded as per the legend), and proteins (UniProt accession numbers) are shown in the columns.

3.3.6 Validation by quantitative Western Blotting

B2M is a secreted protein that has been previously quantified in the peripheral blood of cancer patients, including those from patients with UM.[209] B2M was identified as a key protein in the 18 protein signature that discriminated between the HR and LR samples. The presence of B2M was validated in matched undiluted secretome aliquots from the same samples using the Wes system of Simple Western™. By spiking with known concentrations of recombinant B2M protein relative quantitative results (in the order of fentomoles) were obtained (Figure 3.11).

As demonstrated in Figure 3.12, B2M was detected in all secretome samples; secretomes from LR UM had consistently low levels of B2M, whereas the secretomes from HR UM were more variable in their expression of this protein. Although there was no exact correspondence between the MS and Wes data, overall B2M was most highly expressed in secretomes from HR UM.

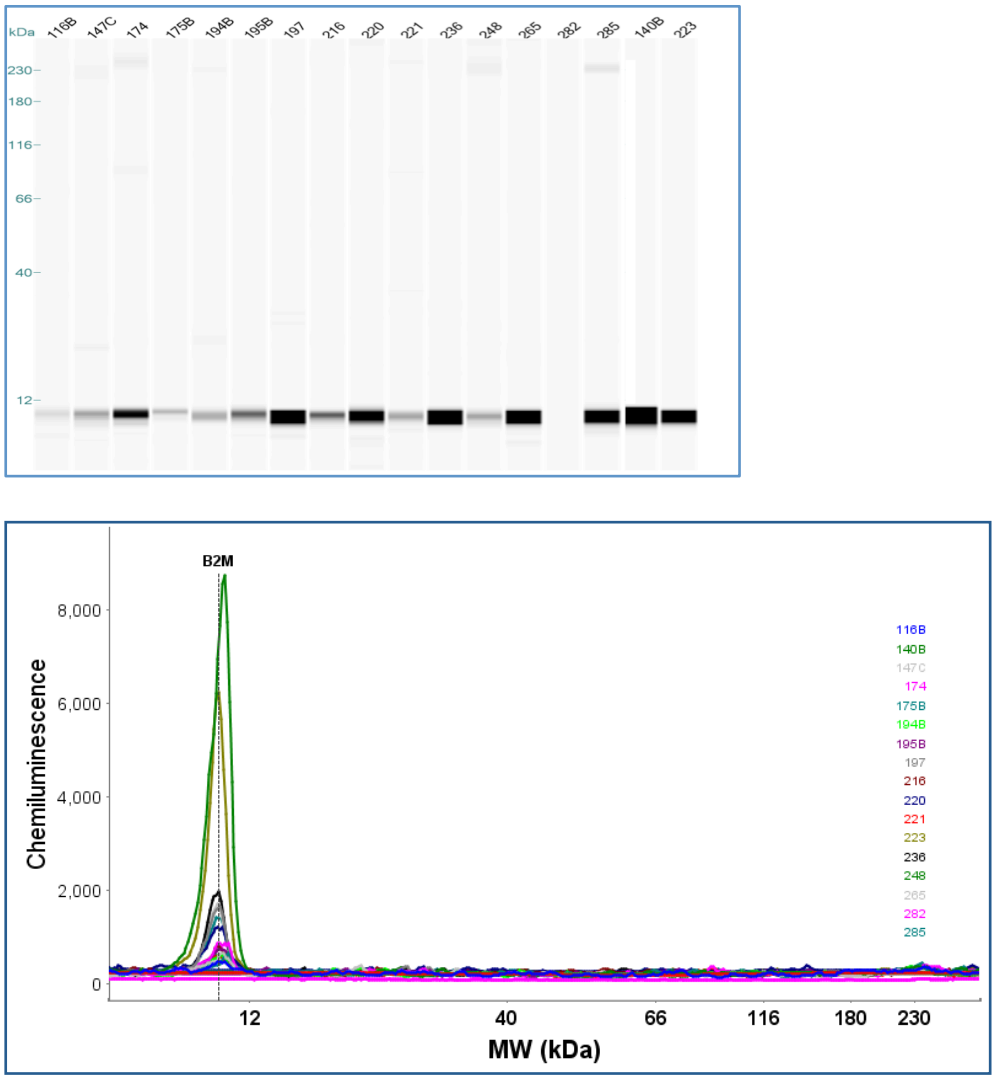

Figure 3.11 Lane view (top) and peak view (bottom) of beta2 microglobulin protein expression determined by Wes.

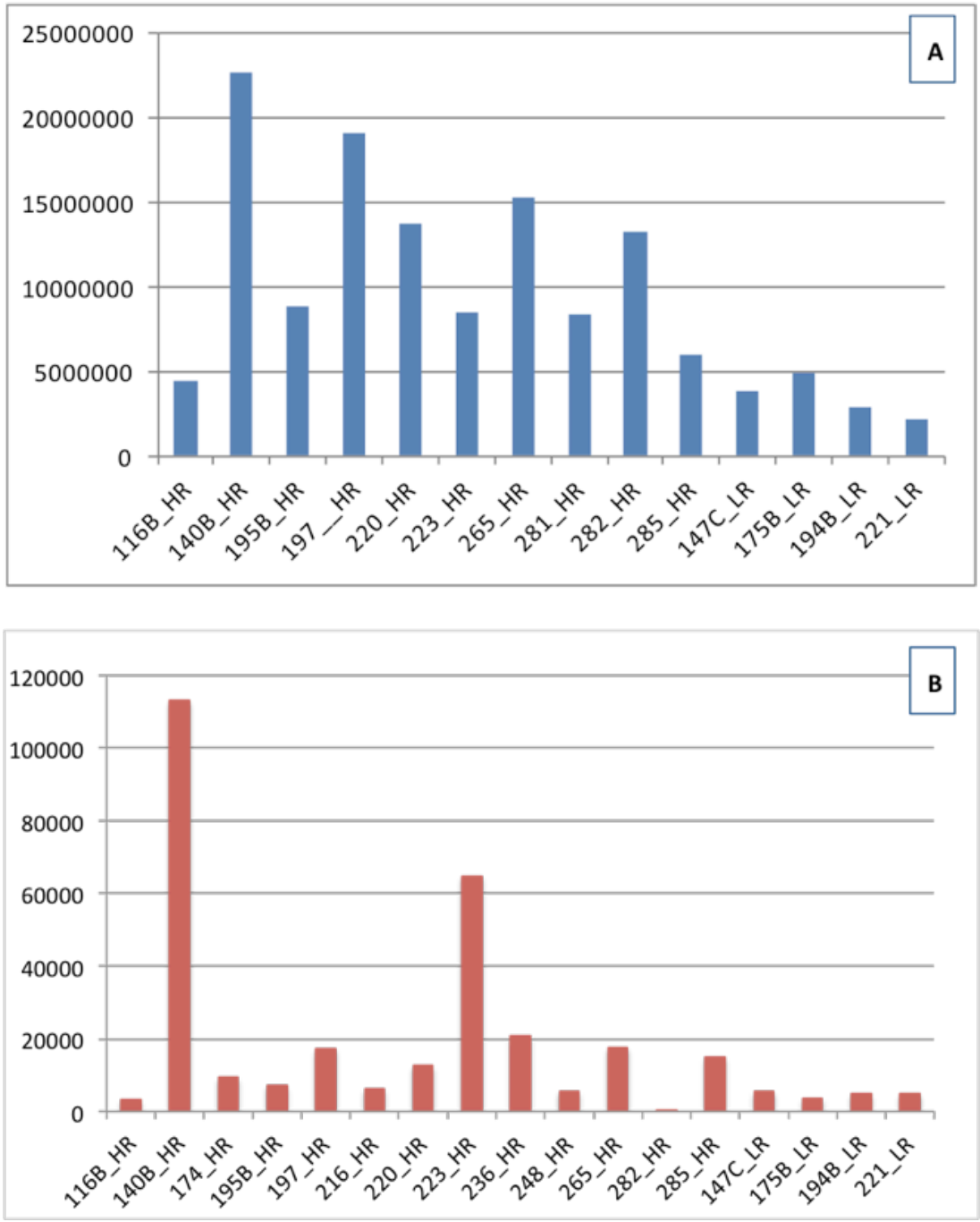

Figure 3.12 Relative quantification of Beta-2 microglobulin protein expression determined by mass spectrometry (A) and Wes (in fmol/µl) (B).

3.4 Discussion

The study of the cell secretome has been proposed as a feasible strategy, in a number of cancers, to identify putative biomarkers that are more likely to be detected in body fluids.[210] To date, a single secretome study published for UM cells[110] concluded that primary cell cultures would be more informative than UM cell lines for biologically relevant studies.

In the current study we analysed the secretome from a panel of primary UM cells and choroidal melanocytes in short-term culture, with the aim of recapitulating the multiform biological landscape of UM. To ensure that variability would be truly biological and not technical, we adopted an accurate, sensitive and robust approach, keeping sample handling to a minimum. In particular, we avoided all filtration and concentration steps, and introduced an innovative method for protein extraction and digestion using magnetic beads. We prospectively collected all samples and then processed them in a single MS experiment, normalising peak intensities for semi quantitative analysis.[192] Finally, we used a recently developed automated capillary immunoassay system to validate and quantify one of the proteins identified by MS. As a result of these steps, we could demonstrate differential protein expression between the secretomes of normal melanocytes and choroidal UM cells, as well as between those of HR and LR UM. Moreover, hierarchical clustering analyses revealed that a panel of 18 proteins could discriminate HR UM from LR UM. Of the 18 proteins identified, some have been previously identified in plasma. Moreover, several of the identified proteins are

related to immune-surveillance, which is extremely interesting given that immunotherapy is a promising therapeutic option for UM patients.[211]

Two proteins in particular have been previously implicated in UM: B2M and macrophage migration inhibitory factor (MIF). B2M is a light chain of the major histocompatibility complex (MHC) class I molecule that is associated with antigen presentation to cytotoxic T lymphocytes.[212] Cancer cells are believed to avoid immune surveillance by down-regulating the expression of MHC class I via the secretion of free B2M.[213] At the same time, there is convincing evidence that B2M may act as a growth-promoting factor and signal molecule, as increased levels positively correlate with advanced-stage tumours.[214]

In UM, expression of B2M, as determined by IHC on tumour sections, has been associated with development of metastasis.[215] Moreover, increased plasma levels of B2M have been correlated with high metastatic risk M3 UM in a study by Triozzi et al.[209] In this study, ELISA was used to assess the concentration of B2M in the plasma of 76 UM patients with known chromosome 3 status (determined by FISH). Using a recursive partitioning algorithm, a cut-off point of 3000 pg/ml (normal blood range for B2M is 1100-2600 pg/ml) was established. Based on this threshold, 33% of M3 versus 5% of D3 patients ($p=0.002$) where considered to have elevated B2M levels. An independent association of elevated plasma B2M levels and M3 status of the tumour was confirmed in multivariate analysis. The authors concluded that plasma levels of B2M may become a prognostic biomarker of HR UM patients. The fact that we also identified B2M as potential biomarker based on our secretome studies is a proof of the validity of our experimental design. Moreover, the variable levels of B2M protein expression in the individual secretome samples

(Figure 3.12) shows that our approach is able to preserve the known biological variability occurring in vivo.

MIF is a pleiotropic cytokine that, among other functions, inhibits natural killer (NK) cell-mediated cytolysis, and is well known to contribute to the immune privilege of the eye.[216] The presence of MIF in intraocular fluids protects tumours against NK cell-mediated surveillance and promotes their growth.[217] The liver is an organ with exceptionally high levels of NK activity. The importance of NK cells in controlling UM systemic metastases has been shown in a mouse model of intraocular melanoma, where multiple systemic metastases developed following in vivo depletion of NK cells with anti-asialo-GM1 Ab.[218] Repp et al. have shown that UM cells can produce MIF, with cell lines derived from UM metastasis producing approximately twice as much biologically active MIF as cultures derived from a primary UM.[219] Very recently, Costa-Silva et al. have demonstrated in murine models of pancreatic carcinoma that MIF is highly expressed in tumour-derived exosomes and that it is responsible for pre-metastatic niche formation in the liver.[220] Moreover, high exosomal MIF levels were present in the plasma of patients who later on developed metastatic disease, indicating the potential prognostic value of MIF as a biomarker. This corroborates our interest for MIF in UM as both a biomarker and a potential therapeutic target, and we will investigate its expression in UM-derived exosomes.

3.4.1 Strengths of our work

Cell lines have been widely used for secretome studies because they are easily accessible, grow well in culture, and can be used for multiple experiments with

minimal inter-sample variability. This homogeneity, however, is also a major limitation from the translational point of view, as it does not reflect the biological variability seen in patients. Moreover, there is increasing scepticism regarding the use of long-standing cell lines, as their genetic and phenotypic characteristics may significantly differ from the original tumour, and many cell lines have been misclassified over time.[221] More specifically for UM cell lines, many previously believed to be distinct were actually derived from the same patients (OCM1 = MUM2C, OCM3 = OCM8, and M619 = C918 = MUM2B) and for some, BRAF mutations were identified, bringing into question their uveal origin.[222]

In this study we used short-term primary UM cultures that, although difficult to obtain, more closely represent the tumours seen in vivo. From 32 UM tumour samples grown in culture, only four were obtained from LR UM samples. This can be attributed to two main reasons: 1) sample selection, as only very large tumours would provide enough spare tissue to be used for culture, and large tumour size is an established risk factor for development of metastatic disease;[223] 2) the low survival rate of D3 cells in vitro. These cells seem more “fragile” and often do not survive the first 24 hours in culture. Moreover, they grow so slowly that the culture flask can be overgrown by fibroblast/mesenchymal-like cells.

One of the potential drawbacks regarding the use of primary cultures is the necessity to phenotype the cells grown in culture. We performed rigorous phenotypic characterisation of our cells by immunofluorescence, as well as genetic analysis to compare the genetic profile to that of the original tumour. MLPA analysis demonstrated a discordant chromosome 3 result between the tumour and the cultured cells in only 1/ 21 (4%) cases analysed. This may have been due to the

outgrowth of non-tumour cells. The corresponding secretome sample was discarded from the analysis leading to the 18-protein signature.

As expected, the primary UM cultures demonstrated inter-sample phenotypic heterogeneity, especially among the HR tumours, which was also reflected in the protein composition of the secretome samples.

Another unique aspect of this work is the production of secretome from primary human normal uveal melanocytes, which to the best of our knowledge has never been done before. Human choroidal melanocytes are difficult to obtain, as there is a tight time limit (8 hours post mortem) within which their viability can be ensured. In collaboration with Dr Michele Madigan from Sidney, the protocol for secretome production, established in our laboratory was reproduced for normal choroidal melanocytes and the samples were then shipped to Liverpool on dry ice. Proteomic analysis was performed together with the UM secretome samples. Detailed analyses of the protein profile of normal melanocytes versus that of UM cells were outside the remit of the current study, but will be performed as part of further studies aimed to increase our understanding of the biological process of UM development within the eye.

Another strength of this study is the quality of the proteomic analysis. The protein content of the SFM was preserved by keeping handling to a minimum and by avoiding enrichment steps such as ultrafiltration. The extraction of proteins from such a diluted sample was possible due to the innovative use of StrataClean beads, followed by on-bead digestion.

A label-free MS approach was also preferred since it provides a wide range of benefits when compared to other proteomic techniques, such as iTRAQ, including:

reduced protein loading; no labelling reagent costs; reduced fractionation and sample handling; increased sequence coverage per protein; increased overall proteome coverage; ability to compare more conditions within a single experiment.[126] The equipment used (Q ExactiveTM) is a "state of the art" LC-MS/MS system which combines quadruple precursor ion selection with high-resolution, accurate-mass Orbitrap detection to deliver exceptional performance and versatility. Peptide identification and quantification was performed using Progenesis®, a software that uses the ion intensities recorded in the MS data to provide reliable measurements of peptides and is therefore more accurate than spectral count.

3.4.2 Limitations of our work and future perspectives

Although short-term primary UM cell cultures preserve the genetic and immunophenotypical characteristics of the original tumour, we know that a 2D environment is still far from ideal. There has been a recent move from 2D cell monolayers to three-dimensional (3D) cultures, motivated by the need to work with cellular models that mimic the functions of living tissues. Other members of our team are currently working on these aspects, by culturing cells on matrices, or as 3D spheroids, and in co-cultures with other cell types such as macrophages. Once such model systems have been optimised, secretome collection and analysis from 3D culture will no doubt provide further novel insight into UM biology.

Another limitation of our model is the need to use SFM to avoid albumin interference with the detection of smaller proteins. Differing depletion protocols and incubation times were assessed during the course of this study and although 48

hours was selected for secretome analysis there is always the possibility that differences in the secretome produced at other time points i.e. 12 and 24 hours may occur. In future, FACS analysis of the cells at different incubation points to assess early apoptotic signs might be preferable as compared to count of dead cells with trypan blue and incubation time in SFM might then be adjusted accordingly.

Cell death with release of intracellular proteins may explain the relatively low percentage (34%) of putative secreted proteins identified in our samples using the available bioinformatics tools (SecretomeP, Protein IP, TMHMM). Further analyses with software such as Ingenuity® Pathway Analysis (IPA) will be performed to investigate the nature of biological pathways activated or inhibited in our samples and aid interpreting these results.

Should cellular debris be an issue, lectin affinity capture prior to MS could be performed, in order to enrich secreted proteins, based on the assumption that secreted proteins are usually glycosylated. This approach was adopted by Yao et al.[224] for colorectal cancer ex vivo explants incubated in SFM and demonstrated a significant increase in the detection efficiency of secreted proteins, evidenced by an increased percentage of spectral counts belonging to the secreted proteins as well as an increase in the number of secreted proteins detected.

Another possible explanation for the presence of membrane and intracellular proteins in our secretome samples is that these are related to exosomes and other extracellular microvesicles secreted by UM cells, as previously suggested.[134] Exosomes are fascinating entities that are increasingly thought to play an important role in many of the biological processes regulating tumour progression, especially because of their ability to horizontally transport genetic and /or protein molecules

and for their proposed role in preparing the metastatic niche.[225] Indeed, the discovery that such a high percentage of exosomal proteins could be identified in our secretome samples has led to a further project within our research group, which aims to identify and characterise exosomes produced by UM cells and to compare the proteomic profiles of these with the current proteomic dataset.

Future avenues opened by this work also include further analyses of the proteomic data with software such as IPA to investigate the biological pathways up or down-regulated in these tumours in more detail and as compared with normal choroidal melanocytes in order to understand the biological processes in addition to searching for a biomarker of metastatic progression.

3.4.3 Conclusions

The aim of this current work was to identify one or more secreted proteins that could be used as a blood-borne biomarker of metastatic disease in UM patients. We identified a panel of 18 proteins that could discriminate between patients at a high or low risk of developing metastatic disease, which now require further validation by ELISA based methods in the associated remaining secretome prior to testing in patient blood samples. In addition, performing proteomic analyses has taught us about the importance of sample collection and storage, therefore we are now in the process of standardising our blood collection procedure to minimise protein loss. Further analysis of the protein dataset will be performed using IPA.

Chapter 4

Detection of circulating tumour cells in uveal melanoma patients using the CellSearch® system

4.1 Introduction

Circulating tumour cells (CTC) were first described in 1869 by Thomas Ashworth in a man with metastatic cancer as "cells similar to those in the tumors seen in the blood".[226] Investigations into the clinical significance of CTC, however, only really began in the 1990's, with the description of a polymerase chain reaction (PCR)-based methods to detect tyrosinase mRNA, a key enzyme in melanin synthesis, in patients with cutaneous melanoma.[227]

Further, the introduction of immunocytochemical techniques for the isolation of cancer cells from the circulation has enabled researchers to investigate the biological relevance and clinical significance of CTC.[228] For example in breast carcinomas, the presence of CTC was included in the international AJCC tumour staging system,[229, 230] whilst the biological relevance of CTCs in most other cancer types, including UM, remains unclear.[231]

The search for CTC in the blood of cancer patients generally includes an enrichment step and a detection step.[232] The enrichment step is applied to compensate for the rarity of CTC in the bloodstream, estimated as one in 10^5-10^6 mononuclear cells.[233] Enrichment can be achieved through positive selection methods based on the physical or biological properties of CTC, for example by filtration, density gradient centrifugation, immunomagnetic capture and immunoselection under low-flow conditions.[234] Alternatively, negative selection methods have been described, where leucocytes and other "contaminating" mononuclear cells are detected using antibodies directed at cell surface markers such as the pan-leukocyte marker CD45 and discarded by immunoselection.[235]

The detection step allows for confirmation and enumeration of CTC. This can be achieved by flow cytometry, immunocytochemistry, PCR-based analysis of tumour-cell-associated DNA and RNA or FISH.[234]

Studies conducted in UM have mainly used reverse transcriptase (RT-) PCR for the detection of mRNA levels of tyrosinase,[236-239] either alone or in conjunction with melanoma antigen recognized by T-cells 1 (MART-1)[233, 240-242] and/or gp100 melanoma antigen,[243] as surrogate markers for the presence of CTC (Table 4.1). In one of these studies, Pinzani et al.[241] performed a direct comparison in 16 patients between the results obtained by the tyrosinase qRT-PCR assay and those obtained using the isolation by size of epithelial tumour cells (ISET) platform, a filtration-based, marker-independent method of CTC detection that relies on cell size and morphology. CTC were detected by ISET in 5 of the 16 samples, which also tested positive for tyrosinase levels, showing a direct correlation between the two tests. In addition, tyrosinase levels in the 11 ISET-negative patients were undetectable. Despite this, mRNA analysis is renowned to be susceptible to false positives, resulting from 'illegitimate' transcription or contamination,[244] while ISET is a time-consuming operator-dependent system not ideal for the clinical setting.

To overcome these limitations an alternative approach has been adopted: immunomagnetic cell sorting with the anti-melanoma antibody, which recognises the melanoma-associated chondroitin sulphate proteoglycan (MCSP) antigen, also known as high-molecular weight melanoma associated antigen (HMW-MAA).[245-247]

Ulmer et al. were the first to suggest this approach for UM patients, adopting a technique previously used to examine for CTC in cutaneous melanoma patients.[248] These authors examined whole blood from 52 UM patients without metastatic

disease, and identified CTC (1-5 cells / 50 mL) in 10 of the samples (19%), showing a positive relationship with established clinical prognostic factors associated with increased risk of metastatic disease.[245] In contrast, a later study from the same group on 94 patients tested before and after treatment of the ocular tumour showed that CTC could only be detected in 14% of patients, without any significant association with established prognostic parameters.[246]

Taken together, data produced to date from the various CTC studies conducted in UM (Table 4.1) have been inconsistent, complicated mainly by variations in the test procedures. As previously demonstrated in cutaneous melanoma, comparative analyses of the same patient samples by different platforms/methodologies can lead to dissimilar results,[249] hence the clinical and biological implications of CTC enumeration largely depends on the technology applied.[250] The result of this is that none of the above-described techniques has as yet been adopted in clinical practice for UM patients.

Table 4.1 CTC in UM: summary of published studies at the time ours began.

Author (Year)	Marker	Primary disease: no. CTC+ / total pts sample (%)	Metastatic disease: no. CTC+ / total pts sample (%)	Controls: no. CTC+ / total pts sample	Summary
Real Time Polymerase Chain Reaction studies					
Tobal et al. (1993)	Tyrosinase	1/4 (25)	2/2 (100)	-	The one CTC+ patient developed metastasis 9 months later
Foss et al. (1995)	Tyrosinase	0/36 (0)	-	2/31	Despite of a demonstrated sensitivity of 1cell/ml, no CTC were found in UM nor advanced cutaneous melanoma patients
El-Shabrawi et al. (1998)	Tyrosinase	2/12 (17)	-	-	During the 12-month follow-up, 1/2 CTC+ patients developed mets, none of the others did.
Boldin et al. (2005)	Tyrosinase	16/41 (39)	-	-	Prospective, 5yrs follow-up. 11/16 CTC+ pts became CTC- after local treatment. CTC+ correlates with 5-yrs survival.
Keilholz et al. (2004)	Tyrosinase MART-1 gp100	3/21 (14)	12/17 (71)	0/21 for tyrosinase. 3/21 for MART-1 17/21 for gp100	2/3 CTC+ patients developed metastasis during 6-month f-up.
Schuster et al. (2007)	Tyrosinase MART-1	11/110 (10)	-	-	CTC+ as independent prognostic factor for development of metastasis (22-month f-up)
Callejo et al. (2007)	Tyrosinase MART-1	29/30 (97) over multiple visits	-	0/30 for both markers	Prospective longitudinal study, multiple samples per patient. Pt enrolled at diagnosis (5/30) or after treatment, none with metastatic disease. CTC+ months after enucleation/resection.
Pinzani et al. (2010)	Tyrosinase	20/41 (49)	-	3/16, hence cut-off value established	Longitudinal study, 55-month f-up. CTC+ as independent prognostic factor for progression-free and overall survival
	ISET	5/16 (31)	-	-	Direct correlation found between CTC values and tyrosinase levels
Schuster et al. (2011)	Tyrosinase MART-1	-	43/68 (63)	-	CTC+ as independent prognostic factor for progression-free and overall survival in metastatic UM patients
Immunomagnetic cell sorting studies					
Ulmer et al. (2008)	MCSP	10/52 (19)	-	0/20	CTC+ associated with clinicopathologic risk factors (LBD>14mm, CB involvement)
Suesskind et al. (2011)	MCSP	13/94 (14)	-	-	No changes in CTC level before and after ocular treatment. No correlation with prognostic parameters
Eide et al. (2009)	MCSP	4/ 249 (2)	-	-	Prospective, 9-year long study. **Bone marrow** was also tested with 98/328 (30%) positive results.

CTC= circulating tumour cells; MART-1= Melanoma antigen recognised by T-cells-1; MCSP= Melanoma-associated chondroitin sulphate proteoglycan; ISET= Isolation by size of epithelial tumour cells; LBD= largest basal diameter; CB= ciliary body;

In order to overcome test inconsistencies and to facilitate comprehensive CTC analysis in rare cancers such as UM, where the samples are likely to be collected at multiple clinical sites over time, an automated and standardised platform is needed. To date, the only platform for CTC enumeration to gain U.S. Food and Drug Administration (FDA) approval for prognostication in metastatic breast,[250] colorectal,[251] and prostate carcinoma[252] is the CellSearch® System (Veridex LLC, NJ). More recently, CTC detection by CellSearch® has also been demonstrated to be of prognostic significance in lung carcinoma[253] and cutaneous melanoma.[254] At the time of commencing this study in September 2011, no data existed for the detection of CTC in UM patients using this platform.

The overall goal of this study was to evaluate the prevalence, clinical significance, and biomarker potential of CTCs using the CellSearch® technology in UM patients at different stages of the disease. To achieve this, we investigated whether the presence of CTC in blood samples from UM patients could be detected and enumerated by the CellSearch® system using the CellTracks® circulating melanoma cell (CMC) kit (previously developed for cutaneous melanoma) and correlated with known clinical, histopathological and genetic features of increased metastatic risk.

The CMC kit enriches CTC using ferromagnetic beads coated in melanoma cell adhesion molecule (MelCAM or CD146) and defines them according to morphological characteristics, positive expression of MCSP, and absence of the leukocyte marker CD45. In addition, it contains a 4th channel that can be loaded with a customised antibody. An exploratory endpoint of this study was to validate the expression of the enrichment (CD146) and detection (MSCP) antigens present in the CMC kit, using UM cell lines grown as adherent and non-adherent cultures.

We also investigated the expression of an additional cell surface antigen that could be used in the 4th channel: CD184, also known as C-X-C chemokine receptor type 4 (CXCR-4) or fusin, a G-protein-coupled chemokine receptor specific for stromal-derived-factor-1. CD184 was initially recognised for its involvement in HIV entry and leukocyte trafficking, but it is now also accepted as an important player in the development of metastatic disease in multiple cancer types.[255] In particular, CD184 expression has been detected by flow cytometry on almost 80% of CTC isolated from the peripheral blood of metastatic cutaneous melanoma patients.[256]

4.2 Patients and methods

4.2.1 Patient population

4.2.1.1 Inclusion criteria

Consenting patients were entered into this study if they had received treatment for their primary UM at the Liverpool Ocular Oncology Centre (LOOC) or if they were diagnosed with metastatic UM at the Clatterbridge Cancer Centre (CCC) between October 2011 and March 2012. All patient samples were pseudo-anonymised prior to release from the OOB. Project specific ethical approval for this study was obtained from the National Research Ethics Service (NRES Ref No. 11/NW/0568).

Patients affected by metastatic UM and treated at the Christie Hospital NHS Trust in Manchester during the same time period were also included in this study. Patient consent and ethical approval for this part of the study formed part of the CEP144 project, Clinical and Experimental Pharmacology (CEP) Group, Cancer Research UK, Manchester Institute.

4.2.1.2 Exclusion criteria

Samples from patients affected at any time by another malignancy were excluded.

4.2.1.3 Metastatic risk stratification

Patients with a primary UM and without evidence of metastatic disease were classified as being at either at HR or LR of developing metastatic disease using the LUMPO, as detailed in Chapter 1.

Details about the clinical, histopathological and genetic characteristics of the tumour, as well as follow-up information about the patient, were provided in a pseudo-anonymised manner by the custodian of the OOB.

To avoid possible bias, sample analysis was performed without any knowledge of the risk stratification of the patient.

4.2.2 Sample collection and analysis

4.2.2.1 Sample collection

For each patient, a 10ml blood sample was drawn by venepuncture directly into a CellSave® tube (Veridex LLC, NJ), containing ethylenediaminetetraacetic acid (EDTA) and a custom preservative, allowing sample preservation at room temperature for up to 96 hours. Samples collected at the LOOC and CCC were shipped to the CEP group using the Royal Mail Safebox™, with Special Delivery™ Next Day postage. Samples collected at the Christie Hospital were transferred to the CEP group via internal porters.

Each sample was assigned a unique study code (linked to the pseudoanonymised OOB code) and entered onto a database prior to processing.

Samples from metastatic patients were collected prior to beginning any chemotherapy.

4.2.2.2 Sample analysis using the CellSearch® platform

The CellSearch® System (Veridex LLC, NJ) comprises the CellTracks® Autoprep system, the CellSearch® CMC Kit and the CellTracks® Analyser II (Figure 4.1). The

Autoprep system is semi-automated for CTC enrichment. The CMC kit contains the following reagents:

- ferrofluid consisting of iron nanoparticles coated with a polymer layer and conjugated to the MelCAM (CD146) antibody for CTC enrichment
- phycoerythrin (PE)-conjugated mouse monoclonal antibody to MCSP for CTC detection
- allophycocyanin (APC)-conjugated mouse antibody to CD45 and CD34 for detection and negative selection of blood components
- 4,6-diamidino-2-phenylindole (DAPI) to stain the nucleus
- a proprietary buffer to wash, permeabilise and re-suspend the cells.

The CMC kit also comprises a 4th channel that can be customised with user-defined antibodies.

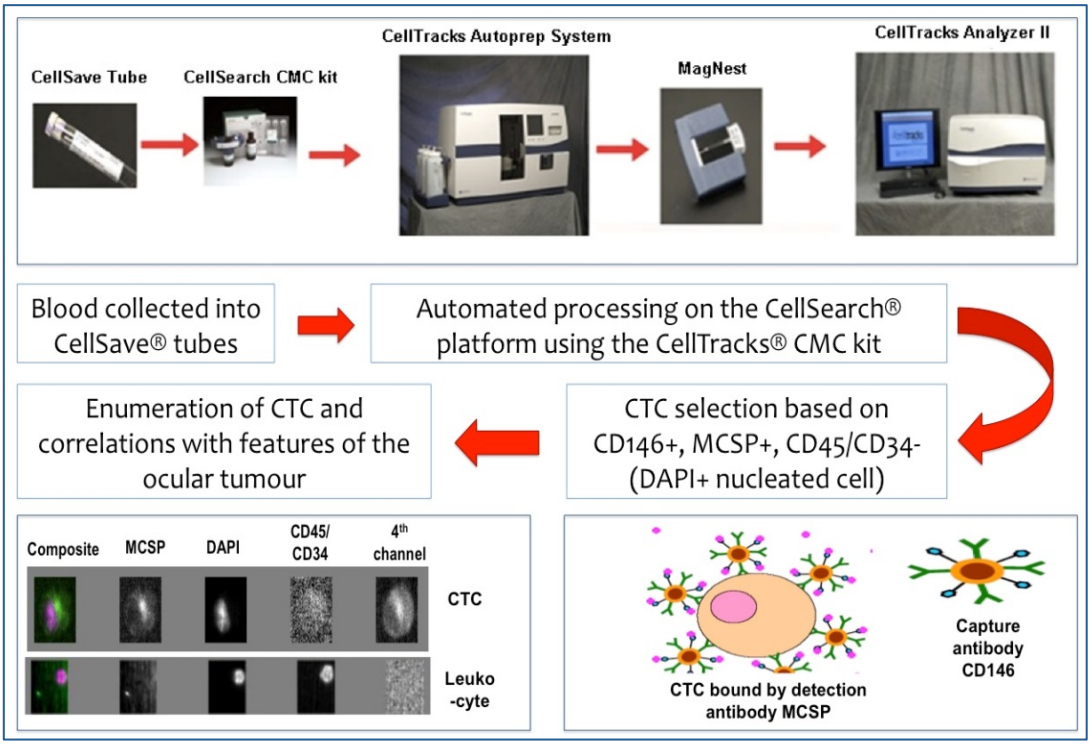

Figure 4.1 Schematic highlighting the processes undertaken in the detection of CTC using the CellSearch® system and the CellTracks® CMC kit.

For each sample, 7.5ml blood was transferred to a 15ml conical tube and 6.5ml of CMC kit dilution buffer was added. The samples were mixed by inverting five times and then centrifuged at 800xg for 10 minutes to separate the plasma layer from the cellular pellet. Samples were loaded onto the CellTracks® Autoprep system and the automated process performed whereby the plasma was aspirated and the ferrofluid containing CD146 was added to the cellular pellet. Captured cells were then drawn to the sides of the column by a magnetic field and unattached cells and blood were aspirated. Captured cells were re-suspended in buffer and permeabilising agent applied prior to staining with the fluorochrome conjugated antibodies detailed above. Magnetic separation was again applied to aspirate excess reagent and the enriched sample was resuspended and placed into a MagNest® presentation device. The MagNest® presentation device is a cartridge located between two magnets that draw the cells to the cartridge surface thus enabling scanning by the CellTracks® Analyser II system. The MagNest® was rested in the dark for a minimum of 20 minutes prior to scanning.

The CellTracks® Analyser II is a four-colour fluorescence microscope. The MagNest® was placed in the analyser and scanned for each of the four fluorescent probes. Cells stained with MCSP/endothelial markers and DAPI were presented for analysis. Melanoma CTC were defined as MCSP and DAPI positive, and CD45 and CD34 negative (MCSP+, DAPI+, CD45-, CD34-). White blood cells and endothelial cells were CD45, CD34 and DAPI positive, but MCSP negative (CD45+, CD34+, DAPI+, MCSP-). The total number of CTC present in each sample was recorded.

4.2.2.3 Data analysis

Correlations were drawn between the number of CTC identified in each sample and the clinical, histopathological and genetic data of the corresponding primary tumour, as well as the survival data at study completion. All data were analysed using the statistics software SPSS.

As this was an exploratory pilot study, no formal power calculation to set sample size was performed to detect clinical significance.

4.2.3 Assessment of antigen expression on uveal melanoma cells

4.2.3.1 Cell culture

Five cell lines established from primary (Mel 270[257] and 92.1[258]) and metastatic (Omm1[259], Omm2.3[257], Omm2.5[257]) UMs, kindly provided by Dr M Jager (Leiden, The Netherlands), were grown in adherent and non-adherent culture conditions as previously described.[196] All cells were grown in RPMI medium (PAA Laboratories, Somerset, UK) supplemented with 10% FBS (PAA Laboratories), 2 mM L-glutamine (Sigma, Dorset, UK), and antibiotics and incubated at 37°C with 5% CO^2. For adherent cultures, $1x10^6$ cells were seeded in a 25-cm2 flask and grown to 85% confluence.

For non-adherent cultures, $1x10^6$ cells were seeded in a 25-cm^2 flask previously coated with poly 2-hydroxyethyl methacrylate (poly-HEMA; Sigma) to prevent cell attachment. Cells were grown in suspension for 48 hours only, as the aim was to measure cell surface antigen expression, not to facilitate 3D spheroid induction.

As an exploratory endpoint, cells from one primary short-term UM cell culture (S156-13 p1), established as described in Chapter 3, were also grown in adherent and suspension conditions and stained using the same protocol as per cell lines (below).

4.2.3.2 Multicolour flow cytometry

Single cells were collected using non-enzymatic cell dissociation solution (Sigma Aldrich C5789), counted and resuspended at $2x10^6$/ml in FACS buffer (1% BSA, 0.1% NaN3 in PBS). Cells were stained at 4°C for 15 min with the following fluorochrome conjugated anti-human monoclonal antibodies: CD146-fluorescein isothiocyanate (FITC), MCSP-phycoerythrin (PE) (both Miltenyi Biotech, Germany) and CD184-PE cyanine dye 7 (PE-Cy7) (BD Pharmingen, Germany). Isotype-matched IgG antibodies were used as controls. Fixable Viability Dye eFluor® 450 (eBioscience Ltd, Hatfield, UK) was used to assess cellular viability. Stained cells were kept on ice, in the dark, and immediately analysed, without adding any fixative.

Samples were measured with the LSRFortessa, using BDTM CompBeads to optimise compensation settings for multicolour flow cytometric analyses. Data were analysed with Diva 7.0 software (all BD Biosciences). Single live UM cells positive for the markers above were identified by gating out dead cells (stained by the viability dye), and determining the negative population using isotype controls. Experiments were repeated three times with cells at different passage numbers.

4.3 Results

4.3.1 Detection of CTC in patient samples

A total of 37 patients were included in the study: 22 affected by primary UM and treated at the LOOC; 5 diagnosed with metastatic UM at the CCC; 10 treated for metastatic UM at the Christie Hospital, Manchester. Four of these samples (two from LOOC and two from CCC) could not be analysed because of a temporary shortage of reagents. Hence, 33 samples were successfully analysed by the CellSearch platform for CTC detection and enumeration. The number of CTC identified ranged between 0 and 510 (Figure 4.2). CTC were detected in seven out of 13 metastatic patients (range 1-510), in five out of 14 HR UM patients (range 1-2). No CTC were detected in the six LR UM patients.

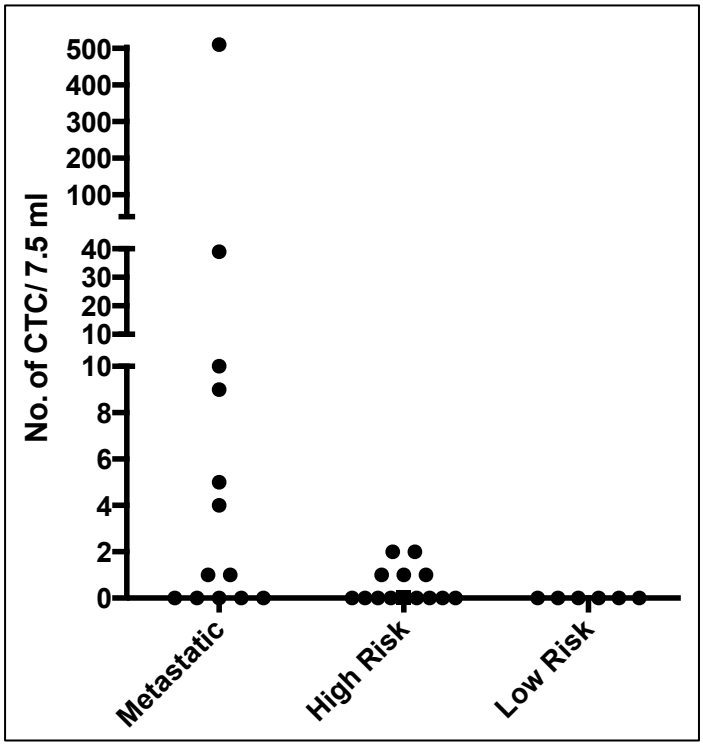

Figure 4.2 Number of CTC identified in UM patients at different stages of the disease using the CellSearch® platform

4.3.1.1 Correlation between CTC number and metastatic risk

In patients with primary UM, the presence of 1 or more CTC was significantly correlated with the presence of monosomy 3 in the tumour (Chi-square, $p<0.01$) detected using MLPA or MSA but not with any other clinical or histopathological prognostic factor (Table 4.2)

During the 2-year follow-up period, three out of the 14 HR patients developed metastatic disease. CTC had been detected at the time of ocular treatment in one of these patients, whereas no CTC had been identified in the other two individuals.

Table 4.2 CTC count in patients with primary UM prior to ocular treatment

Patient No.	No. of CTC	Age (Years)	Sex	LBD (mm)	Height (mm)	CBI	EOE	Epithelioid cells	Genetic	MD during follow-up
HR1	1	62	M	16.9	10.2	No	No	Yes	3L, 8G	No
HR2	1	77	F	14.2	3.3	No	No	No	3L	No
HR3	1	73	M	16.4	5	No	No	Yes	3L, 8G	No
HR4	2	73	M	11.9	3.1	No	No	Yes	3L, 8G	No
HR5	2	72	M	15.6	15.2	No	No	Yes	3L, 8G	Yes §
HR6	0	70	M	16.2	10.9	Yes	No	Yes	3L, 8G	Yes
HR7	0	68	F	19.5	11.4	Yes	No	Yes	3L, 8G	No
HR8	0	65	M	18.2	2.3	No	No	Yes	3L, 8G	No
HR9	0	35	M	14.5	3.8	No	No	No	3L	No
HR10	0	63	M	19.1	13.5	Yes	No	Yes	3L, 8G	Yes §
HR11	0	72	M	12.5	3.2	No	No	N/A	3L	No
HR12	0	44	M	9.7	4.2	No	No	Yes	3L, 8G	N/A
HR13	0	62	M	14.9	3.8	No	No	No	3L, 8G	N/A
HR14	0	74	F	14.3	5.8	No	No	No	3L	N/A
LR1	0	71	F	13.5	5.3	No	No	No	3N, 8G	No
LR2	0	74	M	10.1	3.1	No	No	No	3N	No
LR3	0	61	F	13.1	7.5	No	No	No	3N, 8G	No
LR4	0	62	F	14.7	4.1	No	No	Yes	3N	No
LR5	0	60	M	13.3	2.9	No	No	No	3N,8N	No
LR6	0	60	F	12.7	7.4	No	No	No	3N, 8G	No

LBD = largest basal diameter; CBI = ciliary body invasion; EOE = extra-ocular extension; MD = metastatic disease; HR = high risk; LR = low risk; M = male; F = female; N/A = not available. §= patient deceased.

4.3.1.2 Correlation between CTC numbers and overall survival

Of the 13 samples from UM patients with overt metastatic disease successfully analysed, CTC were identified in eight samples (61%). The blood sample for CTC analysis was collected before the start of chemotherapy in all cases, but one patient (M4) had undergone surgical liver resection of isolated metastases two years before. Details of the systemic treatment received by each patient are outlined in Table 4.3.

During the 18 months of follow-up, 12 of 13 patients died of metastatic disease. The data would suggest that patients with ≥1 CTC have a shorter mean overall survival time as compared with those patients in whom no CTC were detectable (72 vs 318 days). However, given the overall small number of patients in our series and the fact that the two groups (CTC positive vs CTC negative) included a different number of patients, there were insufficient numbers to do formal statistic. Moreover, the patients were included independently of their performance status, tumour burden, or hepatic function. Since all of these factors play a role in survival, no clinically meaningful conclusions could be drawn at this point.

Table 4.3 CTC count in patients with metastatic UM

Patient No.	No. of CTC	Age (years)	Sex	Time to mets (years)	Metastatic sites	Systemic treatment	Time to death (days)
M1	510	48	M	1	liver	DTIC	40
M2	5	60	M	2	liver,adrenal gland	DTIC	173
M3	0	67	F	2	liver	DTIC	397
M4	0	64	M	18	liver	DTIC*	495
M5	39	82	F	2	liver	None	112
M6	1	71	M	12	liver, kidney	None	43
M7	4	77	M	2	liver	DTIC	102
M8	10	74	F	4	liver	None	63
M9	1	74	M	2	liver	None	4
M10	0	62	F	5	liver,pancreas,lung	None	60
M11	9	67	M	0[§]	liver	None	42
M12	0	25	M	3	spine	Surgery	Alive
M13	0	64	M	2	liver	DTIC	102

*§= metastatic disease diagnosed at the same time as the ocular tumour; DTIC = Dacarbazine; *= this patient had liver resection of an isolated metastasis two years earlier*

4.3.2 Cell surface antigen expression in UM cells

4.3.2.1 Expression in UM cell lines

The CD146 antigen, used for positive enrichment in the CellSearch platform, was detected in > 99% of live cells in all five cell lines, irrespective of whether they were grown in adherent or non-adherent culture conditions. In contrast, expression of the MCSP antigen, used for detection in the CMC kit, demonstrated heterogeneous levels of expression both within and between cell lines. The strongest expression was detected in the Mel270 cell line, where there appear to be two populations of cells, one negative and one positive for MCSP. The chemokine receptor CD184 was detectable in all UM cell lines, but only in a very low percentage of the cells. (Table 4.4). The type of culture conditions, i.e. adherent or non-adherent, did not significantly influence protein expression. (Figure 4.3)

Table 4.4 Percentage of UM cells positive for CD146, MCSP, CD184 measured by multicolour flow cytometry. Percentages refer only to the live cell population, as determined by viability dye exclusion

	Mel 270		92.1		Omm 1		Omm 2.3		Omm 2.5	
	Adh	Susp	Adh	Susp	Adh	Susp	Adh	Susp	Adh	Susp
Alive	87.1	85.3	85.9	84.9	84.2	84.8	86.6	86.5	88.4	82.7
CD146	99.8	99.6	99.6	99.5	99.9	99.9	99.8	99.8	99.8	99.2
MCSP	40.3	38.4	0.3	0.4	0.8	0.1	0.5	0.2	2.0	3.1
CD184	1.9	1.0	1.0	1.5	1.8	0.6	0.3	0.7	2.9	3.6

Adh = adherent culture; Susp = suspension culture

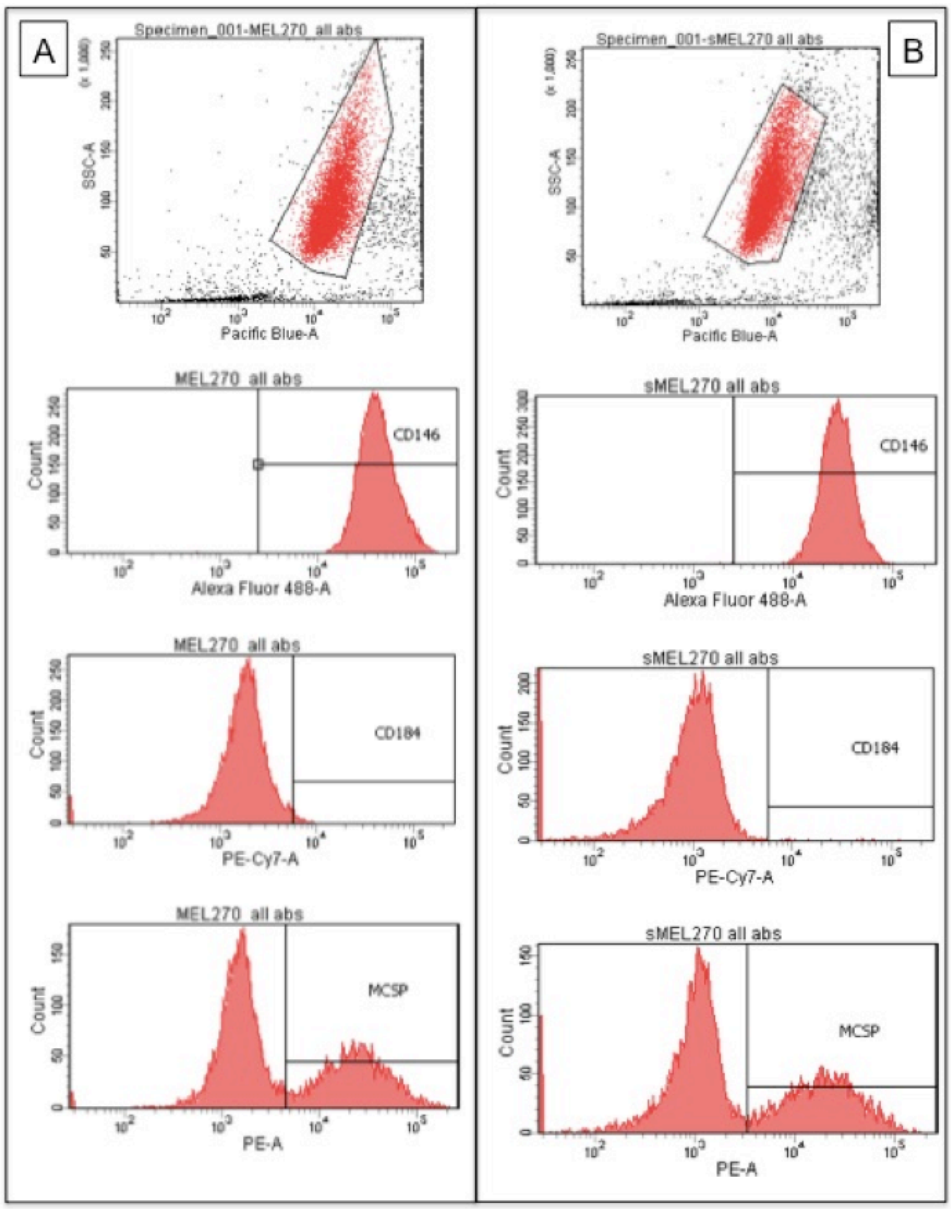

Figure 4.3 Representative images of cell surface antigen expression in the Mel 270 cell line grown in adherent (A) and suspension (B) conditions

4.3.2.2 Expression in one UM short-term primary culture

Primary cells grew well in both conditions, forming spontaneous large clumps in both adherent and suspension cultures (Figure 4.4). The cells were harvested and underwent the same staining protocol as for the cell lines. Difficulties in obtaining a single cell suspension and the multiple centrifugation wash steps during the protocol, resulted in a reduction in the percentage of viable cells for flow cytometric analysis to 33.4% and 41.8% in the adherent and suspension cultures, respectively (Figure 4.5).

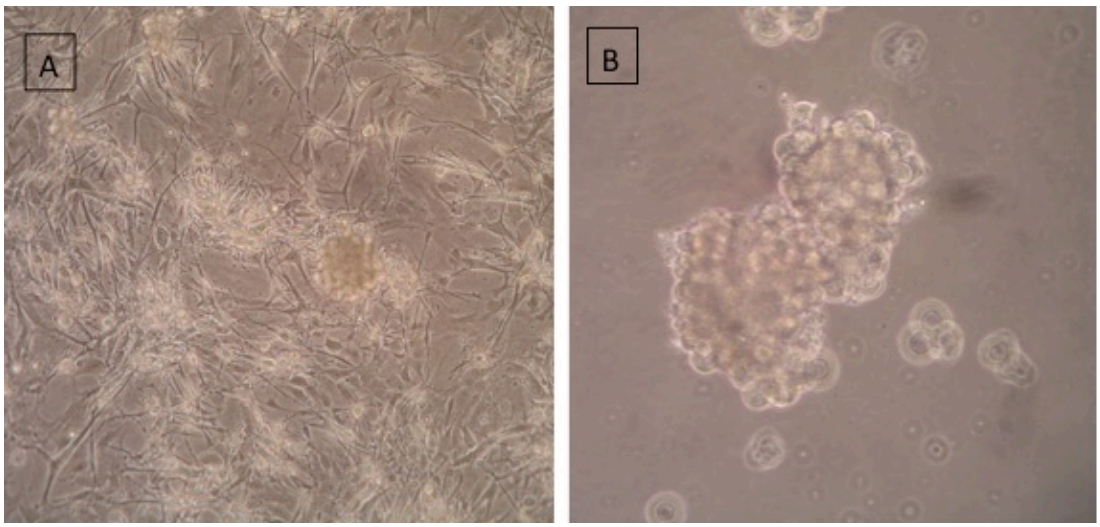

Figure 4.4 Primary UM cells (S156-13) in short term culture under adherent (A, 10X) and suspension (B, 40X) conditions.

Flow cytometric analysis of the viable single cell populations demonstrated antigen expression in adherent and suspension cells, respectively, as follows: MCSP, 98% and 85% suspension; CD146, 50% and 17%; CD184, 21% and 23%.

4.4 Discussion

In this Chapter, we report the prevalence and prognostic value of CTC in patients with primary UM as well as those with overt metastatic disease using the FDA approved CellSearch® platform and CMC kit. This is currently the only system that would be suitable to be used in multicentre clinical trials, which are the future of rare diseases, such as UM.

The main use of the CellSearch® platform in other cancers has been in the metastatic setting, for prognostic purposes and to monitor response to treatment. In this study patients with only primary UM were also included in the hope that CTC could provide more information on the development of metastatic disease in HR patients. At the time of initiating this study, there were no data available regarding the utility of this platform in UM patients.

4.4.1 Prognostic value of CTC in patients with only ocular disease

Our data demonstrate that at the diagnosis of patients with primary UM, ≥1 CTC were detectable in 25% of individuals. The presence of one or more CTC in the peripheral blood was more frequently associated with M3 in the primary tumour. None of the six LR patients had detectable CTC in their peripheral blood. Despite this, there was no correlation between other clinical or histopathological features of the primary tumour and the presence of CTC in the peripheral blood. This is in line with previous reports, where the presence of CTC determined by PCR for tyrosinase and Melan A showed no correlation with established clinico-pathological prognostic factors.[233, 239, 240, 246]

To validate the prognostic value of CTC in terms of predicting the development of metastatic disease, it is necessary to follow the patient for at least 10 years.[260] In the two-year follow-up period for this study, three out of 20 patients developed metastases: all patients were classified as HR, but only one of them had detectable CTC. No conclusions can therefore be drawn at this point.

4.4.2 Prognostic value of CTC in metastatic UM patients

Using the CMC Kit in the CellSearch® system, one or more CTC were detected in the peripheral blood of 61% of the metastatic patients in this study, all of whom were tested prior to any chemotherapeutic treatment.

In a similar study of 40 metastatic UM patients using this platform just recently published,[261] CTC were detected in only 30% of cases, with a range of 1-20 cells / 7.5 ml of blood. It should be noted, however, that all patients were either on first-line treatment or had received previous multiple treatments prior to CTC analysis, which may have had an impact on the number of detectable CTCs in the peripheral blood. This is in contrast to our study, where the blood sample for CTC analysis was taken prior to beginning any systemic therapy. In the above-mentioned study, CTC positivity was strongly associated with a reduced progression free survival and overall survival time by univariate analysis. However, in a multivariate analysis time to first metastatic relapse, performance status, and tumour volume were the only independent prognostic indicators of reduced overall survival.

It should be recognised that in both the published work and our current study, heterogeneity of the clinical cohort analysed highlights the importance of comprehensive clinical information and the ability to recruit a large number of

patients is needed to be able to create comparable groups with similar characteristics, which is only possible through multicentre studies in such a rare tumour as UM.

4.4.3 Validation of cell surface antigens used by the CellSearch® Melanoma Kit

The number of CTC detected by the CellSearch® system in UM patients, was surprisingly low as compared with the cutoff used for prognostic significance in other cancers: 50 CTC for small cell lung cancer; 5 CTC for breast, prostate, and non–small cell lung cancer; and 3 CTC for colorectal cancer. One possible explanation for the low numbers of CTC detected is that the antigens used for enrichment and detection are suboptimal for this cancer type, resulting in false-negative results.

The enrichment antigen, CD146, also known as MelCAM or MUC18, is a cell adhesion molecule, which has been demonstrated previously in UM cells and cell lines by proteomics,[109] and RT-PCR, immunoblotting, and immunocytochemistry.[262] Variations in the expression levels of MUC18 between the UM cell lines are reported in both studies.

The detection antigen MCSP, also known as HMW-MAA, which is recognised by the monoclonal antibody 9.2.27,[263] has been used previously for CTC detection in UM using immunomagnetic methods.[245-247] Selection of this antigen is based on a single paper showing moderate immunohistochemical expression in 18/19 FFPE choroidal melanoma sections.[264]

We hypothesised that expression of these two antigens could be influenced by their growth in anchorage dependent and independent conditions, the latter more closely mimicking UM cells circulating in the blood. Based on our analysis, CD146 was widely expressed in all cell lines in both adherent and non-adherent conditions suggesting good performance of the enrichment step. In contrast, the detection antibody MCSP was expressed only by a limited number of cells both within and between the UM cell lines, perhaps explaining the absence/low levels of CTC detection in many UM patient samples. In contrast, cells isolated from a single primary UM specimen and grown in short term culture showed low numbers of CD146 positive cells, particularly when grown in suspension, while expression of MCSP was detected in almost every cell analysed. Of further interest was the more widespread expression of CD184. These data highlight the need for further studies using UM cells isolated from patient specimens. In this respect, magnetic-activated cell sorting (MACS), could be preferable over FACS, as it requires less sample handling (in particular rinse/centrifugation steps) and allows for large input volumes.[265]

In a recently published paper, similar concerns about the use of MCSP for CTC detection in UM were raised.[266] The authors went on to apply a dual immune-magnetic enriched assay using antibodies against two melanoma markers: NKI/beteb (analogue to CD146) and NKI/C3 (analogue to CD63), which had been previously tested in UM cell lines.[267] Using an indirect labelling approach, in which the mononuclear cell fraction was first incubated with the antibody cocktail and then added to the immunobeads, a detection sensitivity of 2 tumour cells/ 10ml of blood, as shown by spiking experiments with the 92.1 cell line, was achieved. Using

this method, CTC were detected in 29 out of 31 (93.5%) patients with primary non-metastatic UM, with a median count of 3.5 cells / 10 ml of blood (range: 0-10 cells). However, as reported in the previous studies, no correlation was found between the number of CTC and any clinical prognostic factors. Furthermore, there was no follow-up information to draw conclusions about survival. The most interesting aspect of this approach is that intact and viable CTC could be identified and successfully cultured for the majority of UM patients. This opens the avenue to further molecular characterization of CTC as well as enhancing our understanding of the biology of these cells and elements of the metastatic process.

4.4.4 CTC and cancer stem cells

Recent data have suggested an interesting functional confluence between CTC and cancer stem cells (CSC), as different functional statuses of the same subpopulation of cancer cells.[268] The concept of dynamic phenotype and heterogeneity amongst CTC has led to the development of a hypothetical model with three types of CTC: a) bystander CTC; b) pathogenically active CTC; and c) migrating CSC.[269]

Bystander CTC are more differentiated cancer cells that have no proliferative potential and have entered the circulation by a passive mechanism such as inflammation at the site of the primary cancer. Enumeration of this subpopulation would be of no clinical value.

Pathogenically active CTC are those that play a role in cancer dissemination and metastasis. Characterization and enumeration of this subpopulation over time would provide useful diagnostic and prognostic information.

Migrating CSC are characterised by peculiar genotypic and phenotypic plasticity, being able to assume stem cell-like characteristics as well as undergo epithelial-mesenchymal transition (EMT). This would be the subpopulation of greatest pathogenic value in terms of cancer aggressiveness and resistance to therapy. However, the currently used detection methods for CTC are not efficient enough to identify this CTC subpopulation.[270]

For this reason, we simultaneously tested the expression of the two cell surface markers used for enrichment (CD146) and detection (MCSP) of CTC as well as that of a putative stem cell marker, CD184, which had previously been shown to be expressed on the surface of CTC in metastatic cutaneous melanoma.[256] In both adherent and suspension UM cell lines, the expression of CD184 was minimal, in line with one previous report,[271] and did not correlate with MCSP status. In the one primary sample, on the contrary, 22% of cells were positive for this marker. It should be noted that detection of the CD184 chemokine receptor is influenced by microenvironmental conditions leading to its internalisation. Hence caution should be taken when assaying this cell surface marker in the laboratory, and once again, studies on a larger series of primary samples are very much needed.

4.4.5 Conclusions and future directions

The heterogeneity and intriguing plasticity of CTC in the bloodstream, essential for their high adaptability to the changing microenvironment, makes the discovery of a specific and sensible assay for CTC detection very difficult.[269] Our study shows that the CellSearch® platform with the current CMC kit does not seem suitable for enumeration of CTC in UM patients at any stage of disease. However, our work also

shows that determining which antibody may be most suitable remains difficult, as studies of surface antigen expression on cell lines are not truly representative. Advances in the characterization of primary UM samples are warranted and could lead to the identification of alternative cell markers for the development of a UM customised kit.

In the meanwhile, other groups have focused on the detection of circulating tumour DNA (ctDNA)[272] or cell-free DNA (cfDNA),[273] rather than CTC, in the search for a solid and reproducible technique that can overcome antibody-based limitations. This is based on the knowledge that approximately 80% of UM bear mutually exclusive somatic mutations in the GNAQ or GNA11 genes. One recent study investigated the presence of CTC (using the CellSearch® platform) and ctDNA (using bidirectional pyrophosphorolysis-activated polymerization) in a cohort of 40 metastatic UM patients and showed that ctDNA is more frequently detected and has greater prognostic value in multivariate analysis than CTC enumeration.[261] In addition, ctDNA is more promising as clinical tool because it has a dynamic range of values, and therefore could be used to monitor treatment response. To date, there is no information about the presence or not of ctDNA in primary UM patients. In metastatic patients, a strong correlation has been shown between tumour burden and ctDNA levels, with low tumour burden being the only clear limit to ctDNA detection.[272] It is therefore not clear whether ctDNA could be used as a biomarker for monitoring the development of metastasis in HR patients; however, this is also worth investigating in the future.

In conclusion, the analysis of CTC in the peripheral blood of UM patients is still far from being clinically useful, but it requires pursuit in terms of CTC capture and

characterisation (rather than enumeration), as it could provide unparalleled means to understand metastatic biology and identify relevant therapeutic targets.

Chapter 5

Choroidal tumour biopsies for risk stratification in uveal melanoma patients

5.1 Introduction

As discussed in Chapter 1, almost 50% of patients with choroidal melanoma develop metastatic disease, which is only rarely clinically detectable at the time of diagnosis of the ocular tumour and which may develop months to years after apparent good health. Metastatic disease almost always involves the liver initially, and usually has a fatal outcome.[274] However, there are increasing therapeutic options, such as hepatic tumour resection,[89] intra-hepatic chemotherapy,[275] and immunotherapy with agents such as ipilimumab.[211] The best results are obtained in patients when metastases have been identified early within the liver, are few in number, and are potentially surgically resectable.[78, 89, 90] To identify UM patients with increased metastatic risk and who thus require more intensive liver screening, chromosomal aberrations or GEP of the primary tumour is assessed and incorporated into risk stratification at many oncology centres. At the LOOC a computerized neural network[276] was developed and validated to produce survival estimates that are relevant to individual patients (i.e., 'personalized prognostication')[277] based on affordable molecular and histopathological analyses, financed by the National Health Service (NHS) England, and which is routinely used to guide the screening protocol for metastatic disease.[90]

Between 1999 and 2007, such prognostic tests were offered to consented patients treated by local resection or enucleation, in whom tumour tissue was readily available.[278] Advances in survival prediction and in the treatment of metastases prompted LOOC to start offering prognostic tumour biopsy to as many patients as possible, including those treated by brachytherapy or PBR.[76] Intraocular tumour

biopsies have been performed in Liverpool since 1993 mainly for diagnostic purposes,[279, 280] hence the surgical expertise was already there. Indeed, the LOOC was the first to describe a trans-retinal (TR) approach using a 25G vitreous cutter[281] and have since developed a variety of approaches for trans-retinal and trans-scleral (TS) tumour sampling, depending on size and location.

To facilitate the processing of prognostic samples, in November 2010, the Liverpool Ocular Oncology Molecular Pathology Service was established in the accredited laboratory of the Department of Cellular Pathology, Royal Liverpool University Hospital NHS Trust. This has allowed all prognostic testing, including molecular genetic analyses by MLPA or MSA, to be performed 'in house', with close collaboration between the Department of Cellular Pathology and the LOOC clinical team.

Nevertheless, prognostic intraocular biopsies are not always successful, especially for thin tumours (<3 mm thick)[282] and the procedures themselves bear potential risks, including: tumour dissemination; surgical complications, such as vitreous haemorrhage or retinal detachment; endophthalmitis; and failure to obtain a result. The issue of tumour dissemination has been addressed in a number of previous publications, which showed no clinical evidence of intraocular, extra ocular or orbital spread following either trans-scleral or trans-retinal biopsy.[283-290] The two aspects that clinicians still need to consider and discuss with prospective patients are the risk of developing vitreo-retinal complications, with potential visual loss and/or need for further surgery,[279] and the risk of not obtaining a result, either because of inadequate sampling or laboratory processing.[38] The failure to obtain a result is indeed an important aspect to consider because psychological studies have

shown that patients find an uncertain prognosis more stressful than a poor prognosis.[291]

Prognostic tumour biopsy and personalised prognostication in UM is also important for translational research, as it provides essential information that allows for segregation into HR versus LR of associated material, such as blood samples. For example, the study on CTC described in Chapter 4 relied on tumour biopsies for determination of metastatic risk in those patients treated conservatively. While collecting this information, it became apparent that molecular genetic results could not be obtained in some cases; therefore an audit of the prognostic biopsy process was started. In particular, we were interested in understanding whether there was room for improvement in the surgical techniques, in the sample handling, and in its processing.

The aims of the study in this Chapter were to retrospectively evaluate the process of choroidal melanoma biopsy conducted by LOOC over an 18-month period, to assess the yield of prognostic information provided weighed against surgical complications, to identify possible 'pitfalls' in the process, to describe the change of practice undertaken, and to re-assess the results after a further 12 months.

5.2 Patients and methods

5.2.1 Patients

Patients were included in this study if treated for choroidal melanoma with Ruthenium-106 plaque brachytherapy or PBR at the LOOC between January 2011 and June 2013 and if a prognostic biopsy was performed. The study population comprised two groups: 1) a retrospective cohort of patients treated between January 2011 and June 2012; and 2) a prospective cohort of patients treated between July 2012 and June 2013 in which the impact of the adopted changes to procedure was assessed.

The inclusion/exclusion criteria, data collection, follow-up protocols were identical in both groups. On the contrary, the surgical technique and the sample processing were modified as a result of the audit process, hence are different between the two groups, as explained in Table 5.1.

Table 5.1 Differences in practice between group 1 and group 2.

	Group 1	Group 2
Time period	01/2011 – 06/2012	07/2012 – 06/2013
Biopsy techniques (TR or TS approach depending on tumour location, with TR being preferred for post-equatorial UM)	For all tumours irrespective of thickness TR: 25G vitreous cutter TS: 25G FNAB	Tumours <3mm thick: TR: "sideway approach" TS: "flap biopsy" Tumours >3mm thick: TR: 25G vitreous cutter TS: 25G FNAB
Blood sample	From selected patients	Collected in all cases and sent to the lab with the matched biopsy specimen
Specimen handling	3-4 cytospin slides prepared for all biopsy samples; remaining sample used for genetic analyses	Only 1 cytospin slide prepared for morphological examination; majority of the specimen preserved for genetic analyses

Patients were excluded if the tumour arose in the iris, and if the biopsy was performed for diagnostic purposes. Clinical data were collected from patient records and included: age, gender, affected eye, tumour characteristics (location, largest basal diameter and thickness measured by B-scan ultrasonography). Surgical data included: type of treatment for uveal melanoma (plaque or PBR), type of biopsy (trans-scleral or trans-retinal), time of biopsy compared to treatment commencement, surgeon, intraoperative complications, follow-up examination at 1 day, 1 month, and any other further visit.

Tumours were biopsied either trans-sclerally or trans-retinally depending on their size, location and treatment. Those treated with a ruthenium plaque were biopsied either: (a) trans-sclerally if they extended pre-equatorially and if the tumour thickness exceeded 2mm; or (b) trans-retinally, if the tumour was considered inaccessible with this approach because it was small and/or posterior. Tumours treated with PBR were biopsied trans-retinally as soon as possible after completion of the radiotherapy, i.e., on the last day of the radiotherapy or, if this was not possible, within a period of two weeks.

Written informed consent was obtained in all cases prior to performing the biopsy. In addition to being advised of the possible risks associated with the surgery, patients were informed of the screening/follow-up procedures following prognostic testing. Contra-indications to biopsy were poor vision in the fellow eye and patients on any anti-coagulant therapy.

Generic consent for the use of data, tissues and images for research, teaching and audit was obtained prospectively from all patients. Approval for this study was

obtained from the Royal Liverpool University Hospital (project reference number 4031-11/129).

5.2.2 Surgical Techniques

5.2.2.1 Trans-retinal biopsies

Trans-retinal biopsies were performed under local anaesthesia with a 25-gauge vitreous cutter, using a 3-port sutureless vitrectomy kit, as previously described.[281] Briefly, the vitreous cutter was advanced across the vitreous cavity and through the retina into the centre of the tumour, avoiding any retinal blood vessels. To obtain more tissue samples, the vitreous cutter was repeatedly inserted into and withdrawn from the tumour, with maximum suction and low cutting rate (Figure 5.1).

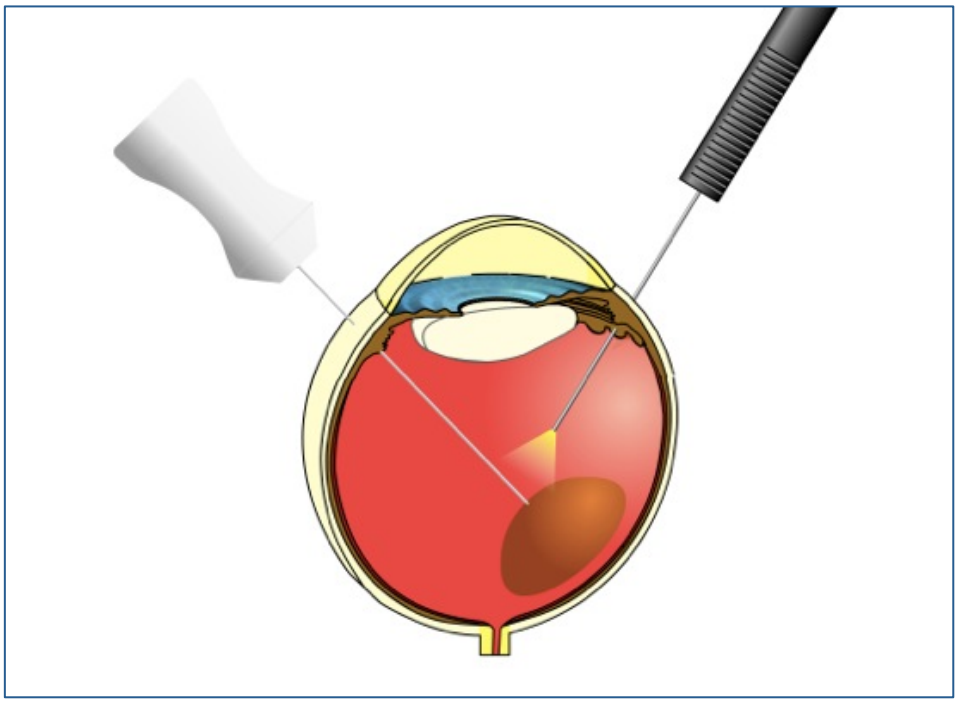

Figure 5.1 Schematic representation of the transretinal tumour biopsy technique using a 25G vitreous cutter introduced via pars-plana through the vitreous cavity. The tumour is visualised using a fundus lens (not shown) and a light pipe, shown in black on the right hand side of the image *(Courtesy of Mr C. Groenewald; vitreoretinal surgeon, LOOC).*

A modified technique has been developed for thinner choroidal tumours (i.e., less than 3 mm thick) and applied to study group 2. In such tumours, the retinotomy was placed near the tumour margin and the retina was lifted slightly away by moving the cutter sideways towards the centre of the tumour. Raising the intraocular pressure for about one minute controlled bleeding on removing the cutter from the tumour. Vitrectomy, endo-laser photocoagulation and internal tamponade were not required in any case. The specimen was ejected through the vitreous cutter into a sterile universal tube by flushing the line with BSS.

5.2.2.2 Trans-scleral biopsies

Trans-scleral fine-needle aspiration biopsies (FNAB) were performed with a 25-gauge needle, which was attached to a 20ml syringe by flexible plastic tubing. (Figure 5.2).

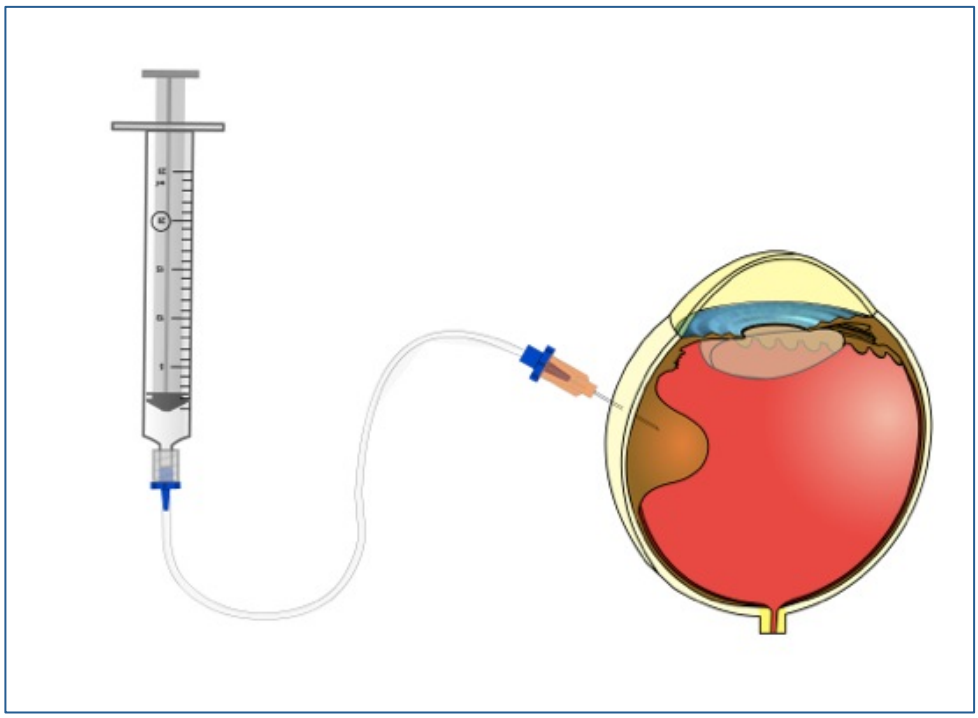

Figure 5.2 Schematic representation of the trans-scleral fine-needle aspiration biopsy technique using a 25G needle. *(Courtesy of Mr C. Groenewald; vitreoretinal surgeon, LOOC).*

An ink-mark was made on the needle at an appropriate distance from the tip corresponding to the thickness of the tumour, plus 1-2 mm extra, so that the mark would not be wiped away by contact with the sclera. The needle was abraded with artery forceps beforehand, in order to create a rough surface on which the ink would stay. The needle was passed obliquely through the sclera for 3-4 mm before being adjusted, in order to enter the tumour. Traction was applied to the plunger of the syringe while the needle tip was moved from side to side and backwards and forwards. Immediately after removing the needle, the scleral track was compressed with a cotton bud and diathermied with bipolar cautery to reduce any risk of tumour seeding outside the eye. The specimen was collected by filling the syringe with BSS and flushing the content of the tubing and needle into a sterile universal tube.

The following modification to the procedure was adopted for all patients included in study group 2: a trans-scleral incisional biopsy approach ("flap biopsy") was developed by Professor Damato, lead of the LOOC at the time, to sample anterior tumours less than 3 mm thick being treated by brachytherapy (Figure 5.3). A partial-thickness, lamellar scleral flap was created over the centre of the tumour and hinged posteriorly. Essen forceps[292] were repeatedly introduced into the tumour through a deep scleral incision, rinsing the forceps with BSS into a sterile universal tube to collect the cell pellets (at least two). The superficial scleral flap was glued in place with histoacryl adhesive and the plaque placed over the flap.

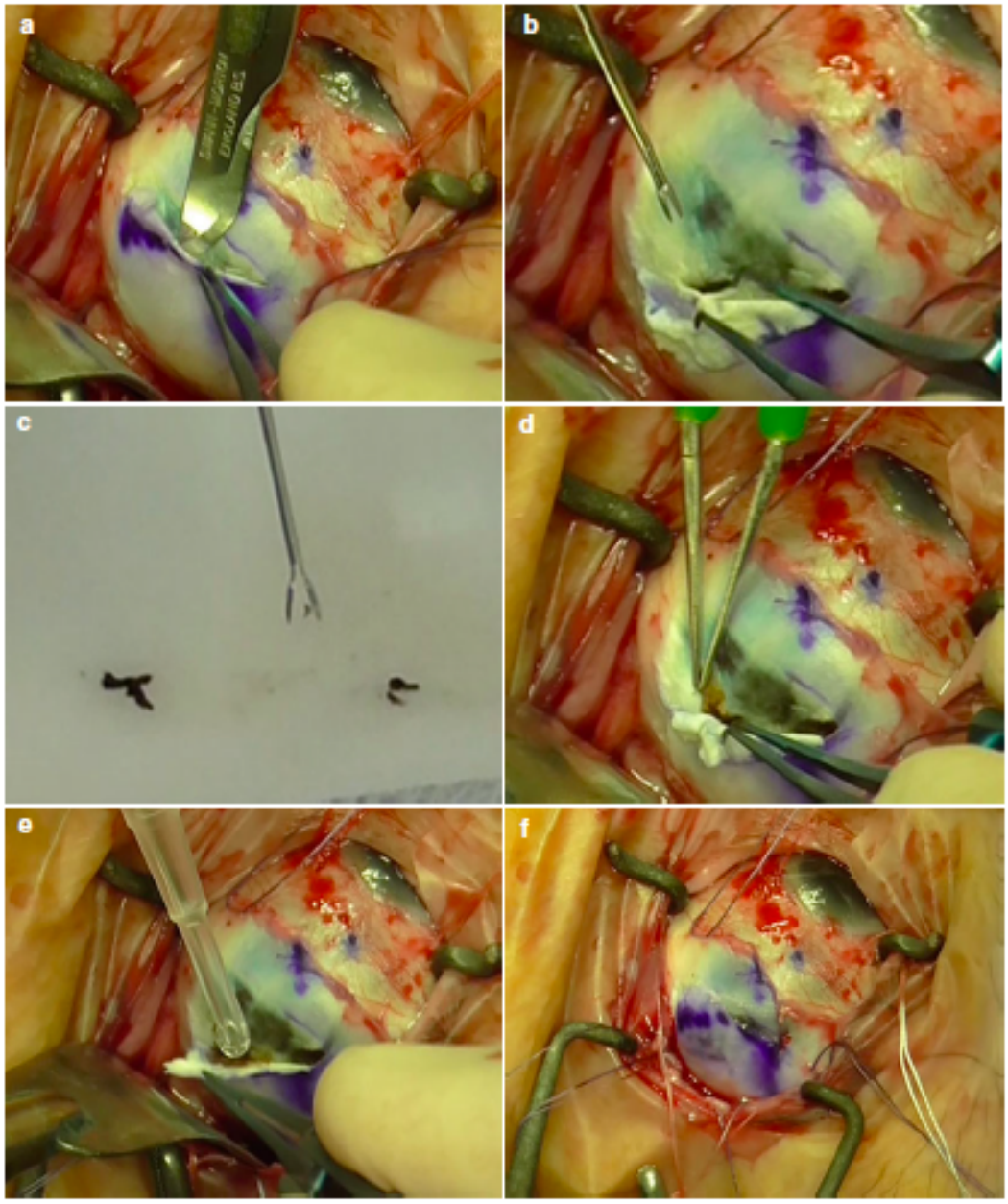

Figure 5.3 The "flap biopsy" technique developed for thin anterior choroidal tumours. A superficial, lamellar scleral flap is created (a); a deep scleral incision is made for introduction of Essen forceps into the tumour (b); the specimens are collected onto a tissue before transferring into a container (c); any pigment is treated with bipolar cautery (d); the flap is closed with tissue glue (e); if necessary, sutures are placed (f); the radioactive plaque is then inserted overlying the biopsy site. *(Courtesy of Prof. B. Damato*[293]*)*

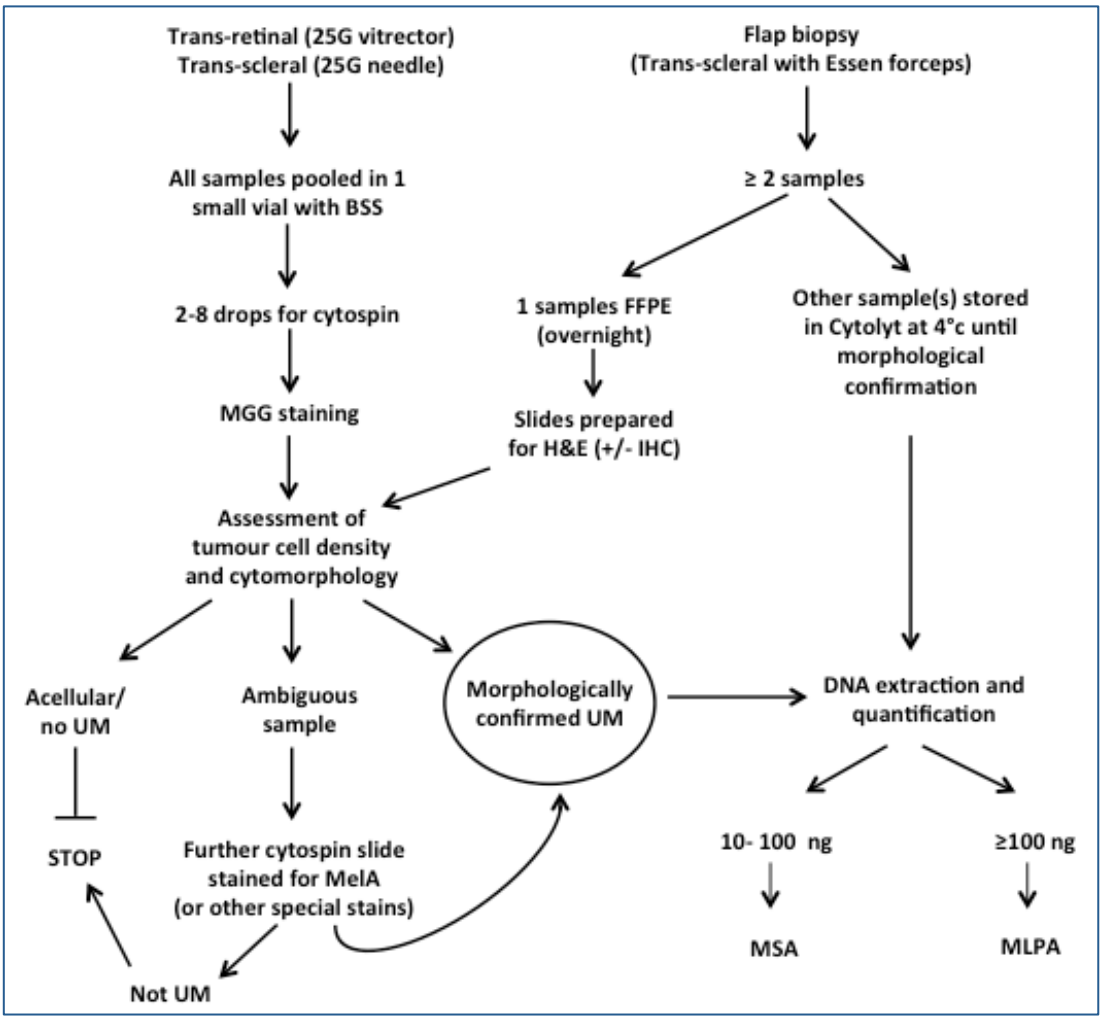

Figure 5.4 Flow diagram illustrating the pathway designed for the optimal processing of prognostic biopsy samples, depending on the surgical technique used (study group 2). Please note how cytomorphological evaluation of the sample is key in determining further steps, including molecular genetic analyses. *(Legend: BSS: balanced salt solution; MGG: May-Grünwald-Giemsa; UM: uveal melanoma; H&E: haematoxylin and eosin)*

5.2.3 Sample processing

Specimens were transported immediately without fixative to the pathology laboratory, where the sample was used as follows:

- Study group 1: 3 to 4 cytospin slides were prepared for cytomorphological analysis and immunocytochemistry; the remainder of the specimen was used for DNA extraction and subsequent molecular genetic analyses.

- Study group 2: a single cytospin slide was prepared for cytomorphological analysis allowing the preservation of the majority of the sample for DNA extraction and subsequent molecular analyses. Moreover, two different pathways were devised for handling of trans-retinal and trans-scleral FNAB versus trans-scleral flap biopsies, as the latter surgical technique yields small fragments of tumour rather than cells (Figure 5.4).

5.2.3.1 Molecular genetic analyses

Following morphological examination and confirmation of the presence of UM cells in the sample by experienced ophthalmic pathologists, DNA was extracted from the residual sample and used for molecular genetic analyses, either by MLPA or MSA, depending on the DNA yield obtained, as detailed below.

For DNA extraction, tissues were incubated for 16 hours at 56°C (Thermomixer Comfort, Eppendorf, Stevenage, UK) in 125 µl of P-buffer (50 mM Tris-HCl pH 8.2, 1 mM EDTA, 100 mM NaCl, 0.5% Tween-20, 0.5% NP40, 20 mM dithiothreitol) containing 8.2 mg of Proteinase K (Qiagen, Crawley, UK). Samples were further incubated at 37°C, following the addition of 8.2 mg of Proteinase K for 24 hours. Genomic DNA was extracted using the DNeasy Blood and Tissue kit (Qiagen) and the DNA eluted in 15-25 µl of AE buffer. DNA concentration was quantified by fluorometry (Qubit fluorometer and Broad Range DNA Quantification assay, Life Technologies, Glasgow, UK) and its quality was assessed by multiplex PCR (adapted from Dongen et al)[294], as previously described by Dopierala et al.[197]

When at least 100 ng of amplifiable DNA was obtained, MLPA was performed with the P027.B1 assay produced by MRC-Holland (Amsterdam, The Netherlands). This

kit has been specifically designed for use in UM to determine copy number alterations for gene loci on chromosomes 1, 3, 6 and 8. The kit comprises a set of 50 probes (12 control, 38 test), each hybridizing to a specific genomic sequence. As MLPA is a high-resolution multiplex PCR-based method, it is not target sequences that are amplified in the reaction, but MLPA probes that hybridise to the target sequence. In contrast to a standard multiplex PCR, a single pair of PCR primers are used for DNA amplification. The resulting amplification products can be analysed by capillary electrophoresis. By comparing the peak pattern of a tumour sample to that of non-tumour reference samples, gene dosage quotients (DQ) for individual loci are determined. Six FFPE non-tumour, normal choroid, control samples and a negative (no template) control were analysed alongside the UM test samples in each reaction. MLPA was performed in a G-Storm GS1 Thermal Cycler (Genetic Research Instrumentation Ltd, Essex, UK) as per the manufacturers' instructions and quantified using the 3130XL Genetic Analyser and GeneMapper software (Applied Biosystems, Paisley, UK). Peak heights were taken as a measure of intensity. MLPA data were analyzed using an adapted version of the Excel spreadsheet designed by Dr. Andrew Wallace of the National Genetics Reference Laboratory (NGRL), Manchester, UK (http:/www.ngrl.org.uk/Manchester/). The adapted analysis method allows for the removal of any control loci from an individual MLPA assay if the DQ is not within the range for a normal (disomic) copy number (0.85–1.14). MLPA data were considered reliable if the number of control loci within the normal range was ≥6 and if the standard deviation (SD) of their DQs was <0.2. The DQ for each gene loci was categorized as suggested by the NGRL as

follows: deletion (D), ≤0.65; borderline loss (E), 0.65-0.84; normal=diploid (N), 0.85-1.14; borderline amplification (Q), 1.15-1.35; and amplification (A) >1.35.

When the yield of DNA was <100 ng, MSA was used to detect regions of loss of heterozygosity on chromosome 3. Microsatellites are small repeat regions of 1-6 base pairs generally found in the non-coding regions of the genome. The region containing the microsatellite is amplified by PCR using forward and reverse primers that flank the microsatellite. The size of the DNA amplified can then be determined by the number of repeats present in the microsatellite on that allele. One of each primer pair is fluorescently tagged to allow quantitation by capillary electrophoresis. A comparison of the peak area of tumour DNA (biopsy specimens) and normal DNA (matched blood sample) allows the determination of allele ratio in the tumour.

The protocol for MSA analysis of chromosome 3 (p and q arms) used in this study is based on the validated method published by Dr Zeschnigk's group.[295]

5.2.3.2 Cytomorphological assessment

In an effort to understand whether examination of cytospin slides (which can be done within a few hours) could predict the likelihood to obtain a genetic result (process which requires several days), May-Grünwald-Giemsa (MGG)-stained cytospin slides for all patients in study group 1 were retrieved from the Pathology archives, the pathology report reviewed, and the cytospins scored by three independent observers in terms of the overall degree of cellularity (i.e. percentage

of the cytospin area occupied by cells of any type). This percentage was then broken down into the proportions occupied by; 1) tumour cells, 2) red blood cells, 3) white blood cells and 4) other cells, such as macrophages. In the case of discrepancy, slides were re-assessed together with the reporting pathologist and a consensus reached. Examples of this scoring system are given in Figure 5.5. Correlations were drawn between the score of tumour cellularity on the slide and the amount of DNA extracted from the sample.

5.2.4 Data analysis

All patient data were retrieved and all samples analysed according to their ability to: (1) yield cytomorphological information; and (2) provide chromosome 3 classification. Secondary analyses included: intraoperative complications; postoperative complications; tumour dissemination.

All statistical analyses were carried out using SPSS (IBM) version 20 (SPSS Science, Chicago, IL) in collaboration with Prof Azzam Taktak, Consultant Clinical Scientist, Department of Clinical Physics and Engineering, University of Liverpool.

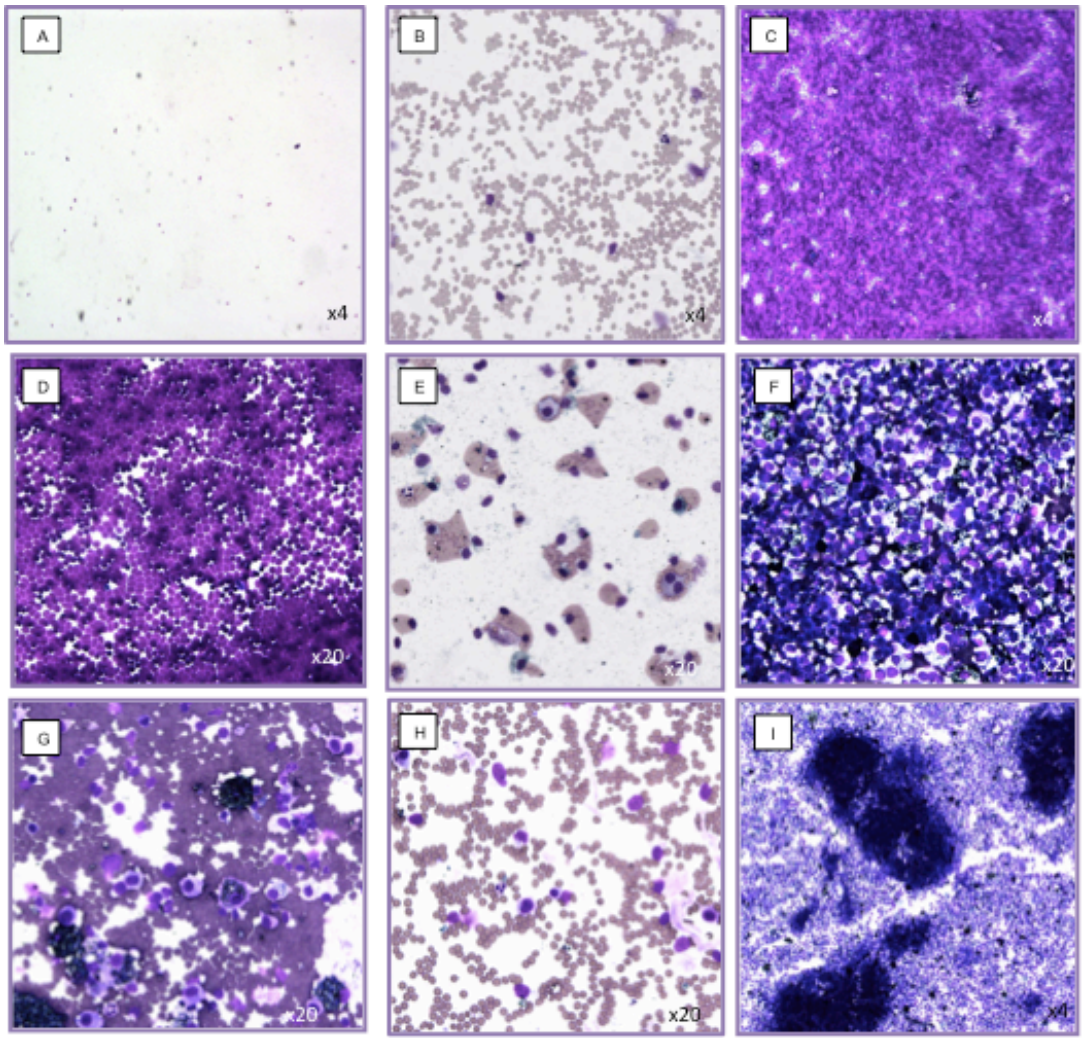

Figure 5.5 Scoring of choroidal melanoma biopsy content (cytospin slides stained with MGG). The overall cellularity of the specimen is classified as: A) low – 5%; B) medium – 50%; C) high -100%. The presence of melanoma cells (as percentage of the overall cellularity) is classified as: D) absent – 0%; E) medium – 30%; F) high – 100%. The presence of other cell types (as percentage of the overall cellularity) is also noted, for example: G) erythrocytes- 80%, and macrophages – 10%; H) leucocytes – 5%. The use of Essen forceps in trans-scleral incisional biopsies allows for preservation of clumps of uveal melanoma tissue, rather than loose cells, as shown in figure 1I.

5.3 Results

5.3.1 Clinical characteristics

Between January 2011 and June 2013 (i.e. 18 months), 232 consecutive UM patients underwent prognostic tumour biopsy of a choroidal melanoma. The patients (123 male, 109 female) had a median age of 59 years (range, 25 – 82). The tumour was located in the right eye in 111 patients and in the left eye in 121. The site of origin was considered to be the choroid in 190 patients and ciliary body in 42. The tumours had a median LBD of 11.4 mm (range 4.1-20.8) and a median thickness of 3.4 mm (range 0.7-10.3), with 47% measuring less than 3 mm in thickness.

As detailed in Table 5.2, the clinical characteristics of the tumours in group 1 and group 2 were not statistically significantly different. In particular, although the number of patients differed between the two groups, the tumour size distribution within the groups was comparable, as illustrated in Figure 5.6.

Table 5.2 Clinical characteristics of the study population

	Overall n= 232	Group 1 n= 142	Group 2 n= 90	P value
Sex				0.312*
Male	*123*	*72*	*51*	
Female	*109*	*70*	*39*	
Age Mean (SD)	59 (13.948)	60 (13.317)	58 (14.892)	0.474+
Eye				0.601*
Right	*111*	*66*	*45*	
Left	*121*	*76*	*45*	
Tumour height Mean (SD)	3.4 (1.808)	3.4 (1.8451)	3.6 (1.7368)	0.066°
LBD Mean (SD)	11.4 (3.0883)	11.4 (3.0678)	11.4 (3.1374)	0.921+
Tumour location				0.081*
Pre-equatorial	*32*	*14*	*18*	
Post-equatorial	*109*	*68*	*41*	
Mixed	*91*	*60*	*31*	
Tumour treatment				0.115*
Ru Plaque	*151*	*69*	*53*	
Proton beam	*81*	*31*	*37*	

SD: standard deviation; LBD: largest basal diameter; Ru: ruthenium-106
** χ2 test between the two groups;+ Student's t-test; ° Mann-Whitney test*

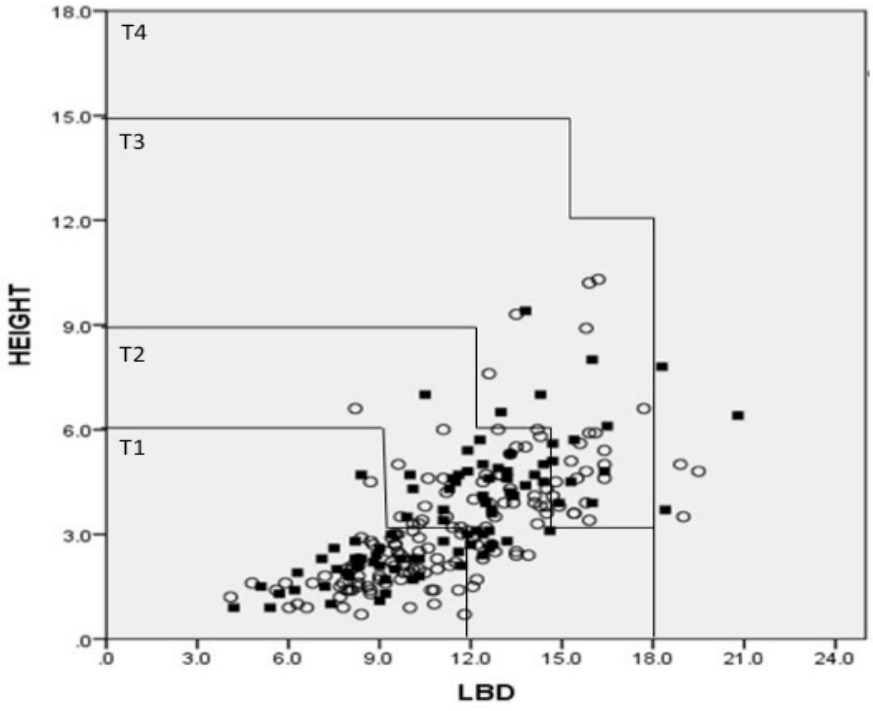

Figure 5.6 Scatterplot showing the size distribution of the tumors according to the TNM staging for both groups. O: group 1; ■: group 2.

5.3.2 Surgical results

Treatment consisted of: Ruthenium plaque in 151 cases (65%) and PBR in 81 cases (35%). The surgical treatment was similar in group 1 and group 2 (Student's T test, p=0.115).

Overall, the mean tumour thickness was significantly lower for trans-retinal biopsies (3.09±0.175 mm) than for trans-scleral biopsies (3.8±0.141 mm) (T-test, p = 0.003). The mean LBD was also significantly lower for trans-retinal biopsies (10.48±3.06 mm) than for trans-scleral biopsies (12.6±2.7 mm) (T-test, p < 0.001).

Sixty-one percent (86/142) of tumours in group 1 and 50% (45/90) of tumours in group 2 were biopsied trans-retinally. For both groups, the biopsy technique adopted for tumours of different height categories, as suggested by McCannel et al.[283], are detailed in Table 5.3. Tumours < 3 mm in thickness are the most challenging ones to safely biopsy. In group 1, only 22% (16/72) of these were biopsied transclerally at the time of plaque insertion, whereas all other patients required a separate surgical procedure for trans-retinal biopsy. Changes in practice and improvements in the biopsy technique (flap biopsy) adopted for cases in group 2 resulted in an increase to 37% (14/38) of thin tumours undergoing trans-scleral biopsy

5.3.2.1 Surgical complications

Group 1

Trans-scleral biopsy was without complication in 71% (40/56) of cases. Thirteen out of 56 patients experienced limited sub-retinal or localised perilesional bleeding. A single case had mild transient vitreous haemorrhage and in two cases, retinal

perforation occurred: one patient required further surgery for retinal detachment repair, whereas the other was successfully managed with pneumatic retinopexy and laser.

Trans-retinal biopsy was without complication in 67% (58/86) of cases. Limited and transient sub-retinal bleeding occurred in three cases, perilesional bleeding occurred in five cases and mild vitreous haemorrhage was noted in 15. All of the above resolved spontaneously during the follow-up time. Further surgery was needed in 6% (5/86) of cases: to manage severe vitreous haemorrhage in four patients, and to repair retinal detachment in one.

Group 2

Peri-lesional bleeding was noted in only one case (2%) among the 45 patients who underwent trans-scleral biopsy. With the newly introduced flap technique no cases of retinal perforation or retinal detachment occurred; however, one patient needed further surgery to repair a scleral wound dehiscence caused by poor suturing of the conjunctiva over the flap after plaque removal. For patients undergoing trans-retinal biopsy, the rate of peri-operative complications was similar to that in group 1 (14/45, 31%). In seven cases there was limited sub-retinal or peri-lesional bleeding, which resolved spontaneously. Of seven patients who developed vitreous haemorrhage: one needed vitrectomy; two decided to undergo enucleation because of old age and poor visual acuity of the eye related to tumour size and location; four were kept under observation and the haemorrhage resolved spontaneously.

Table 5.3 Morphological and genetic results, grouped by tumour height and biopsy technique

	GROUP 1 (n=142)			GROUP 2 (n=90)		
	Tumour Height			Tumour Height		
	< 3 mm	3-5 mm	> 5 mm	< 3 mm	3-5 mm	> 5 mm
	n= 72 (51%)	n= 51 (36%)	n= 19 (13%)	n= 38 (42%)	n= 38 (42%)	n= 14 (16%)
Cytomorphology						
Not defined	7	3	0	3	0	0
Spindle	41	25	11	23	18	6
Mixed	8	12	2	5	11	4
Epithelioid	11	7	4	6	9	4
No UM cells	5	4	2	1	0	0
Genetic test						
MLPA	10	14	8	8	17	6
MSA	40	20	6	28	17	8
None	22	17	5	2	4	0
Biopsy technique						
Trans-retinal	56	19	11	24	13	8
Trans-scleral	16	32	8	14	25	6

UM= uveal melanoma, MLPA= multiplex ligation-dependent probe amplification, MSA= microsatellite analysis

5.3.3 Follow-up

Follow-up information was available for 213/232 patients (92%), as the others were overseas patients. Over a median follow-up period of 9 months (range 2-32), no case of endophthalmitis, orbital dissemination or local treatment failure was noted.

5.3.3.1 Metastatic disease

Overall, 15/232 (6%) UM patients developed metastatic disease during the follow-up time. The chromosome 3 status for these patients was: monosomy 3 in 8 cases, allelic imbalance in 2 cases, disomy 3 in 1 case, indeterminate in 1 case. For 3 cases no genetic information could be obtained, as the biopsy did not yield sufficient DNA for genetic analyses.

5.3.4 Cytomorphological results

In group 1, cytospins stained with MGG were prepared for the cytomorphological assessment of all biopsy specimens. Confirmation of the presence of melanoma cells was possible in 131/142 (92%) biopsy samples. For 11 biopsies, the sample provided was either completely acellular or devoid of tumour cells; 2/86 (2%) were trans-retinal biopsies and 9/56 (16%) trans-scleral biopsies. The median overall cellularity of the cytospin was 50% (range 1-100%). Tumour thickness did not influence the overall biopsy cellularity (Mann-Whitney Z=-0.146, p=0.884). The median tumour cell component of the cytospin was 20% (range 0-100%), with red blood cells accounting for the majority of other cells. This was not influenced by surgical technique. As expected, tumour cell composition of the cytospin showed a strong positive correlation with the DNA yield (Spearman's r=0.732, p<0.001). Macrophages were present in 16/142 (11%) samples. White blood cells were also present in 23/142 (16%) of samples, but only rarely contributed to more than 5% of overall biopsy cellularity.

Overall, biopsies provided cytopathological information in 92% (131/142) of cases in group 1 and 99% (89/90) of cases in group 2. Details of cytomorphological classification were taken from the official report issued by the Ophthalmic Pathologists and used in the prognostication algorithm for the individual patient. UM cells were classified as (group 1 and group 2, respectively): spindle in 77/142 (54%) and 47/90 (52%); mixed in 22/142 (15%) and 20/90 (22%); epithelioid in 22/142 (15%) and 19/90 (21%); definite UM cells but with ambiguous morphology in 10/142 (7%) and 3/90 (3%). Details of the cytomorphology for biopsies grouped by tumour thickness are shown in Table 5.3.

5.3.5 Genetic results

As mentioned, genetic studies were only performed on samples with confirmed UM cellularity and a yield of amplifiable DNA ≥10ng. These guidelines reduced the number of samples eligible for genetic analyses. A detailed explanation of the attrition of specimens is provided in Figure 5.7.

In group 1, of the 131 cases for which cytomorphological confirmation for the presence of melanoma cells was possible, 27 (21%) yielded insufficient DNA for genetic analysis by either MLPA or MSA. The breakdown of these 27 cases is as follows: 17 were trans-retinal samples and 10 were trans-scleral biopsies. There was no significant difference in the tumour thickness between those cases yielding sufficient DNA and those that did not (T-test between mean heights, p =0.688)

Genetic testing was performed in 98 of the remaining 104 DNA samples; in six cases, DNA was extracted; however, the concentration was below that required for MLPA and matched bloods were not available with which to perform MSA. Of the 98 cases, 66 were analysed by MSA and 32 by MLPA. Fifty-one cases were reported as disomy 3 and 40 cases as monosomy 3. Three cases passed the quality control assessment for MLPA data but could not be unequivocally classified as either disomy 3 or monosomy 3. Four cases, in which MSA was performed, showed allelic imbalance. In conclusion, genetic analysis was performed in 75% (98/131) of cases in group 1. Of the 98 cases for which genetic analyses were performed, chromosome 3 classification, as either disomy 3 or monosomy 3, was possible in 93% (91/98). Overall in group 1 genetic analysis successfully yielded a result for chromosome 3 status in 70% (91/131) of cases with confirmed UM cells.

In group 2, of the 89 cases for which cytomorphological confirmation for the presence of melanoma cells was possible, six (7%) yielded insufficient DNA for genetic analysis by either MLPA or MSA (Figure 5.7). The breakdown of these six cases is as follows: two cases were trans-retinal samples and four were trans-scleral biopsies. There was no significant difference in the tumour thickness between those cases yielding sufficient DNA and those that did not (T-test between mean heights, $p = 0.677$).

Genetic testing was performed in all 83 remaining DNA samples in Group 2: 52 were analysed by MSA and 31 by MLPA. Fifty-five cases were reported as disomy 3 and 24 cases as monosomy 3. Three cases, in which MSA was performed, showed allelic imbalance. One case examined by MLPA could not be classified as either disomy 3 or monosomy 3. In conclusion, genetic analysis was possible in 93% (83/89) of cases in group 2. Of the 83 cases in which genetic analyses were performed, chromosome 3 classification, as either disomy 3 or monosomy 3, was possible in 95% (79/83). Overall in group 2 genetic analysis successfully yielded a result for chromosome 3 status in 89% (79/89) of cases with confirmed UM cells.

Details of the genetic test performed for biopsies grouped by tumour thickness are shown in Table 5.3. Following introduction of the new procedures, an improvement in the overall capacity to provide a chromosome 3 classification was achieved. This was particularly evident in the very thin tumour group (<3 mm), where the success rate increased from 69% (50/72) in group 1 to 95% (36/38) in group 2 (Z-test for Binomial distribution, $p < 0.001$).

Figure 5.7 Flowchart explaining the attrition of specimens for genetic assessment

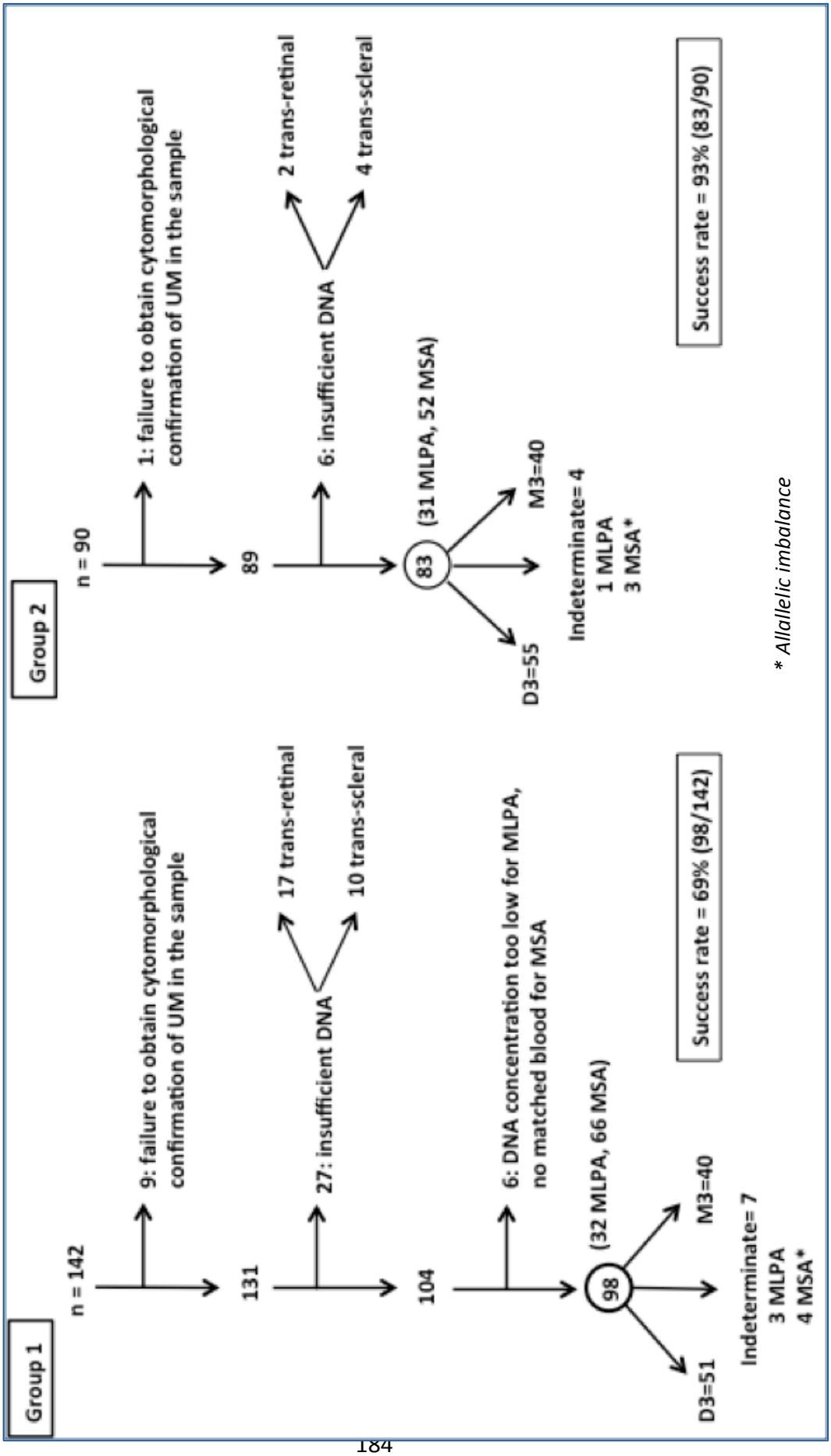

5.4 Discussion

We audited the results of prognostic biopsies for UM patients treated in LOOC over an 18-month time period by retrospectively assessing the yield of prognostic information provided weighed against surgical complications (study group 1). We identified possible 'pitfalls' in the process and implemented a change of practice, which was assessed prospectively over 12 months (study group 2), showing an improvement in the cytogenetic results obtained and a reduction in surgical complications.

In contrast to previous studies,[282, 283, 285, 296, 297] we do not perform molecular genetic analyses on the specimen without cytomorphological examination, as the presence of macrophages or leucocytes (or indeed a different malignancy!) may affect the results and provide false reassurance to the patients.[298] In this study, we reviewed the cytospin slides for all tumours and assessed the presence of tumour cells, showing a strong correlation with the amount of DNA extracted from the specimen. Moreover, it is well known that the presence of epithelioid melanoma cells is a poor prognostic factor,[223] hence cytomorphological examination adds meaningful information to our predictive model even in the absence of molecular genetic results. For all of the above reasons, we believe that cytomorphological examination of a cytospin slide is essential, and should be performed prior to any molecular genetic analysis in UM.

Monosomy 3 remains the strongest predictive factor for the development of metastatic disease,[72] thus, the aim for all prognostic biopsies is that they should yield enough DNA with which to perform molecular analyses. About 50 % of the

tumours in our series were thinner than 3 mm, which is a notorious challenge for obtaining meaningful samples.[284] In agreement with other authors,[282, 296, 299] we found in the first phase of this study that trans-scleral FNAB of small UM is successful for molecular analysis only in about 70% of cases; therefore we have adopted alternative surgical techniques to obviate such problem. Through this combination of techniques, the overall success of biopsy (i.e. giving the patient cytomorphological and chromosome 3 information) in this series did not depend on tumour thickness. Trans-retinal biopsy using a 25G vitreous cutter has been used in 60% of the cases in this series, providing successful specimens even in tumours less than 1 mm in thickness. However, such a technique is associated with a higher rate of local complications, mainly intravitreal bleeding. Therefore, the senior author has developed a new trans-scleral approach, creating a scleral flap and introducing the Essen forceps through a small incision over the tumour. Such a technique, adopted only since July 2012, is now being routinely used for pre-equatorial melanomas of less than 3 mm in thickness. Further studies with a longer follow-up are underway and will be necessary to determine the long-term risks and benefits associated with such an approach. Preliminary results presented here, however, are promising for the large size of the specimens obtained and the lack of complications when such biopsy is performed at the time of plaque insertion, as long as care is taken in properly closing the conjunctiva over the flap after plaque removal.

To enhance our capacity to provide genetic results to the patient, we have introduced MSA for determination of chromosome 3 status, which requires only 10ng DNA as compared with a minimum of 100ng for MLPA. MSA was used for genetic testing in the majority of biopsies obtained from UM <3 mm in thickness.

At present, the other most widely utilised technique for analysis of small samples is GEP. As detailed in Chapter 1, this commercial platform has been developed using a panel of 15 genes (12 test genes and 3 control genes), the expression of which assigns UM to two prognostic subgroups: class 1 (low metastatic risk) and class 2 (high metastatic risk). A collaborative study on 459 patients reported a success rate of providing a prognostic class in 97% of cases. Although this figure is slightly higher than that reported for Group 2 cases in our study, there is currently insufficient follow-up of these patients to determine the accuracy of these prognostic data for patient survival. Moreover, GEP analysis is performed in a commercial setting (Castle Biosciences, Inc.) with high costs that would not be covered by NHS England. Many other European colleagues are faced with similar economic restraints;[300] hence our efforts are to provide the best possible service at an affordable cost. Moreover, GEP analysis is routinely performed without any matched cytological analysis of the sample. A recent study of 159 patients with matched biopsies being sent for cytological as well as GEP analysis showed that cytological diagnosis was possible for only 125/159 (79%) samples whereas GEP gave results in all but one (99%).[297] The authors interpret this as very positive, whereas we look at it with concern and stress the importance of a cytological diagnosis to confirm the presence of UM cells in the sample prior to DNA extraction, given that GEP provided a prognostic result for a tumour subsequently identified as a choroidal metastasis.[298] Augsburger et al.[301] have recently reported an 11% discrepancy in GEP classification of the same UM when biopsied (FNAB) at two different sites, which were then tested independently. The authors conclude that "sampling of a clinically diagnosed posterior uveal melanoma at a single site for prognostic GEP

testing is associated with a substantial probability of misclassification" and recommend two-site sampling and independent GEP testing, making the whole process even more expensive.

The issue of intratumoural genetic heterogeneity has been debated for a long time, and one of the potential criticisms to any study of prognostic biopsies, is that a single biopsy may be subject to sampling error for monosomy 3.[302] We have recently performed a retrospective analysis of genetic data from 28 cases for which both a biopsy and a secondary tumour specimen from the same UM (enucleation or endoresection) had been tested by MSA or MLPA. The data from this analysis showed 100% concordance between the chromosome 3 status of the biopsy and the subsequent secondary tumour specimen (Coupland et al 2015, ARVO abstract 2013; manuscript submitted). Nevertheless, we discuss the risk for tumour heterogeneity with the patient and clearly state it on the report, which is written by a dedicated Ophthalmic Pathologist who interprets the genetic data in the light of the clinical and cytomorphological characteristics of each individual tumour. A definitive answer on the accuracy of prognostication for biopsies samples as described in this study will only be available after many years of follow-up, but this was not the aim of the current study.

Performing a prognostic biopsy may also be questioned due to the lack of current effective treatment modalities for those patients who develop metastatic disease. However, with the identification of new therapeutic targets and the introduction of clinical trials for adjuvant systemic treatment,[303] prognostication is essential to identify those patients who could benefit from such treatments before the development of clinically evident, advanced metastatic disease, which is known to

be refractory to therapy. Our studies also demonstrate that prognostication is welcomed by the patients in order to help prepare themselves and their family for any eventuality.[291] We have found that the unhappiest patients are those whose biopsy has failed to yield a prognostic result. We therefore consider biopsy failure to be a serious complication, which is why we have developed a variety of surgical techniques and laboratory methods to address this problem.

Specific limitations of our study are linked mainly to the retrospective nature of the audit, for example; biopsies being performed by different surgeons with different techniques, lack of matched blood samples with which to perform MSA analyses in a few cases. However, we believe that these reflect important "real life" experiences that are useful to colleagues planning to establish prognostic testing in their units. Performing and interpreting prognostic biopsies is a challenge both for the clinical and the laboratory team and requires close collaboration between the two. While performing this audit we identified and solved pitfalls in the process, such as: clearly stating in the request form whether a biopsy was for diagnostic or prognostic analyses, so that only a minimum number of cytospin slides would be prepared, saving most of the specimen for DNA extraction; collecting a small blood sample for all patients undergoing prognostic biopsy, so that baseline DNA could be extracted for MSA analysis should the uveal specimen be too small for MLPA; informing the clinical team if a transcleral FNAB specimen done at the time of plaque insertion was acellular, so that another sample could be collected trans-retinally at the time of plaque removal.

In conclusion, prognostic biopsy is a safe procedure that can yield useful prognostic information in over 90% of cases (cytomorphology in 99%, chromosome 3 status in

93%). Using a combination of surgical techniques depending on the size and location of the tumour improves the chances of getting an adequate specimen for cytomorphological and molecular genetic analyses. Cytomorphological examination of a cytospin from the specimen is essential to determine cellular composition and thus reduce the risk of a falsely reassuring prognosis. Using a combination of molecular prognostic techniques such as MLPA and MSA maximises the chance of providing a genetic result from the biopsy specimen. A close collaboration between the clinical and molecular pathology team is essential to optimise the success of the overall process and provide the patient with meaningful information.

Chapter 6

Summary

6.1 Conclusions and future perspectives

Despite successful treatment of the primary tumour, UM remains a fatal disease in those patients who develop metastatic disease. Survival is improved by early detection of liver metastases, which can then be treated with locoregional therapies.

As discussed in Chapter 1, previous work done by members of the LOORG has focused on genetic analyses of UM, leading to the creation and clinical validation of a prognostic tool to stratify patients as being at HR or LR of developing metastatic disease. However, the mechanisms responsible for the development of metastatic disease in UM are still largely unknown; therefore no adjuvant treatment is currently offered to HR patients to prevent development of fatal disease. As the time to discovery of clinically detectable metastases can range from months to decades, a secreted biomarker(s) that could be routinely tested in blood is much needed.

The scope of the work presented in this thesis was to use proteomics as a tool to identify potential novel, UM-specific biomarkers. Moreover, the proteomic data acquired would complement our genomic and transcriptomic information, with the ultimate aim of increasing our understanding of UM development and dissemination.

In Chapter 2 we described the use of iTRAQ labelling and MS to compare the proteome of UM tissue samples at HR versus LR of developing metastatic disease.

The quantification of proteins in our samples, proteomic analysis and further IHC validation has led to the identification of two novel prognostic and potentially therapeutic targets, S100A6 and the tumour suppressor PDCD4. Further examination of these two proteins will be undertaken; S100A6 as prognostic biomarker in the peripheral blood of UM patients, and PDCD4 as potential therapeutic target. In particular, immunoprecipitation studies in lung cancer have shown that PDCD4 is part of a molecular complex that also comprises the ribosomal protein S6 kinase 2 (S6K2) and the heterogeneous nuclear ribonucleoprotein A1 (hnRBNPA1). This mediates chemoresistance by promoting the translation of the anti-apoptotic proteins BCL-XL and XIAP.[304, 305] A collaboration has been established with Prof. Michael Seckl and his group at Imperial College in London to investigate the relationship between hnRNPA1/SK62/PDCD4 in UM. Further studies to investigate the relationship between PDCD4 and its regulation by the oncogene microRNA-21 as described for other tumours[176, 306, 307] are also warranted.

In Chapter 3 we described another proteomic approach to identify potential biomarkers of metastatic disease in UM: comparative proteomic analyses of the secretome from short-term primary cultures of HR and LR UM, as well as normal choroidal melanocytes, using label-free nanoLC-MS/MS. This led to the identification and quantitation of almost 2000 proteins, with more than 30% of these identified as secreted and/or previously identified in exosomes. Using these data an 18 protein signature, able to discriminate between HR and LR UM was identified.. Further validation of the non-exosomal secreted proteins within the 18 protein signature will be necessary in secretome samples and in the peripheral

blood of UM patients. This has the potential of being translated into a clinically useful assay to detect early development of metastatic disease. Furthermore, in view of the number of exosomal proteins identified in the secretome and the current interest in the role of these extracellular microvesicles in tumour biology, further work is now being undertaken within the LOORG to study the role of exosomes in UM. In particular, analysis of their cargo and how this may aid tumour progression will be conducted.

Further interrogation of proteomic data derived from both the secretome analysis and iTRAQ run A will be performed using the IPA software to increase our understanding of the differences between normal choroid, LR UM and HR UM in terms of protein expression and pathway activation and this information fed back into the ongoing analyses.

In recent years, there has been a body of evidence across a number of tumour types supporting the clinical utility of detecting and characterising CTC. As reported in Chapter 4, we conducted a pilot study on peripheral blood samples using the FDA approved CellSearch® platform to enumerate CTC in UM patients at LR, HR or with overt metastatic disease. CTC were detected in HR tumours and were not present in LR UM, however, only two of the 14 HR UM displayed ≥2 CTC. Although, the number of CTCs detected in the patients with overt metastatic disease was significantly higher it also varied widely, ranging from no CTC detected to 510 CTC in a single patient. These data called into question the prognostic value of using such a system for CTC detection in UM. We also conducted a small study to examine expression of the chemokine receptor CD184 in a panel of UM cell lines in

the search of alternative surface markers for CTC. This work showed that determining which antibody may be most suitable remains difficult, as studies of surface antigen expression on cell lines may not be truly representative of primary UM cells. Advances in the characterisation of primary UM samples are required and could lead to the identification of alternative cell markers for the development of a UM customised CTC detection kit. Moreover, CTC capture and characterisation (rather than enumeration) is an important field of research worth pursuing, as it could provide unparalleled means to understand metastatic biology and identify relevant therapeutic targets.

Chapter 5 describes an audit of the procedures undertaken during the acquisition and processing of prognostic biopsies from UM tumours treated conservatively. In this audit, pitfalls and limitations of procedures were identified leading to the introduction of modifications to both the surgical technique and the specimen handling and downstream analyses. By introducing revisions to both surgical and pathological procedures the success rate for achieving cytomorphological and genetic classification increased from 69% to 93%. This is an important improvement in the ocular oncology service provision as more and more patients, who are being treated by radiotherapy, wish to know their prognosis, and in particular their chromosome 3 status. This would become even more important should an adjuvant treatment be approved for HR UM patients, as those with an unsuccessful biopsy and therefore incomplete risk stratification may be denied treatment.

In conclusion, the work conducted throughout this PhD has provided further insight into the molecular characteristics that can differentiate between the aggressive high metastatic risk UM from those with a low metastatic risk. Unlike the genetic code, measuring changes in protein expression allows us to monitor what is happening in patients in “real-time”, generating unique insight into the biological processes occurring during tumour development and progression. Proteomics itself, however, is not without its challenges, due to dynamic changes in expression, splice variants and the influence of post-translational modifications. Thus, the greatest biological insight is likely to come from the integration of proteomic data with the genomic and transcriptomic data already generated by LOORG.

Finally, this PhD has been a unique learning experience for me personally, not only in terms of laboratory techniques and scientific outputs, but also especially in terms of independent thinking, problem solving and perseverance.

Appendices

- **Appendix 1** Comparison of the proteins identified in the different iTRAQ runs
- **Appendix 2** Semi-quantitative immunohistochemical validation of iTRAQ relative quantification
- **Appendix 3** Optimization of secretome production
- **Appendix 4** Details of the 18 protein signature discriminating between HR and LR secretome samples

Please open the CD-ROM attached to visualise the files above

Bibliography

1. Egan KM, Seddon JM, Glynn RJ, et al. Epidemiologic aspects of uveal melanoma. Surv Ophthalmol 1988;32(4):239-51.

2. Singh AD, Topham A. Incidence of uveal melanoma in the United States: 1973-1997. Ophthalmology 2003;110(5):956-61.

3. Yonekawa Y, Kim IK. Epidemiology and management of uveal melanoma. Hematol Oncol Clin North Am 2012;26(6):1169-84.

4. Hu DN, Yu GP, McCormick SA, et al. Population-based incidence of uveal melanoma in various races and ethnic groups. Am J Ophthalmol 2005;140(4):612-7.

5. Singh AD, Shields CL, Shields JA, Sato T. Uveal melanoma in young patients. Arch Ophthalmol 2000;118(7):918-23.

6. Singh AD, De Potter P, Fijal BA, et al. Lifetime prevalence of uveal melanoma in white patients with oculo(dermal) melanocytosis. Ophthalmology 1998;105(1):195-8.

7. Singh AD, Shields CL, Shields JA, et al. Uveal melanoma and familial atypical mole and melanoma (FAM-M) syndrome. Ophthalmic Genet 1995;16(2):53-61.

8. Specht CS, Smith TW. Uveal malignant melanoma and von Recklinghausen's neurofibromatosis. Cancer 1988;62(4):812-7.

9. Singh AD, Damato B, Howard P, Harbour JW. Uveal melanoma: genetic aspects. Ophthalmol Clin North Am 2005;18(1):85-97, viii.

10. Singh AD, Shields CL, De Potter P, et al. Familial uveal melanoma. Clinical observations on 56 patients. Arch Ophthalmol 1996;114(4):392-9.

11. Abdel-Rahman MH, Pilarski R, Cebulla CM, et al. Germline BAP1 mutation predisposes to uveal melanoma, lung adenocarcinoma, meningioma, and other cancers. J Med Genet 2011;48(12):856-9.

12. Hoiom V, Edsgard D, Helgadottir H, et al. Hereditary uveal melanoma: a report of a germline mutation in BAP1. Genes Chromosomes Cancer 2013;52(4):378-84.

13. Cebulla CM, Binkley EM, Pilarski R, et al. Analysis of BAP1 Germline Gene Mutation in Young Uveal Melanoma Patients. Ophthalmic Genet 2015:1-6.

14. Vajdic CM, Kricker A, Giblin M, et al. Sun exposure predicts risk of ocular melanoma in Australia. Int J Cancer 2002;101(2):175-82.

15. Eagle Jr R. Eye pathology: an atlas and text, Second ed. Philadelphia, PA Lippincott Williams & Wilkins, 2011.

16. Damato BE, Coupland SE. Differences in uveal melanomas between men and women from the British Isles. Eye (Lond) 2012;26(2):292-9.

17. Damato EM, Damato BE. Detection and time to treatment of uveal melanoma in the United Kingdom: an evaluation of 2,384 patients. Ophthalmology 2012;119(8):1582-9.

18. Accuracy of diagnosis of choroidal melanomas in the Collaborative Ocular Melanoma Study. COMS report no. 1. Arch Ophthalmol 1990;108(9):1268-73.

19. Kujala E, Damato B, Coupland SE, et al. Staging of ciliary body and choroidal melanomas based on anatomic extent. J Clin Oncol 2013;31(22):2825-31.

20. Kivela T, Kujala E. Prognostication in eye cancer: the latest tumor, node, metastasis classification and beyond. Eye (Lond) 2013;27(2):243-52.

21. Shields CL, Shields JA, Kiratli H, et al. Risk factors for growth and metastasis of small choroidal melanocytic lesions. Ophthalmology 1995;102(9):1351-61.

22. Shields CL, Demirci H, Materin MA, et al. Clinical factors in the identification of small choroidal melanoma. Can J Ophthalmol 2004;39(4):351-7.

23. Shields CL, Furuta M, Berman EL, et al. Choroidal nevus transformation into melanoma: analysis of 2514 consecutive cases. Arch Ophthalmol 2009;127(8):981-7.

24. Kivela T. Diagnosis of uveal melanoma. Dev Ophthalmol 2012;49:1-15.

25. Stanga PE, Lim JI, Hamilton P. Indocyanine green angiography in chorioretinal diseases: indications and interpretation: an evidence-based update. Ophthalmology 2003;110(1):15-21; quiz 2-3.

26. Shields JA, Mashayekhi A, Ra S, Shields CL. Pseudomelanomas of the posterior uveal tract: the 2006 Taylor R. Smith Lecture. Retina 2005;25(6):767-71.

27. The American Brachytherapy Society consensus guidelines for plaque brachytherapy of uveal melanoma and retinoblastoma. Brachytherapy 2014;13(1):1-14.

28. Jampol LM, Moy CS, Murray TG, et al. The COMS randomized trial of iodine 125 brachytherapy for choroidal melanoma: IV. Local treatment failure and enucleation in the first 5 years after brachytherapy. COMS report no. 19. Ophthalmology 2002;109(12):2197-206.

29. Damato B, Patel I, Campbell IR, et al. Local tumor control after 106Ru brachytherapy of choroidal melanoma. Int J Radiat Oncol Biol Phys 2005;63(2):385-91.

30. Gunduz K, Shields CL, Shields JA, et al. Radiation complications and tumor control after plaque radiotherapy of choroidal melanoma with macular involvement. Am J Ophthalmol 1999;127(5):579-89.

31. Bergman L, Nilsson B, Lundell G, et al. Ruthenium brachytherapy for uveal melanoma, 1979-2003: survival and functional outcomes in the Swedish population. Ophthalmology 2005;112(5):834-40.

32. Desjardins L, Lumbroso-Le Rouic L, Levy-Gabriel C, et al. Treatment of uveal melanoma by accelerated proton beam. Dev Ophthalmol 2012;49:41-57.

33. Damato B, Kacperek A, Chopra M, et al. Proton beam radiotherapy of iris melanoma. Int J Radiat Oncol Biol Phys 2005;63(1):109-15.

34. Brockhurst RJ. Tantalum buttons for localization of malignant melanoma in proton beam therapy. Ophthalmic Surg 1980;11(5):352.

35. Kim IK, Lane AM, Egan KM, et al. Natural history of radiation papillopathy after proton beam irradiation of parapapillary melanoma. Ophthalmology 2010;117(8):1617-22.

36. Modorati G, Miserocchi E, Galli L, et al. Gamma knife radiosurgery for uveal melanoma: 12 years of experience. Br J Ophthalmol 2009;93(1):40-4.

37. Muller K, Naus N, Nowak PJ, et al. Fractionated stereotactic radiotherapy for uveal melanoma, late clinical results. Radiother Oncol 2012;102(2):219-24.

38. Damato B. Progress in the management of patients with uveal melanoma. The 2012 Ashton Lecture. Eye (Lond) 2012.

39. Konstantinidis L, Groenewald C, Coupland SE, Damato B. Trans-scleral local resection of toxic choroidal melanoma after proton beam radiotherapy. Br J Ophthalmol 2014;98(6):775-9.

40. Damato B, Foulds WS. Indications for trans-scleral local resection of uveal melanoma. Br J Ophthalmol 1996;80(11):1029-30.

41. Damato B, Groenewald C, McGalliard J, Wong D. Endoresection of choroidal melanoma. Br J Ophthalmol 1998;82(3):213-8.

42. Damato B. Adjunctive plaque radiotherapy after local resection of uveal melanoma. Front Radiat Ther Oncol 1997;30:123-32.

43. Puusaari I, Damato B, Kivela T. Transscleral local resection versus iodine brachytherapy for uveal melanomas that are large because of tumour height. Graefes Arch Clin Exp Ophthalmol 2007;245(4):522-33.

44. The COMS randomized trial of iodine 125 brachytherapy for choroidal melanoma: V. Twelve-year mortality rates and prognostic factors: COMS report No. 28. Arch Ophthalmol 2006;124(12):1684-93.

45. Favilla I, Favilla ML, Gosbell AD, et al. Photodynamic therapy: a 5-year study of its effectiveness in the treatment of posterior uveal melanoma, and evaluation of haematoporphyrin uptake and photocytotoxicity of melanoma cells in tissue culture. Melanoma Res 1995;5(5):355-64.

46. Campbell WG, Pejnovic TM. Treatment of amelanotic choroidal melanoma with photodynamic therapy. Retina 2012;32(7):1356-62.

47. Shields CL, Shields JA, Cater J, et al. Transpupillary thermotherapy for choroidal melanoma: tumor control and visual results in 100 consecutive cases. Ophthalmology 1998;105(4):581-90.

48. Singh AD, Kivela T, Seregard S, et al. Primary transpupillary thermotherapy of "small" choroidal melanoma: is it safe? Br J Ophthalmol 2008;92(6):727-8.

49. Mashayekhi A, Shields CL, Rishi P, et al. Primary transpupillary thermotherapy for choroidal melanoma in 391 cases: importance of risk factors in tumor control. Ophthalmology 2015;122(3):600-9.

50. Damato B. Does ocular treatment of uveal melanoma influence survival? Br J Cancer 2010;103(3):285-90.

51. Ardjomand N, Komericki P, Langmann G, et al. Lymph node metastases arising from uveal melanoma. Wien Klin Wochenschr 2005;117(11-12):433-5.

52. Torres V, Triozzi P, Eng C, et al. Circulating tumor cells in uveal melanoma. Future Oncol 2011;7(1):101-9.

53. Lorigan JG, Wallace S, Mavligit GM. The prevalence and location of metastases from ocular melanoma: imaging study in 110 patients. AJR Am J Roentgenol 1991;157(6):1279-81.

54. Fuchs E. Das Sarkom des Uvealtractus. Graefe's Arch Ophthalmol 1882;XII(2):233.

55. Paget S. The distribution of secondary growths in cancer of the breast. 1889. Cancer Metastasis Rev 1989;8(2):98-101.

56. Logan PT, Fernandes BF, Di Cesare S, et al. Single-cell tumor dormancy model of uveal melanoma. Clin Exp Metastasis 2008;25(5):509-16.

57. Yang H, Fang G, Huang X, et al. In-vivo xenograft murine human uveal melanoma model develops hepatic micrometastases. Melanoma Res 2008;18(2):95-103.

58. Grossniklaus HE. Progression of ocular melanoma metastasis to the liver: the 2012 Zimmerman lecture. JAMA Ophthalmol 2013;131(4):462-9.

59. Yang H, Dithmar S, Grossniklaus HE. Interferon alpha 2b decreases hepatic micrometastasis in a murine model of ocular melanoma by activation of intrinsic hepatic natural killer cells. Invest Ophthalmol Vis Sci 2004;45(7):2056-64.

60. Jager MJ, Ly LV, El Filali M, Madigan MC. Macrophages in uveal melanoma and in experimental ocular tumor models: Friends or foes? Prog Retin Eye Res 2011;30(2):129-46.

61. Eskelin S, Pyrhonen S, Summanen P, et al. Tumor doubling times in metastatic malignant melanoma of the uvea: tumor progression before and after treatment. Ophthalmology 2000;107(8):1443-9.

62. De Croock L, Verbraeken H. Metastatic uveal melanoma: diagnosis and treatment. A literature review. Bull Soc Belge Ophtalmol 2002(286):59-63.

63. Blanco PL, Lim LA, Miyamoto C, Burnier MN. Uveal melanoma dormancy: an acceptable clinical endpoint? Melanoma Res 2012;22(5):334-40.

64. Damato B. Choroidal melanoma endoresection, dandelions and allegory-based medicine. Br J Ophthalmol 2008;92(8):1013-4.

65. Damato BE, Heimann H, Kalirai H, Coupland SE. Age, survival predictors, and metastatic death in patients with choroidal melanoma: tentative evidence of a therapeutic effect on survival. JAMA Ophthalmol 2014;132(5):605-13.

66. Shields CL, Kaliki S, Furuta M, et al. American Joint Committee on Cancer classification of posterior uveal melanoma (tumor size category) predicts prognosis in 7731 patients. Ophthalmology 2013;120(10):2066-71.

67. McLean IW, Zimmerman LE, Evans RM. Reappraisal of Callender's spindle a type of malignant melanoma of choroid and ciliary body. Am J Ophthalmol 1978;86(4):557-64.

68. Angi M, Damato B, Kalirai H, et al. Immunohistochemical assessment of mitotic count in uveal melanoma. Acta Ophthalmol 2011;89(2):e155-60.

69. Kivela T, Makitie T, Al-Jamal RT, Toivonen P. Microvascular loops and networks in uveal melanoma. Can J Ophthalmol 2004;39(4):409-21.

70. McLean IW, Keefe KS, Burnier MN. Uveal melanoma. Comparison of the prognostic value of fibrovascular loops, mean of the ten largest nucleoli, cell type, and tumor size. Ophthalmology 1997;104(5):777-80.

71. de la Cruz PO, Jr., Specht CS, McLean IW. Lymphocytic infiltration in uveal malignant melanoma. Cancer 1990;65(1):112-5.

72. Prescher G, Bornfeld N, Hirche H, et al. Prognostic implications of monosomy 3 in uveal melanoma. Lancet 1996;347(9010):1222-5.

73. White VA, Chambers JD, Courtright PD, et al. Correlation of cytogenetic abnormalities with the outcome of patients with uveal melanoma. Cancer 1998;83(2):354-9.

74. Caines R, Eleuteri A, Kalirai H, et al. Cluster analysis of multiplex ligation-dependent probe amplification data in choroidal melanoma. Mol Vis 2015;21:1-11.

75. Kilic E, Naus NC, van Gils W, et al. Concurrent loss of chromosome arm 1p and chromosome 3 predicts a decreased disease-free survival in uveal melanoma patients. Invest Ophthalmol Vis Sci 2005;46(7):2253-7.

76. Damato B, Dopierala JA, Coupland SE. Genotypic profiling of 452 choroidal melanomas with multiplex ligation-dependent probe amplification. Clin Cancer Res 2010;16(24):6083-92.

77. Eleuteri A DB, Coupland SE and Taktak AFG. Enhancing survival prognostication in patients with choroidal melanoma by integrating pathologic,

clinical and genetic predictors of metastasis. Int J Biomedical Engineering and Technology 2012;8(1):18-35.

78. Marshall E, Romaniuk C, Ghaneh P, et al. MRI in the detection of hepatic metastases from high-risk uveal melanoma: a prospective study in 188 patients. Br J Ophthalmol 2013;97(2):159-63.

79. Lander ES. Array of hope. Nat Genet. 1999 Jan;21(1 Suppl):3-4.

80. Onken MD, Worley LA, Ehlers JP, Harbour JW. Gene expression profiling in uveal melanoma reveals two molecular classes and predicts metastatic death. Cancer Res 2004;64(20):7205-9.

81. Onken MD, Worley LA, Tuscan MD, et al. An accurate, clinically feasible multi-gene expression assay for predicting metastasis in uveal melanoma. J Mol Diagn. 2010 Jul;12(4):461-8.

82. Kalirai H, Coupland S. An update on ocular melanoma. Diagnostic Histopathology 2015;21:19-25.

83. Singh AD, Turell ME, Topham AK. Uveal melanoma: trends in incidence, treatment, and survival. Ophthalmology 2011;118(9):1881-5.

84. Eschelman DJ, Gonsalves CF, Sato T. Transhepatic therapies for metastatic uveal melanoma. Semin Intervent Radiol 2013;30(1):39-48.

85. Buder K, Gesierich A, Gelbrich G, Goebeler M. Systemic treatment of metastatic uveal melanoma: review of literature and future perspectives. Cancer Med 2013;2(5):674-86.

86. Albert DM, Niffenegger AS, Willson JK. Treatment of metastatic uveal melanoma: review and recommendations. Surv Ophthalmol 1992;36(6):429-38.

87. Augsburger JJ, Correa ZM, Shaikh AH. Effectiveness of treatments for metastatic uveal melanoma. Am J Ophthalmol 2009;148(1):119-27.

88. Luke JJ, Triozzi PL, McKenna KC, et al. Biology of Advanced Uveal Melanoma and Next Steps for Clinical Therapeutics. Pigment Cell Melanoma Res 2014.

89. Mariani P, Piperno-Neumann S, Servois V, et al. Surgical management of liver metastases from uveal melanoma: 1.6 years' experience at the Institut Curie. Ejso 2009;35(11):1192-7.

90. Gomez D, Wetherill C, Cheong J, et al. The Liverpool uveal melanoma liver metastases pathway: outcome following liver resection. J Surg Oncol 2014;109(6):542-7.

91. Diener-West M, Reynolds SM, Agugliaro DJ, et al. Screening for metastasis from choroidal melanoma: the Collaborative Ocular Melanoma Study Group Report 23. J Clin Oncol 2004;22(12):2438-44.

92. Reiniger IW, Schaller UC, Haritoglou C, et al. "Melanoma inhibitory activity" (MIA): a promising serological tumour marker in metastatic uveal melanoma. Graefes Arch Clin Exp Ophthalmol 2005;243(11):1161-6.

93. Bauer R, Humphries M, Fassler R, et al. Regulation of integrin activity by MIA. J Biol Chem 2006;281(17):11669-77.

94. Schaller UC, Bosserhoff AK, Neubauer AS, et al. Melanoma inhibitory activity: a novel serum marker for uveal melanoma. Melanoma Res 2002;12(6):593-9.

95. Barak V, Frenkel S, Kalickman I, et al. Serum markers to detect metastatic uveal melanoma. Anticancer Res 2007;27(4A):1897-900.

96. Chen H, Xu C, Jin Q, Liu Z. S100 protein family in human cancer. Am J Cancer Res 2014;4(2):89-115.

97. von Schoultz E, Hansson LO, Djureen E, et al. Prognostic value of serum analyses of S-100 beta protein in malignant melanoma. Melanoma Res 1996;6(2):133-7.

98. Missotten GS, Tang NE, Korse CM, et al. Prognostic value of S-100-beta serum concentration in patients with uveal melanoma. Arch Ophthalmol 2003;121(8):1117-9.

99. Rittling SR, Chambers AF. Role of osteopontin in tumour progression. Br J Cancer 2004;90(10):1877-81.

100. Kadkol SS, Lin AY, Barak V, et al. Osteopontin expression and serum levels in metastatic uveal melanoma: a pilot study. Invest Ophthalmol Vis Sci 2006;47(3):802-6.

101. Hendler K, Pe'er J, Kaiserman I, et al. Trends in liver function tests: a comparison with serum tumor markers in metastatic uveal melanoma (part 2). Anticancer Res 2011;31(1):351-7.

102. Barak V, Kaiserman I, Frenkel S, et al. The dynamics of serum tumor markers in predicting metastatic uveal melanoma (part 1). Anticancer Res 2011;31(1):345-9.

103. Ludwig JA, Weinstein JN. Biomarkers in cancer staging, prognosis and treatment selection. Nat Rev Cancer 2005;5(11):845-56.

104. Mallick P, Kuster B. Proteomics: a pragmatic perspective. Nat Biotechnol 2010;28(7):695-709.

105. Domon B, Aebersold R. Options and considerations when selecting a quantitative proteomics strategy. Nat Biotechnol 2010;28(7):710-21.

106. Gorg A, Obermaier C, Boguth G, et al. The current state of two-dimensional electrophoresis with immobilized pH gradients. Electrophoresis 2000;21(6):1037-53.

107. Rabilloud T. The Whereabouts of 2D Gels in Quantitative Proteomics. Methods Mol Biol 2012;893:25-35.

108. Pardo M, Garcia A, Thomas B, et al. Proteome analysis of a human uveal melanoma primary cell culture by 2-DE and MS. Proteomics 2005;5(18):4980-93.

109. Pardo M, Garcia A, Thomas B, et al. The characterization of the invasion phenotype of uveal melanoma tumour cells shows the presence of MUC18 and HMG-1 metastasis markers and leads to the identification of DJ-1 as a potential serum biomarker. Int J Cancer 2006;119(5):1014-22.

110. Pardo M, Garcia A, Antrobus R, et al. Biomarker discovery from uveal melanoma secretomes: identification of gp100 and cathepsin D in patient serum. J Proteome Res 2007;6(7):2802-11.

111. Zuidervaart W, Hensbergen PJ, Wong MC, et al. Proteomic analysis of uveal melanoma reveals novel potential markers involved in tumor progression. Invest Ophthalmol Vis Sci 2006;47(3):786-93.

112. Coupland SE, Vorum H, Mandal N, et al. Proteomics of uveal melanomas suggests HSP-27 as a possible surrogate marker of chromosome 3 loss. Invest Ophthalmol Vis Sci 2010;51(1):12-20.

113. Tannu NS, Hemby SE. Two-dimensional fluorescence difference gel electrophoresis for comparative proteomics profiling. Nat Protoc 2006;1(4):1732-42.

114. Karas M, Hillenkamp F. Laser desorption ionization of proteins with molecular masses exceeding 10,000 daltons. Anal Chem 1988;60(20):2299-301.

115. Fenn JB, Mann M, Meng CK, et al. Electrospray ionization for mass spectrometry of large biomolecules. Science 1989;246(4926):64-71.

116. Aebersold R, Mann M. Mass spectrometry-based proteomics. Nature 2003;422(6928):198-207.

117. Cottrell JS. Protein identification by peptide mass fingerprinting. Pept Res 1994;7(3):115-24.

118. Lam TC, Chun RK, Li KK, To CH. Application of proteomic technology in eye research: a mini review. Clin Exp Optom 2008;91(1):23-33.

119. Shen Y, Zhao R, Berger SJ, et al. High-efficiency nanoscale liquid chromatography coupled on-line with mass spectrometry using nanoelectrospray ionization for proteomics. Anal Chem 2002;74(16):4235-49.

120. Peng J, Elias JE, Thoreen CC, et al. Evaluation of multidimensional chromatography coupled with tandem mass spectrometry (LC/LC-MS/MS) for large-scale protein analysis: the yeast proteome. J Proteome Res 2003;2(1):43-50.

121. Qian WJ, Jacobs JM, Camp DG, 2nd, et al. Comparative proteome analyses of human plasma following in vivo lipopolysaccharide administration using multidimensional separations coupled with tandem mass spectrometry. Proteomics 2005;5(2):572-84.

122. Liang S, Xu Z, Xu X, et al. Quantitative proteomics for cancer biomarker discovery. Comb Chem High Throughput Screen 2012;15(3):221-31.

123. Beynon RJ, Pratt JM. Metabolic labeling of proteins for proteomics. Mol Cell Proteomics 2005;4(7):857-72.

124. Panchaud A, Affolter M, Moreillon P, Kussmann M. Experimental and computational approaches to quantitative proteomics: status quo and outlook. J Proteomics 2008;71(1):19-33.

125. Megger DA, Bracht T, Meyer HE, et al. Label-free quantification in clinical proteomics. Biochim Biophys Acta. 2013;1834(8):1581-90.

126. Patel VJ, Thalassinos K, Slade SE, et al. A comparison of labeling and label-free mass spectrometry-based proteomics approaches. J Proteome Res 2009;8(7):3752-9.

127. Nesvizhskii AI, Vitek O, Aebersold R. Analysis and validation of proteomic data generated by tandem mass spectrometry. Nat Methods 2007;4(10):787-97.

128. Picotti P, Rinner O, Stallmach R, et al. High-throughput generation of selected reaction-monitoring assays for proteins and proteomes. Nat Methods 2010;7(1):43-6.

129. Jay NL, Gillies M. Proteomic analysis of ophthalmic disease. Clin Experiment Ophthalmol 2012.

130. Missotten GS, Beijnen JH, Keunen JE, Bonfrer JM. Proteomics in uveal melanoma. Melanoma Res 2003;13(6):627-9.

133. Bande MF, Santiago M, Blanco MJ, et al. Serum DJ-1/PARK 7 is a potential biomarker of choroidal nevi transformation. Invest Ophthalmol Vis Sci 2012;53(1):62-7.

137. Linge A, Kennedy S, O'Flynn D, et al. Differential expression of fourteen proteins between uveal melanoma from patients who subsequently developed distant metastases versus those who did Not. Invest Ophthalmol Vis Sci 2012;53(8):4634-43.

138. Ramasamy P, Murphy CC, Clynes M, et al. Proteomics in uveal melanoma. Exp Eye Res 2014;118:1-12.

139. Yan LB, Shi K, Bing ZT, et al. Proteomic analysis of energy metabolism and signal transduction in irradiated melanoma cells. Int J Ophthalmol 2013;6(3):286-94.

140. Wang F, Bing Z, Zhang Y, et al. Quantitative proteomic analysis for radiation-induced cell cycle suspension in 92-1 melanoma cell line. J Radiat Res 2013;54(4):649-62.

141. Coupland SE, Lake SL, Zeschnigk M, Damato BE. Molecular pathology of uveal melanoma. Eye (Lond) 2013;27(2):230-42.

142. Findeisen P, Neumaier M. Mass spectrometry based proteomics profiling as diagnostic tool in oncology: current status and future perspective. Clin Chem Lab Med 2009;47(6):666-84.

143. Pardo M, Dwek RA, Zitzmann N. Proteomics in uveal melanoma research: opportunities and challenges in biomarker discovery. Expert Rev Proteomics 2007;4(2):273-86.

144. Jmor F, Kalirai H, Taktak A, et al. HSP-27 protein expression in uveal melanoma: correlation with predicted survival. Acta Ophthalmol 2012;90(6):534-9.

145. Latterich M, Abramovitz M, Leyland-Jones B. Proteomics: new technologies and clinical applications. Eur J Cancer 2008;44(18):2737-41.

146. Bunai K, Yamane K. Effectiveness and limitation of two-dimensional gel electrophoresis in bacterial membrane protein proteomics and perspectives. J Chromatogr B Analyt Technol Biomed Life Sci 2005;815(1-2):227-36.

147. Choe LH, Aggarwal K, Franck Z, Lee KH. A comparison of the consistency of proteome quantitation using two-dimensional electrophoresis and shotgun isobaric tagging in Escherichia coli cells. Electrophoresis 2005;26(12):2437-49.

148. Tonack S, Jenkinson C, Cox T, et al. iTRAQ reveals candidate pancreatic cancer serum biomarkers: influence of obstructive jaundice on their performance. Br J Cancer 2013;108(9):1846-53.

149. Tonack S, Aspinall-O'Dea M, Jenkins RE, et al. A technically detailed and pragmatic protocol for quantitative serum proteomics using iTRAQ. J Proteomics 2009;73(2):352-6.

150. Glen A, Gan CS, Hamdy FC, et al. iTRAQ-facilitated proteomic analysis of human prostate cancer cells identifies proteins associated with progression. J Proteome Res 2008;7(3):897-907.

151. Griffiths SD, Burthem J, Unwin RD, et al. The use of isobaric tag peptide labeling (iTRAQ) and mass spectrometry to examine rare, primitive hematopoietic cells from patients with chronic myeloid leukemia. Mol Biotechnol 2007;36(2):81-9.

152. Ross PL, Huang YN, Marchese JN, et al. Multiplexed protein quantitation in Saccharomyces cerevisiae using amine-reactive isobaric tagging reagents. Mol Cell Proteomics 2004;3(12):1154-69.

153. Aggarwal K, Choe LH, Lee KH. Shotgun proteomics using the iTRAQ isobaric tags. Brief Funct Genomic Proteomic 2006;5(2):112-20.

154. Bradford MM. A rapid and sensitive method for the quantitation of microgram quantities of protein utilizing the principle of protein-dye binding. Anal Biochem 1976;72:248-54.

155. Walsh J, Jenkins RE, Wong M, et al. Identification and quantification of the basal and inducible Nrf2-dependent proteomes in mouse liver: Biochemical, pharmacological and toxicological implications. J Proteomics 2014.

156. Bohm M, Sawicka K, Siebrasse JP, et al. The transformation suppressor protein Pdcd4 shuttles between nucleus and cytoplasm and binds RNA. Oncogene 2003;22(31):4905-10.

157. Onken MD, Worley LA, Char DH, et al. Collaborative Ocular Oncology Group report number 1: prospective validation of a multi-gene prognostic assay in uveal melanoma. Ophthalmology 2012;119(8):1596-603.

158. Schafer BW, Wicki R, Engelkamp D, et al. Isolation of a YAC clone covering a cluster of nine S100 genes on human chromosome 1q21: rationale for a new nomenclature of the S100 calcium-binding protein family. Genomics 1995;25(3):638-43.

159. Salama I, Malone PS, Mihaimeed F, Jones JL. A review of the S100 proteins in cancer. Eur J Surg Oncol 2008;34(4):357-64.

160. Cochran AJ, Holland GN, Wen DR, et al. Detection of cytoplasmic S-100 protein in primary and metastatic intraocular melanomas. Invest Ophthalmol Vis Sci 1983;24(8):1153-5.

161. Kan-Mitchell J, Rao N, Albert DM, et al. S100 immunophenotypes of uveal melanomas. Invest Ophthalmol Vis Sci 1990;31(8):1492-6.

162. Van Ginkel PR, Gee RL, Walker TM, et al. The identification and differential expression of calcium-binding proteins associated with ocular melanoma. Biochim Biophys Acta 1998;1448(2):290-7.

163. Keijser S, Missotten GS, Bonfrer JM, et al. Immunophenotypic markers to differentiate between benign and malignant melanocytic lesions. Br J Ophthalmol 2006;90(2):213-7.

164. Gaynor R, Irie R, Morton D, Herschman HR. S100 protein is present in cultured human malignant melanomas. Nature 1980;286(5771):400-1.

165. Cochran AJ, Holland GN, Saxton RE, et al. Detection and quantification of S-100 protein in ocular tissues and fluids from patients with intraocular melanoma. Br J Ophthalmol 1988;72(11):874-9.

166. Zhang J, Zhang K, Jiang X, Zhang J. S100A6 as a Potential Serum Prognostic Biomarker and Therapeutic Target in Gastric Cancer. Dig Dis Sci 2014.

167. Cmarik JL, Min H, Hegamyer G, et al. Differentially expressed protein Pdcd4 inhibits tumor promoter-induced neoplastic transformation. Proc Natl Acad Sci U S A 1999;96(24):14037-42.

168. Chen Y, Knosel T, Kristiansen G, et al. Loss of PDCD4 expression in human lung cancer correlates with tumour progression and prognosis. J Pathol 2003;200(5):640-6.

169. Jansen AP, Camalier CE, Stark C, Colburn NH. Characterization of programmed cell death 4 in multiple human cancers reveals a novel enhancer of drug sensitivity. Mol Cancer Ther 2004;3(2):103-10.

170. Wen YH, Shi X, Chiriboga L, et al. Alterations in the expression of PDCD4 in ductal carcinoma of the breast. Oncol Rep 2007;18(6):1387-93.

171. Wang Q, Sun Z, Yang HS. Downregulation of tumor suppressor Pdcd4 promotes invasion and activates both beta-catenin/Tcf and AP-1-dependent transcription in colon carcinoma cells. Oncogene 2008;27(11):1527-35.

172. Wei NA, Liu SS, Leung TH, et al. Loss of Programmed cell death 4 (Pdcd4) associates with the progression of ovarian cancer. Mol Cancer 2009;8:70.

173. Lankat-Buttgereit B, Goke R. The tumour suppressor Pdcd4: recent advances in the elucidation of function and regulation. Biol Cell 2009;101(6):309-17.

174. Blees JS, Schmid T, Thomas CL, et al. Development of a high-throughput cell-based reporter assay to identify stabilizers of tumor suppressor Pdcd4. J Biomol Screen 2010;15(1):21-9.

175. Schmid T, Jansen AP, Baker AR, et al. Translation inhibitor Pdcd4 is targeted for degradation during tumor promotion. Cancer Res 2008;68(5):1254-60.

176. Asangani IA, Rasheed SA, Nikolova DA, et al. MicroRNA-21 (miR-21) post-transcriptionally downregulates tumor suppressor Pdcd4 and stimulates invasion, intravasation and metastasis in colorectal cancer. Oncogene 2008;27(15):2128-36.

177. Gao F, Wang X, Zhu F, et al. PDCD4 gene silencing in gliomas is associated with 5'CpG island methylation and unfavourable prognosis. J Cell Mol Med 2009;13(10):4257-67.

178. Dorrello NV, Peschiaroli A, Guardavaccaro D, et al. S6K1- and betaTRCP-mediated degradation of PDCD4 promotes protein translation and cell growth. Science 2006;314(5798):467-71.

179. Vikhreva PN, Shepelev MV, Korobko IV. mTOR-dependent transcriptional repression of Pdcd4 tumor suppressor in lung cancer cells. Biochim Biophys Acta 2014;1839(1):43-9.

180. Amirouchene-Angelozzi N, Nemati F, Gentien D, et al. Establishment of novel cell lines recapitulating the genetic landscape of uveal melanoma and preclinical validation of mTOR as a therapeutic target. Mol Oncol 2014.

181. Wang D, Guo S, Han SY, et al. Distinct roles of different fragments of PDCD4 in regulating the metastatic behavior of B16 melanoma cells. Int J Oncol 2013;42(5):1725-33.

182. Vikhreva PN, Korobko IV. Expression of Pdcd4 tumor suppressor in human melanoma cells. Anticancer Res 2014;34(5):2315-8.

183. Galan JA, Geraghty KM, Lavoie G, et al. Phosphoproteomic analysis identifies the tumor suppressor PDCD4 as a RSK substrate negatively regulated by 14-3-3. Proc Natl Acad Sci U S A 2014;111(29):E2918-27.

184. Van Raamsdonk CD, Griewank KG, Crosby MB, et al. Mutations in GNA11 in uveal melanoma. N Engl J Med 2010;363(23):2191-9.

185. Xue H, Lu B, Zhang J, et al. Identification of serum biomarkers for colorectal cancer metastasis using a differential secretome approach. J Proteome Res 2010;9(1):545-55.

186. Hanash SM, Pitteri SJ, Faca VM. Mining the plasma proteome for cancer biomarkers. Nature 2008;452(7187):571-9.

187. Jacobs JM, Adkins JN, Qian WJ, et al. Utilizing human blood plasma for proteomic biomarker discovery. J Proteome Res 2005;4(4):1073-85.

188. Tjalsma H, Bolhuis A, Jongbloed JD, et al. Signal peptide-dependent protein transport in Bacillus subtilis: a genome-based survey of the secretome. Microbiol Mol Biol Rev 2000;64(3):515-47.

189. Xue H, Lu B, Lai M. The cancer secretome: a reservoir of biomarkers. J Transl Med. 2008;6:52.

190. Piersma SR, Fiedler U, Span S, et al. Workflow comparison for label-free, quantitative secretome proteomics for cancer biomarker discovery: method

evaluation, differential analysis, and verification in serum. J Proteome Res 2010;9(4):1913-22.

191. Lin Q, Tan HT, Lim HS, Chung MC. Sieving through the cancer secretome. Biochim Biophys Acta 2013;1834(11):2360-71.

192. Pham TV, Piersma SR, Oudgenoeg G, Jimenez CR. Label-free mass spectrometry-based proteomics for biomarker discovery and validation. Expert Review of Molecular Diagnostics 2012;12(4):343-59.

193. Rogers LJ, Suchowerska N, Khan A, et al. Profiling of the secretome of human cancer cells: Preparation of supernatant for proteomic analysis. Electrophoresis 2014;35(18):2626-33.

194. Villarreal L, Mendez O, Salvans C, et al. Unconventional secretion is a major contributor of cancer cell line secretomes. Mol Cell Proteomics 2013;12(5):1046-60.

195. Skehan P, Storeng R, Scudiero D, et al. New colorimetric cytotoxicity assay for anticancer-drug screening. J Natl Cancer Inst 1990;82(13):1107-12.

196. Kalirai H, Damato BE, Coupland SE. Uveal melanoma cell lines contain stem-like cells that self-renew, produce differentiated progeny and survive chemotherapy. Invest Ophthalmol Vis Sci 2011.

197. Dopierala J, Damato BE, Lake SL, et al. Genetic heterogeneity in uveal melanoma assessed by multiplex ligation-dependent probe amplification. Invest Ophthalmol Vis Sci 2010;51(10):4898-905.

198. Hu DN, McCormick SA, Ritch R, Pelton-Henrion K. Studies of human uveal melanocytes in vitro: isolation, purification and cultivation of human uveal melanocytes. Invest Ophthalmol Vis Sci 1993;34(7):2210-9.

199. Makridakis M, Vlahou A. Secretome proteomics for discovery of cancer biomarkers. J Proteomics 2010;73(12):2291-305.

200. Polisetty RV, Gupta MK, Nair SC, et al. Glioblastoma cell secretome: analysis of three glioblastoma cell lines reveal 148 non-redundant proteins. J Proteomics 2011;74(10):1918-25.

201. Strober W. Trypan blue exclusion test of cell viability. Curr Protoc Immunol 2001;Appendix 3:Appendix 3B.

202. Caccia D, Dugo M, Callari M, Bongarzone I. Bioinformatics tools for secretome analysis. Biochim Biophys Acta 2013;1834(11):2442-53.

203. Petersen TN, Brunak S, von Heijne G, Nielsen H. SignalP 4.0: discriminating signal peptides from transmembrane regions. Nat Methods 2011;8(10):785-6.

204. Bendtsen JD, Jensen LJ, Blom N, et al. Feature-based prediction of non-classical and leaderless protein secretion. Protein Eng Des Sel 2004;17(4):349-56.

205. Sonnhammer EL, von Heijne G, Krogh A. A hidden Markov model for predicting transmembrane helices in protein sequences. Proc Int Conf Intell Syst Mol Biol 1998;6:175-82.

206. Beynon RJ, Doherty MK, Pratt JM, Gaskell SJ. Multiplexed absolute quantification in proteomics using artificial QCAT proteins of concatenated signature peptides. Nat Methods 2005;2(8):587-9.

207. Peffers MJ, Beynon RJ, Clegg PD. Absolute quantification of selected proteins in the human osteoarthritic secretome. Int J Mol Sci 2013;14(10):20658-81.

208. Chen JQ, Heldman MR, Herrmann MA, et al. Absolute quantitation of endogenous proteins with precision and accuracy using a capillary Western system. Anal Biochem 2013;442(1):97-103.

209. Triozzi PL, Elson P, Aldrich W, et al. Elevated blood beta-2 microglobulin is associated with tumor monosomy-3 in patients with primary uveal melanoma. Melanoma Res 2013;23(1):1-7.

210. Schaaij-Visser TB, de Wit M, Lam SW, Jimenez CR. The cancer secretome, current status and opportunities in the lung, breast and colorectal cancer context. Biochim Biophys Acta 2013;1834(11):2242-58.

211. Khattak MA, Fisher R, Hughes P, et al. Ipilimumab activity in advanced uveal melanoma. Melanoma Res 2013;23(1):79-81.

212. Margalit A, Sheikhet HM, Carmi Y, et al. Induction of antitumor immunity by CTL epitopes genetically linked to membrane-anchored beta2-microglobulin. J Immunol 2006;176(1):217-24.

213. Chiou SJ, Chen CH. Decipher beta2-microglobulin: gain- or loss-of-function (a mini-review). Med Sci Monit Basic Res 2013;19:271-3.

214. Huang WC, Wu D, Xie Z, et al. beta2-microglobulin is a signaling and growth-promoting factor for human prostate cancer bone metastasis. Cancer Res 2006;66(18):9108-16.

215. Krishnakumar S, Abhyankar D, Lakshmi SA, et al. HLA expression in choroidal melanomas: correlation with clinicopathological features. Curr Eye Res 2004;28(6):409-16.

216. Apte RS, Niederkorn JY. Isolation and characterization of a unique natural killer cell inhibitory factor present in the anterior chamber of the eye. J Immunol 1996;156(8):2667-73.

217. Apte RS, Mayhew E, Niederkorn JY. Local inhibition of natural killer cell activity promotes the progressive growth of intraocular tumors. Invest Ophthalmol Vis Sci 1997;38(6):1277-82.

218. Ma D, Luyten GP, Luider TM, Niederkorn JY. Relationship between natural killer cell susceptibility and metastasis of human uveal melanoma cells in a murine model. Invest Ophthalmol Vis Sci 1995;36(2):435-41.

219. Repp AC, Mayhew ES, Apte S, Niederkorn JY. Human uveal melanoma cells produce macrophage migration-inhibitory factor to prevent lysis by NK cells. J Immunol 2000;165(2):710-5.

220. Costa-Silva B, Aiello NM, Ocean AJ, et al. Pancreatic cancer exosomes initiate pre-metastatic niche formation in the liver. Nat Cell Biol 2015;17(6):816-26.

221. Lacroix M. Persistent use of "false" cell lines. Int J Cancer 2008;122(1):1-4.

222. Folberg R, Kadkol SS, Frenkel S, et al. Authenticating cell lines in ophthalmic research laboratories. Invest Ophthalmol Vis Sci 2008;49(11):4697-701.

223. Seddon JM, Albert DM, Lavin PT, Robinson N. A prognostic factor study of disease-free interval and survival following enucleation for uveal melanoma. Arch Ophthalmol 1983;101(12):1894-9.

224. Yao L, Lao W, Zhang Y, et al. Identification of EFEMP2 as a serum biomarker for the early detection of colorectal cancer with lectin affinity capture assisted secretome analysis of cultured fresh tissues. J Proteome Res 2012;11(6):3281-94.

225. Peinado H, Aleckovic M, Lavotshkin S, et al. Melanoma exosomes educate bone marrow progenitor cells toward a pro-metastatic phenotype through MET. Nat Med 2012;18(6):883-91.

226. Ashworth TR. A case of cancer in which cells similar to those in the tumors were seen in the blood after death. Australian Medical Journal 1869(14):146-7.

227. Smith B, Selby P, Southgate J, et al. Detection of melanoma cells in peripheral blood by means of reverse transcriptase and polymerase chain reaction. Lancet 1991;338(8777):1227-9.

228. Roberts S, Watne A, Mc GR, et al. Technique and results of isolation of cancer cells from the circulating blood. AMA Arch Surg 1958;76(3):334-46.

229. Singletary SE, Greene FL, Sobin LH. Classification of isolated tumor cells: clarification of the 6th edition of the American Joint Committee on Cancer Staging Manual. Cancer 2003;98(12):2740-1.

230. Harris L, Fritsche H, Mennel R, et al. American Society of Clinical Oncology 2007 update of recommendations for the use of tumor markers in breast cancer. J Clin Oncol 2007;25(33):5287-312.

231. Riethdorf S, Wikman H, Pantel K. Review: Biological relevance of disseminated tumor cells in cancer patients. Int J Cancer 2008;123(9):1991-2006.

232. Alunni-Fabbroni M, Sandri MT. Circulating tumour cells in clinical practice: Methods of detection and possible characterization. Methods 2010;50(4):289-97.

233. Callejo SA, Antecka E, Blanco PL, et al. Identification of circulating malignant cells and its correlation with prognostic factors and treatment in uveal melanoma. A prospective longitudinal study. Eye (Lond) 2007;21(6):752-9.

234. Yu M, Stott S, Toner M, et al. Circulating tumor cells: approaches to isolation and characterization. J Cell Biol 2011;192(3):373-82.

235. Joshi P, Jacobs B, Derakhshan A, et al. Enrichment of circulating melanoma cells (CMCs) using negative selection from patients with metastatic melanoma2014.

236. Tobal K, Sherman LS, Foss AJ, Lightman SL. Detection of melanocytes from uveal melanoma in peripheral blood using the polymerase chain reaction. Invest Ophthalmol Vis Sci 1993;34(9):2622-5.

237. Foss AJ, Guille MJ, Occleston NL, et al. The detection of melanoma cells in peripheral blood by reverse transcription-polymerase chain reaction. Br J Cancer 1995;72(1):155-9.

238. El-Shabrawi Y, Langmann G, Hutter H, et al. Comparison of current methods and PCR for the diagnosis of metastatic disease in uveal malignant melanoma. Ophthalmologica 1998;212(1):80.

239. Boldin I, Langmann G, Richtig E, et al. Five-year results of prognostic value of tyrosinase in peripheral blood of uveal melanoma patients. Melanoma Res 2005;15(6):503-7.

240. Schuster R, Bechrakis NE, Stroux A, et al. Circulating tumor cells as prognostic factor for distant metastases and survival in patients with primary uveal melanoma. Clin Cancer Res 2007;13(4):1171-8.

241. Pinzani P, Mazzini C, Salvianti F, et al. Tyrosinase mRNA levels in the blood of uveal melanoma patients: correlation with the number of circulating tumor cells and tumor progression. Melanoma Res 2010;20(4):303-10.

242. Schuster R, Bechrakis NE, Stroux A, et al. Prognostic Relevance of Circulating Tumor Cells in Metastatic Uveal Melanoma. Oncology 2011;80(1-2):57-62.

243. Keilholz U, Goldin-Lang P, Bechrakis NE, et al. Quantitative detection of circulating tumor cells in cutaneous and ocular melanoma and quality assessment by real-time reverse transcriptase-polymerase chain reaction. Clin Cancer Res 2004;10(5):1605-12.

244. Mocellin S, Hoon D, Ambrosi A, et al. The prognostic value of circulating tumor cells in patients with melanoma: a systematic review and meta-analysis. Clin Cancer Res 2006;12(15):4605-13.

245. Ulmer A, Beutel J, Susskind D, et al. Visualization of circulating melanoma cells in peripheral blood of patients with primary uveal melanoma. Clin Cancer Res 2008;14(14):4469-74.

246. Suesskind D, Ulmer A, Schiebel U, et al. Circulating melanoma cells in peripheral blood of patients with uveal melanoma before and after different therapies and association with prognostic parameters: a pilot study. Acta Ophthalmol 2011;89(1):17-24.

247. Eide N, Faye RS, Hoifodt HK, et al. Immunomagnetic detection of micrometastatic cells in bone marrow in uveal melanoma patients. Acta Ophthalmol 2009;87(8):830-6.

248. Ulmer A, Schmidt-Kittler O, Fischer J, et al. Immunomagnetic enrichment, genomic characterization, and prognostic impact of circulating melanoma cells. Clin Cancer Res 2004;10(2):531-7.

249. Khoja L, Backen A, Sloane R, et al. A pilot study to explore circulating tumour cells in pancreatic cancer as a novel biomarker. Br J Cancer 2012;106(3):508-16.

250. Cristofanilli M, Budd GT, Ellis MJ, et al. Circulating tumor cells, disease progression, and survival in metastatic breast cancer. N Engl J Med 2004;351(8):781-91.

251. Cohen SJ, Punt CJ, Iannotti N, et al. Relationship of circulating tumor cells to tumor response, progression-free survival, and overall survival in patients with metastatic colorectal cancer. J Clin Oncol 2008;26(19):3213-21.

252. de Bono JS, Scher HI, Montgomery RB, et al. Circulating tumor cells predict survival benefit from treatment in metastatic castration-resistant prostate cancer. Clin Cancer Res 2008;14(19):6302-9.

253. Krebs MG, Sloane R, Priest L, et al. Evaluation and prognostic significance of circulating tumor cells in patients with non-small-cell lung cancer. J Clin Oncol 2011;29(12):1556-63.

254. Khoja L, Lorigan P, Zhou C, et al. Biomarker Utility of Circulating Tumor Cells in Metastatic Cutaneous Melanoma. J Invest Dermatol 2012.

255. Chatterjee S, Behnam Azad B, Nimmagadda S. The intricate role of CXCR4 in cancer. Adv Cancer Res 2014;124:31-82.

256. Fusi A, Liu Z, Kummerlen V, et al. Expression of chemokine receptors on circulating tumor cells in patients with solid tumors. J Transl Med 2012;10:52.

257. Chen PW, Murray TG, Uno T, et al. Expression of MAGE genes in ocular melanoma during progression from primary to metastatic disease. Clin Exp Metastasis 1997;15(5):509-18.

258. De Waard-Siebinga I, Blom DJ, Griffioen M, et al. Establishment and characterization of an uveal-melanoma cell line. Int J Cancer 1995;62(2):155-61.

259. Luyten GP, Naus NC, Mooy CM, et al. Establishment and characterization of primary and metastatic uveal melanoma cell lines. Int J Cancer 1996;66(3):380-7.

260. Demicheli R, Fornili M, Biganzoli E. Bimodal mortality dynamics for uveal melanoma: a cue for metastasis development traits? BMC Cancer 2014;14:392.

261. Bidard FC, Madic J, Mariani P, et al. Detection rate and prognostic value of circulating tumor cells and circulating tumor DNA in metastatic uveal melanoma. Int J Cancer 2014;134(5):1207-13.

262. Lai K, Sharma V, Jager MJ, et al. Expression and distribution of MUC18 in human uveal melanoma. Virchows Arch 2007;451(5):967-76.

263. Morgan AC, Jr., Galloway DR, Reisfeld RA. Production and characterization of monoclonal antibody to a melanoma specific glycoprotein. Hybridoma 1981;1(1):27-36.

264. Li Y, Madigan MC, Lai K, et al. Human uveal melanoma expresses NG2 immunoreactivity. Br J Ophthalmol 2003;87(5):629-32.

265. Benez A, Geiselhart A, Handgretinger R, et al. Detection of circulating melanoma cells by immunomagnetic cell sorting. J Clin Lab Anal 1999;13(5):229-33.

266. Tura A, Luke J, Merz H, et al. Identification of circulating melanoma cells in uveal melanoma patients by dual-marker immunoenrichment. Invest Ophthalmol Vis Sci 2014;55(7):4395-404.

267. Cools-Lartigue JJ, McCauley CS, Marshall JC, et al. Immunomagnetic isolation and in vitro expansion of human uveal melanoma cell lines. Mol Vis 2008;14:50-5.

268. Chaffer CL, Weinberg RA. A perspective on cancer cell metastasis. Science 2011;331(6024):1559-64.

269. Scatena R, Bottoni P, Giardina B. Circulating tumour cells and cancer stem cells: a role for proteomics in defining the interrelationships between function, phenotype and differentiation with potential clinical applications. Biochim Biophys Acta 2013;1835(2):129-43.

270. Kasimir-Bauer S, Hoffmann O, Wallwiener D, et al. Expression of stem cell and epithelial-mesenchymal transition markers in primary breast cancer patients with circulating tumor cells. Breast Cancer Res 2012;14(1):R15.

271. Thill M, Berna MJ, Grierson R, et al. Expression of CD133 and other putative stem cell markers in uveal melanoma. Melanoma Res 2011;21(5):405-16.

272. Madic J, Piperno-Neumann S, Servois V, et al. Pyrophosphorolysis-activated polymerization detects circulating tumor DNA in metastatic uveal melanoma. Clin Cancer Res 2012;18(14):3934-41.

273. Metz CH, Scheulen M, Bornfeld N, et al. Ultradeep sequencing detects GNAQ and GNA11 mutations in cell-free DNA from plasma of patients with uveal melanoma. Cancer Med 2013;2(2):208-15.

274. Diener-West M, Reynolds SM, Agugliaro DJ, et al. Development of metastatic disease after enrollment in the COMS trials for treatment of choroidal melanoma - Collaborative ocular melanoma study group report no. 26. Archives of Ophthalmology 2005;123(12):1639-43.

275. Heusner TA, Antoch G, Wittkowski-Sterczewski A, et al. Transarterial hepatic chemoperfusion of uveal melanoma metastases: survival and response to treatment. Rofo 2011;183(12):1151-60.

276. Damato B, Eleuteri A, Fisher AC, et al. Artificial neural networks estimating survival probability after treatment of choroidal melanoma. Ophthalmology 2008;115(9):1598-607.

277. Damato B, Coupland SE. Translating uveal melanoma cytogenetics into clinical care. Arch Ophthalmol 2009;127(4):423-9.

278. Damato B, Duke C, Coupland SE, et al. Cytogenetics of uveal melanoma: a 7-year clinical experience. Ophthalmology 2007;114(10):1925-31.

279. Grixti AA, M.; Damato, B.; Jmor, F.; Konstantinidis, L.; Groenewald, C.; Heimann, H. Vitreo-retinal surgery for complications of choroidal tumour biopsy. Ophthalmology 2014.

280. Konstantinidis L, Rospond-Kubiak I, Zeolite I, et al. Management of patients with uveal metastases at the Liverpool Ocular Oncology Centre. Br J Ophthalmol 2014;98(1):92-8.

281. Sen J, Groenewald C, Hiscott PS, et al. Transretinal choroidal tumor biopsy with a 25-gauge vitrector. Ophthalmology 2006;113(6):1028-31.

282. Shields CL, Materin MA, Teixeira L, et al. Small choroidal melanoma with chromosome 3 monosomy on fine-needle aspiration biopsy. Ophthalmology 2007;114(10):1919-24.

283. McCannel TA, Chang MY, Burgess BL. Multi-year follow-up of fine-needle aspiration biopsy in choroidal melanoma. Ophthalmology 2012;119(3):606-10.

284. Cohen VM, Dinakaran S, Parsons MA, Rennie IG. Transvitreal fine needle aspiration biopsy: the influence of intraocular lesion size on diagnostic biopsy result. Eye (Lond) 2001;15(Pt 2):143-7.

285. Shields CL, Ganguly A, Bianciotto CG, et al. Prognosis of uveal melanoma in 500 cases using genetic testing of fine-needle aspiration biopsy specimens. Ophthalmology 2011;118(2):396-401.

286. Fastenberg DM, Finger PT, Chess Q, et al. Vitrectomy retinotomy aspiration biopsy of choroidal tumors. Am J Ophthalmol 1990;110(4):361-5.

287. Bechrakis NE, Foerster MH, Bornfeld N. Biopsy in indeterminate intraocular tumors. Ophthalmology 2002;109(2):235-42.

288. Kvanta A, Seregard S, Kopp ED, et al. Choroidal biopsies for intraocular tumors of indeterminate origin. Am J Ophthalmol 2005;140(6):1002-6.

289. Abi-Ayad N, Grange JD, Salle M, Kodjikian L. Transretinal uveal melanoma biopsy with 25-gauge vitrectomy system. Acta Ophthalmol 2013;91(3):279-81.

290. Seregard S, All-Ericsson C, Hjelmqvist L, et al. Diagnostic incisional biopsies in clinically indeterminate choroidal tumours. Eye (Lond) 2013;27(2):115-8.

291. Cook SA, Damato B, Marshall E, Salmon P. Psychological aspects of cytogenetic testing of uveal melanoma: preliminary findings and directions for future research. Eye (Lond) 2009;23(3):581-5.

292. Akgul H, Otterbach F, Bornfeld N, Jurklies B. Intraocular biopsy using special forceps: a new instrument and refined surgical technique. Br J Ophthalmol 2011;95(1):79-82.

293. Damato B, Angi M, Coupland S, et al. Miscellaneous uveal biopsy techniques. In: Damato B, Singh A, eds. Clinical Ophthalmic Oncology

. Berlin Heidelberg

: Springer-Verlag

, 2014.

294. van Dongen JJ, Langerak AW, Bruggemann M, et al. Design and standardization of PCR primers and protocols for detection of clonal immunoglobulin and T-cell receptor gene recombinations in suspect lymphoproliferations: report of the BIOMED-2 Concerted Action BMH4-CT98-3936. Leukemia 2003;17(12):2257-317.

295. Thomas S, Putter C, Weber S, et al. Prognostic significance of chromosome 3 alterations determined by microsatellite analysis in uveal melanoma: a long-term follow-up study. Br J Cancer 2012;106(6):1171-6.

296. Shields CL, Ganguly A, Materin MA, et al. Chromosome 3 analysis of uveal melanoma using fine-needle aspiration biopsy at the time of plaque radiotherapy in 140 consecutive cases. Trans Am Ophthalmol Soc 2007;105:43-52; discussion -3.

297. Correa ZM, Augsburger JJ. Sufficiency of FNAB aspirates of posterior uveal melanoma for cytologic versus GEP classification in 159 patients, and relative prognostic significance of these classifications. Graefes Arch Clin Exp Ophthalmol 2014;252(1):131-5.

298. Seider MI, Stewart PJ, Mishra KK, Damato BE. Uveal melanoma gene expression profile test result provided for uveal metastasis. Ophthalmic Surg Lasers Imaging Retina 2014;45(5):441-2.

299. Young TA, Burgess BL, Rao NP, et al. Transscleral fine-needle aspiration biopsy of macular choroidal melanoma. Am J Ophthalmol 2008;145(2):297-302.

300. Cassoux N, Rodrigues MJ, Plancher C, et al. Genome-wide profiling is a clinically relevant and affordable prognostic test in posterior uveal melanoma. Br J Ophthalmol 2014;98(6):769-74.

301. Augsburger JJ, Correa ZM, Augsburger BD. Frequency and implications of discordant gene expression profile class in posterior uveal melanomas sampled by fine needle aspiration biopsy. Am J Ophthalmol 2015;159(2):248-56.

302. Maat W, Jordanova ES, van Zelderen-Bhola SL, et al. The heterogeneous distribution of monosomy 3 in uveal melanomas: implications for prognostication based on fine-needle aspiration biopsies. Arch Pathol Lab Med 2007;131(1):91-6.

303. Leyvraz S, Keilholz U. Ocular melanoma: what's new? Curr Opin Oncol 2012;24(2):162-9.

304. Pardo OE, Wellbrock C, Khanzada UK, et al. FGF-2 protects small cell lung cancer cells from apoptosis through a complex involving PKCepsilon, B-Raf and S6K2. EMBO J 2006;25(13):3078-88.

305. Roy R, Durie D, Li H, et al. hnRNPA1 couples nuclear export and translation of specific mRNAs downstream of FGF-2/S6K2 signalling. Nucleic Acids Res 2014;42(20):12483-97.

306. Bera A, Das F, Ghosh-Choudhury N, et al. microRNA-21-induced dissociation of PDCD4 from rictor contributes to Akt-IKKbeta-mTORC1 axis to regulate renal cancer cell invasion. Exp Cell Res 2014.

307. Shen F, Mo MH, Chen L, et al. MicroRNA-21 Down-regulates Rb1 Expression by Targeting PDCD4 in Retinoblastoma. J Cancer 2014;5(9):804-12.

Appendix 1. Comparison of the proteins detected in the different iTRAQ runs

		Run A		Run B		Run C	
Accession	Name	Peptides (95%)	Coverage (95%)	Peptides (95%)	Coverage (95%)	Peptides (95%)	Coverage (95%)
A0AVT1	Ubiquitin-like modifier-activating enzyme 6	10	11.69	2	1.24	2	2.19
A0FGR8	Extended synaptotagmin-2	4	6.19	3	4.89	2	3.26
A0M8Q6	Ig lambda-7 chain C region	0	0.00	13	32.08	11	32.08
A1L0T0	Acetolactate synthase-like protein	37	45.25	23	35.76	24	32.75
A2RTX5	Probable threonyl-tRNA synthetase 2, cytoplasmic	1	1.62	1	1.62	2	2.62
A4D1P6	WD repeat-containing protein 91	8	12.99	5	6.96	8	13.25
A5YKK6	CCR4-NOT transcription complex subunit 1	4	1.47	7	2.86	3	0.76
A6NCN2	Keratin-81-like protein	3	3.09	0	0.00	0	0.00
A6NDU8	UPF0600 protein C5orf51	1	4.76	0	0.00	0	0.00
A6NHG4	D-dopachrome decarboxylase-like protein	8	40.30	4	23.88	3	17.91
A6NHR9	Structural maintenance of chromosomes flexible hinge domain-containing protein 1	2	1.15	2	0.55	3	1.25
A6NIZ1	Ras-related protein Rap-1b-like protein	21	55.98	13	34.24	14	47.28
A6NL28	Putative tropomyosin alpha-3 chain-like protein	18	23.77	9	16.59	11	16.59
A8MTJ3	Guanine nucleotide-binding protein G(t) subunit alpha-3	4	7.91	0	0.00	3	7.91
A8MWD9	Small nuclear ribonucleoprotein G-like protein	3	15.79	0	0.00	3	15.79
A8MXV4	Nucleoside diphosphate-linked moiety X motif 19, mitochondrial	2	9.87	1	6.13	0	0.00
B2RPK0	Putative high mobility group protein B1-like 1	7	15.64	0	0.00	0	0.00
B9A064	Immunoglobulin lambda-like polypeptide 5	15	33.18	11	27.57	12	33.18
C4AMC7	Putative WAS protein family homolog 3	2	7.34	1	3.02	1	3.02
C9JLW8	Protein FAM195B	3	29.90	0	0.00	1	11.34
O00115	Deoxyribonuclease-2-alpha	3	12.22	0	0.00	0	0.00
O00116	Alkyldihydroxyacetonephosphate synthase, peroxisomal	4	6.84	2	5.32	3	7.29
O00139	Kinesin-like protein KIF2A	3	5.38	0	0.00	0	0.00
O00148	ATP-dependent RNA helicase DDX39A	28	39.11	0	0.00	16	25.06
O00151	PDZ and LIM domain protein 1	6	16.11	0	0.00	2	13.07
O00154	Cytosolic acyl coenzyme A thioester hydrolase	14	22.89	8	18.68	8	19.74
O00159	Myosin-Ic	51	35.84	36	28.32	26	21.07
O00161	Synaptosomal-associated protein 23	3	12.80	0	0.00	0	0.00
O00170	AH receptor-interacting protein	3	11.21	4	14.55	1	4.24
O00178	GTP-binding protein 1	2	4.78	0	0.00	0	0.00
O00186	Syntaxin-binding protein 3	4	9.29	0	0.00	0	0.00
O00192	Armadillo repeat protein deleted in velo-cardio-facial syndrome	2	2.60	0	0.00	0	0.00
O00193	Small acidic protein	2	12.57	0	0.00	0	0.00
O00203	AP-3 complex subunit beta-1	12	12.98	3	3.66	9	8.13
O00217	NADH dehydrogenase [ubiquinone] iron-sulfur protein 8, mitochondrial	6	23.33	3	18.10	5	18.10
O00231	26S proteasome non-ATPase regulatory subunit 11	13	31.04	10	24.41	6	11.85
O00232	26S proteasome non-ATPase regulatory subunit 12	10	23.68	7	13.60	6	10.53
O00233	26S proteasome non-ATPase regulatory subunit 9	6	16.14	2	8.97	0	0.00
O00244	Copper transport protein ATOX1	2	25.00	1	25.00	1	25.00
O00255	Menin	1	2.28	0	0.00	0	0.00
O00264	Membrane-associated progesterone receptor component 1	11	31.79	6	12.31	3	7.69
O00273	DNA fragmentation factor subunit alpha	3	13.60	5	20.24	2	9.97
O00299	Chloride intracellular channel protein 1	22	61.41	17	43.57	14	43.57
O00303	Eukaryotic translation initiation factor 3 subunit F	11	25.21	8	17.65	7	17.93
O00330	Pyruvate dehydrogenase protein X component, mitochondrial	2	4.59	2	4.79	0	0.00
O00399	Dynactin subunit 6	1	7.37	0	0.00	0	0.00
O00401	Neural Wiskott-Aldrich syndrome protein	1	1.58	0	0.00	0	0.00
O00410	Importin-5	26	20.69	13	9.21	15	12.67
O00422	Histone deacetylase complex subunit SAP18	1	10.46	2	10.46	1	10.46
O00429	Dynamin-1-like protein	27	35.87	10	18.75	8	12.36
O00442	RNA 3'-terminal phosphate cyclase	3	7.65	0	0.00	4	10.38
O00468	Agrin	11	6.31	5	2.74	5	2.54
O00471	Exocyst complex component 5	3	4.94	0	0.00	0	0.00
O00479	High mobility group nucleosome-binding domain-containing protein 4	4	26.67	0	0.00	1	7.78
O00483	NADH dehydrogenase [ubiquinone] 1 alpha subcomplex subunit 4	3	27.16	3	27.16	5	27.16
O00487	26S proteasome non-ATPase regulatory subunit 14	2	10.65	4	28.71	3	17.74
O00560	Syntenin-1	42	55.03	27	46.31	32	51.01
O00567	Nucleolar protein 56	33	39.73	21	33.00	19	31.99
O00571	ATP-dependent RNA helicase DDX3X	14	25.53	15	21.90	15	21.30
O00584	Ribonuclease T2	2	9.77	0	0.00	1	3.91
O00625	Pirin	32	50.69	24	56.55	8	33.79
O00629	Importin subunit alpha-4	9	17.47	5	11.32	4	4.80
O00754	Lysosomal alpha-mannosidase	5	5.93	3	4.75	1	1.48
O00764	Pyridoxal kinase	12	29.17	8	28.21	6	16.67
O14556	Glyceraldehyde-3-phosphate dehydrogenase, testis-specific	37	50.25	35	50.00	30	47.06
O14561	Acyl carrier protein, mitochondrial	14	28.21	8	17.95	6	17.95
O14579	Coatomer subunit epsilon	8	38.31	6	30.84	4	18.18
O14602	Eukaryotic translation initiation factor 1A, Y-chromosomal	4	14.58	0	0.00	2	14.58
O14617	AP-3 complex subunit delta-1	18	15.18	11	10.67	13	10.49
O14618	Copper chaperone for superoxide dismutase	3	17.88	3	17.88	3	17.88
O14672	Disintegrin and metalloproteinase domain-containing protein 10	3	5.35	2	3.34	1	2.01
O14727	Apoptotic protease-activating factor 1	1	1.12	0	0.00	1	1.12
O14735	CDP-diacylglycerol--inositol 3-phosphatidyltransferase	4	10.80	1	6.10	3	6.10
O14737	Programmed cell death protein 5	11	38.40	3	29.60	4	19.20
O14744	Protein arginine N-methyltransferase 5	4	6.12	0	0.00	0	0.00
O14745	Na(+)/H(+) exchange regulatory cofactor NHE-RF1	6	17.32	6	19.83	5	17.32
O14773	Tripeptidyl-peptidase 1	57	36.94	35	36.94	31	36.94
O14776	Transcription elongation regulator 1	5	4.28	4	3.10	4	3.10
O14787	Transportin-2	4	4.68	3	4.13	3	4.46

O14818	Proteasome subunit alpha type-7	14	39.92	9	30.24	10	36.29
O14828	Secretory carrier-associated membrane protein 3	18	30.84	7	24.21	8	24.21
O14841	5-oxoprolinase	17	17.86	8	9.86	8	9.32
O14874	[3-methyl-2-oxobutanoate dehydrogenase [lipoamide]] kinase, mitochondrial	2	8.50	0	0.00	0	0.00
O14879	Interferon-induced protein with tetratricopeptide repeats 3	6	11.22	0	0.00	0	0.00
O14880	Microsomal glutathione S-transferase 3	23	33.55	11	33.55	7	32.24
O14907	Tax1-binding protein 3	2	13.71	0	0.00	0	0.00
O14908	PDZ domain-containing protein GIPC1	2	14.11	0	0.00	0	0.00
O14949	Cytochrome b-c1 complex subunit 8	3	15.85	0	0.00	2	15.85
O14950	Myosin regulatory light chain 12B	22	68.02	12	34.88	13	36.05
O14964	Hepatocyte growth factor-regulated tyrosine kinase substrate	7	10.81	5	6.56	2	3.09
O14972	Down syndrome critical region protein 3	2	8.08	0	0.00	0	0.00
O14976	Cyclin-G-associated kinase	4	3.20	3	1.30	5	3.28
O14979	Heterogeneous nuclear ribonucleoprotein D-like	17	21.19	16	17.86	10	17.38
O14980	Exportin-1	29	24.84	23	22.04	14	15.78
O15020	Spectrin beta chain, brain 2	12	5.98	0	0.00	0	0.00
O15027	Protein transport protein Sec16A	3	2.16	0	0.00	0	0.00
O15061	Synemin	3	2.24	6	4.41	4	3.20
O15067	Phosphoribosylformylglycinamidine synthase	20	16.74	7	6.58	10	7.02
O15083	ERC protein 2	1	1.15	0	0.00	1	1.25
O15116	U6 snRNA-associated Sm-like protein LSm1	3	12.03	3	26.32	4	15.79
O15118	Niemann-Pick C1 protein	3	2.82	1	0.94	2	1.88
O15126	Secretory carrier-associated membrane protein 1	3	10.95	0	0.00	0	0.00
O15127	Secretory carrier-associated membrane protein 2	4	13.07	0	0.00	2	6.08
O15131	Importin subunit alpha-6	1	2.61	0	0.00	3	5.78
O15143	Actin-related protein 2/3 complex subunit 1B	7	20.16	1	4.84	2	4.84
O15144	Actin-related protein 2/3 complex subunit 2	9	30.00	3	10.33	6	17.33
O15145	Actin-related protein 2/3 complex subunit 3	8	35.39	4	14.61	4	13.48
O15160	DNA-directed RNA polymerases I and III subunit RPAC1	3	11.27	0	0.00	3	15.90
O15173	Membrane-associated progesterone receptor component 2	10	33.18	6	28.70	6	28.70
O15198	Mothers against decapentaplegic homolog 9	3	6.21	0	0.00	0	0.00
O15211	Ral guanine nucleotide dissociation stimulator-like 2	4	6.56	0	0.00	0	0.00
O15212	Prefoldin subunit 6	7	27.91	4	20.16	3	20.16
O15226	NF-kappa-B-repressing factor	1	1.88	0	0.00	0	0.00
O15230	Laminin subunit alpha-5	25	9.77	13	3.98	9	3.90
O15234	Protein CASC3	1	1.28	0	0.00	0	0.00
O15260	Surfeit locus protein 4	7	20.45	6	17.47	6	17.47
O15294	UDP-N-acetylglucosamine--peptide N-acetylglucosaminyltransferase 110 kDa subunit	1	1.05	1	1.05	1	1.05
O15355	Protein phosphatase 1G	5	10.81	2	7.51	2	7.51
O15371	Eukaryotic translation initiation factor 3 subunit D	9	14.42	8	14.42	8	11.86
O15372	Eukaryotic translation initiation factor 3 subunit H	3	13.07	2	7.39	0	0.00
O15400	Syntaxin-7	34	45.98	17	49.04	20	49.04
O15488	Glycogenin-2	3	9.38	4	9.38	2	7.19
O15498	Synaptobrevin homolog YKT6	3	17.68	1	11.11	2	10.61
O15511	Actin-related protein 2/3 complex subunit 5	2	7.95	2	7.95	0	0.00
O15533	Tapasin	3	10.27	3	14.51	1	7.14
O43143	Putative pre-mRNA-splicing factor ATP-dependent RNA helicase DHX15	19	23.02	13	17.48	9	13.96
O43149	Zinc finger ZZ-type and EF-hand domain-containing protein 1	5	1.35	0	0.00	4	1.69
O43156	TEL2-interacting protein 1 homolog	2	1.74	1	1.74	1	1.74
O43169	Cytochrome b5 type B	10	50.68	12	37.67	7	37.67
O43172	U4/U6 small nuclear ribonucleoprotein Prp4	2	5.75	0	0.00	0	0.00
O43175	D-3-phosphoglycerate dehydrogenase	11	16.89	5	8.25	4	7.32
O43181	NADH dehydrogenase [ubiquinone] iron-sulfur protein 4, mitochondrial	8	28.57	2	13.71	3	22.86
O43237	Cytoplasmic dynein 1 light intermediate chain 2	9	27.03	6	19.11	3	9.35
O43242	26S proteasome non-ATPase regulatory subunit 3	14	25.28	8	15.36	8	12.55
O43290	U4/U6.U5 tri-snRNP-associated protein 1	3	4.75	0	0.00	3	3.38
O43301	Heat shock 70 kDa protein 12A	9	14.67	2	4.00	0	0.00
O43324	Eukaryotic translation elongation factor 1 epsilon-1	3	11.49	3	20.11	0	0.00
O43390	Heterogeneous nuclear ribonucleoprotein R	27	28.59	24	23.85	17	22.12
O43396	Thioredoxin-like protein 1	11	36.33	4	15.57	6	24.57
O43399	Tumor protein D54	11	39.32	9	33.01	8	33.01
O43402	Neighbor of COX4	3	11.90	2	7.62	0	0.00
O43423	Acidic leucine-rich nuclear phosphoprotein 32 family member C	3	9.40	3	4.70	0	0.00
O43447	Peptidyl-prolyl cis-trans isomerase H	2	9.04	2	9.04	0	0.00
O43464	Serine protease HTRA2, mitochondrial	9	24.89	4	12.23	0	0.00
O43488	Aflatoxin B1 aldehyde reductase member 2	14	22.28	8	15.32	10	17.55
O43491	Band 4.1-like protein 2	15	17.21	4	5.47	12	15.92
O43592	Exportin-T	1	1.04	0	0.00	2	2.49
O43598	Deoxyribonucleoside 5'-monophosphate N-glycosidase	11	34.48	8	32.76	5	21.84
O43615	Mitochondrial import inner membrane translocase subunit TIM44	9	20.13	3	5.97	3	8.41
O43670	Zinc finger protein 207	5	5.44	3	2.72	2	2.72
O43674	NADH dehydrogenase [ubiquinone] 1 beta subcomplex subunit 5, mitochondrial	2	12.70	0	0.00	0	0.00
O43678	NADH dehydrogenase [ubiquinone] 1 alpha subcomplex subunit 2	4	32.32	0	0.00	1	21.21
O43681	ATPase ASNA1	8	24.14	8	16.95	4	13.51
O43684	Mitotic checkpoint protein BUB3	2	9.15	0	0.00	3	9.15
O43707	Alpha-actinin-4	136	59.39	72	43.25	87	44.46
O43708	Maleylacetoacetate isomerase	3	6.48	0	0.00	0	0.00
O43747	AP-1 complex subunit gamma-1	12	14.48	5	8.64	6	8.27
O43752	Syntaxin-6	10	37.65	2	9.80	4	23.14
O43765	Small glutamine-rich tetratricopeptide repeat-containing protein alpha	10	19.81	4	11.50	5	10.86
O43776	Asparaginyl-tRNA synthetase, cytoplasmic	30	33.94	17	28.28	18	26.46
O43790	Keratin, type II cuticular Hb6	3	3.09	0	0.00	0	0.00
O43795	Myosin-Ib	7	7.57	6	6.51	6	5.90

O43809	Cleavage and polyadenylation specificity factor subunit 5	2	15.86	3	10.57	1	6.61
O43813	LanC-like protein 1	7	8.52	5	8.52	4	8.52
O43819	Protein SCO2 homolog, mitochondrial	2	9.40	0	0.00	0	0.00
O43823	A-kinase anchor protein 8	1	2.89	0	0.00	3	4.62
O43837	Isocitrate dehydrogenase [NAD] subunit beta, mitochondrial	6	15.32	2	4.16	3	11.69
O43852	Calumenin	18	42.22	16	36.19	10	26.98
O43865	Putative adenosylhomocysteinase 2	4	6.23	5	6.79	4	8.30
O43920	NADH dehydrogenase [ubiquinone] iron-sulfur protein 5	4	23.58	2	23.58	2	23.58
O60216	Double-strand-break repair protein rad21 homolog	3	6.97	1	3.17	2	4.91
O60220	Mitochondrial import inner membrane translocase subunit Tim8 A	3	11.34	2	11.34	2	11.34
O60256	Phosphoribosyl pyrophosphate synthase-associated protein 2	6	27.10	0	0.00	7	22.76
O60262	Guanine nucleotide-binding protein G(I)/G(S)/G(O) subunit gamma-7	5	44.12	0	0.00	3	44.12
O60264	SWI/SNF-related matrix-associated actin-dependent regulator of chromatin subfamily	5	5.32	0	0.00	2	2.38
O60271	C-Jun-amino-terminal kinase-interacting protein 4	6	4.32	5	4.54	9	9.69
O60287	Nucleolar pre-ribosomal-associated protein 1	2	1.10	2	1.10	0	0.00
O60313	Dynamin-like 120 kDa protein, mitochondrial	13	15.00	5	7.19	3	2.19
O60343	TBC1 domain family member 4	10	8.32	4	3.16	6	6.47
O60443	Non-syndromic hearing impairment protein 5	7	14.72	0	0.00	1	2.42
O60486	Plexin-C1	13	8.04	4	4.34	8	6.70
O60493	Sorting nexin-3	2	8.64	3	15.43	2	8.64
O60506	Heterogeneous nuclear ribonucleoprotein Q	37	29.53	31	32.58	25	27.77
O60547	GDP-mannose 4,6 dehydratase	2	7.26	2	6.72	0	0.00
O60568	Procollagen-lysine,2-oxoglutarate 5-dioxygenase 3	8	11.79	7	14.50	4	7.45
O60610	Protein diaphanous homolog 1	5	3.38	2	2.12	1	0.86
O60613	15 kDa selenoprotein	2	9.88	1	9.88	1	9.88
O60645	Exocyst complex component 3	5	7.14	4	7.14	3	4.37
O60664	Perilipin-3	32	60.83	19	49.31	17	43.32
O60684	Importin subunit alpha-7	1	2.61	0	0.00	3	5.78
O60701	UDP-glucose 6-dehydrogenase	7	14.17	0	0.00	4	10.73
O60716	Catenin delta-1	37	26.03	18	17.56	19	19.32
O60739	Eukaryotic translation initiation factor 1b	10	52.21	5	35.40	0	0.00
O60749	Sorting nexin-2	13	20.81	3	5.20	5	12.72
O60762	Dolichol-phosphate mannosyltransferase	5	8.46	4	8.46	2	8.46
O60763	General vesicular transport factor p115	13	11.85	8	10.29	6	6.76
O60784	Target of Myb protein 1	6	15.85	5	12.40	3	8.54
O60814	Histone H2B type 1-K	61	67.46	61	62.70	43	57.94
O60825	6-phosphofructo-2-kinase/fructose-2,6-biphosphatase 2	4	7.13	0	0.00	0	0.00
O60826	Coiled-coil domain-containing protein 22	10	14.99	7	16.75	8	18.50
O60831	PRA1 family protein 2	2	6.18	1	6.18	1	6.18
O60832	H/ACA ribonucleoprotein complex subunit 4	14	25.68	4	12.65	1	2.53
O60841	Eukaryotic translation initiation factor 5B	10	8.93	5	6.80	8	9.59
O60879	Protein diaphanous homolog 2	2	2.72	1	0.82	0	0.00
O60888	Protein CutA	8	30.73	6	40.78	2	22.91
O60936	Nucleolar protein 3	1	8.68	1	8.68	1	8.68
O75044	SLIT-ROBO Rho GTPase-activating protein 2	3	2.43	3	1.12	0	0.00
O75083	WD repeat-containing protein 1	39	43.07	20	30.69	15	37.13
O75116	Rho-associated protein kinase 2	5	3.82	1	0.72	0	0.00
O75122	CLIP-associating protein 2	2	1.24	0	0.00	0	0.00
O75131	Copine-3	14	12.29	6	8.38	6	6.70
O75165	DnaJ homolog subfamily C member 13	16	6.78	10	4.90	14	5.08
O75208	Ubiquinone biosynthesis protein COQ9, mitochondrial	3	12.26	0	0.00	0	0.00
O75223	Gamma-glutamylcyclotransferase	1	5.32	2	17.55	3	22.87
O75251	NADH dehydrogenase [ubiquinone] iron-sulfur protein 7, mitochondrial	2	4.22	2	4.22	2	10.80
O75306	NADH dehydrogenase [ubiquinone] iron-sulfur protein 2, mitochondrial	24	37.80	17	29.81	10	21.38
O75323	Protein NipSnap homolog 2	7	16.78	2	6.99	0	0.00
O75340	Programmed cell death protein 6	9	29.84	8	40.84	7	47.64
O75347	Tubulin-specific chaperone A	8	27.78	7	18.52	4	10.19
O75348	V-type proton ATPase subunit G 1	6	27.97	4	27.97	4	20.34
O75351	Vacuolar protein sorting-associated protein 4B	7	14.86	3	4.28	0	0.00
O75352	Mannose-P-dolichol utilization defect 1 protein	2	9.72	1	5.67	1	5.67
O75367	Core histone macro-H2A.1	32	42.74	27	38.98	22	36.56
O75368	SH3 domain-binding glutamic acid-rich-like protein	27	90.35	20	84.21	15	77.19
O75369	Filamin-B	38	15.95	19	8.46	26	9.80
O75380	NADH dehydrogenase [ubiquinone] iron-sulfur protein 6, mitochondrial	1	17.74	1	17.74	1	17.74
O75390	Citrate synthase, mitochondrial	41	33.26	23	37.77	25	31.12
O75396	Vesicle-trafficking protein SEC22b	11	45.12	7	34.42	11	34.42
O75400	Pre-mRNA-processing factor 40 homolog A	3	3.03	2	1.36	2	3.03
O75431	Metaxin-2	3	13.31	2	8.37	1	4.94
O75436	Vacuolar protein sorting-associated protein 26A	4	9.79	0	0.00	1	2.14
O75439	Mitochondrial-processing peptidase subunit beta	10	20.65	8	18.61	7	15.95
O75448	Mediator of RNA polymerase II transcription subunit 24	1	1.42	0	0.00	0	0.00
O75477	Erlin-1	4	8.38	0	0.00	5	16.18
O75489	NADH dehydrogenase [ubiquinone] iron-sulfur protein 3, mitochondrial	25	47.73	19	47.35	20	47.35
O75494	Serine/arginine-rich splicing factor 10	7	23.28	9	23.28	5	18.70
O75521	Enoyl-CoA delta isomerase 2, mitochondrial	6	13.71	0	0.00	3	7.87
O75531	Barrier-to-autointegration factor	16	48.31	12	40.45	7	40.45
O75533	Splicing factor 3B subunit 1	20	18.63	15	13.96	13	11.66
O75534	Cold shock domain-containing protein E1	2	2.88	1	1.63	3	4.01
O75607	Nucleoplasmin-3	3	27.53	2	21.35	2	21.35
O75608	Acyl-protein thioesterase 1	4	25.22	1	6.09	3	15.22
O75628	GTP-binding protein REM 1	1	3.69	0	0.00	0	0.00
O75629	Protein CREG1	4	9.54	0	0.00	2	9.54
O75643	U5 small nuclear ribonucleoprotein 200 kDa helicase	33	15.64	25	11.47	20	10.96

O75688	Protein phosphatase 1B	4	8.14	1	3.76	1	3.76
O75694	Nuclear pore complex protein Nup155	11	7.26	10	7.76	8	5.97
O75746	Calcium-binding mitochondrial carrier protein Aralar1	15	19.91	11	14.75	7	10.03
O75781	Paralemmin-1	2	7.49	1	4.91	2	7.49
O75792	Ribonuclease H2 subunit A	2	7.36	1	2.68	0	0.00
O75817	Ribonuclease P protein subunit p20	1	10.71	0	0.00	0	0.00
O75821	Eukaryotic translation initiation factor 3 subunit G	13	26.88	3	10.31	3	7.50
O75822	Eukaryotic translation initiation factor 3 subunit J	3	8.53	0	0.00	0	0.00
O75843	AP-1 complex subunit gamma-like 2	2	4.08	0	0.00	1	1.15
O75874	Isocitrate dehydrogenase [NADP] cytoplasmic	18	39.61	10	23.19	13	31.40
O75891	Cytosolic 10-formyltetrahydrofolate dehydrogenase	5	5.99	5	6.32	3	4.10
O75915	PRA1 family protein 3	10	20.21	7	16.49	10	16.49
O75923	Dysferlin	8	4.90	1	0.91	0	0.00
O75937	DnaJ homolog subfamily C member 8	4	25.69	2	7.51	1	3.16
O75947	ATP synthase subunit d, mitochondrial	21	71.43	8	47.83	10	47.83
O75955	Flotillin-1	17	35.13	15	27.40	12	23.65
O75964	ATP synthase subunit g, mitochondrial	10	52.43	4	35.92	3	25.24
O76003	Glutaredoxin-3	6	15.82	3	12.24	3	8.36
O76021	Ribosomal L1 domain-containing protein 1	5	12.24	8	17.55	4	11.22
O76024	Wolframin	5	4.49	2	2.14	2	2.70
O76031	ATP-dependent Clp protease ATP-binding subunit clpX-like, mitochondrial	2	3.79	0	0.00	0	0.00
O76054	SEC14-like protein 2	1	2.73	2	4.96	1	4.96
O76094	Signal recognition particle 72 kDa protein	5	5.22	6	6.56	6	14.16
O94760	N(G),N(G)-dimethylarginine dimethylaminohydrolase 1	2	7.72	0	0.00	0	0.00
O94766	Galactosylgalactosylxylosylprotein 3-beta-glucuronosyltransferase 3	2	7.16	0	0.00	0	0.00
O94804	Serine/threonine-protein kinase 10	11	9.92	6	5.37	5	6.40
O94826	Mitochondrial import receptor subunit TOM70	9	15.79	3	4.93	1	3.95
O94832	Myosin-Id	49	28.13	21	16.40	26	23.06
O94874	E3 UFM1-protein ligase 1	10	13.10	3	6.42	4	6.93
O94875	Sorbin and SH3 domain-containing protein 2	1	1.82	0	0.00	0	0.00
O94886	Transmembrane protein 63A	2	3.72	0	0.00	2	3.72
O94901	SUN domain-containing protein 1	4	5.05	0	0.00	4	5.67
O94905	Erlin-2	8	22.12	7	18.88	12	34.81
O94915	Protein furry homolog-like	1	0.60	0	0.00	0	0.00
O94919	Endonuclease domain-containing 1 protein	6	7.40	2	2.60	6	11.60
O94925	Glutaminase kidney isoform, mitochondrial	3	6.13	0	0.00	0	0.00
O94973	AP-2 complex subunit alpha-2	13	15.87	13	18.64	11	12.57
O94979	Protein transport protein Sec31A	9	7.62	6	6.64	6	4.02
O95071	E3 ubiquitin-protein ligase UBR5	2	1.25	2	0.68	0	0.00
O95155	Ubiquitin conjugation factor E4 B	4	3.00	0	0.00	0	0.00
O95168	NADH dehydrogenase [ubiquinone] 1 beta subcomplex subunit 4	3	16.28	2	21.71	0	0.00
O95169	NADH dehydrogenase [ubiquinone] 1 beta subcomplex subunit 8, mitochondrial	4	21.51	0	0.00	3	22.58
O95182	NADH dehydrogenase [ubiquinone] 1 alpha subcomplex subunit 7	2	17.70	2	18.58	0	0.00
O95197	Reticulon-3	2	1.07	2	1.07	0	0.00
O95202	LETM1 and EF-hand domain-containing protein 1, mitochondrial	16	18.00	2	4.87	2	3.79
O95208	Epsin-2	2	1.56	1	1.56	1	1.56
O95219	Sorting nexin-4	3	4.89	0	0.00	0	0.00
O95232	Luc7-like protein 3	3	6.25	4	6.25	4	9.49
O95260	Arginyl-tRNA--protein transferase 1	2	5.60	2	5.60	0	0.00
O95292	Vesicle-associated membrane protein-associated protein B/C	5	15.64	0	0.00	4	10.70
O95299	NADH dehydrogenase [ubiquinone] 1 alpha subcomplex subunit 10, mitochondrial	11	26.20	8	19.72	2	6.20
O95302	Peptidyl-prolyl cis-trans isomerase FKBP9	4	8.42	3	5.61	0	0.00
O95336	6-phosphogluconolactonase	20	48.06	14	54.65	11	39.92
O95372	Acyl-protein thioesterase 2	4	19.05	6	19.05	1	7.79
O95373	Importin-7	11	9.73	6	5.78	7	8.09
O95379	Tumor necrosis factor alpha-induced protein 8	1	10.10	1	10.10	0	0.00
O95394	Phosphoacetylglucosamine mutase	1	3.14	0	0.00	0	0.00
O95428	Papilin	1	1.57	1	1.57	0	0.00
O95433	Activator of 90 kDa heat shock protein ATPase homolog 1	7	15.68	7	15.68	6	10.06
O95456	Proteasome assembly chaperone 1	2	10.42	0	0.00	0	0.00
O95470	Sphingosine-1-phosphate lyase 1	1	2.64	1	2.64	0	0.00
O95479	GDH/6PGL endoplasmic bifunctional protein	8	9.35	6	6.70	5	7.33
O95486	Protein transport protein Sec24A	2	2.75	2	2.75	2	2.75
O95487	Protein transport protein Sec24B	7	3.78	5	3.23	3	1.73
O95571	Protein ETHE1, mitochondrial	5	22.05	3	23.23	3	12.20
O95573	Long-chain-fatty-acid--CoA ligase 3	4	7.64	3	6.39	4	8.19
O95671	N-acetylserotonin O-methyltransferase-like protein	2	6.92	0	0.00	1	2.74
O95674	Phosphatidate cytidylyltransferase 2	5	15.06	3	11.69	4	10.79
O95678	Keratin, type II cytoskeletal 75	3	2.90	0	0.00	0	0.00
O95716	Ras-related protein Rab-3D	10	26.03	6	27.40	6	15.53
O95721	Synaptosomal-associated protein 29	6	18.22	2	8.91	0	0.00
O95747	Serine/threonine-protein kinase OSR1	5	9.49	4	12.14	0	0.00
O95777	N-alpha-acetyltransferase 38, NatC auxiliary subunit	5	41.67	8	52.08	7	52.08
O95782	AP-2 complex subunit alpha-1	11	10.95	9	10.13	9	9.01
O95817	BAG family molecular chaperone regulator 3	1	2.61	0	0.00	2	6.96
O95822	Malonyl-CoA decarboxylase, mitochondrial	5	15.21	2	4.06	1	4.06
O95831	Apoptosis-inducing factor 1, mitochondrial	14	21.53	11	18.92	9	14.19
O95834	Echinoderm microtubule-associated protein-like 2	6	12.48	7	15.25	10	18.03
O95861	3'(2'),5'-bisphosphate nucleotidase 1	4	20.13	3	16.56	2	12.66
O95865	N(G),N(G)-dimethylarginine dimethylaminohydrolase 2	8	43.86	5	19.30	3	15.44
O95870	Abhydrolase domain-containing protein 16A	3	3.58	1	1.97	1	1.97
O95881	Thioredoxin domain-containing protein 12	3	17.44	0	0.00	0	0.00
O96000	NADH dehydrogenase [ubiquinone] 1 beta subcomplex subunit 10	6	20.93	2	14.53	1	8.14

O96008	Mitochondrial import receptor subunit TOM40 homolog	14	21.33	10	18.28	0	0.00
O96013	Serine/threonine-protein kinase PAK 4	1	1.86	1	2.20	2	8.80
O96019	Actin-like protein 6A	2	7.46	0	0.00	0	0.00
P00167	Cytochrome b5	3	25.37	2	15.67	3	25.37
P00338	L-lactate dehydrogenase A chain	79	68.67	65	58.73	59	46.08
P00352	Retinal dehydrogenase 1	10	16.57	11	18.96	10	24.75
P00367	Glutamate dehydrogenase 1, mitochondrial	46	47.67	17	29.39	18	31.54
P00387	NADH-cytochrome b5 reductase 3	37	64.12	23	53.82	14	46.51
P00390	Glutathione reductase, mitochondrial	8	11.11	5	8.81	4	8.81
P00403	Cytochrome c oxidase subunit 2	7	35.24	4	17.18	6	26.43
P00441	Superoxide dismutase [Cu-Zn]	30	46.10	23	46.10	15	32.47
P00450	Ceruloplasmin	32	25.54	30	20.09	20	12.30
P00488	Coagulation factor XIII A chain	11	16.26	10	14.62	12	16.26
P00505	Aspartate aminotransferase, mitochondrial	31	45.58	18	41.16	18	28.60
P00558	Phosphoglycerate kinase 1	94	75.30	77	67.63	66	62.11
P00568	Adenylate kinase isoenzyme 1	9	35.57	6	37.11	6	36.08
P00734	Prothrombin	14	15.27	7	12.70	6	10.93
P00738	Haptoglobin	13	18.72	17	32.27	12	14.04
P00747	Plasminogen	9	10.74	6	6.05	6	7.04
P00748	Coagulation factor XII	2	2.93	0	0.00	0	0.00
P00751	Complement factor B	11	11.13	11	12.96	7	8.25
P00846	ATP synthase subunit a	3	4.43	0	0.00	0	0.00
P00915	Carbonic anhydrase 1	12	27.59	25	40.23	25	43.68
P00918	Carbonic anhydrase 2	14	26.15	11	21.54	14	28.46
P00973	2'-5'-oligoadenylate synthase 1	1	5.25	0	0.00	0	0.00
P01008	Antithrombin-III	8	15.73	10	18.97	2	5.82
P01009	Alpha-1-antitrypsin	60	63.64	57	54.55	47	43.30
P01011	Alpha-1-antichymotrypsin	15	27.19	13	30.97	15	28.61
P01019	Angiotensinogen	9	17.32	9	23.51	7	18.35
P01023	Alpha-2-macroglobulin	57	30.80	81	38.20	47	28.83
P01024	Complement C3	114	46.90	115	42.15	98	44.62
P01034	Cystatin-C	1	7.53	0	0.00	2	21.92
P01042	Kininogen-1	8	8.70	5	7.45	4	7.45
P01111	GTPase NRas	8	25.40	7	25.40	4	17.46
P01112	GTPase HRas	9	30.16	7	25.40	4	17.46
P01593	Ig kappa chain V-I region AG	5	16.67	7	31.48	18	31.48
P01594	Ig kappa chain V-I region AU	5	16.67	6	16.67	8	16.67
P01599	Ig kappa chain V-I region Gal	5	16.67	6	16.67	8	16.67
P01600	Ig kappa chain V-I region Hau	5	16.67	6	16.67	9	22.22
P01601	Ig kappa chain V-I region HK101 (Fragment)	7	25.64	6	15.38	9	20.51
P01607	Ig kappa chain V-I region Rei	5	16.67	6	16.67	8	16.67
P01608	Ig kappa chain V-I region Roy	5	16.67	6	16.67	8	16.67
P01610	Ig kappa chain V-I region WEA	5	16.67	6	16.67	9	22.22
P01611	Ig kappa chain V-I region Wes	2	16.67	0	0.00	3	22.22
P01617	Ig kappa chain V-II region TEW	1	21.24	0	0.00	0	0.00
P01620	Ig kappa chain V-III region SIE	5	39.45	9	31.19	9	39.45
P01622	Ig kappa chain V-III region Ti	4	31.19	9	31.19	8	31.19
P01623	Ig kappa chain V-III region WOL	5	39.45	9	31.19	9	39.45
P01625	Ig kappa chain V-IV region Len	4	23.68	3	23.68	4	23.68
P01701	Ig lambda chain V-I region NEW	2	7.21	1	7.21	0	0.00
P01702	Ig lambda chain V-I region NIG-64	2	7.21	1	7.21	0	0.00
P01714	Ig lambda chain V-III region SH	2	7.41	1	7.41	0	0.00
P01715	Ig lambda chain V-IV region Bau	1	7.55	0	0.00	0	0.00
P01764	Ig heavy chain V-III region VH26	2	25.64	2	25.64	3	25.64
P01765	Ig heavy chain V-III region TIL	1	16.52	2	26.09	3	26.09
P01766	Ig heavy chain V-III region BRO	6	25.00	6	25.00	2	25.00
P01774	Ig heavy chain V-III region POM	1	15.97	1	15.97	2	15.97
P01776	Ig heavy chain V-III region WAS	1	16.24	1	16.24	2	16.24
P01777	Ig heavy chain V-III region TEI	4	15.97	5	15.97	1	15.97
P01779	Ig heavy chain V-III region TUR	1	16.38	1	16.38	2	16.38
P01834	Ig kappa chain C region	55	80.19	44	80.19	61	80.19
P01857	Ig gamma-1 chain C region	95	51.21	90	57.58	76	59.09
P01859	Ig gamma-2 chain C region	50	42.64	49	44.48	43	46.01
P01860	Ig gamma-3 chain C region	35	38.46	31	37.40	24	35.81
P01861	Ig gamma-4 chain C region	65	34.56	64	49.54	57	48.62
P01871	Ig mu chain C region	8	15.49	14	25.00	4	12.61
P01876	Ig alpha-1 chain C region	22	33.99	12	23.51	14	26.06
P01880	Ig delta chain C region	2	6.51	0	0.00	0	0.00
P01889	HLA class I histocompatibility antigen, B-7 alpha chain	18	29.01	6	14.09	13	25.97
P01891	HLA class I histocompatibility antigen, A-68 alpha chain	15	23.84	0	0.00	9	16.71
P01892	HLA class I histocompatibility antigen, A-2 alpha chain	19	29.59	8	18.08	10	17.53
P01903	HLA class II histocompatibility antigen, DR alpha chain	9	29.13	5	24.41	3	17.72
P02042	Hemoglobin subunit delta	122	91.16	137	85.03	120	74.83
P02452	Collagen alpha-1(I) chain	73	42.90	92	42.83	21	19.74
P02458	Collagen alpha-1(II) chain	58	29.05	3	3.16	0	0.00
P02489	Alpha-crystallin A chain	10	30.06	7	24.86	3	17.34
P02511	Alpha-crystallin B chain	27	60.57	12	41.71	12	45.71
P02538	Keratin, type II cytoskeletal 6A	2	1.24	0	0.00	0	0.00
P02545	Prelamin-A/C	227	68.98	158	58.13	142	56.93
P02647	Apolipoprotein A-I	83	65.54	67	58.05	56	49.81
P02649	Apolipoprotein E	20	49.53	14	37.54	13	35.96
P02652	Apolipoprotein A-II	15	41.00	10	37.00	6	39.00
P02654	Apolipoprotein C-I	1	10.84	0	0.00	0	0.00

P02656	Apolipoprotein C-III	2	27.27	2	27.27	1	16.16
P02671	Fibrinogen alpha chain	20	15.01	12	10.85	17	13.63
P02675	Fibrinogen beta chain	25	32.18	32	37.68	28	36.46
P02679	Fibrinogen gamma chain	12	17.00	11	12.58	13	18.76
P02730	Band 3 anion transport protein	12	15.48	26	21.19	22	16.03
P02743	Serum amyloid P-component	6	20.63	3	14.80	3	9.87
P02748	Complement component C9	10	10.38	7	11.27	7	7.51
P02749	Beta-2-glycoprotein 1	4	8.41	5	6.67	5	10.72
P02750	Leucine-rich alpha-2-glycoprotein	3	15.85	5	12.68	2	10.95
P02751	Fibronectin	15	7.67	18	10.85	17	11.48
P02760	Protein AMBP	3	10.23	3	8.52	5	20.17
P02763	Alpha-1-acid glycoprotein 1	16	33.33	15	32.84	14	33.33
P02765	Alpha-2-HS-glycoprotein	12	21.25	13	30.52	7	24.25
P02766	Transthyretin	14	70.07	17	70.07	9	40.82
P02768	Serum albumin	475	76.35	363	75.04	296	76.68
P02774	Vitamin D-binding protein	22	28.06	20	23.21	19	23.21
P02786	Transferrin receptor protein 1	3	5.40	4	5.40	0	0.00
P02787	Serotransferrin	124	51.72	104	48.57	71	37.25
P02790	Hemopexin	31	37.01	24	26.19	22	32.25
P02792	Ferritin light chain	2	17.14	0	0.00	2	17.14
P03989	HLA class I histocompatibility antigen, B-27 alpha chain	14	26.24	4	14.09	7	19.89
P04004	Vitronectin	10	12.97	8	14.85	6	8.79
P04040	Catalase	25	40.99	20	28.65	14	26.38
P04062	Glucosylceramidase	2	8.02	2	4.10	1	5.04
P04066	Tissue alpha-L-fucosidase	4	6.01	3	6.01	1	2.36
P04075	Fructose-bisphosphate aldolase A	101	72.53	68	71.43	57	74.73
P04080	Cystatin-B	8	57.14	3	55.10	0	0.00
P04083	Annexin A1	22	39.60	21	29.77	22	37.28
P04114	Apolipoprotein B-100	9	2.28	15	4.41	6	1.78
P04179	Superoxide dismutase [Mn], mitochondrial	16	32.88	8	16.22	13	16.22
P04181	Ornithine aminotransferase, mitochondrial	4	10.02	0	0.00	0	0.00
P04196	Histidine-rich glycoprotein	14	19.43	14	17.90	9	15.81
P04206	Ig kappa chain V-III region GOL	4	31.19	10	37.61	8	31.19
P04217	Alpha-1B-glycoprotein	14	41.62	10	24.85	7	15.35
P04222	HLA class I histocompatibility antigen, Cw-3 alpha chain	23	36.34	0	0.00	20	19.67
P04229	HLA class II histocompatibility antigen, DRB1-1 beta chain	8	21.80	4	13.53	4	18.42
P04259	Keratin, type II cytoskeletal 6B	4	3.01	0	0.00	0	0.00
P04264	Keratin, type II cytoskeletal 1	28	37.89	26	19.72	10	10.56
P04271	Protein S100-B	10	48.91	10	40.22	4	32.61
P04275	von Willebrand factor	5	2.74	2	1.42	3	1.88
P04350	Tubulin beta-4A chain	152	76.80	108	75.00	87	71.85
P04406	Glyceraldehyde-3-phosphate dehydrogenase	147	73.43	129	69.55	80	61.79
P04431	Ig kappa chain V-I region Walker	5	13.95	6	13.95	9	18.60
P04432	Ig kappa chain V-I region Daudi	5	13.95	6	13.95	10	22.48
P04433	Ig kappa chain V-III region VG (Fragment)	4	23.48	0	0.00	0	0.00
P04632	Calpain small subunit 1	13	57.84	11	30.22	10	30.22
P04792	Heat shock protein beta-1	50	78.05	50	84.88	43	78.05
P04839	Cytochrome b-245 heavy chain	1	2.98	0	0.00	1	2.98
P04843	Dolichyl-diphosphooligosaccharide--protein glycosyltransferase subunit 1	44	48.11	31	37.23	31	31.47
P04844	Dolichyl-diphosphooligosaccharide--protein glycosyltransferase subunit 2	37	33.76	33	29.00	31	33.28
P04899	Guanine nucleotide-binding protein G(i) subunit alpha-2	12	30.70	8	15.49	7	18.87
P05023	Sodium/potassium-transporting ATPase subunit alpha-1	62	33.82	41	29.52	35	27.86
P05091	Aldehyde dehydrogenase, mitochondrial	11	18.38	10	20.70	11	18.38
P05109	Protein S100-A8	4	32.26	7	32.26	9	33.33
P05114	Non-histone chromosomal protein HMG-14	8	41.00	6	40.00	1	13.00
P05141	ADP/ATP translocase 2	59	52.68	43	53.69	35	51.68
P05155	Plasma protease C1 inhibitor	16	21.80	8	12.20	12	18.40
P05156	Complement factor I	1	2.23	0	0.00	0	0.00
P05161	Ubiquitin-like protein ISG15	12	25.45	1	7.88	1	12.12
P05165	Propionyl-CoA carboxylase alpha chain, mitochondrial	7	12.64	1	2.06	2	3.43
P05166	Propionyl-CoA carboxylase beta chain, mitochondrial	12	26.72	5	11.50	5	11.32
P05198	Eukaryotic translation initiation factor 2 subunit 1	20	42.86	12	24.13	9	21.59
P05204	Non-histone chromosomal protein HMG-17	7	30.00	3	22.22	2	21.11
P05362	Intercellular adhesion molecule 1	7	10.71	6	11.09	8	11.09
P05386	60S acidic ribosomal protein P1	18	67.54	14	67.54	11	51.75
P05387	60S acidic ribosomal protein P2	26	77.39	25	77.39	27	76.52
P05388	60S acidic ribosomal protein P0	30	56.78	29	56.78	30	55.84
P05413	Fatty acid-binding protein, heart	8	34.59	7	27.82	5	34.59
P05455	Lupus La protein	26	35.29	12	18.63	11	24.51
P05534	HLA class I histocompatibility antigen, A-24 alpha chain	16	20.00	0	0.00	3	7.40
P05546	Heparin cofactor 2	4	5.81	4	7.01	2	4.01
P05549	Transcription factor AP-2-alpha	3	6.64	3	6.64	3	6.64
P05556	Integrin beta-1	7	8.15	5	4.64	4	6.64
P05783	Keratin, type I cytoskeletal 18	10	26.28	0	0.00	0	0.00
P05787	Keratin, type II cytoskeletal 8	17	18.01	14	12.84	11	14.91
P06132	Uroporphyrinogen decarboxylase	3	13.08	0	0.00	0	0.00
P06241	Tyrosine-protein kinase Fyn	4	4.84	2	3.35	0	0.00
P06280	Alpha-galactosidase A	2	6.76	0	0.00	2	6.76
P06309	Ig kappa chain V-II region GM607 (Fragment)	1	20.51	0	0.00	0	0.00
P06312	Ig kappa chain V-IV region (Fragment)	4	22.31	3	22.31	4	22.31
P06313	Ig kappa chain V-IV region JI	4	20.30	3	20.30	4	20.30
P06314	Ig kappa chain V-IV region B17	4	20.15	3	20.15	4	20.15
P06316	Ig lambda chain V-I region BL2	2	6.15	1	6.15	0	0.00

P06396	Gelsolin	69	42.33	50	33.25	39	29.28
P06454	Prothymosin alpha	23	29.73	13	27.03	6	26.13
P06576	ATP synthase subunit beta, mitochondrial	148	73.53	108	72.40	93	67.86
P06681	Complement C2	3	3.72	1	1.60	1	1.60
P06702	Protein S100-A9	6	37.72	11	49.12	16	49.12
P06703	Protein S100-A6	5	35.56	1	8.89	2	8.89
P06727	Apolipoprotein A-IV	23	34.34	11	18.18	11	17.42
P06733	Alpha-enolase	177	77.65	168	72.58	107	60.83
P06737	Glycogen phosphorylase, liver form	90	41.20	71	40.85	96	39.32
P06744	Glucose-6-phosphate isomerase	47	44.09	32	40.32	25	28.49
P06748	Nucleophosmin	58	44.56	41	41.50	41	38.78
P06753	Tropomyosin alpha-3 chain	28	26.41	23	20.77	19	17.61
P06756	Integrin alpha-V	15	15.08	9	8.87	5	6.30
P06865	Beta-hexosaminidase subunit alpha	25	25.90	22	25.33	19	27.22
P06888	Ig lambda chain V-I region EPS	2	7.34	1	7.34	0	0.00
P06899	Histone H2B type 1-J	59	67.46	60	62.70	41	57.14
P07093	Glia-derived nexin	4	13.82	3	10.55	4	10.55
P07099	Epoxide hydrolase 1	16	24.40	8	15.38	11	12.09
P07108	Acyl-CoA-binding protein	5	32.18	0	0.00	0	0.00
P07195	L-lactate dehydrogenase B chain	64	56.89	36	53.59	42	47.01
P07203	Glutathione peroxidase 1	10	56.65	4	26.60	7	40.89
P07205	Phosphoglycerate kinase 2	25	25.90	28	25.66	21	19.66
P07237	Protein disulfide-isomerase	60	52.36	39	37.99	41	38.58
P07305	Histone H1.0	6	20.62	4	15.46	3	11.34
P07339	Cathepsin D	50	46.60	30	36.41	43	44.66
P07355	Annexin A2	94	69.03	67	64.31	61	57.23
P07357	Complement component C8 alpha chain	2	3.08	0	0.00	0	0.00
P07384	Calpain-1 catalytic subunit	18	18.07	13	15.83	10	12.32
P07437	Tubulin beta chain	193	75.90	133	74.32	123	73.87
P07602	Proactivator polypeptide	35	15.08	10	10.31	13	13.17
P07686	Beta-hexosaminidase subunit beta	43	34.17	11	14.57	22	17.99
P07711	Cathepsin L1	5	14.71	0	0.00	0	0.00
P07737	Profilin-1	28	72.14	21	57.14	22	50.00
P07738	Bisphosphoglycerate mutase	1	5.02	2	12.36	0	0.00
P07741	Adenine phosphoribosyltransferase	15	37.22	12	48.33	12	46.11
P07814	Bifunctional aminoacyl-tRNA synthetase	24	19.05	17	10.98	10	4.63
P07858	Cathepsin B	27	35.69	13	19.47	14	23.89
P07900	Heat shock protein HSP 90-alpha	148	51.91	97	39.62	86	36.61
P07902	Galactose-1-phosphate uridylyltransferase	5	10.03	2	6.60	3	9.50
P07910	Heterogeneous nuclear ribonucleoproteins C1/C2	34	43.46	23	37.58	20	42.16
P07919	Cytochrome b-c1 complex subunit 6, mitochondrial	8	56.04	9	64.84	5	57.14
P07947	Tyrosine-protein kinase Yes	4	4.79	2	3.31	0	0.00
P07948	Tyrosine-protein kinase Lyn	3	3.13	0	0.00	0	0.00
P07954	Fumarate hydratase, mitochondrial	31	45.49	17	42.35	12	29.02
P08107	Heat shock 70 kDa protein 1A/1B	102	53.98	72	46.65	58	42.12
P08123	Collagen alpha-2(I) chain	60	37.85	70	41.29	26	22.55
P08133	Annexin A6	91	55.42	72	46.95	64	43.24
P08134	Rho-related GTP-binding protein RhoC	26	51.30	0	0.00	16	51.30
P08195	4F2 cell-surface antigen heavy chain	60	40.16	34	30.32	30	37.30
P08236	Beta-glucuronidase	8	16.13	0	0.00	3	2.77
P08237	6-phosphofructokinase, muscle type	24	30.77	13	17.82	14	13.33
P08238	Heat shock protein HSP 90-beta	121	50.83	81	44.61	63	38.95
P08240	Signal recognition particle receptor subunit alpha	3	4.86	0	0.00	0	0.00
P08294	Extracellular superoxide dismutase [Cu-Zn]	6	15.42	3	13.33	0	0.00
P08397	Porphobilinogen deaminase	6	16.07	6	16.90	5	10.80
P08473	Neprilysin	2	1.47	0	0.00	4	4.67
P08559	Pyruvate dehydrogenase E1 component subunit alpha, somatic form, mitochondrial	13	33.59	8	17.69	5	13.08
P08574	Cytochrome c1, heme protein, mitochondrial	23	36.62	17	36.62	11	29.54
P08581	Hepatocyte growth factor receptor	3	2.45	0	0.00	0	0.00
P08582	Melanotransferrin	2	2.17	0	0.00	0	0.00
P08603	Complement factor H	8	6.90	4	2.27	1	0.97
P08621	U1 small nuclear ribonucleoprotein 70 kDa	5	5.03	5	5.03	3	5.03
P08631	Tyrosine-protein kinase HCK	3	3.04	0	0.00	0	0.00
P08670	Vimentin	344	83.05	220	83.69	237	78.33
P08697	Alpha-2-antiplasmin	3	6.72	3	8.76	0	0.00
P08708	40S ribosomal protein S17	21	48.89	20	48.89	20	41.48
P08729	Keratin, type II cytoskeletal 7	8	5.54	0	0.00	0	0.00
P08758	Annexin A5	168	79.69	153	81.88	114	73.75
P08865	40S ribosomal protein SA	39	56.61	35	53.90	31	53.90
P08962	CD63 antigen	5	6.72	0	0.00	0	0.00
P09012	U1 small nuclear ribonucleoprotein A	2	6.38	6	15.25	0	0.00
P09104	Gamma-enolase	40	51.15	37	55.53	29	44.70
P09110	3-ketoacyl-CoA thiolase, peroxisomal	2	9.67	1	3.07	2	7.07
P09211	Glutathione S-transferase P	101	68.57	64	60.95	83	62.38
P09234	U1 small nuclear ribonucleoprotein C	2	11.32	0	0.00	0	0.00
P09382	Galectin-1	33	62.96	16	57.04	21	57.04
P09417	Dihydropteridine reductase	10	32.79	3	16.39	3	14.34
P09429	High mobility group protein B1	9	21.40	7	21.86	1	5.58
P09455	Retinol-binding protein 1	12	45.19	6	33.33	7	24.44
P09467	Fructose-1,6-bisphosphatase 1	2	8.88	0	0.00	2	9.17
P09486	SPARC	4	12.54	0	0.00	0	0.00
P09488	Glutathione S-transferase Mu 1	8	29.82	4	22.48	0	0.00
P09493	Tropomyosin alpha-1 chain	24	24.30	17	17.96	14	15.14

P09496	Clathrin light chain A	5	18.95	0	0.00	4	12.10
P09497	Clathrin light chain B	2	6.11	0	0.00	0	0.00
P09525	Annexin A4	35	54.23	22	36.68	17	38.87
P09543	2',3'-cyclic-nucleotide 3'-phosphodiesterase	15	25.42	8	13.54	7	14.96
P09622	Dihydrolipoyl dehydrogenase, mitochondrial	21	35.56	18	30.06	17	31.63
P09651	Heterogeneous nuclear ribonucleoprotein A1	45	33.87	39	37.37	24	30.38
P09661	U2 small nuclear ribonucleoprotein A'	7	24.71	4	16.47	3	12.16
P09669	Cytochrome c oxidase subunit 6C	3	32.00	3	32.00	0	0.00
P09769	Tyrosine-protein kinase Fgr	3	3.02	0	0.00	0	0.00
P09874	Poly [ADP-ribose] polymerase 1	26	20.12	16	14.40	9	8.88
P09914	Interferon-induced protein with tetratricopeptide repeats 1	7	13.81	0	0.00	2	5.23
P09936	Ubiquitin carboxyl-terminal hydrolase isozyme L1	4	8.07	0	0.00	0	0.00
P09960	Leukotriene A-4 hydrolase	15	20.13	9	11.29	9	14.40
P09972	Fructose-bisphosphate aldolase C	35	40.93	20	36.81	18	29.95
P0C0L4	Complement C4-A	56	25.57	41	20.76	42	24.14
P0C0L5	Complement C4-B	58	27.12	42	22.31	43	25.69
P0C0S5	Histone H2A.Z	17	45.31	17	49.22	7	28.91
P0C0S8	Histone H2A type 1	54	47.69	55	37.69	35	37.69
P0C263	Serine/threonine-protein kinase SBK2	1	4.60	0	0.00	0	0.00
P0C7P4	Putative cytochrome b-c1 complex subunit Rieske-like protein 1	11	34.28	0	0.00	0	0.00
P0C870	JmjC domain-containing protein 7	1	4.43	0	0.00	0	0.00
P0CB43	Protein FAM203B	7	32.82	4	21.79	5	25.13
P0CG05	Ig lambda-2 chain C regions	23	75.47	20	55.66	15	59.43
P0CG06	Ig lambda-3 chain C regions	22	68.87	20	55.66	15	59.43
P0CG38	POTE ankyrin domain family member I	49	8.84	0	0.00	31	7.72
P0CW22	40S ribosomal protein S17-like	21	48.89	20	48.89	20	41.48
P10155	60 kDa SS-A/Ro ribonucleoprotein	11	16.73	4	10.78	7	16.36
P10253	Lysosomal alpha-glucosidase	18	21.01	11	13.87	12	15.97
P10301	Ras-related protein R-Ras	4	16.51	4	16.51	3	5.51
P10412	Histone H1.4	44	49.32	29	45.21	19	27.85
P10415	Apoptosis regulator Bcl-2	3	4.18	3	16.74	4	16.74
P10515	Dihydrolipoyllysine-residue acetyltransferase component of pyruvate dehydrogenase	14	16.23	6	6.80	9	11.90
P10523	S-arrestin	21	40.74	12	26.91	11	20.74
P10599	Thioredoxin	12	48.57	12	40.00	10	31.43
P10606	Cytochrome c oxidase subunit 5B, mitochondrial	13	38.76	8	31.78	5	37.21
P10619	Lysosomal protective protein	5	10.63	3	6.88	0	0.00
P10644	cAMP-dependent protein kinase type I-alpha regulatory subunit	16	31.76	13	31.23	9	19.42
P10721	Mast/stem cell growth factor receptor Kit	2	1.64	1	1.03	1	1.13
P10745	Retinol-binding protein 3	56	38.01	31	28.87	37	31.19
P10768	S-formylglutathione hydrolase	20	61.70	13	39.72	15	37.59
P10809	60 kDa heat shock protein, mitochondrial	152	69.46	113	65.62	95	67.19
P10909	Clusterin	20	30.07	17	25.39	17	22.49
P11021	78 kDa glucose-regulated protein	99	49.69	76	47.55	72	40.52
P11047	Laminin subunit gamma-1	10	7.52	4	3.23	7	5.16
P11137	Microtubule-associated protein 2	12	6.62	2	1.42	1	0.77
P11142	Heat shock cognate 71 kDa protein	145	54.95	96	46.59	87	43.65
P11166	Solute carrier family 2, facilitated glucose transporter member 1	7	6.50	4	4.47	4	3.86
P11172	Uridine 5'-monophosphate synthase	4	10.42	3	8.12	2	5.62
P11177	Pyruvate dehydrogenase E1 component subunit beta, mitochondrial	25	40.95	16	33.43	7	17.27
P11182	Lipoamide acyltransferase component of branched-chain alpha-keto acid dehydrogen	3	8.30	0	0.00	0	0.00
P11216	Glycogen phosphorylase, brain form	111	44.72	66	39.62	80	40.81
P11277	Spectrin beta chain, erythrocyte	9	5.62	15	9.83	15	7.49
P11279	Lysosome-associated membrane glycoprotein 1	4	8.63	3	6.00	3	6.00
P11310	Medium-chain specific acyl-CoA dehydrogenase, mitochondrial	8	17.81	10	20.67	5	15.68
P11387	DNA topoisomerase 1	4	3.40	2	3.27	4	5.49
P11413	Glucose-6-phosphate 1-dehydrogenase	10	20.97	10	20.58	10	18.06
P11586	C-1-tetrahydrofolate synthase, cytoplasmic	25	25.45	18	20.75	17	20.43
P11717	Cation-independent mannose-6-phosphate receptor	6	1.85	1	0.44	0	0.00
P11766	Alcohol dehydrogenase class-3	12	20.86	9	20.86	7	20.32
P11940	Polyadenylate-binding protein 1	31	38.21	15	17.77	13	15.72
P12004	Proliferating cell nuclear antigen	4	18.01	4	13.03	5	22.99
P12034	Fibroblast growth factor 5	1	4.85	0	0.00	0	0.00
P12035	Keratin, type II cytoskeletal 3	2	1.11	0	0.00	0	0.00
P12081	Histidyl-tRNA synthetase, cytoplasmic	9	17.29	2	3.34	3	5.50
P12109	Collagen alpha-1(VI) chain	16	17.90	20	13.42	17	16.05
P12110	Collagen alpha-2(VI) chain	7	9.32	8	8.44	7	8.64
P12111	Collagen alpha-3(VI) chain	40	15.36	50	15.68	34	12.12
P12235	ADP/ATP translocase 1	44	53.36	36	46.64	26	49.66
P12236	ADP/ATP translocase 3	49	54.70	37	48.66	31	51.68
P12268	Inosine-5'-monophosphate dehydrogenase 2	7	10.89	5	6.23	4	7.98
P12270	Nucleoprotein TPR	21	9.40	11	5.20	14	5.67
P12271	Retinaldehyde-binding protein 1	18	41.96	13	35.02	13	21.77
P12277	Creatine kinase B-type	25	49.34	20	37.80	20	48.03
P12694	2-oxoisovalerate dehydrogenase subunit alpha, mitochondrial	4	12.36	4	11.01	2	8.99
P12814	Alpha-actinin-1	88	44.62	51	32.74	57	38.12
P12830	Cadherin-1	12	14.40	5	8.05	8	12.59
P12931	Proto-oncogene tyrosine-protein kinase Src	3	3.36	2	3.36	0	0.00
P12955	Xaa-Pro dipeptidase	31	41.78	20	31.24	20	25.56
P12956	X-ray repair cross-complementing protein 6	61	43.02	55	42.69	46	40.72
P13010	X-ray repair cross-complementing protein 5	46	39.48	41	43.58	38	36.89
P13073	Cytochrome c oxidase subunit 4 isoform 1, mitochondrial	5	17.16	4	17.16	1	5.92
P13164	Interferon-induced transmembrane protein 1	4	27.20	0	0.00	0	0.00
P13473	Lysosome-associated membrane glycoprotein 2	4	4.88	6	4.88	4	7.32

P13489	Ribonuclease inhibitor	31	45.99	18	30.37	24	34.06
P13639	Elongation factor 2	104	46.62	64	43.47	60	36.60
P13645	Keratin, type I cytoskeletal 10	3	6.51	17	23.29	0	0.00
P13647	Keratin, type II cytoskeletal 5	2	1.19	0	0.00	0	0.00
P13667	Protein disulfide-isomerase A4	28	33.95	18	25.43	15	26.36
P13671	Complement component C6	1	1.93	1	1.93	1	1.93
P13674	Prolyl 4-hydroxylase subunit alpha-1	5	13.86	5	14.04	5	15.73
P13686	Tartrate-resistant acid phosphatase type 5	6	13.85	4	9.54	4	9.54
P13693	Translationally-controlled tumor protein	9	51.74	5	28.49	4	15.70
P13716	Delta-aminolevulinic acid dehydratase	6	19.70	7	15.45	5	11.52
P13760	HLA class II histocompatibility antigen, DRB1-4 beta chain	6	12.03	3	4.89	2	4.89
P13761	HLA class II histocompatibility antigen, DRB1-7 beta chain	6	13.16	3	4.89	4	13.53
P13796	Plastin-2	23	26.00	18	25.20	22	30.62
P13797	Plastin-3	41	35.40	23	26.03	29	21.59
P13798	Acylamino-acid-releasing enzyme	8	13.11	8	10.11	7	7.10
P13804	Electron transfer flavoprotein subunit alpha, mitochondrial	33	54.05	19	35.44	18	31.53
P13807	Glycogen [starch] synthase, muscle	14	17.50	14	15.88	9	14.65
P13861	cAMP-dependent protein kinase type II-alpha regulatory subunit	19	32.18	11	29.46	12	25.74
P13929	Beta-enolase	31	38.94	22	28.80	0	0.00
P13987	CD59 glycoprotein	10	17.19	4	15.63	7	15.63
P14136	Glial fibrillary acidic protein	24	22.69	19	16.67	0	0.00
P14174	Macrophage migration inhibitory factor	30	52.17	19	48.70	16	51.30
P14209	CD99 antigen	4	7.57	2	7.57	0	0.00
P14314	Glucosidase 2 subunit beta	25	30.30	15	23.11	18	25.00
P14324	Farnesyl pyrophosphate synthase	5	7.16	3	7.16	3	7.16
P14406	Cytochrome c oxidase subunit 7A2, mitochondrial	7	27.71	9	27.71	7	27.71
P14543	Nidogen-1	2	2.33	3	2.41	0	0.00
P14550	Alcohol dehydrogenase [NADP+]	27	54.15	24	41.23	14	25.85
P14618	Pyruvate kinase isozymes M1/M2	101	71.56	83	65.35	74	59.51
P14625	Endoplasmin	76	41.34	49	33.37	44	30.01
P14672	Solute carrier family 2, facilitated glucose transporter member 4	2	5.11	0	0.00	0	0.00
P14678	Small nuclear ribonucleoprotein-associated proteins B and B'	7	28.33	6	18.33	3	8.75
P14679	Tyrosinase	2	8.13	3	10.02	2	6.99
P14854	Cytochrome c oxidase subunit 6B1	6	45.35	3	26.74	3	13.95
P14866	Heterogeneous nuclear ribonucleoprotein L	28	38.20	13	18.34	15	26.83
P14868	Aspartyl-tRNA synthetase, cytoplasmic	27	37.52	19	27.35	14	21.96
P14927	Cytochrome b-c1 complex subunit 7	10	30.63	10	30.63	4	20.72
P15104	Glutamine synthetase	2	9.92	5	9.65	4	9.65
P15121	Aldose reductase	13	30.38	5	18.35	5	17.41
P15153	Ras-related C3 botulinum toxin substrate 2	4	15.10	4	19.79	5	23.96
P15289	Arylsulfatase A	1	3.35	4	6.51	2	3.35
P15311	Ezrin	32	34.47	23	28.67	25	28.50
P15531	Nucleoside diphosphate kinase A	26	63.16	19	58.55	12	46.05
P15559	NAD(P)H dehydrogenase [quinone] 1	5	17.15	1	7.30	4	21.53
P15586	N-acetylglucosamine-6-sulfatase	10	14.13	2	3.80	4	10.87
P15735	Phosphorylase b kinase gamma catalytic chain, testis/liver isoform	2	7.64	0	0.00	0	0.00
P15880	40S ribosomal protein S2	11	18.09	14	22.87	10	24.23
P15927	Replication protein A 32 kDa subunit	2	12.59	0	0.00	0	0.00
P16070	CD44 antigen	29	12.13	16	9.43	11	6.87
P16083	Ribosyldihydronicotinamide dehydrogenase [quinone]	2	11.69	0	0.00	1	7.79
P16104	Histone H2A.x	58	41.96	61	37.06	41	37.06
P16152	Carbonyl reductase [NADPH] 1	45	67.51	36	67.51	35	57.76
P16219	Short-chain specific acyl-CoA dehydrogenase, mitochondrial	14	35.19	10	25.49	10	24.03
P16278	Beta-galactosidase	6	12.41	2	4.28	3	7.09
P16401	Histone H1.5	22	37.61	18	36.28	14	30.97
P16403	Histone H1.2	39	43.66	28	43.66	19	28.64
P16435	NADPH--cytochrome P450 reductase	10	17.87	4	10.64	4	7.24
P16615	Sarcoplasmic/endoplasmic reticulum calcium ATPase 2	28	23.32	16	14.11	17	13.72
P16930	Fumarylacetoacetase	6	18.85	2	5.01	0	0.00
P16949	Stathmin	6	29.53	9	34.90	5	22.82
P16989	DNA-binding protein A	8	18.82	7	20.70	8	19.62
P17066	Heat shock 70 kDa protein 6	50	20.53	0	0.00	0	0.00
P17096	High mobility group protein HMG-I/HMG-Y	5	23.36	3	22.43	3	23.36
P17152	Transmembrane protein 11, mitochondrial	3	12.50	2	8.33	1	8.33
P17174	Aspartate aminotransferase, cytoplasmic	21	38.01	18	27.12	15	24.94
P17480	Nucleolar transcription factor 1	12	12.30	3	5.63	4	5.89
P17540	Creatine kinase S-type, mitochondrial	9	30.07	0	0.00	3	12.41
P17568	NADH dehydrogenase [ubiquinone] 1 beta subcomplex subunit 7	4	25.55	1	10.95	1	7.30
P17612	cAMP-dependent protein kinase catalytic subunit alpha	3	12.25	0	0.00	3	9.69
P17643	5,6-dihydroxyindole-2-carboxylic acid oxidase	24	27.56	7	11.36	23	24.39
P17655	Calpain-2 catalytic subunit	17	22.43	9	15.29	7	8.71
P17812	CTP synthase 1	3	7.78	1	2.71	2	4.74
P17844	Probable ATP-dependent RNA helicase DDX5	25	24.10	18	21.82	11	17.75
P17858	6-phosphofructokinase, liver type	31	30.38	23	33.97	19	17.31
P17900	Ganglioside GM2 activator	1	10.36	2	10.36	1	10.36
P17931	Galectin-3	11	22.00	6	16.00	8	16.00
P17980	26S protease regulatory subunit 6A	13	32.57	9	22.10	15	21.18
P17987	T-complex protein 1 subunit alpha	39	45.32	26	33.81	25	42.81
P18031	Tyrosine-protein phosphatase non-receptor type 1	5	17.24	0	0.00	3	12.64
P18077	60S ribosomal protein L35a	1	8.18	1	6.36	0	0.00
P18085	ADP-ribosylation factor 4	24	47.78	19	38.89	18	41.11
P18124	60S ribosomal protein L7	15	39.92	13	32.26	11	22.18
P18135	Ig kappa chain V-III region HAH	5	33.33	9	26.36	9	33.33

P18136	Ig kappa chain V-III region HIC	5	33.33	9	26.36	9	33.33
P18206	Vinculin	38	22.75	17	16.14	18	14.99
P18428	Lipopolysaccharide-binding protein	1	3.95	0	0.00	0	0.00
P18463	HLA class I histocompatibility antigen, B-37 alpha chain	16	26.52	7	17.40	11	23.76
P18583	Protein SON	1	0.58	1	0.58	1	0.58
P18615	Negative elongation factor E	1	3.42	1	4.74	0	0.00
P18621	60S ribosomal protein L17	5	21.74	7	21.74	5	8.70
P18669	Phosphoglycerate mutase 1	37	62.99	27	62.99	24	58.66
P18754	Regulator of chromosome condensation	9	27.08	4	15.44	7	16.86
P18858	DNA ligase 1	2	1.52	0	0.00	1	1.52
P18859	ATP synthase-coupling factor 6, mitochondrial	4	40.74	0	0.00	0	0.00
P19013	Keratin, type II cytoskeletal 4	4	3.18	0	0.00	0	0.00
P19105	Myosin regulatory light chain 12A	22	68.42	12	35.09	13	36.26
P19174	1-phosphatidylinositol-4,5-bisphosphate phosphodiesterase gamma-1	3	3.02	0	0.00	0	0.00
P19320	Vascular cell adhesion protein 1	1	2.44	0	0.00	0	0.00
P19338	Nucleolin	71	32.54	62	28.87	54	23.38
P19367	Hexokinase-1	37	25.19	30	19.63	26	15.70
P19388	DNA-directed RNA polymerases I, II, and III subunit RPABC1	2	8.09	0	0.00	0	0.00
P19404	NADH dehydrogenase [ubiquinone] flavoprotein 2, mitochondrial	10	17.67	6	13.25	5	9.24
P19447	TFIIH basal transcription factor complex helicase XPB subunit	2	4.22	0	0.00	0	0.00
P19525	Interferon-induced, double-stranded RNA-activated protein kinase	5	6.53	1	2.18	1	2.18
P19623	Spermidine synthase	4	10.26	5	17.55	3	7.62
P19634	Sodium/hydrogen exchanger 1	3	3.44	0	0.00	1	1.59
P19652	Alpha-1-acid glycoprotein 2	7	22.89	0	0.00	0	0.00
P19784	Casein kinase II subunit alpha'	3	7.14	0	0.00	2	8.86
P19823	Inter-alpha-trypsin inhibitor heavy chain H2	9	11.21	9	7.72	1	1.59
P19827	Inter-alpha-trypsin inhibitor heavy chain H1	7	8.67	11	10.43	9	10.43
P19838	Nuclear factor NF-kappa-B p105 subunit	2	3.82	2	3.82	4	5.16
P19971	Thymidine phosphorylase	22	32.16	16	26.14	15	23.86
P20020	Plasma membrane calcium-transporting ATPase 1	4	4.69	0	0.00	4	4.05
P20039	HLA class II histocompatibility antigen, DRB1-11 beta chain	8	22.18	5	16.92	4	18.42
P20042	Eukaryotic translation initiation factor 2 subunit 2	9	23.72	6	20.12	5	13.51
P20073	Annexin A7	13	18.44	4	8.20	7	12.30
P20231	Tryptase beta-2	6	13.09	3	9.82	2	7.64
P20290	Transcription factor BTF3	2	22.82	6	32.04	5	22.82
P20338	Ras-related protein Rab-4A	5	20.66	0	0.00	0	0.00
P20340	Ras-related protein Rab-6A	9	33.17	4	23.08	4	16.35
P20591	Interferon-induced GTP-binding protein Mx1	57	47.13	5	11.78	1	2.27
P20618	Proteasome subunit beta type-1	13	32.37	10	35.27	12	31.54
P20645	Cation-dependent mannose-6-phosphate receptor	9	26.35	4	12.64	6	19.13
P20674	Cytochrome c oxidase subunit 5A, mitochondrial	26	65.33	22	65.33	6	36.00
P20700	Lamin-B1	38	40.61	25	29.69	16	21.84
P20774	Mimecan	5	20.47	7	20.47	4	13.09
P20810	Calpastatin	11	18.36	9	11.16	9	10.45
P20936	Ras GTPase-activating protein 1	5	5.64	0	0.00	0	0.00
P20962	Parathymosin	11	22.55	9	22.55	3	21.57
P21266	Glutathione S-transferase Mu 3	17	35.56	17	35.11	14	39.11
P21281	V-type proton ATPase subunit B, brain isoform	43	53.03	36	57.34	37	50.88
P21283	V-type proton ATPase subunit C 1	13	21.20	7	21.20	7	19.90
P21291	Cysteine and glycine-rich protein 1	12	36.79	9	35.75	5	32.12
P21333	Filamin-A	169	43.18	98	33.62	124	35.59
P21359	Neurofibromin	5	2.61	3	1.16	3	1.62
P21399	Cytoplasmic aconitate hydratase	14	19.69	13	20.92	13	19.57
P21589	5'-nucleotidase	8	20.38	4	10.80	0	0.00
P21796	Voltage-dependent anion-selective channel protein 1	40	75.27	28	75.27	26	51.59
P21810	Biglycan	11	19.57	16	17.12	9	17.12
P21912	Succinate dehydrogenase [ubiquinone] iron-sulfur subunit, mitochondrial	11	23.93	9	18.57	3	12.50
P21953	2-oxoisovalerate dehydrogenase subunit beta, mitochondrial	3	10.46	2	7.14	3	10.46
P21964	Catechol O-methyltransferase	31	61.25	19	44.65	20	48.71
P21980	Protein-glutamine gamma-glutamyltransferase 2	17	17.03	16	14.99	15	16.89
P22033	Methylmalonyl-CoA mutase, mitochondrial	1	1.47	3	5.33	1	2.13
P22059	Oxysterol-binding protein 1	3	5.20	3	5.20	2	5.20
P22061	Protein-L-isoaspartate(D-aspartate) O-methyltransferase	14	54.63	6	35.68	4	24.23
P22087	rRNA 2'-O-methyltransferase fibrillarin	15	49.84	16	53.89	6	24.92
P22102	Trifunctional purine biosynthetic protein adenosine-3	25	25.05	16	16.63	11	14.75
P22234	Multifunctional protein ADE2	10	22.35	6	16.24	10	16.00
P22314	Ubiquitin-like modifier-activating enzyme 1	61	39.32	57	33.08	48	29.96
P22392	Nucleoside diphosphate kinase B	30	75.00	25	70.39	14	63.82
P22570	NADPH:adrenodoxin oxidoreductase, mitochondrial	17	30.14	5	14.46	5	12.22
P22626	Heterogeneous nuclear ribonucleoproteins A2/B1	63	52.97	46	52.69	38	48.44
P22695	Cytochrome b-c1 complex subunit 2, mitochondrial	33	44.15	27	38.41	19	34.44
P22914	Beta-crystallin S	1	6.18	0	0.00	0	0.00
P23246	Splicing factor, proline- and glutamine-rich	38	27.02	26	17.82	21	16.27
P23258	Tubulin gamma-1 chain	13	25.50	8	28.38	8	26.39
P23284	Peptidyl-prolyl cis-trans isomerase B	25	47.22	18	39.81	16	36.57
P23297	Protein S100-A1	35	45.74	26	45.74	16	38.30
P23368	NAD-dependent malic enzyme, mitochondrial	10	15.41	3	6.16	0	0.00
P23381	Tryptophanyl-tRNA synthetase, cytoplasmic	81	66.03	34	43.31	34	42.68
P23396	40S ribosomal protein S3	25	48.56	24	46.91	24	41.56
P23497	Nuclear autoantigen Sp-100	5	7.51	2	2.27	2	2.96
P23526	Adenosylhomocysteinase	43	36.34	28	29.63	25	23.38
P23527	Histone H2B type 1-O	59	67.46	60	62.70	41	57.14
P23528	Cofilin-1	53	61.45	46	56.02	40	50.60

P23588	Eukaryotic translation initiation factor 4B	8	6.22	0	0.00	2	2.13
P23610	Factor VIII intron 22 protein	2	9.97	0	0.00	1	6.20
P23634	Plasma membrane calcium-transporting ATPase 4	17	15.87	9	11.76	9	8.06
P23786	Carnitine O-palmitoyltransferase 2, mitochondrial	6	13.22	6	12.92	1	1.52
P24534	Elongation factor 1-beta	17	42.22	5	28.00	5	12.44
P24539	ATP synthase subunit b, mitochondrial	13	31.64	4	13.67	4	13.67
P24666	Low molecular weight phosphotyrosine protein phosphatase	5	32.28	4	24.68	4	32.28
P24752	Acetyl-CoA acetyltransferase, mitochondrial	30	48.71	26	43.09	17	38.17
P24844	Myosin regulatory light polypeptide 9	12	44.19	8	34.30	0	0.00
P24941	Cyclin-dependent kinase 2	9	20.47	4	12.08	5	12.08
P25311	Zinc-alpha-2-glycoprotein	15	32.89	12	32.89	13	23.15
P25325	3-mercaptopyruvate sulfurtransferase	10	32.32	13	40.40	7	34.68
P25398	40S ribosomal protein S12	18	45.45	8	32.58	7	39.39
P25685	DnaJ homolog subfamily B member 1	6	15.59	2	3.82	1	3.82
P25705	ATP synthase subunit alpha, mitochondrial	134	58.59	91	49.01	88	48.82
P25786	Proteasome subunit alpha type-1	17	45.25	16	50.95	9	36.50
P25787	Proteasome subunit alpha type-2	17	48.29	14	38.89	13	38.46
P25788	Proteasome subunit alpha type-3	9	24.31	7	14.12	6	14.12
P25789	Proteasome subunit alpha type-4	7	19.16	6	19.54	4	16.09
P26006	Integrin alpha-3	6	4.76	2	1.90	0	0.00
P26038	Moesin	64	52.34	43	44.54	46	41.77
P26196	Probable ATP-dependent RNA helicase DDX6	10	21.33	5	7.66	6	9.73
P26358	DNA (cytosine-5)-methyltransferase 1	1	0.87	0	0.00	0	0.00
P26368	Splicing factor U2AF 65 kDa subunit	9	23.37	6	20.00	5	11.58
P26373	60S ribosomal protein L13	12	41.71	3	13.74	7	22.27
P26440	Isovaleryl-CoA dehydrogenase, mitochondrial	18	28.61	6	18.20	7	15.60
P26447	Protein S100-A4	4	27.72	0	0.00	0	0.00
P26572	Alpha-1,3-mannosyl-glycoprotein 2-beta-N-acetylglucosaminyltransferase	5	17.30	0	0.00	3	5.62
P26599	Polypyrimidine tract-binding protein 1	30	37.48	34	33.90	21	22.79
P26639	Threonyl-tRNA synthetase, cytoplasmic	11	7.61	4	3.04	6	7.88
P26640	Valyl-tRNA synthetase	57	32.91	39	24.21	32	20.81
P26641	Elongation factor 1-gamma	32	32.27	19	26.54	17	24.71
P26885	Peptidyl-prolyl cis-trans isomerase FKBP2	7	38.73	5	9.16	8	54.23
P27105	Erythrocyte band 7 integral membrane protein	15	40.97	8	34.72	9	35.42
P27144	Adenylate kinase isoenzyme 4, mitochondrial	2	21.08	2	9.87	0	0.00
P27169	Serum paraoxonase/arylesterase 1	2	11.27	2	11.27	1	6.76
P27348	14-3-3 protein theta	50	55.92	35	40.00	37	47.35
P27635	60S ribosomal protein L10	12	33.18	11	33.18	10	27.57
P27694	Replication protein A 70 kDa DNA-binding subunit	7	16.07	5	12.99	4	7.30
P27695	DNA-(apurinic or apyrimidinic site) lyase	39	66.04	23	45.28	15	39.94
P27701	CD82 antigen	2	10.49	0	0.00	0	0.00
P27708	CAD protein	17	7.64	15	7.55	16	9.53
P27797	Calreticulin	31	45.08	18	29.26	14	25.66
P27816	Microtubule-associated protein 4	19	16.32	13	15.63	11	11.11
P27824	Calnexin	44	30.41	25	16.89	24	20.61
P27987	Inositol-trisphosphate 3-kinase B	6	10.04	0	0.00	0	0.00
P28062	Proteasome subunit beta type-8	11	21.38	7	16.30	3	5.07
P28065	Proteasome subunit beta type-9	3	14.16	0	0.00	0	0.00
P28066	Proteasome subunit alpha type-5	17	30.71	13	29.88	10	26.56
P28070	Proteasome subunit beta type-4	10	26.89	5	15.15	8	23.11
P28072	Proteasome subunit beta type-6	3	8.79	0	0.00	0	0.00
P28074	Proteasome subunit beta type-5	7	25.10	6	21.29	1	6.08
P28161	Glutathione S-transferase Mu 2	8	37.61	6	24.31	5	18.35
P28288	ATP-binding cassette sub-family D member 3	2	4.40	3	7.89	4	10.02
P28289	Tropomodulin-1	2	10.58	1	4.74	2	10.58
P28331	NADH-ubiquinone oxidoreductase 75 kDa subunit, mitochondrial	34	40.72	23	29.44	24	30.54
P28340	DNA polymerase delta catalytic subunit	2	2.62	1	1.26	1	1.26
P28482	Mitogen-activated protein kinase 1	15	27.78	5	15.28	8	22.50
P28827	Receptor-type tyrosine-protein phosphatase mu	2	1.93	0	0.00	2	2.20
P28838	Cytosol aminopeptidase	52	52.99	26	36.99	23	34.30
P29144	Tripeptidyl-peptidase 2	2	1.92	4	5.93	2	2.08
P29218	Inositol monophosphatase 1	13	37.91	6	22.38	6	18.05
P29401	Transketolase	54	49.44	51	38.04	39	29.21
P29590	Protein PML	14	13.15	4	5.33	6	6.80
P29692	Elongation factor 1-delta	33	49.47	15	36.30	15	35.59
P29728	2'-5'-oligoadenylate synthase 2	3	5.29	0	0.00	0	0.00
P29762	Cellular retinoic acid-binding protein 1	3	34.31	2	24.09	0	0.00
P29966	Myristoylated alanine-rich C-kinase substrate	36	47.89	22	43.37	20	40.06
P29992	Guanine nucleotide-binding protein subunit alpha-11	6	25.07	5	18.94	5	18.66
P30038	Delta-1-pyrroline-5-carboxylate dehydrogenase, mitochondrial	11	14.39	8	8.88	5	7.28
P30040	Endoplasmic reticulum resident protein 29	18	37.93	14	37.93	10	27.20
P30041	Peroxiredoxin-6	38	68.30	23	57.59	24	58.04
P30042	ES1 protein homolog, mitochondrial	28	49.25	18	41.42	13	35.07
P30043	Flavin reductase (NADPH)	15	39.32	18	50.00	15	46.60
P30044	Peroxiredoxin-5, mitochondrial	35	39.72	25	39.25	23	45.79
P30046	D-dopachrome decarboxylase	11	55.08	5	36.44	4	29.66
P30048	Thioredoxin-dependent peroxide reductase, mitochondrial	40	47.66	19	44.53	19	32.42
P30049	ATP synthase subunit delta, mitochondrial	13	36.90	9	28.57	7	28.57
P30050	60S ribosomal protein L12	22	50.30	19	45.45	10	45.45
P30084	Enoyl-CoA hydratase, mitochondrial	18	45.17	11	33.79	13	43.45
P30085	UMP-CMP kinase	16	46.43	12	27.55	7	24.49
P30086	Phosphatidylethanolamine-binding protein 1	67	78.07	39	68.45	36	68.45
P30101	Protein disulfide-isomerase A3	98	59.01	72	53.07	60	51.88

P30153	Serine/threonine-protein phosphatase 2A 65 kDa regulatory subunit A alpha isoform	37	41.43	25	22.41	23	28.18
P30405	Peptidyl-prolyl cis-trans isomerase F, mitochondrial	3	21.74	1	14.01	0	0.00
P30419	Glycylpeptide N-tetradecanoyltransferase 1	5	11.49	5	10.28	4	7.66
P30447	HLA class I histocompatibility antigen, A-23 alpha chain	16	20.00	0	0.00	3	7.40
P30460	HLA class I histocompatibility antigen, B-8 alpha chain	21	32.32	8	17.40	14	23.76
P30462	HLA class I histocompatibility antigen, B-14 alpha chain	18	29.56	7	17.40	12	25.97
P30475	HLA class I histocompatibility antigen, B-39 alpha chain	15	26.24	5	14.09	9	22.65
P30479	HLA class I histocompatibility antigen, B-41 alpha chain	19	29.83	7	17.40	11	17.40
P30480	HLA class I histocompatibility antigen, B-42 alpha chain	21	32.32	8	17.40	30	25.97
P30481	HLA class I histocompatibility antigen, B-44 alpha chain	13	23.76	4	14.09	5	14.09
P30483	HLA class I histocompatibility antigen, B-45 alpha chain	11	20.72	4	14.09	5	14.09
P30485	HLA class I histocompatibility antigen, B-47 alpha chain	12	23.76	4	14.09	6	17.40
P30486	HLA class I histocompatibility antigen, B-48 alpha chain	13	25.41	4	6.63	12	22.38
P30487	HLA class I histocompatibility antigen, B-49 alpha chain	13	24.03	4	14.09	12	17.40
P30488	HLA class I histocompatibility antigen, B-50 alpha chain	13	24.03	4	14.09	12	17.40
P30519	Heme oxygenase 2	8	21.20	4	17.72	4	21.84
P30520	Adenylosuccinate synthetase isozyme 2	5	17.54	4	15.13	1	3.07
P30533	Alpha-2-macroglobulin receptor-associated protein	11	13.45	4	8.12	5	8.12
P30536	Translocator protein	3	13.61	3	18.34	0	0.00
P30566	Adenylosuccinate lyase	6	16.12	0	0.00	0	0.00
P30622	CAP-Gly domain-containing linker protein 1	6	4.31	0	0.00	2	2.02
P30626	Sorcin	7	27.78	4	18.69	5	24.24
P30711	Glutathione S-transferase theta-1	11	30.83	4	20.00	5	30.83
P30740	Leukocyte elastase inhibitor	9	14.78	7	25.59	6	14.78
P30837	Aldehyde dehydrogenase X, mitochondrial	45	46.23	37	36.56	31	32.88
P31040	Succinate dehydrogenase [ubiquinone] flavoprotein subunit, mitochondrial	34	34.94	17	27.26	14	18.98
P31146	Coronin-1A	2	3.47	0	0.00	2	3.47
P31150	Rab GDP dissociation inhibitor alpha	18	28.86	0	0.00	12	26.40
P31153	S-adenosylmethionine synthase isoform type-2	12	24.05	6	18.99	7	14.68
P31689	DnaJ homolog subfamily A member 1	8	24.94	0	0.00	0	0.00
P31930	Cytochrome b-c1 complex subunit 1, mitochondrial	40	47.92	37	47.92	21	33.75
P31937	3-hydroxyisobutyrate dehydrogenase, mitochondrial	32	46.43	24	38.69	28	38.99
P31939	Bifunctional purine biosynthesis protein PURH	47	44.93	29	35.30	36	43.92
P31942	Heterogeneous nuclear ribonucleoprotein H3	18	23.99	14	19.94	10	13.87
P31943	Heterogeneous nuclear ribonucleoprotein H	32	36.08	33	34.52	24	32.07
P31946	14-3-3 protein beta/alpha	46	63.41	31	38.21	32	41.87
P31948	Stress-induced-phosphoprotein 1	31	34.62	18	20.99	16	17.50
P31949	Protein S100-A11	11	40.95	11	49.52	9	49.52
P32119	Peroxiredoxin-2	32	32.32	30	40.40	26	31.82
P32189	Glycerol kinase	2	4.47	0	0.00	0	0.00
P32322	Pyrroline-5-carboxylate reductase 1, mitochondrial	2	9.72	1	4.08	0	0.00
P32455	Interferon-induced guanylate-binding protein 1	4	6.08	2	2.70	0	0.00
P32456	Interferon-induced guanylate-binding protein 2	2	2.71	2	2.71	0	0.00
P32969	60S ribosomal protein L9	11	47.92	9	42.71	4	29.17
P33121	Long-chain-fatty-acid--CoA ligase 1	17	22.78	6	11.60	11	19.91
P33176	Kinesin-1 heavy chain	25	28.35	10	10.28	10	9.35
P33240	Cleavage stimulation factor subunit 2	2	5.20	4	8.67	2	4.68
P33316	Deoxyuridine 5'-triphosphate nucleotidohydrolase, mitochondrial	16	46.03	6	24.60	6	20.63
P33778	Histone H2B type 1-B	59	67.46	60	62.70	41	57.14
P33993	DNA replication licensing factor MCM7	2	3.62	0	0.00	0	0.00
P34059	N-acetylgalactosamine-6-sulfatase	1	1.72	2	3.26	0	0.00
P34896	Serine hydroxymethyltransferase, cytosolic	15	28.36	7	20.91	10	24.22
P34897	Serine hydroxymethyltransferase, mitochondrial	12	18.45	0	0.00	4	11.51
P34913	Epoxide hydrolase 2	3	12.07	6	12.79	5	10.99
P34932	Heat shock 70 kDa protein 4	36	33.57	26	25.83	24	24.40
P35052	Glypican-1	1	3.23	0	0.00	0	0.00
P35221	Catenin alpha-1	51	40.84	19	15.34	27	27.59
P35222	Catenin beta-1	30	33.80	20	24.58	21	26.25
P35232	Prohibitin	64	75.74	48	76.10	30	64.71
P35241	Radixin	19	16.98	11	13.21	15	17.84
P35244	Replication protein A 14 kDa subunit	3	14.05	2	14.05	2	14.05
P35251	Replication factor C subunit 1	1	0.87	1	0.96	0	0.00
P35268	60S ribosomal protein L22	7	18.75	6	18.75	6	18.75
P35270	Sepiapterin reductase	16	55.17	7	24.90	6	20.69
P35527	Keratin, type I cytoskeletal 9	5	12.68	4	8.83	0	0.00
P35555	Fibrillin-1	6	1.99	1	0.31	3	1.50
P35573	Glycogen debranching enzyme	18	16.45	9	6.72	7	6.20
P35579	Myosin-9	255	48.21	197	43.27	191	40.26
P35580	Myosin-10	136	38.56	84	25.15	90	29.45
P35606	Coatomer subunit beta'	12	15.78	7	9.82	10	13.58
P35610	Sterol O-acyltransferase 1	1	2.91	2	3.82	1	2.91
P35611	Alpha-adducin	4	7.06	0	0.00	0	0.00
P35613	Basigin	10	12.47	8	14.55	9	15.84
P35658	Nuclear pore complex protein Nup214	6	3.40	3	2.11	0	0.00
P35659	Protein DEK	4	6.40	3	6.13	3	6.13
P35749	Myosin-11	52	11.41	44	14.15	40	10.95
P35813	Protein phosphatase 1A	5	10.21	2	7.07	3	4.71
P35914	Hydroxymethylglutaryl-CoA lyase, mitochondrial	7	18.77	7	18.77	4	12.00
P35998	26S protease regulatory subunit 7	14	27.02	7	17.09	7	21.48
P36269	Gamma-glutamyltransferase 5	6	13.82	5	8.36	4	8.36
P36405	ADP-ribosylation factor-like protein 3	4	24.73	3	21.43	2	18.13
P36507	Dual specificity mitogen-activated protein kinase kinase 2	11	32.00	0	0.00	2	10.75
P36542	ATP synthase subunit gamma, mitochondrial	15	27.85	12	18.79	7	15.44

P36543	V-type proton ATPase subunit E 1	12	25.22	10	15.93	6	14.60
P36551	Coproporphyrinogen-III oxidase, mitochondrial	5	11.23	0	0.00	0	0.00
P36578	60S ribosomal protein L4	40	33.72	31	28.57	23	31.62
P36776	Lon protease homolog, mitochondrial	30	24.40	16	12.10	14	12.20
P36871	Phosphoglucomutase-1	12	29.18	7	18.51	9	20.82
P36915	Guanine nucleotide-binding protein-like 1	10	15.49	3	4.45	4	9.06
P36954	DNA-directed RNA polymerase II subunit RPB9	3	18.40	3	18.40	0	0.00
P36955	Pigment epithelium-derived factor	21	34.93	16	26.79	18	32.54
P36957	Dihydrolipoyllysine-residue succinyltransferase component of 2-oxoglutarate dehydrc	23	35.10	16	22.74	13	22.74
P36959	GMP reductase 1	12	33.62	5	4.35	5	9.27
P36969	Phospholipid hydroperoxide glutathione peroxidase, mitochondrial	1	7.11	0	0.00	0	0.00
P37108	Signal recognition particle 14 kDa protein	3	17.65	0	0.00	0	0.00
P37198	Nuclear pore glycoprotein p62	10	20.69	7	8.24	3	5.56
P37235	Hippocalcin-like protein 1	6	19.69	2	4.15	1	4.15
P37802	Transgelin-2	37	62.31	10	32.66	20	46.73
P37837	Transaldolase	28	33.23	14	18.69	11	21.36
P37840	Alpha-synuclein	11	47.86	4	30.00	7	41.43
P38117	Electron transfer flavoprotein subunit beta	16	41.18	9	33.33	8	34.12
P38159	Heterogeneous nuclear ribonucleoprotein G	7	16.88	2	6.65	2	3.58
P38571	Lysosomal acid lipase/cholesteryl ester hydrolase	2	5.76	0	0.00	0	0.00
P38606	V-type proton ATPase catalytic subunit A	35	43.11	27	32.74	29	39.22
P38646	Stress-70 protein, mitochondrial	81	50.07	55	38.29	51	38.29
P38919	Eukaryotic initiation factor 4A-III	16	27.25	14	31.63	12	20.92
P39019	40S ribosomal protein S19	12	49.66	9	37.24	7	28.97
P39023	60S ribosomal protein L3	20	32.01	19	28.29	11	20.35
P39060	Collagen alpha-1(XVIII) chain	11	7.13	6	6.78	5	3.71
P39210	Protein Mpv17	2	13.07	1	13.07	2	13.07
P39656	Dolichyl-diphosphooligosaccharide--protein glycosyltransferase 48 kDa subunit	12	21.49	9	16.67	10	19.08
P39687	Acidic leucine-rich nuclear phosphoprotein 32 family member A	14	23.69	12	19.28	15	19.28
P39748	Flap endonuclease 1	3	10.00	0	0.00	0	0.00
P40121	Macrophage-capping protein	8	18.10	4	3.74	8	18.10
P40222	Alpha-taxilin	3	5.49	0	0.00	0	0.00
P40227	T-complex protein 1 subunit zeta	37	44.44	30	32.96	31	36.35
P40306	Proteasome subunit beta type-10	3	7.33	1	7.33	1	7.33
P40429	60S ribosomal protein L13a	5	17.24	4	10.84	2	10.84
P40616	ADP-ribosylation factor-like protein 1	6	34.25	5	25.97	6	39.78
P40763	Signal transducer and activator of transcription 3	12	12.86	8	8.96	7	11.43
P40925	Malate dehydrogenase, cytoplasmic	29	33.23	21	33.23	23	29.04
P40926	Malate dehydrogenase, mitochondrial	84	71.60	54	67.16	44	58.28
P40939	Trifunctional enzyme subunit alpha, mitochondrial	70	54.13	42	41.15	43	38.14
P40967	Melanocyte protein PMEL	21	18.91	18	16.04	16	14.37
P41091	Eukaryotic translation initiation factor 2 subunit 3	10	13.98	6	11.02	4	8.69
P41219	Peripherin	24	12.34	0	0.00	0	0.00
P41222	Prostaglandin-H2 D-isomerase	1	8.95	2	8.95	2	17.37
P41229	Lysine-specific demethylase 5C	1	0.90	0	0.00	0	0.00
P41240	Tyrosine-protein kinase CSK	3	9.33	4	10.89	2	6.00
P41250	Glycyl-tRNA synthetase	9	12.58	8	12.58	6	12.58
P41252	Isoleucyl-tRNA synthetase, cytoplasmic	24	16.96	11	9.27	15	13.07
P41567	Eukaryotic translation initiation factor 1	10	63.72	6	50.44	7	50.44
P42126	Enoyl-CoA delta isomerase 1, mitochondrial	12	25.83	5	12.58	4	9.27
P42167	Lamina-associated polypeptide 2, isoforms beta/gamma	13	22.25	10	17.84	14	26.87
P42224	Signal transducer and activator of transcription 1-alpha/beta	13	20.67	15	17.07	13	16.40
P42226	Signal transducer and activator of transcription 6	5	6.61	2	2.71	1	1.18
P42229	Signal transducer and activator of transcription 5A	6	11.21	4	7.43	5	6.55
P42285	Superkiller viralicidic activity 2-like 2	8	6.62	7	3.45	4	5.57
P42345	Serine/threonine-protein kinase mTOR	6	3.22	9	4.20	5	2.16
P42356	Phosphatidylinositol 4-kinase alpha	10	7.14	4	2.89	5	3.13
P42566	Epidermal growth factor receptor substrate 15	6	8.48	2	2.79	0	0.00
P42677	40S ribosomal protein S27	3	22.62	0	0.00	0	0.00
P42704	Leucine-rich PPR motif-containing protein, mitochondrial	73	38.09	50	27.04	49	29.20
P42765	3-ketoacyl-CoA thiolase, mitochondrial	9	29.22	5	17.38	6	16.12
P42785	Lysosomal Pro-X carboxypeptidase	6	9.88	2	4.23	1	4.23
P42858	Huntingtin	11	4.49	6	2.23	3	1.53
P43007	Neutral amino acid transporter A	4	4.51	0	0.00	3	4.51
P43034	Platelet-activating factor acetylhydrolase IB subunit alpha	7	20.24	1	2.93	5	13.66
P43121	Cell surface glycoprotein MUC18	14	23.68	2	5.73	9	19.97
P43155	Carnitine O-acetyltransferase	3	5.91	0	0.00	0	0.00
P43243	Matrin-3	38	29.16	23	25.27	21	21.02
P43246	DNA mismatch repair protein Msh2	7	7.17	2	3.21	3	4.39
P43304	Glycerol-3-phosphate dehydrogenase, mitochondrial	21	27.65	13	21.87	14	17.74
P43307	Translocon-associated protein subunit alpha	3	9.09	3	5.25	4	9.09
P43320	Beta-crystallin B2	2	11.71	1	7.32	2	11.22
P43487	Ran-specific GTPase-activating protein	3	16.92	3	5.47	2	5.47
P43490	Nicotinamide phosphoribosyltransferase	12	25.05	4	5.91	9	15.07
P43652	Afamin	3	5.68	6	8.35	2	2.17
P43686	26S protease regulatory subunit 6B	15	22.97	15	17.94	9	15.07
P43897	Elongation factor Ts, mitochondrial	4	16.31	0	0.00	1	5.23
P45880	Voltage-dependent anion-selective channel protein 2	22	50.34	11	29.25	19	35.71
P45954	Short/branched chain specific acyl-CoA dehydrogenase, mitochondrial	7	10.65	2	5.09	0	0.00
P45974	Ubiquitin carboxyl-terminal hydrolase 5	34	34.62	15	22.14	9	13.17
P46013	Antigen KI-67	1	0.40	0	0.00	0	0.00
P46019	Phosphorylase b kinase regulatory subunit alpha, liver isoform	1	1.46	1	1.46	1	1.46
P46060	Ran GTPase-activating protein 1	9	20.10	4	5.79	4	8.35

P46108	Adapter molecule crk	4	24.67	4	20.39	1	9.87
P46109	Crk-like protein	5	17.49	4	10.56	0	0.00
P46199	Translation initiation factor IF-2, mitochondrial	2	3.03	4	6.19	0	0.00
P46379	Large proline-rich protein BAG6	5	7.60	4	6.09	7	11.04
P46439	Glutathione S-transferase Mu 5	3	7.80	0	0.00	0	0.00
P46459	Vesicle-fusing ATPase	12	16.13	6	10.89	6	7.39
P46776	60S ribosomal protein L27a	2	14.19	2	12.16	3	6.76
P46777	60S ribosomal protein L5	19	39.06	15	29.97	14	29.97
P46778	60S ribosomal protein L21	4	31.87	1	6.88	2	9.38
P46779	60S ribosomal protein L28	4	16.06	4	20.44	6	25.55
P46781	40S ribosomal protein S9	18	32.47	10	26.80	8	18.56
P46782	40S ribosomal protein S5	23	33.33	14	28.43	16	28.43
P46783	40S ribosomal protein S10	19	47.88	21	32.73	12	23.64
P46926	Glucosamine-6-phosphate isomerase 1	9	34.95	4	21.45	8	37.02
P46939	Utrophin	13	5.21	7	2.39	5	2.50
P46940	Ras GTPase-activating-like protein IQGAP1	65	33.80	60	29.33	56	26.80
P46976	Glycogenin-1	2	5.71	2	5.71	2	2.86
P46977	Dolichyl-diphosphooligosaccharide--protein glycosyltransferase subunit STT3A	7	9.22	0	0.00	2	2.84
P47755	F-actin-capping protein subunit alpha-2	11	21.68	10	29.37	10	25.87
P47756	F-actin-capping protein subunit beta	17	27.08	12	22.02	7	13.36
P47804	RPE-retinal G protein-coupled receptor	4	7.90	4	7.90	1	4.47
P47813	Eukaryotic translation initiation factor 1A, X-chromosomal	4	14.58	0	0.00	2	14.58
P47897	Glutaminyl-tRNA synthetase	14	18.71	9	12.26	7	8.65
P47914	60S ribosomal protein L29	7	14.47	3	9.43	1	9.43
P47985	Cytochrome b-c1 complex subunit Rieske, mitochondrial	12	37.96	9	27.01	5	21.90
P48047	ATP synthase subunit O, mitochondrial	24	46.48	11	35.21	10	35.21
P48059	LIM and senescent cell antigen-like-containing domain protein 1	1	3.38	0	0.00	0	0.00
P48147	Prolyl endopeptidase	14	23.94	11	17.18	13	18.45
P48163	NADP-dependent malic enzyme	6	8.39	4	9.97	2	4.72
P48426	Phosphatidylinositol-5-phosphate 4-kinase type-2 alpha	15	22.41	11	16.01	15	18.72
P48444	Coatomer subunit delta	14	19.37	5	8.61	10	13.31
P48556	26S proteasome non-ATPase regulatory subunit 8	4	15.43	4	13.71	3	10.86
P48637	Glutathione synthetase	12	23.00	8	20.25	5	15.19
P48643	T-complex protein 1 subunit epsilon	28	30.13	13	24.95	17	26.25
P48651	Phosphatidylserine synthase 1	1	2.96	0	0.00	1	2.96
P48668	Keratin, type II cytoskeletal 6C	2	1.24	0	0.00	0	0.00
P48681	Nestin	7	4.94	2	1.73	7	5.12
P48723	Heat shock 70 kDa protein 13	1	2.76	0	0.00	0	0.00
P48729	Casein kinase I isoform alpha	2	6.23	0	0.00	1	2.97
P48735	Isocitrate dehydrogenase [NADP], mitochondrial	29	36.06	9	21.68	11	21.90
P48960	CD97 antigen	4	8.98	3	5.87	2	3.95
P49006	MARCKS-related protein	1	7.69	2	7.69	3	25.13
P49023	Paxillin	3	8.63	0	0.00	2	5.58
P49189	4-trimethylaminobutyraldehyde dehydrogenase	22	35.63	13	25.10	11	20.85
P49207	60S ribosomal protein L34	1	6.84	0	0.00	0	0.00
P49257	Protein ERGIC-53	9	20.59	8	24.90	5	18.43
P49321	Nuclear autoantigenic sperm protein	3	2.92	0	0.00	0	0.00
P49327	Fatty acid synthase	74	26.64	51	21.66	55	24.41
P49354	Protein farnesyltransferase/geranylgeranyltransferase type-1 subunit alpha	6	15.83	5	10.82	7	15.04
P49368	T-complex protein 1 subunit gamma	42	48.62	21	36.15	23	35.78
P49406	39S ribosomal protein L19, mitochondrial	3	8.22	3	8.22	2	4.79
P49407	Beta-arrestin-1	5	17.70	0	0.00	0	0.00
P49411	Elongation factor Tu, mitochondrial	66	51.77	45	47.35	29	38.50
P49419	Alpha-aminoadipic semialdehyde dehydrogenase	22	35.99	13	32.84	8	15.77
P49458	Signal recognition particle 9 kDa protein	4	25.58	2	25.58	3	25.58
P49585	Choline-phosphate cytidylyltransferase A	3	11.99	2	8.72	2	8.72
P49588	Alanyl-tRNA synthetase, cytoplasmic	28	21.90	15	17.36	16	15.50
P49589	Cysteinyl-tRNA synthetase, cytoplasmic	4	4.95	3	3.61	3	5.48
P49591	Seryl-tRNA synthetase, cytoplasmic	13	17.32	9	13.81	8	10.89
P49593	Protein phosphatase 1F	19	32.82	15	29.52	12	25.99
P49720	Proteasome subunit beta type-3	7	34.63	7	28.29	4	16.59
P49721	Proteasome subunit beta type-2	10	26.87	4	19.90	6	16.92
P49748	Very long-chain specific acyl-CoA dehydrogenase, mitochondrial	38	38.02	17	20.15	16	20.00
P49750	YLP motif-containing protein 1	3	1.49	0	0.00	0	0.00
P49753	Acyl-coenzyme A thioesterase 2, mitochondrial	23	39.54	13	29.40	12	20.91
P49754	Vacuolar protein sorting-associated protein 41 homolog	3	5.74	0	0.00	1	2.58
P49755	Transmembrane emp24 domain-containing protein 10	21	36.53	10	31.05	7	30.59
P49756	RNA-binding protein 25	10	11.63	5	6.29	3	4.86
P49773	Histidine triad nucleotide-binding protein 1	6	40.48	6	34.92	0	0.00
P49789	Bis(5'-adenosyl)-triphosphatase	2	8.84	0	0.00	0	0.00
P49792	E3 SUMO-protein ligase RanBP2	10	3.44	5	2.11	5	2.26
P49821	NADH dehydrogenase [ubiquinone] flavoprotein 1, mitochondrial	22	40.95	8	23.71	11	22.41
P49902	Cytosolic purine 5'-nucleotidase	3	8.20	2	4.99	1	2.32
P49915	GMP synthase [glutamine-hydrolyzing]	5	11.11	2	4.47	3	7.94
P49916	DNA ligase 3	3	4.06	2	2.38	2	2.58
P49959	Double-strand break repair protein MRE11A	5	8.19	6	8.47	3	4.80
P50148	Guanine nucleotide-binding protein G(q) subunit alpha	9	26.74	6	18.94	7	22.56
P50213	Isocitrate dehydrogenase [NAD] subunit alpha, mitochondrial	19	36.34	8	16.94	9	19.67
P50225	Sulfotransferase 1A1	8	26.78	0	0.00	5	16.27
P50226	Sulfotransferase 1A2	8	26.78	0	0.00	5	16.27
P50395	Rab GDP dissociation inhibitor beta	44	50.11	35	37.53	33	31.69
P50402	Emerin	7	20.08	6	20.08	6	14.96
P50453	Serpin B9	25	32.98	17	30.59	13	24.20

P50454	Serpin H1	34	36.60	29	37.80	22	33.49
P50502	Hsc70-interacting protein	15	18.97	8	16.53	8	11.65
P50552	Vasodilator-stimulated phosphoprotein	7	9.74	5	6.58	4	6.58
P50570	Dynamin-2	8	9.77	8	10.46	6	4.60
P50579	Methionine aminopeptidase 2	5	12.76	2	7.74	4	15.06
P50851	Lipopolysaccharide-responsive and beige-like anchor protein	4	1.82	3	1.47	4	1.40
P50897	Palmitoyl-protein thioesterase 1	3	15.03	1	4.90	3	10.78
P50914	60S ribosomal protein L14	9	22.33	7	19.07	5	11.16
P50990	T-complex protein 1 subunit theta	48	52.74	27	34.67	34	36.13
P50991	T-complex protein 1 subunit delta	41	46.57	22	38.78	28	44.90
P50995	Annexin A11	31	29.90	19	28.12	16	22.97
P51114	Fragile X mental retardation syndrome-related protein 1	7	8.53	5	8.53	5	12.56
P51116	Fragile X mental retardation syndrome-related protein 2	8	12.04	0	0.00	5	8.02
P51148	Ras-related protein Rab-5C	22	54.17	13	46.76	13	41.20
P51149	Ras-related protein Rab-7a	35	55.56	27	55.56	26	50.24
P51159	Ras-related protein Rab-27A	10	27.60	0	0.00	5	14.93
P51178	1-phosphatidylinositol-4,5-bisphosphate phosphodiesterase delta-1	4	9.26	0	0.00	3	5.03
P51398	28S ribosomal protein S29, mitochondrial	6	15.83	1	5.03	3	12.56
P51452	Dual specificity protein phosphatase 3	7	23.24	9	23.24	7	23.24
P51532	Transcription activator BRG1	6	3.04	3	2.43	3	1.52
P51553	Isocitrate dehydrogenase [NAD] subunit gamma, mitochondrial	12	29.52	5	20.87	4	21.63
P51570	Galactokinase	12	23.47	8	15.31	7	15.31
P51571	Translocon-associated protein subunit delta	7	17.34	7	17.34	7	17.34
P51572	B-cell receptor-associated protein 31	9	21.95	5	14.63	6	12.20
P51606	N-acylglucosamine 2-epimerase	14	22.25	6	14.99	7	18.03
P51608	Methyl-CpG-binding protein 2	5	13.58	0	0.00	3	8.85
P51648	Fatty aldehyde dehydrogenase	6	14.23	0	0.00	7	10.10
P51659	Peroxisomal multifunctional enzyme type 2	13	14.95	1	0.82	8	11.82
P51665	26S proteasome non-ATPase regulatory subunit 7	14	27.78	9	17.28	5	12.65
P51668	Ubiquitin-conjugating enzyme E2 D1	4	12.24	3	12.24	2	12.24
P51687	Sulfite oxidase, mitochondrial	2	4.40	1	4.40	0	0.00
P51689	Arylsulfatase D	1	2.53	0	0.00	0	0.00
P51790	H(+)/Cl(-) exchange transporter 3	2	1.35	0	0.00	0	0.00
P51798	H(+)/Cl(-) exchange transporter 7	8	11.55	5	5.34	4	7.33
P51810	G-protein coupled receptor 143	13	25.50	7	10.40	7	12.87
P51812	Ribosomal protein S6 kinase alpha-3	6	5.54	3	2.57	1	2.70
P51858	Hepatoma-derived growth factor	17	47.08	8	33.75	5	25.00
P51884	Lumican	19	32.84	15	14.79	15	22.49
P51888	Prolargin	8	19.11	5	9.42	4	9.95
P51948	CDK-activating kinase assembly factor MAT1	1	4.21	0	0.00	1	4.21
P51991	Heterogeneous nuclear ribonucleoprotein A3	31	27.78	21	21.16	18	21.16
P52209	6-phosphogluconate dehydrogenase, decarboxylating	13	20.70	13	20.70	9	15.32
P52272	Heterogeneous nuclear ribonucleoprotein M	56	49.32	48	40.68	31	33.29
P52292	Importin subunit alpha-2	1	4.16	0	0.00	0	0.00
P52294	Importin subunit alpha-1	1	2.60	0	0.00	1	2.60
P52434	DNA-directed RNA polymerases I, II, and III subunit RPABC3	2	8.67	0	0.00	0	0.00
P52565	Rho GDP-dissociation inhibitor 1	23	28.43	17	38.73	19	25.00
P52566	Rho GDP-dissociation inhibitor 2	3	12.44	0	0.00	0	0.00
P52597	Heterogeneous nuclear ribonucleoprotein F	27	31.81	25	29.88	15	16.63
P52630	Signal transducer and activator of transcription 2	8	14.81	3	4.58	6	8.70
P52655	Transcription initiation factor IIA subunit 1	2	2.93	3	7.45	3	7.45
P52735	Guanine nucleotide exchange factor VAV2	3	3.42	0	0.00	0	0.00
P52758	Ribonuclease UK114	2	11.68	0	0.00	2	11.68
P52788	Spermine synthase	6	20.49	6	27.05	4	13.39
P52815	39S ribosomal protein L12, mitochondrial	3	28.79	3	27.78	0	0.00
P52907	F-actin-capping protein subunit alpha-1	19	42.31	19	40.21	16	39.51
P52948	Nuclear pore complex protein Nup98-Nup96	6	4.35	1	0.83	0	0.00
P53004	Biliverdin reductase A	9	26.01	9	30.41	7	17.57
P53007	Tricarboxylate transport protein, mitochondrial	3	9.97	0	0.00	0	0.00
P53041	Serine/threonine-protein phosphatase 5	5	12.63	4	11.42	6	13.43
P53384	Cytosolic Fe-S cluster assembly factor NUBP1	2	5.62	0	0.00	2	14.06
P53396	ATP-citrate synthase	24	23.52	14	12.90	11	9.90
P53597	Succinyl-CoA ligase [ADP/GDP-forming] subunit alpha, mitochondrial	12	30.64	10	21.68	7	15.61
P53618	Coatomer subunit beta	20	22.56	12	15.74	11	16.05
P53621	Coatomer subunit alpha	22	18.30	16	14.95	18	16.50
P53634	Dipeptidyl peptidase 1	6	9.29	4	9.93	1	2.59
P53675	Clathrin heavy chain 2	52	13.41	0	0.00	0	0.00
P53677	AP-3 complex subunit mu-2	1	2.87	0	0.00	0	0.00
P53801	Pituitary tumor-transforming gene 1 protein-interacting protein	3	10.00	0	0.00	0	0.00
P53814	Smoothelin	1	0.87	0	0.00	0	0.00
P53985	Monocarboxylate transporter 1	3	2.40	3	2.40	1	2.40
P53990	IST1 homolog	1	5.22	4	7.69	2	5.22
P53992	Protein transport protein Sec24C	7	7.31	2	2.74	9	7.68
P53999	Activated RNA polymerase II transcriptional coactivator p15	5	18.90	4	18.90	3	18.90
P54136	Arginyl-tRNA synthetase, cytoplasmic	20	23.64	16	25.30	10	16.67
P54577	Tyrosyl-tRNA synthetase, cytoplasmic	10	17.42	5	12.31	4	10.98
P54578	Ubiquitin carboxyl-terminal hydrolase 14	12	21.86	8	18.22	9	25.30
P54619	5'-AMP-activated protein kinase subunit gamma-1	5	10.57	4	9.37	4	9.37
P54652	Heat shock-related 70 kDa protein 2	73	33.33	60	31.46	51	28.33
P54709	Sodium/potassium-transporting ATPase subunit beta-3	8	17.56	7	17.92	6	15.77
P54727	UV excision repair protein RAD23 homolog B	9	18.58	7	21.03	7	16.87
P54802	Alpha-N-acetylglucosaminidase	7	14.54	5	11.44	6	11.44
P54819	Adenylate kinase 2, mitochondrial	29	59.83	24	48.12	17	38.08

P54886	Delta-1-pyrroline-5-carboxylate synthase	4	5.79	0	0.00	0	0.00
P54920	Alpha-soluble NSF attachment protein	10	30.85	9	23.39	6	17.97
P55001	Microfibrillar-associated protein 2	2	5.46	0	0.00	0	0.00
P55010	Eukaryotic translation initiation factor 5	10	14.62	5	10.44	4	5.80
P55039	Developmentally-regulated GTP-binding protein 2	4	12.09	0	0.00	0	0.00
P55058	Phospholipid transfer protein	1	3.04	0	0.00	0	0.00
P55060	Exportin-2	18	18.23	15	11.33	9	8.34
P55072	Transitional endoplasmic reticulum ATPase	104	61.41	83	59.31	69	52.23
P55081	Microfibrillar-associated protein 1	1	4.10	0	0.00	0	0.00
P55084	Trifunctional enzyme subunit beta, mitochondrial	35	37.97	25	31.65	20	35.23
P55145	Mesencephalic astrocyte-derived neurotrophic factor	1	5.49	0	0.00	0	0.00
P55209	Nucleosome assembly protein 1-like 1	11	17.65	10	17.39	8	16.88
P55265	Double-stranded RNA-specific adenosine deaminase	8	8.48	0	0.00	4	4.32
P55268	Laminin subunit beta-2	26	12.24	12	6.56	13	7.45
P55327	Tumor protein D52	3	20.54	0	0.00	0	0.00
P55735	Protein SEC13 homolog	3	11.49	3	18.63	2	15.22
P55769	NHP2-like protein 1	9	49.22	3	18.75	3	18.75
P55786	Puromycin-sensitive aminopeptidase	35	29.82	25	24.05	27	23.29
P55795	Heterogeneous nuclear ribonucleoprotein H2	24	33.18	21	30.07	15	24.72
P55809	Succinyl-CoA:3-ketoacid-coenzyme A transferase 1, mitochondrial	25	40.38	12	25.00	15	28.85
P55854	Small ubiquitin-related modifier 3	4	20.39	3	11.65	1	11.65
P55884	Eukaryotic translation initiation factor 3 subunit B	29	29.12	14	18.06	16	23.46
P55957	BH3-interacting domain death agonist	3	15.38	5	22.05	2	14.36
P56134	ATP synthase subunit f, mitochondrial	8	25.53	4	25.53	4	25.53
P56182	Ribosomal RNA processing protein 1 homolog A	1	3.04	0	0.00	0	0.00
P56192	Methionyl-tRNA synthetase, cytoplasmic	25	24.78	11	14.11	16	20.33
P56377	AP-1 complex subunit sigma-2	4	20.38	1	10.19	2	10.19
P56385	ATP synthase subunit e, mitochondrial	3	34.78	2	34.78	0	0.00
P56537	Eukaryotic translation initiation factor 6	3	19.59	3	23.67	1	9.80
P56545	C-terminal-binding protein 2	5	8.99	0	0.00	4	6.52
P56693	Transcription factor SOX-10	1	1.93	0	0.00	1	5.58
P57053	Histone H2B type F-S	59	62.70	61	62.70	43	57.94
P57088	Transmembrane protein 33	7	15.79	4	6.88	4	4.86
P57105	Synaptojanin-2-binding protein	4	22.76	0	0.00	3	14.48
P57678	Gem-associated protein 4	1	1.61	0	0.00	0	0.00
P57729	Ras-related protein Rab-38	22	49.76	16	45.50	16	49.76
P57740	Nuclear pore complex protein Nup107	4	6.59	2	3.89	0	0.00
P58107	Epiplakin	21	17.07	16	13.75	14	7.33
P58546	Myotrophin	4	14.41	3	14.41	2	14.41
P58876	Histone H2B type 1-D	61	67.46	61	62.70	43	57.94
P59768	Guanine nucleotide-binding protein G(I)/G(S)/G(O) subunit gamma-2	1	22.54	0	0.00	1	22.54
P59998	Actin-related protein 2/3 complex subunit 4	11	41.07	8	41.07	9	36.31
P60033	CD81 antigen	5	15.25	5	15.25	5	15.25
P60174	Triosephosphate isomerase	93	73.08	80	70.63	73	73.08
P60228	Eukaryotic translation initiation factor 3 subunit E	12	17.53	10	15.51	7	16.40
P60660	Myosin light polypeptide 6	42	76.16	30	66.23	23	68.87
P60709	Actin, cytoplasmic 1	187	66.67	138	56.27	119	62.13
P60763	Ras-related C3 botulinum toxin substrate 3	5	19.79	4	19.79	5	23.96
P60842	Eukaryotic initiation factor 4A-I	38	39.66	29	39.66	31	39.66
P60866	40S ribosomal protein S20	6	19.33	6	25.21	3	19.33
P60891	Ribose-phosphate pyrophosphokinase 1	6	22.96	7	19.81	7	21.70
P60900	Proteasome subunit alpha type-6	18	36.99	8	17.48	7	21.14
P60903	Protein S100-A10	2	17.53	0	0.00	3	17.53
P60953	Cell division control protein 42 homolog	19	47.64	16	32.46	18	40.31
P60981	Destrin	5	26.06	3	24.24	2	17.58
P60983	Glia maturation factor beta	9	30.28	5	16.20	5	16.20
P61006	Ras-related protein Rab-8A	7	23.19	5	17.39	7	23.19
P61011	Signal recognition particle 54 kDa protein	2	4.17	0	0.00	0	0.00
P61018	Ras-related protein Rab-4B	4	15.96	0	0.00	0	0.00
P61019	Ras-related protein Rab-2A	27	67.45	11	45.28	19	58.49
P61020	Ras-related protein Rab-5B	12	43.26	9	36.74	8	42.33
P61026	Ras-related protein Rab-10	14	30.00	8	22.50	10	22.50
P61077	Ubiquitin-conjugating enzyme E2 D3	4	12.24	3	12.24	2	12.24
P61081	NEDD8-conjugating enzyme Ubc12	4	17.49	1	6.01	0	0.00
P61086	Ubiquitin-conjugating enzyme E2 K	6	26.00	4	13.50	2	9.50
P61088	Ubiquitin-conjugating enzyme E2 N	19	52.63	11	36.84	7	34.87
P61106	Ras-related protein Rab-14	20	76.28	11	60.00	14	52.56
P61158	Actin-related protein 3	23	35.17	14	27.51	12	25.12
P61160	Actin-related protein 2	18	35.28	13	35.79	13	32.49
P61163	Alpha-centractin	15	26.86	12	22.87	12	29.79
P61201	COP9 signalosome complex subunit 2	7	15.35	0	0.00	1	1.13
P61204	ADP-ribosylation factor 3	38	54.70	31	56.35	28	53.59
P61221	ATP-binding cassette sub-family E member 1	2	2.84	2	4.84	4	7.01
P61224	Ras-related protein Rap-1b	22	61.96	14	40.22	16	53.26
P61225	Ras-related protein Rap-2b	10	32.24	6	26.23	7	32.24
P61247	40S ribosomal protein S3a	14	35.98	14	26.52	15	24.62
P61254	60S ribosomal protein L26	8	26.90	5	20.69	3	20.00
P61289	Proteasome activator complex subunit 3	10	38.98	3	15.35	7	18.90
P61313	60S ribosomal protein L15	9	20.59	8	17.16	6	20.59
P61326	Protein mago nashi homolog	1	13.70	0	0.00	0	0.00
P61353	60S ribosomal protein L27	6	29.41	6	27.94	5	27.94
P61421	V-type proton ATPase subunit d 1	9	19.37	8	17.09	7	19.94
P61457	Pterin-4-alpha-carbinolamine dehydratase	2	9.62	0	0.00	0	0.00

P61586	Transforming protein RhoA	28	69.95	18	44.56	15	52.33
P61604	10 kDa heat shock protein, mitochondrial	24	60.78	14	51.96	14	51.96
P61619	Protein transport protein Sec61 subunit alpha isoform 1	4	7.35	3	12.18	2	10.08
P61758	Prefoldin subunit 3	6	21.32	4	16.24	5	16.24
P61764	Syntaxin-binding protein 1	14	22.05	2	6.40	7	16.50
P61769	Beta-2-microglobulin	5	22.69	0	0.00	1	8.40
P61803	Dolichyl-diphosphooligosaccharide--protein glycosyltransferase subunit DAD1	4	28.32	3	28.32	2	19.47
P61916	Epididymal secretory protein E1	5	15.23	5	15.23	0	0.00
P61923	Coatomer subunit zeta-1	4	16.95	2	16.95	1	10.73
P61956	Small ubiquitin-related modifier 2	3	12.63	3	12.63	1	12.63
P61960	Ubiquitin-fold modifier 1	3	50.59	1	32.94	3	50.59
P61970	Nuclear transport factor 2	9	43.31	3	21.26	2	23.62
P61978	Heterogeneous nuclear ribonucleoprotein K	62	60.91	53	46.65	46	44.92
P61981	14-3-3 protein gamma	36	44.53	24	36.84	22	30.77
P62070	Ras-related protein R-Ras2	3	17.16	0	0.00	0	0.00
P62072	Mitochondrial import inner membrane translocase subunit Tim10	1	21.11	1	7.78	0	0.00
P62081	40S ribosomal protein S7	13	30.41	19	30.41	13	26.29
P62136	Serine/threonine-protein phosphatase PP1-alpha catalytic subunit	27	49.70	18	25.76	13	24.24
P62140	Serine/threonine-protein phosphatase PP1-beta catalytic subunit	25	46.79	19	29.97	15	29.05
P62158	Calmodulin	30	44.30	23	44.30	13	42.95
P62166	Neuronal calcium sensor 1	1	5.79	0	0.00	0	0.00
P62191	26S protease regulatory subunit 4	18	40.45	11	25.91	13	22.05
P62195	26S protease regulatory subunit 8	14	33.99	11	23.15	13	27.09
P62241	40S ribosomal protein S8	19	38.46	15	34.13	19	45.67
P62244	40S ribosomal protein S15a	6	39.23	7	32.31	6	32.31
P62249	40S ribosomal protein S16	16	38.36	14	43.84	7	22.60
P62258	14-3-3 protein epsilon	63	63.53	44	50.59	47	54.90
P62263	40S ribosomal protein S14	7	36.42	8	36.42	9	36.42
P62266	40S ribosomal protein S23	7	23.08	5	28.67	3	11.89
P62269	40S ribosomal protein S18	16	48.03	10	36.18	8	30.26
P62277	40S ribosomal protein S13	15	40.40	18	35.76	10	35.76
P62280	40S ribosomal protein S11	10	39.24	8	29.11	6	22.15
P62304	Small nuclear ribonucleoprotein E	3	11.96	2	11.96	2	11.96
P62306	Small nuclear ribonucleoprotein F	1	15.12	1	15.12	1	15.12
P62308	Small nuclear ribonucleoprotein G	3	15.79	0	0.00	3	15.79
P62310	U6 snRNA-associated Sm-like protein LSm3	2	21.57	1	11.76	0	0.00
P62314	Small nuclear ribonucleoprotein Sm D1	6	54.62	7	36.97	0	0.00
P62316	Small nuclear ribonucleoprotein Sm D2	6	40.68	5	32.20	5	32.20
P62318	Small nuclear ribonucleoprotein Sm D3	11	31.75	7	31.75	4	24.60
P62330	ADP-ribosylation factor 6	3	17.71	4	24.00	1	5.71
P62333	26S protease regulatory subunit 10B	21	44.73	16	33.16	11	30.08
P62424	60S ribosomal protein L7a	17	27.44	9	14.29	9	17.67
P62495	Eukaryotic peptide chain release factor subunit 1	3	6.41	3	9.84	0	0.00
P62633	Cellular nucleic acid-binding protein	3	8.47	2	8.47	2	8.47
P62701	40S ribosomal protein S4, X isoform	19	42.21	18	35.36	13	34.22
P62714	Serine/threonine-protein phosphatase 2A catalytic subunit beta isoform	16	36.57	9	39.16	8	23.30
P62736	Actin, aortic smooth muscle	220	50.13	79	54.64	126	55.17
P62750	60S ribosomal protein L23a	6	20.51	3	8.33	3	13.46
P62753	40S ribosomal protein S6	7	18.07	0	0.00	6	22.09
P62805	Histone H4	59	56.31	42	56.31	26	51.46
P62807	Histone H2B type 1-C/E/F/G/I	61	67.46	61	62.70	43	57.94
P62820	Ras-related protein Rab-1A	23	58.05	14	38.05	15	38.05
P62826	GTP-binding nuclear protein Ran	21	39.35	13	34.26	10	25.93
P62829	60S ribosomal protein L23	6	32.14	8	30.71	8	32.14
P62837	Ubiquitin-conjugating enzyme E2 D2	4	12.24	3	12.24	2	12.24
P62841	40S ribosomal protein S15	5	23.45	0	0.00	0	0.00
P62847	40S ribosomal protein S24	4	28.57	6	28.57	5	28.57
P62851	40S ribosomal protein S25	12	29.60	10	24.00	3	22.40
P62854	40S ribosomal protein S26	5	20.87	0	0.00	4	20.87
P62857	40S ribosomal protein S28	5	46.38	3	17.39	6	46.38
P62873	Guanine nucleotide-binding protein G(I)/G(S)/G(T) subunit beta-1	13	22.35	5	15.29	11	25.29
P62879	Guanine nucleotide-binding protein G(I)/G(S)/G(T) subunit beta-2	11	37.06	4	22.35	7	21.47
P62888	60S ribosomal protein L30	5	24.35	4	24.35	4	24.35
P62899	60S ribosomal protein L31	7	31.20	5	25.60	3	11.20
P62906	60S ribosomal protein L10a	9	29.49	6	19.35	5	23.50
P62910	60S ribosomal protein L32	4	20.74	3	22.22	2	14.81
P62913	60S ribosomal protein L11	7	21.91	3	12.36	5	17.42
P62917	60S ribosomal protein L8	9	18.68	4	10.51	3	10.51
P62937	Peptidyl-prolyl cis-trans isomerase A	79	76.97	55	72.12	51	53.33
P62942	Peptidyl-prolyl cis-trans isomerase FKBP1A	10	39.81	0	0.00	0	0.00
P62979	Ubiquitin-40S ribosomal protein S27a	35	50.00	26	50.00	22	46.15
P62993	Growth factor receptor-bound protein 2	2	10.14	0	0.00	0	0.00
P62995	Transformer-2 protein homolog beta	3	11.81	4	9.72	2	4.86
P63000	Ras-related C3 botulinum toxin substrate 1	6	27.08	4	19.79	6	27.08
P63010	AP-2 complex subunit beta	20	19.32	20	17.61	18	19.64
P63027	Vesicle-associated membrane protein 2	6	35.34	1	14.66	6	29.31
P63092	Guanine nucleotide-binding protein G(s) subunit alpha isoforms short	18	42.89	10	27.66	8	23.35
P63096	Guanine nucleotide-binding protein G(i) subunit alpha-1	7	15.82	6	12.43	5	15.82
P63104	14-3-3 protein zeta/delta	96	68.16	63	54.29	66	47.76
P63151	Serine/threonine-protein phosphatase 2A 55 kDa regulatory subunit B alpha isoform	9	21.48	7	12.53	3	5.59
P63167	Dynein light chain 1, cytoplasmic	4	44.94	3	32.58	0	0.00
P63173	60S ribosomal protein L38	4	48.57	0	0.00	0	0.00
P63208	S-phase kinase-associated protein 1	10	46.63	5	19.63	6	15.95

P63220	40S ribosomal protein S21	8	54.22	6	42.17	0	0.00
P63241	Eukaryotic translation initiation factor 5A-1	25	36.36	26	33.77	15	28.57
P63244	Guanine nucleotide-binding protein subunit beta-2-like 1	30	57.73	25	46.06	20	40.06
P63261	Actin, cytoplasmic 2	187	66.67	138	56.27	119	62.13
P63267	Actin, gamma-enteric smooth muscle	104	46.81	74	51.33	60	51.86
P63279	SUMO-conjugating enzyme UBC9	2	13.92	0	0.00	0	0.00
P63313	Thymosin beta-10	3	47.73	3	47.73	0	0.00
P67775	Serine/threonine-protein phosphatase 2A catalytic subunit alpha isoform	15	32.36	9	39.16	8	23.30
P67809	Nuclease-sensitive element-binding protein 1	25	37.96	15	27.47	20	30.86
P67812	Signal peptidase complex catalytic subunit SEC11A	3	15.64	2	10.61	3	15.64
P67870	Casein kinase II subunit beta	3	15.81	2	10.70	0	0.00
P67936	Tropomyosin alpha-4 chain	37	50.40	27	37.50	25	33.06
P68032	Actin, alpha cardiac muscle 1	110	50.13	79	54.64	63	55.17
P68036	Ubiquitin-conjugating enzyme E2 L3	16	38.96	10	36.36	13	46.10
P68104	Elongation factor 1-alpha 1	107	62.77	75	47.84	58	48.27
P68133	Actin, alpha skeletal muscle	120	50.13	86	54.91	70	55.44
P68363	Tubulin alpha-1B chain	157	74.06	127	65.19	0	0.00
P68366	Tubulin alpha-4A chain	125	62.28	107	54.69	95	60.27
P68371	Tubulin beta-4B chain	169	75.73	118	74.16	0	0.00
P68400	Casein kinase II subunit alpha	5	19.69	3	13.30	1	3.33
P68402	Platelet-activating factor acetylhydrolase IB subunit beta	9	19.21	8	14.41	9	14.41
P68431	Histone H3.1	18	44.85	13	38.24	7	21.32
P68871	Hemoglobin subunit beta	207	93.88	216	93.88	180	91.84
P69849	Nodal modulator 3	10	10.15	5	4.75	6	7.20
P69891	Hemoglobin subunit gamma-1	31	30.61	0	0.00	0	0.00
P69892	Hemoglobin subunit gamma-2	31	30.61	0	0.00	0	0.00
P69905	Hemoglobin subunit alpha	118	85.21	167	87.32	103	64.08
P78324	Tyrosine-protein phosphatase non-receptor type substrate 1	9	16.07	3	7.14	0	0.00
P78344	Eukaryotic translation initiation factor 4 gamma 2	5	2.87	2	1.10	2	1.10
P78347	General transcription factor II-I	11	10.02	4	2.00	2	2.00
P78371	T-complex protein 1 subunit beta	55	55.51	34	45.61	32	47.29
P78385	Keratin, type II cuticular Hb3	3	3.04	0	0.00	0	0.00
P78386	Keratin, type II cuticular Hb5	2	1.38	0	0.00	0	0.00
P78406	mRNA export factor	1	4.08	1	4.08	1	4.08
P78417	Glutathione S-transferase omega-1	17	29.46	13	26.97	16	36.51
P78527	DNA-dependent protein kinase catalytic subunit	127	23.62	79	17.90	70	15.55
P79483	HLA class II histocompatibility antigen, DR beta 3 chain	6	13.16	3	4.89	3	9.77
P80303	Nucleobindin-2	6	12.86	1	2.14	1	2.14
P80362	Ig kappa chain V-I region WAT	5	16.67	6	16.67	9	22.22
P80723	Brain acid soluble protein 1	6	29.96	3	14.54	5	24.23
P80748	Ig lambda chain V-III region LOI	3	21.62	6	22.52	0	0.00
P82663	28S ribosomal protein S25, mitochondrial	2	16.18	1	6.36	0	0.00
P82675	28S ribosomal protein S5, mitochondrial	2	5.12	2	4.65	3	7.67
P82909	28S ribosomal protein S36, mitochondrial	3	35.92	0	0.00	0	0.00
P82932	28S ribosomal protein S6, mitochondrial	1	19.20	0	0.00	0	0.00
P82933	28S ribosomal protein S9, mitochondrial	3	7.83	3	9.09	0	0.00
P83731	60S ribosomal protein L24	6	20.38	3	20.38	3	19.11
P84022	Mothers against decapentaplegic homolog 3	2	5.65	0	0.00	0	0.00
P84077	ADP-ribosylation factor 1	38	54.70	30	53.59	28	53.59
P84090	Enhancer of rudimentary homolog	4	16.35	1	5.77	2	16.35
P84095	Rho-related GTP-binding protein RhoG	3	18.85	3	24.61	4	24.61
P84098	60S ribosomal protein L19	3	7.65	0	0.00	0	0.00
P84103	Serine/arginine-rich splicing factor 3	8	30.49	6	30.49	0	0.00
P84157	Matrix-remodeling-associated protein 7	14	34.31	6	32.35	6	32.35
P84243	Histone H3.3	16	38.24	12	31.62	7	21.32
P85037	Forkhead box protein K1	1	1.77	0	0.00	0	0.00
P86790	Vacuolar fusion protein CCZ1 homolog-like	1	2.49	0	0.00	0	0.00
P86791	Vacuolar fusion protein CCZ1 homolog	1	2.49	0	0.00	0	0.00
P98160	Basement membrane-specific heparan sulfate proteoglycan core protein	29	7.49	34	9.06	26	7.20
P98175	RNA-binding protein 10	1	1.61	0	0.00	0	0.00
P98179	Putative RNA-binding protein 3	4	24.20	4	24.20	4	24.20
P99999	Cytochrome c	25	55.24	18	55.24	11	47.62
Q00059	Transcription factor A, mitochondrial	7	14.63	3	8.54	2	4.06
Q00169	Phosphatidylinositol transfer protein alpha isoform	4	11.48	5	20.00	3	20.00
Q00325	Phosphate carrier protein, mitochondrial	22	21.55	12	19.34	8	13.26
Q00341	Vigilin	16	15.30	10	9.15	10	9.39
Q00577	Transcriptional activator protein Pur-alpha	14	36.96	14	34.16	11	26.71
Q00610	Clathrin heavy chain 1	168	50.75	123	42.99	107	41.01
Q00613	Heat shock factor protein 1	1	5.10	0	0.00	0	0.00
Q00653	Nuclear factor NF-kappa-B p100 subunit	4	4.33	0	0.00	1	1.44
Q00688	Peptidyl-prolyl cis-trans isomerase FKBP3	6	18.30	2	9.82	1	4.91
Q00765	Receptor expression-enhancing protein 5	3	14.81	0	0.00	1	5.29
Q00796	Sorbitol dehydrogenase	20	32.21	13	25.49	15	36.97
Q00839	Heterogeneous nuclear ribonucleoprotein U	56	36.12	46	30.55	30	17.82
Q01081	Splicing factor U2AF 35 kDa subunit	6	12.92	0	0.00	0	0.00
Q01082	Spectrin beta chain, brain 1	154	46.28	88	31.43	80	27.62
Q01085	Nucleolysin TIAR	2	9.33	0	0.00	0	0.00
Q01105	Protein SET	46	32.76	33	26.21	24	26.21
Q01130	Serine/arginine-rich splicing factor 2	5	21.72	6	18.55	0	0.00
Q01433	AMP deaminase 2	3	4.55	1	2.05	3	5.92
Q01469	Fatty acid-binding protein, epidermal	6	39.26	2	6.67	2	6.67
Q01484	Ankyrin-2	3	0.54	0	0.00	4	1.02
Q01518	Adenylyl cyclase-associated protein 1	32	33.68	30	31.16	25	27.79

Q01546	Keratin, type II cytoskeletal 2 oral	2	1.10	0	0.00	0	0.00
Q01628	Interferon-induced transmembrane protein 3	6	24.81	0	0.00	0	0.00
Q01629	Interferon-induced transmembrane protein 2	4	24.24	0	0.00	0	0.00
Q01650	Large neutral amino acids transporter small subunit 1	9	9.47	5	6.31	5	6.31
Q01658	Protein Dr1	1	7.39	0	0.00	1	7.39
Q01813	6-phosphofructokinase type C	12	19.01	6	9.95	7	9.06
Q01844	RNA-binding protein EWS	5	8.54	6	11.89	7	5.79
Q01970	1-phosphatidylinositol-4,5-bisphosphate phosphodiesterase beta-3	3	3.49	1	1.62	2	2.67
Q01995	Transgelin	5	25.37	5	25.37	3	12.44
Q02218	2-oxoglutarate dehydrogenase, mitochondrial	43	29.52	32	25.12	27	17.99
Q02252	Methylmalonate-semialdehyde dehydrogenase [acylating], mitochondrial	24	36.07	15	21.87	13	22.80
Q02318	Sterol 26-hydroxylase, mitochondrial	14	28.81	0	0.00	0	0.00
Q02338	D-beta-hydroxybutyrate dehydrogenase, mitochondrial	3	6.41	5	14.29	2	3.21
Q02447	Transcription factor Sp3	1	2.05	1	2.05	1	2.05
Q02539	Histone H1.1	19	24.19	0	0.00	0	0.00
Q02543	60S ribosomal protein L18a	7	30.68	9	34.66	4	15.34
Q02750	Dual specificity mitogen-activated protein kinase kinase 1	4	9.41	0	0.00	0	0.00
Q02790	Peptidyl-prolyl cis-trans isomerase FKBP4	7	17.86	6	14.38	7	11.76
Q02818	Nucleobindin-1	19	33.84	14	22.34	12	19.31
Q02878	60S ribosomal protein L6	24	31.94	16	28.47	11	22.22
Q02952	A-kinase anchor protein 12	28	16.55	15	11.05	21	14.42
Q02978	Mitochondrial 2-oxoglutarate/malate carrier protein	21	50.64	13	35.99	12	32.48
Q03013	Glutathione S-transferase Mu 4	7	25.23	0	0.00	0	0.00
Q03135	Caveolin-1	6	25.28	3	19.66	2	11.80
Q03154	Aminoacylase-1	12	33.33	15	33.33	3	12.75
Q03252	Lamin-B2	50	48.00	38	40.50	26	29.83
Q03518	Antigen peptide transporter 1	7	14.11	0	0.00	0	0.00
Q04323	UBX domain-containing protein 1	3	24.92	3	24.92	4	16.16
Q04446	1,4-alpha-glucan-branching enzyme	9	14.96	8	12.54	7	8.55
Q04637	Eukaryotic translation initiation factor 4 gamma 1	14	6.50	5	3.44	4	2.25
Q04671	P protein	1	1.19	0	0.00	0	0.00
Q04760	Lactoylglutathione lyase	25	44.57	16	24.46	11	24.46
Q04826	HLA class I histocompatibility antigen, B-40 alpha chain	16	26.52	5	14.09	9	17.40
Q04837	Single-stranded DNA-binding protein, mitochondrial	9	41.89	6	20.27	6	20.27
Q04917	14-3-3 protein eta	29	51.63	22	47.56	23	44.31
Q05397	Focal adhesion kinase 1	6	4.47	0	0.00	3	3.71
Q05519	Serine/arginine-rich splicing factor 11	3	4.34	2	4.34	0	0.00
Q05682	Caldesmon	23	18.41	10	13.62	10	14.00
Q05707	Collagen alpha-1(XIV) chain	5	3.84	0	0.00	0	0.00
Q06124	Tyrosine-protein phosphatase non-receptor type 11	5	11.22	3	7.20	0	0.00
Q06136	3-ketodihydrosphingosine reductase	3	7.53	2	3.31	4	10.54
Q06265	Exosome complex component RRP45	1	2.28	0	0.00	0	0.00
Q06323	Proteasome activator complex subunit 1	22	39.36	21	42.57	19	34.94
Q06546	GA-binding protein alpha chain	2	5.95	2	5.95	2	5.95
Q06787	Fragile X mental retardation 1 protein	8	9.81	4	5.54	4	8.54
Q06830	Peroxiredoxin-1	45	55.28	26	49.25	23	49.25
Q07020	60S ribosomal protein L18	9	25.00	6	25.00	5	19.68
Q07021	Complement component 1 Q subcomponent-binding protein, mitochondrial	36	31.56	22	26.24	20	26.95
Q07065	Cytoskeleton-associated protein 4	15	24.58	11	18.77	12	17.77
Q07157	Tight junction protein ZO-1	5	4.81	0	0.00	7	3.78
Q07666	KH domain-containing, RNA-binding, signal transduction-associated protein 1	11	14.00	9	9.26	2	6.09
Q07812	Apoptosis regulator BAX	4	19.27	2	12.50	0	0.00
Q07817	Bcl-2-like protein 1	1	4.29	0	0.00	0	0.00
Q07866	Kinesin light chain 1	9	17.98	0	0.00	5	10.47
Q07954	Prolow-density lipoprotein receptor-related protein 1	9	2.84	9	2.51	7	2.58
Q07955	Serine/arginine-rich splicing factor 1	20	40.73	14	30.65	10	22.58
Q07960	Rho GTPase-activating protein 1	21	31.44	9	28.70	11	24.60
Q08170	Serine/arginine-rich splicing factor 4	8	11.13	3	6.68	0	0.00
Q08211	ATP-dependent RNA helicase A	55	22.83	42	21.50	32	19.69
Q08257	Quinone oxidoreductase	9	42.25	7	31.00	4	12.46
Q08378	Golgin subfamily A member 3	7	6.34	0	0.00	3	1.94
Q08380	Galectin-3-binding protein	36	31.62	15	14.53	19	18.97
Q08623	Pseudouridine-5'-monophosphatase	3	13.16	5	13.16	3	13.16
Q08722	Leukocyte surface antigen CD47	2	6.19	0	0.00	1	2.48
Q08752	Peptidyl-prolyl cis-trans isomerase D	2	4.05	0	0.00	0	0.00
Q08945	FACT complex subunit SSRP1	6	12.13	6	9.87	2	4.94
Q08AD1	Calmodulin-regulated spectrin-associated protein 2	1	0.60	0	0.00	0	0.00
Q08AM6	Protein VAC14 homolog	11	16.24	6	9.08	7	12.53
Q08J23	tRNA (cytosine(34)-C(5))-methyltransferase	11	16.30	5	8.21	4	6.00
Q09028	Histone-binding protein RBBP4	5	14.59	7	16.71	4	9.18
Q09161	Nuclear cap-binding protein subunit 1	5	5.82	4	5.82	0	0.00
Q09666	Neuroblast differentiation-associated protein AHNAK	170	37.56	134	30.29	146	31.39
Q0VDG4	Secernin-3	1	2.59	1	2.59	1	2.59
Q10567	AP-1 complex subunit beta-1	28	20.02	14	15.28	22	21.81
Q10588	ADP-ribosyl cyclase 2	3	9.75	0	0.00	0	0.00
Q10713	Mitochondrial-processing peptidase subunit alpha	12	24.76	9	17.71	4	10.67
Q12765	Secernin-1	2	3.86	2	3.86	3	7.01
Q12767	Uncharacterized protein KIAA0195	1	0.88	3	2.06	0	0.00
Q12768	WASH complex subunit strumpellin	13	6.47	8	3.71	8	6.13
Q12788	Transducin beta-like protein 3	6	7.92	0	0.00	1	1.61
Q12797	Aspartyl/asparaginyl beta-hydroxylase	21	26.39	5	9.10	11	16.36
Q12802	A-kinase anchor protein 13	2	0.75	0	0.00	0	0.00
Q12824	SWI/SNF-related matrix-associated actin-dependent regulator of chromatin subfamily	2	7.01	0	0.00	1	3.38

Q12849	G-rich sequence factor 1	3	8.75	1	2.50	0	0.00
Q12874	Splicing factor 3A subunit 3	9	20.16	3	10.38	3	10.38
Q12904	Aminoacyl tRNA synthase complex-interacting multifunctional protein 1	8	19.55	8	20.51	6	13.78
Q12905	Interleukin enhancer-binding factor 2	22	43.59	20	46.41	22	42.05
Q12906	Interleukin enhancer-binding factor 3	45	33.67	36	24.05	28	26.62
Q12907	Vesicular integral-membrane protein VIP36	7	18.26	5	12.64	3	9.55
Q12929	Epidermal growth factor receptor kinase substrate 8	10	13.99	3	7.06	4	5.11
Q12931	Heat shock protein 75 kDa, mitochondrial	22	20.74	10	16.48	11	12.07
Q12959	Disks large homolog 1	2	2.32	1	1.00	0	0.00
Q13011	Delta(3,5)-Delta(2,4)-dienoyl-CoA isomerase, mitochondrial	12	41.16	7	25.00	7	27.74
Q13033	Striatin-3	2	2.13	0	0.00	0	0.00
Q13043	Serine/threonine-protein kinase 4	2	4.93	0	0.00	1	3.29
Q13045	Protein flightless-1 homolog	15	9.85	9	4.57	8	6.93
Q13057	Bifunctional coenzyme A synthase	6	13.83	3	6.74	4	8.87
Q13084	39S ribosomal protein L28, mitochondrial	3	19.92	0	0.00	0	0.00
Q13098	COP9 signalosome complex subunit 1	3	4.68	2	5.70	1	3.26
Q13126	S-methyl-5'-thioadenosine phosphorylase	16	55.12	13	50.18	11	46.64
Q13136	Liprin-alpha-1	2	2.58	0	0.00	0	0.00
Q13144	Translation initiation factor eIF-2B subunit epsilon	4	8.46	2	4.58	2	4.30
Q13148	TAR DNA-binding protein 43	7	19.81	6	13.04	4	13.04
Q13151	Heterogeneous nuclear ribonucleoprotein A0	14	30.49	11	25.90	6	15.74
Q13155	Aminoacyl tRNA synthase complex-interacting multifunctional protein 2	11	21.88	8	19.37	4	14.06
Q13162	Peroxiredoxin-4	17	30.26	10	19.19	9	14.39
Q13177	Serine/threonine-protein kinase PAK 2	2	4.96	0	0.00	2	8.97
Q13185	Chromobox protein homolog 3	13	39.34	6	28.42	7	22.40
Q13200	26S proteasome non-ATPase regulatory subunit 2	19	28.74	16	21.70	14	15.31
Q13228	Selenium-binding protein 1	41	45.55	28	39.41	16	33.26
Q13242	Serine/arginine-rich splicing factor 9	4	19.00	0	0.00	0	0.00
Q13247	Serine/arginine-rich splicing factor 6	9	17.73	4	12.21	0	0.00
Q13263	Transcription intermediary factor 1-beta	23	25.75	13	8.62	14	19.04
Q13283	Ras GTPase-activating protein-binding protein 1	13	25.97	7	14.81	6	15.02
Q13303	Voltage-gated potassium channel subunit beta-2	7	23.16	6	23.71	4	18.53
Q13308	Inactive tyrosine-protein kinase 7	4	5.89	4	5.14	3	5.05
Q13315	Serine-protein kinase ATM	3	1.18	2	0.95	2	0.79
Q13347	Eukaryotic translation initiation factor 3 subunit I	7	23.08	0	0.00	5	21.23
Q13362	Serine/threonine-protein phosphatase 2A 56 kDa regulatory subunit gamma isoform	2	4.77	0	0.00	1	2.67
Q13363	C-terminal-binding protein 1	6	14.77	0	0.00	3	6.59
Q13405	39S ribosomal protein L49, mitochondrial	5	30.12	5	23.49	2	15.06
Q13409	Cytoplasmic dynein 1 intermediate chain 2	11	16.61	9	17.40	6	13.79
Q13418	Integrin-linked protein kinase	4	5.53	2	5.31	1	3.10
Q13423	NAD(P) transhydrogenase, mitochondrial	46	33.24	19	16.76	21	19.15
Q13425	Beta-2-syntrophin	5	8.33	0	0.00	3	5.37
Q13428	Treacle protein	6	5.04	4	2.08	3	1.95
Q13435	Splicing factor 3B subunit 2	13	14.86	4	6.37	6	7.04
Q13442	28 kDa heat- and acid-stable phosphoprotein	4	16.57	3	7.73	4	7.73
Q13459	Myosin-IXb	15	9.50	8	5.10	10	5.93
Q13485	Mothers against decapentaplegic homolog 4	2	3.80	0	0.00	2	3.80
Q13488	V-type proton ATPase 116 kDa subunit a isoform 3	3	5.06	0	0.00	0	0.00
Q13491	Neuronal membrane glycoprotein M6-b	2	7.55	0	0.00	0	0.00
Q13492	Phosphatidylinositol-binding clathrin assembly protein	5	9.82	0	0.00	0	0.00
Q13505	Metaxin-1	4	9.01	1	3.00	0	0.00
Q13509	Tubulin beta-3 chain	105	59.56	0	0.00	0	0.00
Q13510	Acid ceramidase	34	44.05	23	31.65	29	37.22
Q13523	Serine/threonine-protein kinase PRP4 homolog	2	2.78	0	0.00	0	0.00
Q13541	Eukaryotic translation initiation factor 4E-binding protein 1	1	22.03	1	22.03	0	0.00
Q13557	Calcium/calmodulin-dependent protein kinase type II subunit delta	5	6.21	3	7.62	1	2.60
Q13561	Dynactin subunit 2	24	48.88	18	33.42	14	24.19
Q13586	Stromal interaction molecule 1	5	9.63	0	0.00	6	11.24
Q13595	Transformer-2 protein homolog alpha	3	12.06	4	11.35	0	0.00
Q13596	Sorting nexin-1	9	21.07	0	0.00	0	0.00
Q13601	KRR1 small subunit processome component homolog	2	6.82	0	0.00	2	6.82
Q13617	Cullin-2	3	5.23	2	2.95	0	0.00
Q13618	Cullin-3	7	9.12	2	3.78	3	4.69
Q13619	Cullin-4A	10	9.88	6	5.80	8	6.46
Q13620	Cullin-4B	11	12.27	4	4.49	8	6.35
Q13630	GDP-L-fucose synthase	13	29.91	7	26.48	5	14.02
Q13637	Ras-related protein Rab-32	13	45.33	11	32.00	13	26.22
Q13642	Four and a half LIM domains protein 1	4	5.26	1	3.71	0	0.00
Q13685	Angio-associated migratory cell protein	1	2.54	0	0.00	0	0.00
Q13724	Mannosyl-oligosaccharide glucosidase	11	15.89	8	11.35	8	9.20
Q13748	Tubulin alpha-3C/D chain	140	66.44	109	53.78	0	0.00
Q13765	Nascent polypeptide-associated complex subunit alpha	10	25.58	6	25.58	6	19.53
Q13813	Spectrin alpha chain, brain	211	50.61	145	39.36	117	33.29
Q13838	Spliceosome RNA helicase DDX39B	36	43.69	26	30.61	21	22.43
Q13867	Bleomycin hydrolase	3	5.49	3	5.93	3	5.93
Q13885	Tubulin beta-2A chain	172	70.11	106	68.99	92	68.54
Q13895	Bystin	7	15.33	4	11.67	3	8.70
Q13907	Isopentenyl-diphosphate Delta-isomerase 1	1	8.81	1	8.81	2	17.18
Q13938	Calcyphosin	2	14.29	0	0.00	0	0.00
Q14008	Cytoskeleton-associated protein 5	5	2.66	0	0.00	0	0.00
Q14011	Cold-inducible RNA-binding protein	7	33.14	8	26.74	7	26.74
Q14019	Coactosin-like protein	5	46.48	2	30.28	2	30.28
Q14103	Heterogeneous nuclear ribonucleoprotein D0	23	30.14	22	19.72	15	20.00

Q14108	Lysosome membrane protein 2	10	16.74	4	8.58	5	8.58
Q14112	Nidogen-2	2	2.11	2	2.11	1	2.11
Q14137	Ribosome biogenesis protein BOP1	5	10.46	6	14.21	3	5.90
Q14139	Ubiquitin conjugation factor E4 A	6	7.04	3	3.94	2	3.94
Q14151	Scaffold attachment factor B2	6	5.04	0	0.00	4	3.78
Q14152	Eukaryotic translation initiation factor 3 subunit A	24	14.98	14	9.41	18	12.01
Q14155	Rho guanine nucleotide exchange factor 7	2	2.37	0	0.00	1	1.49
Q14156	Protein EFR3 homolog A	4	6.94	2	3.65	3	5.36
Q14157	Ubiquitin-associated protein 2-like	6	6.72	4	5.34	2	1.84
Q14160	Protein scribble homolog	14	11.66	5	3.56	2	0.80
Q14165	Malectin	10	29.45	0	0.00	0	0.00
Q14166	Tubulin--tyrosine ligase-like protein 12	10	17.24	5	10.71	9	15.53
Q14185	Dedicator of cytokinesis protein 1	3	2.47	0	0.00	1	1.18
Q14195	Dihydropyrimidinase-related protein 3	11	24.56	9	21.75	5	12.81
Q14203	Dynactin subunit 1	28	25.82	16	14.40	15	15.26
Q14204	Cytoplasmic dynein 1 heavy chain 1	191	31.19	111	19.89	122	24.24
Q14232	Translation initiation factor eIF-2B subunit alpha	3	11.48	2	7.21	0	0.00
Q14240	Eukaryotic initiation factor 4A-II	29	42.01	21	26.54	27	26.54
Q14247	Src substrate cortactin	15	27.82	8	10.55	9	15.09
Q14254	Flotillin-2	23	41.36	15	29.67	13	26.40
Q14257	Reticulocalbin-2	5	26.50	7	24.29	2	13.25
Q14258	E3 ubiquitin/ISG15 ligase TRIM25	9	11.75	4	5.71	4	8.09
Q14315	Filamin-C	17	7.19	0	0.00	7	2.94
Q14318	Peptidyl-prolyl cis-trans isomerase FKBP8	1	3.88	0	0.00	0	0.00
Q14344	Guanine nucleotide-binding protein subunit alpha-13	8	26.79	4	7.43	4	15.65
Q14376	UDP-glucose 4-epimerase	7	28.45	6	20.11	5	21.26
Q14409	Putative glycerol kinase 3	2	4.52	0	0.00	0	0.00
Q14410	Glycerol kinase 2	1	2.17	0	0.00	0	0.00
Q14498	RNA-binding protein 39	11	25.85	5	15.66	5	14.72
Q14533	Keratin, type II cuticular Hb1	3	2.97	0	0.00	0	0.00
Q14558	Phosphoribosyl pyrophosphate synthase-associated protein 1	4	12.64	4	12.08	4	12.64
Q14624	Inter-alpha-trypsin inhibitor heavy chain H4	15	19.78	13	16.77	7	12.90
Q14657	L antigen family member 3	4	37.06	3	37.06	2	37.06
Q14667	UPF0378 protein KIAA0100	1	0.76	1	0.76	1	0.76
Q14683	Structural maintenance of chromosomes protein 1A	5	5.51	3	3.00	0	0.00
Q14690	Protein RRP5 homolog	3	1.98	0	0.00	0	0.00
Q14693	Phosphatidate phosphatase LPIN1	1	2.47	1	2.47	1	2.47
Q14696	LDLR chaperone MESD	5	17.95	1	9.40	2	11.54
Q14697	Neutral alpha-glucosidase AB	71	45.23	48	33.05	45	36.86
Q14728	Major facilitator superfamily domain-containing protein 10	1	2.86	1	2.86	1	2.86
Q14738	Serine/threonine-protein phosphatase 2A 56 kDa regulatory subunit delta isoform	6	13.12	0	0.00	3	6.48
Q14764	Major vault protein	24	25.98	16	21.16	13	15.12
Q14789	Golgin subfamily B member 1	4	1.26	4	1.29	3	1.35
Q14839	Chromodomain-helicase-DNA-binding protein 4	8	5.07	2	1.57	2	1.57
Q14847	LIM and SH3 domain protein 1	15	36.02	5	8.81	4	10.34
Q14894	Thiomorpholine-carboxylate dehydrogenase	1	4.78	0	0.00	0	0.00
Q14914	Prostaglandin reductase 1	5	15.50	4	18.54	5	23.10
Q14956	Transmembrane glycoprotein NMB	30	11.01	18	10.49	22	10.49
Q14974	Importin subunit beta-1	53	30.71	37	28.08	31	26.60
Q14978	Nucleolar and coiled-body phosphoprotein 1	6	5.72	4	3.72	2	2.15
Q14980	Nuclear mitotic apparatus protein 1	54	21.61	30	14.89	33	15.93
Q14999	Cullin-7	3	2.47	2	1.65	0	0.00
Q14C86	GTPase-activating protein and VPS9 domain-containing protein 1	1	1.29	0	0.00	0	0.00
Q15005	Signal peptidase complex subunit 2	3	12.39	3	12.39	2	8.41
Q15008	26S proteasome non-ATPase regulatory subunit 6	10	16.97	9	17.22	9	18.25
Q15019	Septin-2	21	44.04	14	33.24	17	39.61
Q15020	Squamous cell carcinoma antigen recognized by T-cells 3	6	5.19	2	2.18	4	5.50
Q15029	116 kDa U5 small nuclear ribonucleoprotein component	21	17.39	16	17.59	19	16.05
Q15042	Rab3 GTPase-activating protein catalytic subunit	2	2.35	2	1.63	0	0.00
Q15043	Zinc transporter ZIP14	2	2.44	0	0.00	0	0.00
Q15046	Lysyl-tRNA synthetase	9	14.24	9	14.24	9	12.06
Q15056	Eukaryotic translation initiation factor 4H	7	23.79	4	16.53	3	10.89
Q15063	Periostin	13	20.93	25	24.88	17	24.28
Q15075	Early endosome antigen 1	8	7.16	3	2.83	0	0.00
Q15084	Protein disulfide-isomerase A6	38	51.82	19	38.18	23	37.05
Q15102	Platelet-activating factor acetylhydrolase IB subunit gamma	6	26.84	5	23.38	3	12.99
Q15121	Astrocytic phosphoprotein PEA-15	9	36.92	5	22.31	5	34.62
Q15124	Phosphoglucomutase-like protein 5	1	2.65	0	0.00	0	0.00
Q15126	Phosphomevalonate kinase	4	24.48	0	0.00	0	0.00
Q15149	Plectin	257	38.36	132	24.53	147	25.98
Q15155	Nodal modulator 1	10	10.15	5	4.75	6	7.20
Q15165	Serum paraoxonase/arylesterase 2	1	2.54	0	0.00	0	0.00
Q15172	Serine/threonine-protein phosphatase 2A 56 kDa regulatory subunit alpha isoform	1	2.88	0	0.00	1	2.68
Q15181	Inorganic pyrophosphatase	15	42.91	8	20.76	8	24.22
Q15185	Prostaglandin E synthase 3	4	28.13	0	0.00	0	0.00
Q15233	Non-POU domain-containing octamer-binding protein	13	30.57	9	21.87	10	20.59
Q15257	Serine/threonine-protein phosphatase 2A activator	2	2.79	2	2.79	4	6.42
Q15274	Nicotinate-nucleotide pyrophosphorylase [carboxylating]	4	10.44	4	11.78	4	10.44
Q15287	RNA-binding protein with serine-rich domain 1	4	17.70	3	13.77	2	4.92
Q15293	Reticulocalbin-1	11	29.61	9	24.17	6	12.08
Q15345	Leucine-rich repeat-containing protein 41	1	2.22	2	2.83	1	2.22
Q15363	Transmembrane emp24 domain-containing protein 2	6	22.89	0	0.00	0	0.00
Q15365	Poly(rC)-binding protein 1	30	50.84	20	40.17	25	57.02

Q15366	Poly(rC)-binding protein 2	22	37.81	16	22.19	18	27.12
Q15369	Transcription elongation factor B polypeptide 1	6	49.11	2	28.57	0	0.00
Q15370	Transcription elongation factor B polypeptide 2	5	27.12	0	0.00	0	0.00
Q15393	Splicing factor 3B subunit 3	13	9.94	8	7.81	9	9.78
Q15397	Pumilio domain-containing protein KIAA0020	1	1.24	2	2.62	0	0.00
Q15404	Ras suppressor protein 1	2	12.64	0	0.00	1	6.50
Q15417	Calponin-3	7	13.68	5	13.68	2	7.29
Q15424	Scaffold attachment factor B1	8	6.99	5	6.12	4	3.93
Q15435	Protein phosphatase 1 regulatory subunit 7	17	38.61	9	26.94	7	22.22
Q15436	Protein transport protein Sec23A	12	14.64	0	0.00	0	0.00
Q15459	Splicing factor 3A subunit 1	9	15.01	3	4.29	3	5.93
Q15477	Helicase SKI2W	7	8.03	5	7.14	7	5.38
Q15582	Transforming growth factor-beta-induced protein ig-h3	2	4.10	8	13.03	4	8.64
Q15599	Na(+)/H(+) exchange regulatory cofactor NHE-RF2	4	13.95	2	9.79	0	0.00
Q15628	Tumor necrosis factor receptor type 1-associated DEATH domain protein	1	4.49	1	5.13	0	0.00
Q15629	Translocating chain-associated membrane protein 1	2	2.94	0	0.00	0	0.00
Q15631	Translin	16	45.61	14	40.79	12	37.72
Q15637	Splicing factor 1	10	15.65	4	5.32	6	9.86
Q15651	High mobility group nucleosome-binding domain-containing protein 3	1	12.12	0	0.00	0	0.00
Q15654	Thyroid receptor-interacting protein 6	9	24.58	5	18.28	0	0.00
Q15661	Tryptase alpha/beta-1	6	13.09	3	9.82	2	7.64
Q15691	Microtubule-associated protein RP/EB family member 1	3	9.70	1	7.09	1	2.99
Q15717	ELAV-like protein 1	10	31.60	7	15.03	9	27.91
Q15738	Sterol-4-alpha-carboxylate 3-dehydrogenase, decarboxylating	3	12.33	1	5.09	2	9.92
Q15746	Myosin light chain kinase, smooth muscle	2	1.36	1	0.94	2	1.52
Q15758	Neutral amino acid transporter B(0)	2	4.44	4	7.76	2	4.44
Q15785	Mitochondrial import receptor subunit TOM34	2	10.03	0	0.00	1	2.91
Q15796	Mothers against decapentaplegic homolog 2	2	5.14	0	0.00	0	0.00
Q15819	Ubiquitin-conjugating enzyme E2 variant 2	5	39.31	4	26.21	3	21.38
Q15833	Syntaxin-binding protein 2	4	8.94	2	6.07	4	11.47
Q15836	Vesicle-associated membrane protein 3	4	24.00	1	17.00	0	0.00
Q15843	NEDD8	5	30.86	6	30.86	5	30.86
Q15907	Ras-related protein Rab-11B	22	57.80	20	48.62	22	49.08
Q15942	Zyxin	5	13.11	0	0.00	0	0.00
Q16082	Heat shock protein beta-2	3	14.29	0	0.00	0	0.00
Q16181	Septin-7	26	24.26	15	20.37	14	18.54
Q16363	Laminin subunit alpha-4	2	1.43	0	0.00	0	0.00
Q16401	26S proteasome non-ATPase regulatory subunit 5	8	11.71	5	8.13	8	9.52
Q16518	Retinoid isomerohydrolase	29	31.52	16	19.89	16	18.57
Q16531	DNA damage-binding protein 1	17	12.28	6	7.37	10	10.70
Q16537	Serine/threonine-protein phosphatase 2A 56 kDa regulatory subunit epsilon isoform	4	9.64	1	3.00	1	3.00
Q16539	Mitogen-activated protein kinase 14	5	10.56	3	8.33	3	8.33
Q16543	Hsp90 co-chaperone Cdc37	10	17.72	6	14.81	4	5.56
Q16555	Dihydropyrimidinase-related protein 2	22	40.03	27	36.19	22	36.54
Q16563	Synaptophysin-like protein 1	3	10.04	0	0.00	2	4.25
Q16576	Histone-binding protein RBBP7	4	11.29	0	0.00	0	0.00
Q16595	Frataxin, mitochondrial	3	13.33	0	0.00	0	0.00
Q16629	Serine/arginine-rich splicing factor 7	10	32.35	0	0.00	5	13.87
Q16630	Cleavage and polyadenylation specificity factor subunit 6	8	11.62	4	7.44	3	7.08
Q16643	Drebrin	4	6.93	3	4.47	3	6.32
Q16655	Melanoma antigen recognized by T-cells 1	6	32.20	4	27.12	2	19.49
Q16658	Fascin	22	40.16	20	30.22	11	25.56
Q16666	Gamma-interferon-inducible protein 16	4	7.52	3	4.46	8	8.66
Q16695	Histone H3.1t	17	33.09	11	26.47	7	21.32
Q16698	2,4-dienoyl-CoA reductase, mitochondrial	31	35.22	12	33.13	19	34.63
Q16718	NADH dehydrogenase [ubiquinone] 1 alpha subcomplex subunit 5	9	57.76	7	44.83	5	43.97
Q16740	Putative ATP-dependent Clp protease proteolytic subunit, mitochondrial	3	13.72	0	0.00	0	0.00
Q16762	Thiosulfate sulfurtransferase	12	43.10	7	21.21	5	17.17
Q16774	Guanylate kinase	5	28.93	3	20.30	0	0.00
Q16777	Histone H2A type 2-C	55	52.71	55	37.98	36	42.64
Q16778	Histone H2B type 2-E	59	67.46	60	62.70	41	57.14
Q16795	NADH dehydrogenase [ubiquinone] 1 alpha subcomplex subunit 9, mitochondrial	27	39.26	14	25.46	10	27.85
Q16822	Phosphoenolpyruvate carboxykinase [GTP], mitochondrial	5	7.34	2	2.50	3	3.59
Q16836	Hydroxyacyl-coenzyme A dehydrogenase, mitochondrial	23	52.55	14	33.12	8	24.84
Q16851	UTP--glucose-1-phosphate uridylyltransferase	9	20.28	4	12.20	4	11.61
Q16864	V-type proton ATPase subunit F	7	47.90	4	40.34	5	24.37
Q16881	Thioredoxin reductase 1, cytoplasmic	10	17.57	4	8.32	9	16.18
Q16890	Tumor protein D53	1	6.86	1	6.86	1	6.86
Q16891	Mitochondrial inner membrane protein	37	33.11	22	23.48	26	22.82
Q17R60	Interphotoreceptor matrix proteoglycan 1	2	3.26	0	0.00	1	1.88
Q17RN3	Protein FAM98C	1	7.74	0	0.00	0	0.00
Q1KMD3	Heterogeneous nuclear ribonucleoprotein U-like protein 2	18	20.48	16	17.00	10	12.32
Q27J81	Inverted formin-2	17	16.57	9	8.41	17	16.17
Q29718	HLA class I histocompatibility antigen, B-82 alpha chain	13	23.20	5	14.09	8	20.44
Q29836	HLA class I histocompatibility antigen, B-67 alpha chain	15	26.24	5	14.09	9	22.65
Q29974	HLA class II histocompatibility antigen, DRB1-16 beta chain	8	21.80	4	13.53	5	22.18
Q29RF7	Sister chromatid cohesion protein PDS5 homolog A	1	0.97	2	1.65	1	1.50
Q2M389	WASH complex subunit 7	2	1.62	2	2.64	4	4.60
Q2TAA2	Isoamyl acetate-hydrolyzing esterase 1 homolog	10	26.21	3	12.90	2	12.90
Q2TAA5	GDP-Man:Man(3)GlcNAc(2)-PP-Dol alpha-1,2-mannosyltransferase	1	2.24	0	0.00	1	2.24
Q2TAY7	WD40 repeat-containing protein SMU1	3	6.04	0	0.00	2	5.46
Q2VIR3	Putative eukaryotic translation initiation factor 2 subunit 3-like protein	10	13.98	6	11.02	4	8.69
Q2VPB7	Uncharacterized protein DKFZp761E198	1	2.56	2	3.65	1	1.46

Q30154	HLA class II histocompatibility antigen, DR beta 5 chain	7	16.92	4	13.53	3	13.53
Q31610	HLA class I histocompatibility antigen, B-81 alpha chain	13	25.41	4	6.63	12	22.38
Q32MZ4	Leucine-rich repeat flightless-interacting protein 1	11	10.64	4	6.19	3	3.71
Q330K2	UPF0551 protein C8orf38, mitochondrial	2	4.81	0	0.00	0	0.00
Q3KQV9	UDP-N-acetylhexosamine pyrophosphorylase-like protein 1	6	12.43	3	7.50	2	5.72
Q3LXA3	Bifunctional ATP-dependent dihydroxyacetone kinase/FAD-AMP lyase (cyclizing)	5	14.09	7	14.96	4	9.57
Q3SXM5	Inactive hydroxysteroid dehydrogenase-like protein 1	2	5.15	1	4.24	0	0.00
Q3SY69	Mitochondrial 10-formyltetrahydrofolate dehydrogenase	22	21.13	2	3.25	4	4.87
Q3YEC7	Putative GTP-binding protein Parf	5	7.55	2	3.70	3	3.98
Q3ZAQ7	Vacuolar ATPase assembly integral membrane protein VMA21	2	11.88	0	0.00	0	0.00
Q3ZCQ8	Mitochondrial import inner membrane translocase subunit TIM50	12	21.81	8	20.11	9	15.30
Q3ZCW2	Galectin-related protein	1	11.05	0	0.00	1	11.05
Q49A26	Putative oxidoreductase GLYR1	3	2.35	2	2.35	2	2.35
Q4G0N4	NAD kinase domain-containing protein 1	4	11.31	0	0.00	0	0.00
Q4V328	GRIP1-associated protein 1	5	8.56	0	0.00	0	0.00
Q53EL6	Programmed cell death protein 4	26	40.30	17	31.98	24	36.89
Q53EP0	Fibronectin type III domain-containing protein 3B	1	1.16	1	1.16	1	1.16
Q53GL7	Poly [ADP-ribose] polymerase 10	4	6.73	1	1.76	0	0.00
Q53GQ0	Estradiol 17-beta-dehydrogenase 12	12	22.12	6	17.63	7	20.19
Q53GS9	U4/U6.U5 tri-snRNP-associated protein 2	3	6.19	3	2.83	3	6.19
Q53H12	Acylglycerol kinase, mitochondrial	4	13.03	0	0.00	0	0.00
Q53H82	Beta-lactamase-like protein 2	5	14.58	1	3.13	2	10.07
Q53H96	Pyrroline-5-carboxylate reductase 3	4	17.52	0	0.00	0	0.00
Q53T59	HCLS1-binding protein 3	8	34.69	4	14.54	8	21.17
Q562E7	WD repeat-containing protein 81	7	8.76	4	6.85	2	2.70
Q562R1	Beta-actin-like protein 2	63	44.41	0	0.00	0	0.00
Q567U6	Coiled-coil domain-containing protein 93	3	4.75	2	2.69	1	2.06
Q5BJH7	Protein YIF1B	4	16.88	0	0.00	0	0.00
Q5EBL4	RILP-like protein 1	1	2.73	0	0.00	1	2.73
Q5EBM0	UMP-CMP kinase 2, mitochondrial	4	14.70	0	0.00	0	0.00
Q5H9L2	Transcription elongation factor A protein-like 5	1	4.37	1	4.37	0	0.00
Q5HYK3	2-methoxy-6-polyprenyl-1,4-benzoquinol methylase, mitochondrial	3	15.60	0	0.00	0	0.00
Q5JNZ5	Putative 40S ribosomal protein S26-like 1	2	7.83	0	0.00	0	0.00
Q5JPE7	Nodal modulator 2	10	9.79	5	4.58	6	6.95
Q5JPH6	Probable glutamyl-tRNA synthetase, mitochondrial	3	4.78	0	0.00	2	6.12
Q5JRX3	Presequence protease, mitochondrial	27	22.66	6	4.72	5	6.94
Q5JSH3	WD repeat-containing protein 44	2	2.30	0	0.00	0	0.00
Q5JTD0	Tight junction-associated protein 1	1	3.05	0	0.00	0	0.00
Q5JTH9	RRP12-like protein	4	3.78	0	0.00	0	0.00
Q5JTV8	Torsin-1A-interacting protein 1	11	17.32	2	4.63	3	8.75
Q5JTZ9	Alanyl-tRNA synthetase, mitochondrial	8	11.47	0	0.00	0	0.00
Q5JVF3	PCI domain-containing protein 2	2	6.52	0	0.00	0	0.00
Q5JVS0	Intracellular hyaluronan-binding protein 4	2	3.87	0	0.00	0	0.00
Q5JWF2	Guanine nucleotide-binding protein G(s) subunit alpha isoforms XLas	18	16.30	10	10.51	8	8.87
Q5JY77	G-protein coupled receptor-associated sorting protein 1	1	1.29	0	0.00	0	0.00
Q5K4L6	Long-chain fatty acid transport protein 3	1	2.74	2	3.42	1	2.74
Q5QNW6	Histone H2B type 2-F	61	67.46	61	62.70	43	57.94
Q5R3I4	Tetratricopeptide repeat protein 38	4	6.18	2	6.18	3	4.26
Q5RI15	Protein FAM36A	2	22.03	0	0.00	1	11.86
Q5SNT2	Transmembrane protein 201	4	2.85	0	0.00	3	3.60
Q5SRE5	Nucleoporin NUP188 homolog	7	4.52	3	2.52	3	2.29
Q5SRE7	Phytanoyl-CoA dioxygenase domain-containing protein 1	2	12.37	3	12.37	0	0.00
Q5SSJ5	Heterochromatin protein 1-binding protein 3	19	21.70	9	16.27	6	10.13
Q5ST30	Valyl-tRNA synthetase, mitochondrial	3	2.54	0	0.00	0	0.00
Q5SWX8	Protein odr-4 homolog	2	5.73	0	0.00	0	0.00
Q5T0F9	Coiled-coil and C2 domain-containing protein 1B	4	7.46	1	2.45	0	0.00
Q5T160	Probable arginyl-tRNA synthetase, mitochondrial	1	2.77	0	0.00	0	0.00
Q5T2R2	Decaprenyl-diphosphate synthase subunit 1	1	4.34	0	0.00	0	0.00
Q5T440	Putative transferase CAF17, mitochondrial	1	3.37	0	0.00	2	5.90
Q5T4S7	E3 ubiquitin-protein ligase UBR4	11	3.80	3	1.41	8	2.60
Q5T653	39S ribosomal protein L2, mitochondrial	3	18.69	0	0.00	0	0.00
Q5T6V5	UPF0553 protein C9orf64	4	9.97	2	8.21	1	4.40
Q5TFE4	5'-nucleotidase domain-containing protein 1	5	12.53	0	0.00	0	0.00
Q5TFQ8	Signal-regulatory protein beta-1 isoform 3	8	17.09	3	9.04	0	0.00
Q5TI25	Neuroblastoma breakpoint family member 14	1	0.98	0	0.00	0	0.00
Q5TZA2	Rootletin	5	2.43	4	1.59	6	3.42
Q5VT66	MOSC domain-containing protein 1, mitochondrial	1	4.45	0	0.00	0	0.00
Q5VTL8	Pre-mRNA-splicing factor 38B	1	1.83	0	0.00	0	0.00
Q5VWZ2	Lysophospholipase-like protein 1	1	4.22	0	0.00	0	0.00
Q5VYK3	Proteasome-associated protein ECM29 homolog	15	9.38	8	4.99	3	1.95
Q5XKE5	Keratin, type II cytoskeletal 79	2	1.31	0	0.00	0	0.00
Q63HN8	RING finger protein 213	20	8.05	6	2.62	8	3.57
Q63ZY3	KN motif and ankyrin repeat domain-containing protein 2	7	8.58	1	1.06	4	5.87
Q658Y4	Protein FAM91A1	2	3.10	0	0.00	0	0.00
Q66K14	TBC1 domain family member 9B	5	5.52	2	2.08	4	4.72
Q66K74	Microtubule-associated protein 1S	7	7.46	0	0.00	4	5.95
Q68E01	Integrator complex subunit 3	7	10.45	0	0.00	3	6.52
Q68EM7	Rho GTPase-activating protein 17	5	8.97	4	3.63	1	1.02
Q6BCY4	NADH-cytochrome b5 reductase 2	3	13.77	0	0.00	0	0.00
Q6DD88	Atlastin-3	5	16.64	5	13.86	7	13.86
Q6DKK2	Tetratricopeptide repeat protein 19, mitochondrial	5	16.84	0	0.00	2	3.16
Q6DN03	Putative histone H2B type 2-C	10	15.03	0	0.00	5	16.06
Q6DRA6	Putative histone H2B type 2-D	10	17.68	0	0.00	5	18.90

Q6EEV4	Protein GRINL1A, isoforms 4/5	1	16.22	0	0.00	1	16.22
Q6EEV6	Small ubiquitin-related modifier 4	3	12.63	3	12.63	1	12.63
Q6FI13	Histone H2A type 2-A	54	47.69	55	37.69	35	37.69
Q6FI81	Anamorsin	2	3.85	1	3.85	0	0.00
Q6IAA8	Ragulator complex protein LAMTOR1	5	45.34	7	45.34	6	60.25
Q6IAN0	Dehydrogenase/reductase SDR family member 7B	6	16.62	3	9.54	5	13.23
Q6IBS0	Twinfilin-2	7	24.07	5	15.76	5	15.76
Q6ICL3	Uncharacterized protein C22orf25	3	16.30	5	19.20	2	10.14
Q6IN85	Serine/threonine-protein phosphatase 4 regulatory subunit 3A	1	2.04	1	2.04	2	4.32
Q6IQ26	DENN domain-containing protein 5A	1	1.32	0	0.00	0	0.00
Q6JQN1	Acyl-CoA dehydrogenase family member 10	5	4.53	0	0.00	1	1.98
Q6KC79	Nipped-B-like protein	1	0.78	0	0.00	2	0.78
Q6L8Q7	2',5'-phosphodiesterase 12	4	6.24	0	0.00	1	2.30
Q6NUK1	Calcium-binding mitochondrial carrier protein SCaMC-1	11	20.55	9	17.40	4	8.60
Q6NUM9	All-trans-retinol 13,14-reductase	2	3.93	1	1.97	3	4.92
Q6NVV1	Putative 60S ribosomal protein L13a-like MGC87657	3	21.57	4	21.57	2	21.57
Q6NVY1	3-hydroxyisobutyryl-CoA hydrolase, mitochondrial	9	15.03	7	9.07	4	8.81
Q6NZI2	Polymerase I and transcript release factor	14	25.13	14	25.38	10	22.31
Q6P158	Putative ATP-dependent RNA helicase DHX57	1	0.94	0	0.00	0	0.00
Q6P179	Endoplasmic reticulum aminopeptidase 2	1	1.56	0	0.00	0	0.00
Q6P1N0	Coiled-coil and C2 domain-containing protein 1A	2	3.58	0	0.00	0	0.00
Q6P1N9	Putative deoxyribonuclease TATDN1	1	3.70	0	0.00	1	3.70
Q6P1Q0	LETM1 domain-containing protein 1	2	3.61	1	3.61	0	0.00
Q6P1X6	UPF0598 protein C8orf82	6	25.46	3	15.28	1	6.94
Q6P2E9	Enhancer of mRNA-decapping protein 4	6	6.57	5	4.71	4	7.14
Q6P2Q9	Pre-mRNA-processing-splicing factor 8	41	16.19	20	8.22	26	11.26
Q6P4F2	Adrenodoxin-like protein, mitochondrial	2	18.58	0	0.00	0	0.00
Q6P587	Acylpyruvase FAHD1, mitochondrial	3	22.77	0	0.00	0	0.00
Q6P597	Kinesin light chain 3	4	8.13	0	0.00	0	0.00
Q6P6C2	Probable alpha-ketoglutarate-dependent dioxygenase ABH5	2	8.52	0	0.00	0	0.00
Q6P996	Pyridoxal-dependent decarboxylase domain-containing protein 1	5	6.85	2	4.32	3	6.73
Q6PCB7	Long-chain fatty acid transport protein 1	9	13.47	7	16.87	10	14.71
Q6PEY2	Tubulin alpha-3E chain	132	64.44	103	50.22	0	0.00
Q6PGP7	Tetratricopeptide repeat protein 37	3	2.49	2	2.17	3	2.94
Q6PI48	Aspartyl-tRNA synthetase, mitochondrial	8	13.80	9	16.12	7	12.09
Q6PKG0	La-related protein 1	4	4.74	0	0.00	5	7.03
Q6RW13	Type-1 angiotensin II receptor-associated protein	1	10.69	4	24.53	1	10.69
Q6STE5	SWI/SNF-related matrix-associated actin-dependent regulator of chromatin subfamily	2	6.21	0	0.00	0	0.00
Q6U841	Sodium-driven chloride bicarbonate exchanger	1	0.98	0	0.00	0	0.00
Q6UB35	Monofunctional C1-tetrahydrofolate synthase, mitochondrial	2	2.45	2	1.33	6	7.26
Q6UN15	Pre-mRNA 3'-end-processing factor FIP1	3	2.86	1	2.86	1	2.86
Q6UVK1	Chondroitin sulfate proteoglycan 4	29	15.93	14	8.14	10	7.67
Q6UW68	Transmembrane protein 205	5	9.00	2	9.00	1	9.00
Q6UWE0	E3 ubiquitin-protein ligase LRSAM1	1	1.94	0	0.00	0	0.00
Q6UWR7	Ectonucleotide pyrophosphatase/phosphodiesterase family member 6	3	7.05	0	0.00	0	0.00
Q6V1P9	Protocadherin-23	2	0.48	0	0.00	0	0.00
Q6VEQ5	WAS protein family homolog 2	2	7.31	1	3.01	1	3.01
Q6VUC0	Transcription factor AP-2-epsilon	3	6.56	3	6.56	3	6.56
Q6VY07	Phosphofurin acidic cluster sorting protein 1	2	1.45	3	1.45	1	1.45
Q6WCQ1	Myosin phosphatase Rho-interacting protein	5	7.02	0	0.00	4	5.46
Q6WKZ4	Rab11 family-interacting protein 1	5	4.37	0	0.00	3	2.10
Q6XQN6	Nicotinate phosphoribosyltransferase	20	36.62	13	19.14	14	19.14
Q6Y288	Beta-1,3-glucosyltransferase	3	7.83	1	4.02	3	4.02
Q6Y7W6	PERQ amino acid-rich with GYF domain-containing protein 2	3	3.39	0	0.00	1	1.00
Q6YN16	Hydroxysteroid dehydrogenase-like protein 2	10	21.05	5	18.90	4	13.88
Q6ZMZ3	Nesprin-3	2	2.77	0	0.00	1	1.13
Q6ZNW5	GDP-D-glucose phosphorylase C15orf58	2	8.57	0	0.00	0	0.00
Q6ZS17	Protein FAM65A	1	1.39	2	2.21	2	3.02
Q6ZUT9	DENN domain-containing protein 5B	1	1.33	0	0.00	0	0.00
Q6ZUX7	Lipoma HMGIC fusion partner-like 2 protein	1	10.96	0	0.00	1	10.96
Q6ZVM7	TOM1-like protein 2	3	11.05	2	7.10	2	6.51
Q6ZXV5	Transmembrane and TPR repeat-containing protein 3	1	1.09	1	1.09	1	1.09
Q709C8	Vacuolar protein sorting-associated protein 13C	14	4.10	9	3.52	10	3.01
Q71DI3	Histone H3.2	18	44.85	13	38.24	7	21.32
Q71U36	Tubulin alpha-1A chain	152	74.06	119	65.19	113	68.51
Q71UI9	Histone H2A.V	17	45.31	17	49.22	7	28.91
Q75N90	Fibrillin-3	1	0.39	0	0.00	0	0.00
Q765P7	MTSS1-like protein	2	2.94	0	0.00	0	0.00
Q7KZ85	Transcription elongation factor SPT6	2	1.74	0	0.00	0	0.00
Q7KZF4	Staphylococcal nuclease domain-containing protein 1	34	31.98	20	21.98	23	19.89
Q7L014	Probable ATP-dependent RNA helicase DDX46	8	7.76	6	6.40	5	5.24
Q7L2E3	Putative ATP-dependent RNA helicase DHX30	10	7.87	7	5.11	5	4.19
Q7L2H7	Eukaryotic translation initiation factor 3 subunit M	5	16.31	2	7.49	2	7.49
Q7L576	Cytoplasmic FMR1-interacting protein 1	16	13.09	11	9.82	9	7.26
Q7L5D6	Golgi to ER traffic protein 4 homolog	2	4.59	0	0.00	3	4.59
Q7L5N1	COP9 signalosome complex subunit 6	4	8.56	3	8.56	3	8.56
Q7L5Y9	Macrophage erythroblast attacher	1	2.27	0	0.00	0	0.00
Q7L7X3	Serine/threonine-protein kinase TAO1	2	4.00	0	0.00	0	0.00
Q7LG56	Ribonucleoside-diphosphate reductase subunit M2 B	2	5.41	0	0.00	0	0.00
Q7Z2K6	Endoplasmic reticulum metallopeptidase 1	9	7.96	5	3.98	3	3.98
Q7Z2W4	Zinc finger CCCH-type antiviral protein 1	3	5.21	0	0.00	0	0.00
Q7Z2Z2	Elongation factor Tu GTP-binding domain-containing protein 1	2	2.95	0	0.00	1	1.79
Q7Z3C6	Autophagy-related protein 9A	1	1.07	0	0.00	1	1.07

Q7Z3E5	LisH domain-containing protein ARMC9	5	7.22	4	6.85	4	5.02
Q7Z3T8	Zinc finger FYVE domain-containing protein 16	3	2.47	0	0.00	0	0.00
Q7Z406	Myosin-14	51	17.09	33	13.28	35	11.78
Q7Z434	Mitochondrial antiviral-signaling protein	10	13.52	6	8.52	3	8.52
Q7Z460	CLIP-associating protein 1	5	4.23	1	0.91	2	2.15
Q7Z478	ATP-dependent RNA helicase DHX29	3	2.41	0	0.00	0	0.00
Q7Z4H3	HD domain-containing protein 2	4	20.59	0	0.00	3	15.20
Q7Z4I7	LIM and senescent cell antigen-like-containing domain protein 2	1	3.23	0	0.00	0	0.00
Q7Z4Q2	HEAT repeat-containing protein 3	1	1.91	0	0.00	1	1.91
Q7Z4V5	Hepatoma-derived growth factor-related protein 2	4	6.41	0	0.00	1	2.38
Q7Z4W1	L-xylulose reductase	6	28.28	5	24.18	3	11.07
Q7Z6B7	SLIT-ROBO Rho GTPase-activating protein 1	2	1.11	3	1.11	0	0.00
Q7Z6Z7	E3 ubiquitin-protein ligase HUWE1	36	9.05	13	4.98	13	4.71
Q7Z739	YTH domain family protein 3	1	1.54	0	0.00	0	0.00
Q7Z7H8	39S ribosomal protein L10, mitochondrial	2	11.11	1	7.28	2	11.11
Q86SX6	Glutaredoxin-related protein 5, mitochondrial	5	28.03	1	8.92	0	0.00
Q86TV6	Tetratricopeptide repeat protein 7B	1	1.66	4	2.49	1	1.66
Q86TW2	Uncharacterized aarF domain-containing protein kinase 1	1	3.58	0	0.00	0	0.00
Q86TX2	Acyl-coenzyme A thioesterase 1	22	39.67	13	33.73	12	23.99
Q86U28	Iron-sulfur cluster assembly 2 homolog, mitochondrial	3	15.58	0	0.00	2	15.58
Q86U38	Pumilio domain-containing protein C14orf21	4	9.75	1	2.20	3	7.39
Q86U42	Polyadenylate-binding protein 2	2	3.60	5	25.82	4	8.50
Q86U86	Protein polybromo-1	1	1.13	1	1.13	1	1.13
Q86UE4	Protein LYRIC	11	11.51	8	9.62	10	11.68
Q86UP2	Kinectin	17	12.09	9	6.85	10	5.97
Q86UT6	NLR family member X1	8	7.59	4	5.44	5	6.36
Q86UU1	Pleckstrin homology-like domain family B member 1	2	2.03	0	0.00	0	0.00
Q86UX7	Fermitin family homolog 3	22	34.03	10	21.89	18	33.28
Q86UY8	5'-nucleotidase domain-containing protein 3	7	20.62	4	8.03	0	0.00
Q86V81	THO complex subunit 4	3	9.34	0	0.00	3	16.34
Q86VB7	Scavenger receptor cysteine-rich type 1 protein M130	1	0.95	0	0.00	0	0.00
Q86VP6	Cullin-associated NEDD8-dissociated protein 1	58	32.44	41	24.23	38	24.07
Q86VR2	Protein FAM134C	4	8.37	0	0.00	2	5.15
Q86VS8	Protein Hook homolog 3	4	8.36	0	0.00	4	6.41
Q86VU5	Catechol O-methyltransferase domain-containing protein 1	1	9.16	1	9.16	1	9.16
Q86VV8	Rotatin	2	0.63	4	1.98	1	0.63
Q86W42	THO complex subunit 6 homolog	2	8.80	1	5.57	1	5.57
Q86W92	Liprin-beta-1	2	2.18	1	0.89	0	0.00
Q86WA6	Valacyclovir hydrolase	4	11.00	5	14.78	3	8.25
Q86WJ1	Chromodomain-helicase-DNA-binding protein 1-like	1	1.45	1	1.45	1	1.45
Q86WV6	Transmembrane protein 173	3	11.87	0	0.00	3	9.50
Q86X10	Ral GTPase-activating protein subunit beta	2	2.34	0	0.00	3	1.41
Q86X55	Histone-arginine methyltransferase CARM1	3	4.44	0	0.00	3	5.43
Q86X76	Nitrilase homolog 1	6	19.27	0	0.00	0	0.00
Q86X83	COMM domain-containing protein 2	3	22.61	0	0.00	0	0.00
Q86XA9	HEAT repeat-containing protein 5A	2	1.77	0	0.00	1	0.93
Q86XP3	ATP-dependent RNA helicase DDX42	5	7.78	4	7.78	4	7.25
Q86Y56	HEAT repeat-containing protein 2	2	2.81	0	0.00	2	2.81
Q86Y79	Probable peptidyl-tRNA hydrolase	1	4.67	1	4.67	2	7.01
Q86Y82	Syntaxin-12	3	15.58	4	15.58	4	21.01
Q86YN1	Dolichyldiphosphatase 1	1	7.14	0	0.00	0	0.00
Q86YV9	Hermansky-Pudlak syndrome 6 protein	4	6.71	0	0.00	0	0.00
Q8IUD2	ELKS/Rab6-interacting/CAST family member 1	4	3.05	0	0.00	1	1.08
Q8IUX7	Adipocyte enhancer-binding protein 1	9	10.28	5	5.87	0	0.00
Q8IV08	Phospholipase D3	10	13.67	11	17.55	7	13.27
Q8IVD9	NudC domain-containing protein 3	2	6.37	0	0.00	2	10.53
Q8IVF2	Protein AHNAK2	16	12.72	0	0.00	11	7.82
Q8IVH4	Methylmalonic aciduria type A protein, mitochondrial	1	3.83	1	3.83	1	3.83
Q8IVM0	Coiled-coil domain-containing protein 50	3	3.92	0	0.00	0	0.00
Q8IVP5	FUN14 domain-containing protein 1	2	10.97	1	10.97	1	10.97
Q8IW45	Carbohydrate kinase domain-containing protein	5	21.61	0	0.00	0	0.00
Q8IWA5	Choline transporter-like protein 2	3	3.97	3	5.67	0	0.00
Q8IWB7	WD repeat and FYVE domain-containing protein 1	10	18.05	6	14.39	4	8.29
Q8IWE2	Protein NOXP20	2	2.66	0	0.00	1	2.66
Q8IWF6	Protein FAM116A	1	2.14	0	0.00	0	0.00
Q8IWX8	Calcium homeostasis endoplasmic reticulum protein	3	4.37	2	2.73	1	1.53
Q8IXB1	DnaJ homolog subfamily C member 10	1	1.26	0	0.00	1	1.26
Q8IXH7	Negative elongation factor C/D	4	9.15	3	9.15	0	0.00
Q8IXI1	Mitochondrial Rho GTPase 2	3	6.47	0	0.00	0	0.00
Q8IXI2	Mitochondrial Rho GTPase 1	2	3.24	0	0.00	0	0.00
Q8IXT5	RNA-binding protein 12B	2	1.40	2	1.40	2	2.80
Q8IY17	Neuropathy target esterase	3	3.95	4	4.32	3	3.51
Q8IY81	Putative rRNA methyltransferase 3	7	12.28	8	9.68	5	7.20
Q8IYB8	ATP-dependent RNA helicase SUPV3L1, mitochondrial	6	10.81	1	2.16	0	0.00
Q8IYM9	E3 ubiquitin-protein ligase TRIM22	2	6.02	0	0.00	1	4.62
Q8IZ52	Chondroitin sulfate synthase 2	1	2.06	0	0.00	0	0.00
Q8IZ83	Aldehyde dehydrogenase family 16 member A1	11	13.59	7	10.22	7	7.86
Q8IZL8	Proline-, glutamic acid- and leucine-rich protein 1	2	3.63	4	5.66	3	5.22
Q8IZP0	Abl interactor 1	1	2.16	0	0.00	0	0.00
Q8IZQ5	Selenoprotein H	2	18.03	1	9.84	0	0.00
Q8IZR5	CKLF-like MARVEL transmembrane domain-containing protein 4	1	4.27	0	0.00	0	0.00
Q8IZU2	WD repeat-containing protein 17	1	0.53	0	0.00	0	0.00
Q8N0U8	Vitamin K epoxide reductase complex subunit 1-like protein 1	1	5.68	0	0.00	0	0.00

Q8N0V3	Putative ribosome-binding factor A, mitochondrial	2	5.83	0	0.00	1	5.83
Q8N0W3	L-fucose kinase	5	8.12	1	2.40	1	2.40
Q8N0X4	Citrate lyase subunit beta-like protein, mitochondrial	3	11.76	0	0.00	2	5.88
Q8N122	Regulatory-associated protein of mTOR	4	4.42	0	0.00	6	3.15
Q8N163	Protein KIAA1967	14	15.93	11	15.93	10	14.95
Q8N183	Mimitin, mitochondrial	3	21.30	1	10.65	1	10.65
Q8N1B4	Vacuolar protein sorting-associated protein 52 homolog	4	5.81	0	0.00	3	6.50
Q8N1F7	Nuclear pore complex protein Nup93	10	16.00	4	7.81	8	12.33
Q8N1F8	Serine/threonine-protein kinase 11-interacting protein	2	2.09	0	0.00	2	2.09
Q8N1G4	Leucine-rich repeat-containing protein 47	19	28.82	12	18.52	11	21.10
Q8N1N4	Keratin, type II cytoskeletal 78	2	1.35	0	0.00	0	0.00
Q8N257	Histone H2B type 3-B	55	61.90	0	0.00	35	41.27
Q8N2F6	Armadillo repeat-containing protein 10	2	9.62	2	9.62	2	4.66
Q8N2G8	GH3 domain-containing protein	3	6.04	1	2.83	0	0.00
Q8N2H3	Pyridine nucleotide-disulfide oxidoreductase domain-containing protein 2	5	9.47	0	0.00	0	0.00
Q8N2K0	Monoacylglycerol lipase ABHD12	7	22.11	1	5.78	3	6.28
Q8N357	Transmembrane protein C2orf18	2	3.23	1	3.23	0	0.00
Q8N3E9	1-phosphatidylinositol-4,5-bisphosphate phosphodiesterase delta-3	2	3.68	1	2.91	0	0.00
Q8N3U4	Cohesin subunit SA-2	2	3.33	0	0.00	0	0.00
Q8N490	Probable hydrolase PNKD	2	5.45	0	0.00	0	0.00
Q8N4H5	Mitochondrial import receptor subunit TOM5 homolog	1	15.69	0	0.00	0	0.00
Q8N4Q1	Mitochondrial intermembrane space import and assembly protein 40	1	12.68	0	0.00	0	0.00
Q8N5K1	CDGSH iron-sulfur domain-containing protein 2	8	31.11	3	31.11	7	31.11
Q8N5M1	ATP synthase mitochondrial F1 complex assembly factor 2	3	7.96	0	0.00	1	4.15
Q8N5M9	Protein jagunal homolog 1	1	6.56	1	6.56	0	0.00
Q8N5N7	39S ribosomal protein L50, mitochondrial	1	8.23	2	20.25	2	20.89
Q8N6H7	ADP-ribosylation factor GTPase-activating protein 2	1	1.73	0	0.00	0	0.00
Q8N6T3	ADP-ribosylation factor GTPase-activating protein 1	2	8.37	0	0.00	0	0.00
Q8N752	Casein kinase I isoform alpha-like	1	2.97	0	0.00	1	2.97
Q8N766	Uncharacterized protein KIAA0090	8	9.67	9	12.89	6	6.45
Q8N7H5	RNA polymerase II-associated factor 1 homolog	1	2.07	0	0.00	0	0.00
Q8N7J2	Protein FAM123A	1	1.64	0	0.00	0	0.00
Q8N8N7	Prostaglandin reductase 2	4	19.66	1	5.13	1	5.13
Q8N983	39S ribosomal protein L43, mitochondrial	4	16.28	0	0.00	0	0.00
Q8N9N2	Activating signal cointegrator 1 complex subunit 1	1	2.25	0	0.00	0	0.00
Q8NB37	Parkinson disease 7 domain-containing protein 1	3	22.27	0	0.00	1	10.91
Q8NBJ5	Procollagen galactosyltransferase 1	6	9.16	5	7.40	5	7.40
Q8NBJ7	Sulfatase-modifying factor 2	9	22.92	0	0.00	4	10.96
Q8NBM8	Prenylcysteine oxidase-like	3	7.08	3	7.08	0	0.00
Q8NBN3	Transmembrane protein 87A	3	5.40	3	5.05	3	7.75
Q8NBN7	Retinol dehydrogenase 13	6	22.66	4	16.92	6	16.92
Q8NBQ5	Estradiol 17-beta-dehydrogenase 11	5	21.00	4	15.00	4	15.00
Q8NBS9	Thioredoxin domain-containing protein 5	33	44.21	29	36.81	24	28.01
Q8NBU5	ATPase family AAA domain-containing protein 1	1	3.88	0	0.00	1	3.88
Q8NBX0	Saccharopine dehydrogenase-like oxidoreductase	2	8.39	1	5.36	0	0.00
Q8NC44	Protein FAM134A	1	4.60	0	0.00	0	0.00
Q8NC51	Plasminogen activator inhibitor 1 RNA-binding protein	11	18.14	15	22.06	6	15.44
Q8NC56	LEM domain-containing protein 2	12	17.50	4	11.73	5	13.72
Q8NCW5	Apolipoprotein A-I-binding protein	13	31.60	9	20.83	8	24.65
Q8ND90	Paraneoplastic antigen Ma1	1	4.82	0	0.00	1	4.82
Q8NDH3	Probable aminopeptidase NPEPL1	6	12.62	0	0.00	4	4.78
Q8NE01	Metal transporter CNNM3	2	5.80	1	2.55	1	2.55
Q8NE71	ATP-binding cassette sub-family F member 1	8	9.59	5	5.80	4	4.38
Q8NEU8	DCC-interacting protein 13-beta	2	2.11	0	0.00	0	0.00
Q8NF37	Lysophosphatidylcholine acyltransferase 1	7	15.73	1	2.43	1	2.81
Q8NF91	Nesprin-1	3	0.41	0	0.00	0	0.00
Q8NFF5	FAD synthase	5	14.65	3	9.71	3	9.71
Q8NFP9	Neurobeachin	2	0.98	0	0.00	0	0.00
Q8NFV4	Abhydrolase domain-containing protein 11	6	18.73	4	13.97	1	4.13
Q8NFW8	N-acylneuraminate cytidylyltransferase	3	4.84	0	0.00	0	0.00
Q8NG11	Tetraspanin-14	3	10.37	0	0.00	0	0.00
Q8NHP6	Motile sperm domain-containing protein 2	1	4.25	0	0.00	0	0.00
Q8NI22	Multiple coagulation factor deficiency protein 2	2	16.44	2	16.44	3	16.44
Q8NI27	THO complex subunit 2	2	1.44	0	0.00	1	0.57
Q8TAE8	Growth arrest and DNA damage-inducible proteins-interacting protein 1	1	7.21	2	9.46	1	7.21
Q8TAQ2	SWI/SNF complex subunit SMARCC2	7	6.76	4	2.88	4	4.61
Q8TAT6	Nuclear protein localization protein 4 homolog	6	9.87	6	10.20	7	12.83
Q8TB22	Spermatogenesis-associated protein 20	7	11.96	0	0.00	1	1.53
Q8TB36	Ganglioside-induced differentiation-associated protein 1	3	8.10	0	0.00	0	0.00
Q8TB37	Iron-sulfur protein NUBPL	2	11.29	0	0.00	1	5.02
Q8TBA6	Golgin subfamily A member 5	1	1.78	0	0.00	0	0.00
Q8TBC4	NEDD8-activating enzyme E1 catalytic subunit	1	2.16	0	0.00	3	9.72
Q8TBX8	Phosphatidylinositol-5-phosphate 4-kinase type-2 gamma	7	13.78	3	10.45	4	10.45
Q8TC12	Retinol dehydrogenase 11	6	18.55	4	10.06	5	18.55
Q8TCD5	5'(3')-deoxyribonucleotidase, cytosolic type	3	23.38	1	8.96	2	8.96
Q8TCF1	AN1-type zinc finger protein 1	1	3.73	1	2.61	0	0.00
Q8TCJ2	Dolichyl-diphosphooligosaccharide--protein glycosyltransferase subunit STT3B	3	4.12	0	0.00	0	0.00
Q8TCS8	Polyribonucleotide nucleotidyltransferase 1, mitochondrial	4	6.13	0	0.00	0	0.00
Q8TCT9	Minor histocompatibility antigen H13	5	10.34	0	0.00	1	2.65
Q8TD55	Pleckstrin homology domain-containing family O member 2	3	9.80	1	4.69	2	9.80
Q8TDD1	ATP-dependent RNA helicase DDX54	1	2.04	3	3.86	1	1.82
Q8TDN6	Ribosome biogenesis protein BRX1 homolog	5	16.71	4	13.60	2	10.20
Q8TDQ7	Glucosamine-6-phosphate isomerase 2	6	28.62	3	22.46	4	28.62

Q8TDX7	Serine/threonine-protein kinase Nek7	1	4.30	0	0.00	1	3.97
Q8TDZ2	NEDD9-interacting protein with calponin homology and LIM domains	3	3.28	2	1.78	0	0.00
Q8TEM1	Nuclear pore membrane glycoprotein 210	2	1.17	0	0.00	0	0.00
Q8TEQ8	GPI ethanolamine phosphate transferase 3	2	2.57	2	2.57	3	2.57
Q8TES7	Fas-binding factor 1	1	2.91	2	2.91	0	0.00
Q8TET4	Neutral alpha-glucosidase C	1	1.75	1	1.75	0	0.00
Q8TEX9	Importin-4	8	9.16	4	5.18	5	6.66
Q8TF09	Dynein light chain roadblock-type 2	2	12.50	0	0.00	2	12.50
Q8TF74	WAS/WASL-interacting protein family member 2	1	5.23	0	0.00	0	0.00
Q8WU76	Sec1 family domain-containing protein 2	3	3.95	2	1.61	0	0.00
Q8WU79	Stromal membrane-associated protein 2	1	3.03	0	0.00	0	0.00
Q8WU90	Zinc finger CCCH domain-containing protein 15	2	4.93	0	0.00	1	3.29
Q8WUA2	Peptidyl-prolyl cis-trans isomerase-like 4	1	3.25	0	0.00	0	0.00
Q8WUK0	Protein-tyrosine phosphatase mitochondrial 1	3	12.44	1	6.47	0	0.00
Q8WUM0	Nuclear pore complex protein Nup133	5	5.62	3	3.81	4	4.41
Q8WUM4	Programmed cell death 6-interacting protein	18	15.44	8	13.02	8	12.10
Q8WUW1	Protein BRICK1	3	28.00	1	14.67	0	0.00
Q8WUX9	Charged multivesicular body protein 7	2	3.75	1	3.53	2	3.53
Q8WUY1	UPF0670 protein C8orf55	7	29.33	3	16.35	1	7.69
Q8WUY3	Protein prune homolog 2	4	1.46	2	1.26	3	0.97
Q8WVC6	Dephospho-CoA kinase domain-containing protein	4	16.02	1	4.76	1	5.20
Q8WVM0	Dimethyladenosine transferase 1, mitochondrial	1	4.05	0	0.00	0	0.00
Q8WVM8	Sec1 family domain-containing protein 1	8	19.63	6	13.86	11	14.64
Q8WVV9	Heterogeneous nuclear ribonucleoprotein L-like	5	8.86	0	0.00	3	6.09
Q8WVY7	Ubiquitin-like domain-containing CTD phosphatase 1	3	11.95	1	4.40	0	0.00
Q8WWC4	Uncharacterized protein C2orf47, mitochondrial	1	3.44	0	0.00	0	0.00
Q8WWM7	Ataxin-2-like protein	1	0.93	0	0.00	1	2.70
Q8WWP7	GTPase IMAP family member 1	1	5.23	0	0.00	0	0.00
Q8WWX9	Selenoprotein M	2	19.31	0	0.00	0	0.00
Q8WWY3	U4/U6 small nuclear ribonucleoprotein Prp31	5	12.63	2	7.62	0	0.00
Q8WXF1	Paraspeckle component 1	13	21.99	8	14.15	7	13.96
Q8WXH0	Nesprin-2	15	2.66	12	2.14	7	1.13
Q8WYA6	Beta-catenin-like protein 1	3	4.26	0	0.00	1	1.42
Q8WZ82	Ovarian cancer-associated gene 2 protein	2	11.45	1	15.42	2	22.03
Q92481	Transcription factor AP-2-beta	3	6.30	3	6.30	3	6.30
Q92499	ATP-dependent RNA helicase DDX1	22	19.19	20	18.78	15	17.70
Q92506	Estradiol 17-beta-dehydrogenase 8	5	21.46	6	16.86	5	15.71
Q92522	Histone H1x	2	11.74	3	11.74	2	4.70
Q92523	Carnitine O-palmitoyltransferase 1, muscle isoform	1	1.68	4	5.96	0	0.00
Q92542	Nicastrin	8	9.17	4	4.79	4	7.62
Q92552	28S ribosomal protein S27, mitochondrial	2	2.66	1	2.66	1	2.66
Q92556	Engulfment and cell motility protein 1	2	2.34	0	0.00	0	0.00
Q92575	UBX domain-containing protein 4	2	7.87	0	0.00	2	7.87
Q92581	Sodium/hydrogen exchanger 6	1	1.79	0	0.00	0	0.00
Q92597	Protein NDRG1	23	30.71	11	25.63	6	20.05
Q92598	Heat shock protein 105 kDa	24	22.73	10	15.62	11	12.59
Q92599	Septin-8	7	16.36	2	4.14	4	9.32
Q92614	Myosin-XVIIIa	16	10.08	0	0.00	0	0.00
Q92616	Translational activator GCN1	37	18.35	27	12.95	25	13.18
Q92621	Nuclear pore complex protein Nup205	12	8.90	5	4.08	4	2.44
Q92625	Ankyrin repeat and SAM domain-containing protein 1A	2	2.56	0	0.00	0	0.00
Q92665	28S ribosomal protein S31, mitochondrial	4	9.62	5	9.62	2	9.62
Q92688	Acidic leucine-rich nuclear phosphoprotein 32 family member B	15	28.69	11	24.30	12	21.12
Q92696	Geranylgeranyl transferase type-2 subunit alpha	3	3.70	2	1.94	2	1.94
Q92734	Protein TFG	6	18.25	2	6.75	0	0.00
Q92759	General transcription factor IIH subunit 4	1	4.54	1	4.54	2	6.28
Q92781	11-cis retinol dehydrogenase	13	29.87	7	26.42	7	26.42
Q92783	Signal transducing adapter molecule 1	9	19.81	5	16.30	3	9.63
Q92785	Zinc finger protein ubi-d4	2	5.88	0	0.00	0	0.00
Q92804	TATA-binding protein-associated factor 2N	4	5.24	4	3.88	4	3.88
Q92820	Gamma-glutamyl hydrolase	13	27.36	3	9.12	4	13.21
Q92831	Histone acetyltransferase KAT2B	1	1.80	0	0.00	0	0.00
Q92841	Probable ATP-dependent RNA helicase DDX17	31	27.69	15	19.54	13	14.62
Q92859	Neogenin	3	2.46	0	0.00	0	0.00
Q92878	DNA repair protein RAD50	6	5.11	5	4.35	1	1.37
Q92882	Osteoclast-stimulating factor 1	5	17.29	3	17.29	2	5.61
Q92888	Rho guanine nucleotide exchange factor 1	3	4.28	0	0.00	3	3.18
Q92890	Ubiquitin fusion degradation protein 1 homolog	5	13.68	3	7.82	2	7.82
Q92896	Golgi apparatus protein 1	12	10.52	3	2.37	3	2.88
Q92900	Regulator of nonsense transcripts 1	12	11.96	6	7.71	4	6.29
Q92905	COP9 signalosome complex subunit 5	3	6.59	0	0.00	4	9.28
Q92925	SWI/SNF-related matrix-associated actin-dependent regulator of chromatin subfamily	1	3.20	1	2.07	0	0.00
Q92930	Ras-related protein Rab-8B	8	23.19	7	23.19	8	23.19
Q92945	Far upstream element-binding protein 2	35	32.49	31	33.76	20	21.10
Q92947	Glutaryl-CoA dehydrogenase, mitochondrial	4	16.67	1	3.88	0	0.00
Q92973	Transportin-1	9	10.02	7	8.13	6	8.35
Q92974	Rho guanine nucleotide exchange factor 2	1	1.72	0	0.00	0	0.00
Q93008	Probable ubiquitin carboxyl-terminal hydrolase FAF-X	10	4.40	0	0.00	6	2.69
Q93009	Ubiquitin carboxyl-terminal hydrolase 7	7	8.53	4	3.63	4	6.99
Q93034	Cullin-5	3	2.82	0	0.00	0	0.00
Q93050	V-type proton ATPase 116 kDa subunit a isoform 1	28	20.55	11	10.87	11	7.77
Q93052	Lipoma-preferred partner	4	6.70	4	6.70	1	2.45
Q93077	Histone H2A type 1-C	54	47.69	55	37.69	35	37.69

Q93079	Histone H2B type 1-H	61	67.46	61	62.70	43	57.94
Q95365	HLA class I histocompatibility antigen, B-38 alpha chain	15	26.24	5	14.09	9	22.65
Q969E4	Transcription elongation factor A protein-like 3	1	4.50	1	4.50	1	10.50
Q969G3	SWI/SNF-related matrix-associated actin-dependent regulator of chromatin subfamily	2	5.60	0	0.00	0	0.00
Q969H8	UPF0556 protein C19orf10	2	13.87	0	0.00	0	0.00
Q969N2	GPI transamidase component PIG-T	1	2.59	1	2.59	1	2.59
Q969P0	Immunoglobulin superfamily member 8	4	9.30	0	0.00	0	0.00
Q969S9	Ribosome-releasing factor 2, mitochondrial	3	6.16	0	0.00	1	2.44
Q969T4	Ubiquitin-conjugating enzyme E2 E3	2	9.66	0	0.00	0	0.00
Q969V3	Nicalin	9	14.03	4	4.97	7	12.08
Q969X5	Endoplasmic reticulum-Golgi intermediate compartment protein 1	3	11.03	1	8.28	0	0.00
Q969Y2	tRNA modification GTPase GTPBP3, mitochondrial	2	8.94	1	4.27	1	4.27
Q969Z3	MOSC domain-containing protein 2, mitochondrial	1	4.48	0	0.00	0	0.00
Q96A33	Coiled-coil domain-containing protein 47	2	4.55	0	0.00	0	0.00
Q96A65	Exocyst complex component 4	8	10.68	0	0.00	2	3.39
Q96A72	Protein mago nashi homolog 2	1	13.51	0	0.00	0	0.00
Q96AB3	Isochorismatase domain-containing protein 2, mitochondrial	9	38.54	3	17.07	3	17.07
Q96AB6	Protein N-terminal asparagine amidohydrolase	1	7.10	2	7.10	2	7.10
Q96AC1	Fermitin family homolog 2	5	13.24	0	0.00	5	14.41
Q96AE4	Far upstream element-binding protein 1	12	13.98	6	9.32	0	0.00
Q96AG3	Solute carrier family 25 member 46	2	5.50	0	0.00	0	0.00
Q96AG4	Leucine-rich repeat-containing protein 59	13	29.97	8	22.15	2	7.17
Q96AQ6	Pre-B-cell leukemia transcription factor-interacting protein 1	5	7.11	2	3.69	1	2.19
Q96AX1	Vacuolar protein sorting-associated protein 33A	5	5.71	4	8.05	3	5.37
Q96AY2	Crossover junction endonuclease EME1	1	2.11	0	0.00	0	0.00
Q96AY3	Peptidyl-prolyl cis-trans isomerase FKBP10	6	9.62	3	4.81	3	7.22
Q96B97	SH3 domain-containing kinase-binding protein 1	1	2.11	0	0.00	0	0.00
Q96BM9	ADP-ribosylation factor-like protein 8A	4	17.20	0	0.00	0	0.00
Q96BW5	Phosphotriesterase-related protein	3	16.62	0	0.00	0	0.00
Q96BY6	Dedicator of cytokinesis protein 10	1	0.73	0	0.00	0	0.00
Q96C01	Protein FAM136A	1	5.80	0	0.00	0	0.00
Q96C19	EF-hand domain-containing protein D2	4	16.25	4	13.33	0	0.00
Q96C23	Aldose 1-epimerase	10	31.87	6	17.84	3	8.48
Q96C36	Pyrroline-5-carboxylate reductase 2	4	15.00	2	7.81	0	0.00
Q96C86	Scavenger mRNA-decapping enzyme DcpS	16	34.72	11	32.64	11	29.67
Q96C90	Protein phosphatase 1 regulatory subunit 14B	2	8.84	0	0.00	0	0.00
Q96CD0	F-box/LRR-repeat protein 8	2	7.75	2	9.09	2	7.75
Q96CM8	Acyl-CoA synthetase family member 2, mitochondrial	4	9.27	3	6.02	2	2.76
Q96CN7	Isochorismatase domain-containing protein 1	2	8.39	2	11.07	3	14.77
Q96CS3	FAS-associated factor 2	5	16.85	3	8.54	3	9.89
Q96CT7	Coiled-coil domain-containing protein 124	6	24.22	8	24.22	7	18.39
Q96CU9	FAD-dependent oxidoreductase domain-containing protein 1	1	2.68	0	0.00	0	0.00
Q96CV9	Optineurin	2	4.51	0	0.00	0	0.00
Q96CW1	AP-2 complex subunit mu	2	6.44	0	0.00	0	0.00
Q96CW5	Gamma-tubulin complex component 3	4	5.40	2	4.08	3	3.31
Q96CX2	BTB/POZ domain-containing protein KCTD12	8	15.38	4	14.46	3	10.46
Q96D09	G-protein coupled receptor-associated sorting protein 2	1	2.15	0	0.00	0	0.00
Q96D31	Calcium release-activated calcium channel protein 1	1	4.32	1	4.32	1	4.32
Q96D96	Voltage-gated hydrogen channel 1	3	10.26	0	0.00	0	0.00
Q96DB5	Regulator of microtubule dynamics protein 1	11	25.16	3	9.55	7	11.78
Q96DC8	Enoyl-CoA hydratase domain-containing protein 3, mitochondrial	1	5.94	0	0.00	1	5.94
Q96DC9	Ubiquitin thioesterase OTUB2	1	2.99	0	0.00	0	0.00
Q96DG6	Carboxymethylenebutenolidase homolog	2	10.20	2	6.94	2	11.02
Q96DT6	Cysteine protease ATG4C	2	5.68	0	0.00	0	0.00
Q96DV4	39S ribosomal protein L38, mitochondrial	2	7.11	0	0.00	0	0.00
Q96DX5	Ankyrin repeat and SOCS box protein 9	6	12.24	2	6.46	3	6.46
Q96EB1	Elongator complex protein 4	1	4.48	1	4.48	1	4.48
Q96EC8	Protein YIPF6	1	5.09	0	0.00	0	0.00
Q96EL3	39S ribosomal protein L53, mitochondrial	1	13.39	2	16.07	0	0.00
Q96EP5	DAZ-associated protein 1	5	11.30	0	0.00	1	3.69
Q96EY1	DnaJ homolog subfamily A member 3, mitochondrial	7	10.63	2	4.79	4	4.79
Q96EY8	Cob(I)yrinic acid a,c-diamide adenosyltransferase, mitochondrial	6	22.00	0	0.00	2	4.00
Q96FV2	Secernin-2	4	17.88	2	8.47	3	10.82
Q96FW1	Ubiquitin thioesterase OTUB1	16	36.90	9	21.03	9	30.63
Q96G03	Phosphoglucomutase-2	14	21.73	10	15.69	8	17.48
Q96G23	Ceramide synthase 2	2	2.37	0	0.00	1	2.37
Q96GC9	Vacuole membrane protein 1	3	7.39	0	0.00	2	7.39
Q96GD0	Pyridoxal phosphate phosphatase	3	12.84	0	0.00	1	6.76
Q96GK7	Fumarylacetoacetate hydrolase domain-containing protein 2A	14	28.98	6	25.48	4	11.15
Q96GM5	SWI/SNF-related matrix-associated actin-dependent regulator of chromatin subfamily	1	3.30	0	0.00	0	0.00
Q96HE7	ERO1-like protein alpha	9	24.36	0	0.00	6	16.03
Q96HN2	Putative adenosylhomocysteinase 3	4	5.40	0	0.00	2	3.27
Q96HP0	Dedicator of cytokinesis protein 6	1	0.83	1	0.83	1	0.83
Q96HR9	Receptor expression-enhancing protein 6	2	7.06	2	7.06	3	12.50
Q96HS1	Serine/threonine-protein phosphatase PGAM5, mitochondrial	3	13.84	0	0.00	0	0.00
Q96HW7	Integrator complex subunit 4	2	3.22	0	0.00	0	0.00
Q96HY6	DDRGK domain-containing protein 1	14	37.90	7	19.43	5	15.61
Q96I15	Selenocysteine lyase	6	11.01	5	12.81	5	12.81
Q96I24	Far upstream element-binding protein 3	7	5.42	3	4.02	4	4.02
Q96I25	Splicing factor 45	5	14.71	0	0.00	0	0.00
Q96I59	Probable asparaginyl-tRNA synthetase, mitochondrial	8	19.08	7	19.50	3	9.01
Q96I99	Succinyl-CoA ligase [GDP-forming] subunit beta, mitochondrial	17	31.02	12	30.32	13	26.16
Q96IU4	Abhydrolase domain-containing protein 14B	9	34.76	9	28.10	8	28.10

Q96JB5	CDK5 regulatory subunit-associated protein 3	5	12.85	4	7.11	6	10.28
Q96JC1	Vam6/Vps39-like protein	1	1.58	0	0.00	1	1.24
Q96JF0	Beta-galactoside alpha-2,6-sialyltransferase 2	1	2.08	0	0.00	0	0.00
Q96JG6	Coiled-coil domain-containing protein 132	1	1.45	0	0.00	0	0.00
Q96JJ3	Engulfment and cell motility protein 2	2	2.36	0	0.00	0	0.00
Q96JM3	Zinc finger protein 828	1	1.11	0	0.00	0	0.00
Q96K19	RING finger protein 170	2	5.43	0	0.00	0	0.00
Q96K76	Ubiquitin carboxyl-terminal hydrolase 47	3	2.04	0	0.00	1	1.31
Q96KK5	Histone H2A type 1-H	54	48.44	55	38.28	35	38.28
Q96KP1	Exocyst complex component 2	7	6.06	4	6.06	4	4.00
Q96KP4	Cytosolic non-specific dipeptidase	57	53.89	34	37.68	30	43.58
Q96KR6	Transmembrane protein C20orf108	3	18.23	2	18.23	2	18.23
Q96LJ7	Dehydrogenase/reductase SDR family member 1	4	15.97	0	0.00	0	0.00
Q96M27	Protein PRRC1	6	13.71	2	7.64	4	10.34
Q96M96	FYVE, RhoGEF and PH domain-containing protein 4	2	3.66	0	0.00	0	0.00
Q96MW5	Conserved oligomeric Golgi complex subunit 8	5	8.66	0	0.00	0	0.00
Q96N66	Lysophospholipid acyltransferase 7	4	8.47	2	2.54	2	2.54
Q96N67	Dedicator of cytokinesis protein 7	10	4.67	8	5.47	8	4.67
Q96NY7	Chloride intracellular channel protein 6	14	21.88	5	11.79	7	16.05
Q96P48	Arf-GAP with Rho-GAP domain, ANK repeat and PH domain-containing protein 1	2	2.07	1	0.90	2	2.62
Q96P70	Importin-9	6	8.36	4	5.48	3	1.73
Q96PK2	Microtubule-actin cross-linking factor 1, isoform 4	6	1.06	5	0.79	6	1.33
Q96PK6	RNA-binding protein 14	7	10.16	5	8.97	6	7.18
Q96PU5	E3 ubiquitin-protein ligase NEDD4-like	7	5.85	2	1.03	4	3.38
Q96PU8	Protein quaking	4	13.20	0	0.00	3	12.90
Q96PY5	Formin-like protein 2	1	1.29	0	0.00	1	1.29
Q96QK1	Vacuolar protein sorting-associated protein 35	32	32.04	21	25.25	18	23.62
Q96QR8	Transcriptional activator protein Pur-beta	4	23.08	5	24.04	5	24.36
Q96QV6	Histone H2A type 1-A	57	39.69	60	29.77	40	29.77
Q96RF0	Sorting nexin-18	2	4.62	1	2.71	2	4.62
Q96RQ3	Methylcrotonoyl-CoA carboxylase subunit alpha, mitochondrial	1	2.48	1	1.79	1	2.48
Q96RT1	Protein LAP2	2	2.55	0	0.00	2	3.12
Q96RT7	Gamma-tubulin complex component 6	2	1.32	0	0.00	2	1.04
Q96S44	TP53-regulating kinase	4	22.53	0	0.00	1	8.30
Q96S52	GPI transamidase component PIG-S	6	12.61	5	14.23	4	10.81
Q96SB3	Neurabin-2	5	6.26	0	0.00	0	0.00
Q96ST3	Paired amphipathic helix protein Sin3a	2	1.02	2	2.20	2	1.02
Q96SZ5	2-aminoethanethiol dioxygenase	2	14.07	0	0.00	0	0.00
Q96T51	RUN and FYVE domain-containing protein 1	4	6.50	0	0.00	0	0.00
Q96T76	MMS19 nucleotide excision repair protein homolog	10	10.68	5	6.31	5	7.77
Q96TA1	Niban-like protein 1	8	13.40	6	6.03	8	13.94
Q96TC7	Regulator of microtubule dynamics protein 3	5	10.85	3	9.57	3	7.23
Q99426	Tubulin-folding cofactor B	2	11.89	2	8.61	2	11.89
Q99436	Proteasome subunit beta type-7	5	14.44	1	3.61	3	7.22
Q99447	Ethanolamine-phosphate cytidylyltransferase	3	5.91	0	0.00	1	3.60
Q99459	Cell division cycle 5-like protein	4	8.35	1	1.50	1	2.37
Q99460	26S proteasome non-ATPase regulatory subunit 1	25	25.39	14	20.15	15	18.89
Q99471	Prefoldin subunit 5	3	21.43	3	11.69	2	11.69
Q99497	Protein DJ-1	38	78.84	37	78.84	25	70.90
Q99523	Sortilin	11	17.57	8	10.71	8	8.91
Q99536	Synaptic vesicle membrane protein VAT-1 homolog	64	65.39	46	62.09	49	64.38
Q99538	Legumain	1	3.93	1	3.93	1	3.93
Q99567	Nuclear pore complex protein Nup88	4	8.77	3	6.75	0	0.00
Q99569	Plakophilin-4	1	0.84	0	0.00	1	0.84
Q99572	P2X purinoceptor 7	8	10.25	6	8.57	4	6.72
Q99575	Ribonucleases P/MRP protein subunit POP1	1	1.17	0	0.00	0	0.00
Q99584	Protein S100-A13	5	31.63	3	20.41	3	12.24
Q99598	Translin-associated protein X	2	6.55	2	13.45	3	14.14
Q99613	Eukaryotic translation initiation factor 3 subunit C	23	20.48	15	10.30	15	17.85
Q99615	DnaJ homolog subfamily C member 7	2	4.25	0	0.00	0	0.00
Q99623	Prohibitin-2	56	66.89	38	52.51	26	55.52
Q99674	Cell growth regulator with EF hand domain protein 1	2	8.97	0	0.00	0	0.00
Q99700	Ataxin-2	1	0.76	0	0.00	0	0.00
Q99714	3-hydroxyacyl-CoA dehydrogenase type-2	22	70.11	12	49.04	16	67.82
Q99729	Heterogeneous nuclear ribonucleoprotein A/B	11	19.58	10	18.98	8	17.47
Q99733	Nucleosome assembly protein 1-like 4	16	37.60	9	15.20	8	23.20
Q99747	Gamma-soluble NSF attachment protein	1	3.20	0	0.00	2	8.65
Q99757	Thioredoxin, mitochondrial	5	32.53	3	32.53	0	0.00
Q99797	Mitochondrial intermediate peptidase	3	6.17	0	0.00	0	0.00
Q99798	Aconitate hydratase, mitochondrial	109	47.82	69	41.79	46	30.51
Q99805	Transmembrane 9 superfamily member 2	11	9.80	6	5.28	8	5.28
Q99829	Copine-1	14	13.97	4	8.38	8	15.08
Q99832	T-complex protein 1 subunit eta	35	43.46	21	31.31	20	30.76
Q99848	Probable rRNA-processing protein EBP2	2	3.92	0	0.00	0	0.00
Q99873	Protein arginine N-methyltransferase 1	7	8.59	3	6.37	3	6.37
Q99877	Histone H2B type 1-N	61	67.46	61	62.70	43	57.94
Q99878	Histone H2A type 1-J	54	48.44	55	38.28	35	38.28
Q99961	Endophilin-A2	1	3.53	0	0.00	0	0.00
Q9BPW8	Protein NipSnap homolog 1	2	4.93	0	0.00	2	4.93
Q9BPX5	Actin-related protein 2/3 complex subunit 5-like protein	4	16.34	1	17.65	5	33.99
Q9BQ67	Glutamate-rich WD repeat-containing protein 1	3	10.54	2	7.40	2	7.40
Q9BQ69	MACRO domain-containing protein 1	10	22.77	8	19.38	9	19.38
Q9BQ70	Transcription factor 25	1	2.22	0	0.00	0	0.00

Q9BQ95	Evolutionarily conserved signaling intermediate in Toll pathway, mitochondrial	1	3.94	0	0.00	1	3.94
Q9BQA9	Uncharacterized protein C17orf62	1	9.63	0	0.00	0	0.00
Q9BQE5	Apolipoprotein L2	3	6.53	1	3.26	0	0.00
Q9BQG0	Myb-binding protein 1A	16	10.77	12	6.70	8	5.35
Q9BR76	Coronin-1B	10	22.29	8	17.38	4	11.45
Q9BRA2	Thioredoxin domain-containing protein 17	4	26.83	2	11.38	4	19.51
Q9BRF8	Calcineurin-like phosphoesterase domain-containing protein 1	8	24.52	7	21.02	7	20.38
Q9BRG1	Vacuolar protein-sorting-associated protein 25	5	14.20	5	22.16	3	14.20
Q9BRJ2	39S ribosomal protein L45, mitochondrial	2	8.50	1	3.27	1	3.27
Q9BRP4	Proteasomal ATPase-associated factor 1	2	5.10	0	0.00	0	0.00
Q9BRR6	ADP-dependent glucokinase	3	10.26	2	7.45	0	0.00
Q9BRT3	Migration and invasion enhancer 1	2	15.65	0	0.00	0	0.00
Q9BRX8	Redox-regulatory protein PAMM	15	31.88	13	24.45	10	20.96
Q9BRZ2	E3 ubiquitin-protein ligase TRIM56	5	9.40	0	0.00	0	0.00
Q9BS26	Endoplasmic reticulum resident protein 44	15	27.09	8	27.59	7	21.18
Q9BSD7	Cancer-related nucleoside-triphosphatase	7	38.42	4	22.63	2	14.21
Q9BSH5	Haloacid dehalogenase-like hydrolase domain-containing protein 3	7	27.49	4	23.90	2	14.34
Q9BSJ2	Gamma-tubulin complex component 2	4	7.65	0	0.00	0	0.00
Q9BSJ8	Extended synaptotagmin-1	10	11.87	9	9.96	8	9.78
Q9BT09	Protein canopy homolog 3	1	3.60	1	2.52	0	0.00
Q9BT22	Chitobiosyldiphosphodolichol beta-mannosyltransferase	4	8.19	3	6.25	2	6.25
Q9BT40	Inositol polyphosphate 5-phosphatase K	2	5.58	1	2.23	2	2.23
Q9BT78	COP9 signalosome complex subunit 4	11	22.66	5	15.52	6	21.43
Q9BTE6	Alanyl-tRNA editing protein Aarsd1	3	10.68	0	0.00	1	3.64
Q9BTM1	Histone H2A.J	55	55.04	55	37.98	36	44.96
Q9BTT0	Acidic leucine-rich nuclear phosphoprotein 32 family member E	6	24.63	5	23.88	4	21.27
Q9BTU6	Phosphatidylinositol 4-kinase type 2-alpha	2	1.88	2	1.88	2	1.88
Q9BTV4	Transmembrane protein 43	4	19.25	3	16.00	3	16.00
Q9BTW9	Tubulin-specific chaperone D	13	13.67	10	12.42	9	8.73
Q9BTY7	Protein FAM203A	7	32.82	4	21.79	5	25.13
Q9BTZ2	Dehydrogenase/reductase SDR family member 4	3	7.91	0	0.00	0	0.00
Q9BU23	Lipase maturation factor 2	2	2.26	2	4.81	0	0.00
Q9BUF5	Tubulin beta-6 chain	87	62.56	57	47.98	0	0.00
Q9BUJ2	Heterogeneous nuclear ribonucleoprotein U-like protein 1	13	14.60	8	12.73	6	9.81
Q9BUP0	EF-hand domain-containing protein D1	12	44.35	22	48.54	13	44.35
Q9BUQ8	Probable ATP-dependent RNA helicase DDX23	4	5.00	2	2.68	0	0.00
Q9BUR5	Apolipoprotein O	3	18.18	0	0.00	0	0.00
Q9BUT1	3-hydroxybutyrate dehydrogenase type 2	6	22.04	2	13.06	3	13.47
Q9BV10	Dol-P-Man:Man(7)GlcNAc(2)-PP-Dol alpha-1,6-mannosyltransferase	1	3.28	0	0.00	1	3.28
Q9BV36	Melanophilin	19	25.67	7	20.50	14	21.17
Q9BV38	WD repeat-containing protein 18	2	5.56	0	0.00	0	0.00
Q9BV57	1,2-dihydroxy-3-keto-5-methylthiopentene dioxygenase	1	7.26	1	7.26	1	7.26
Q9BV79	Trans-2-enoyl-CoA reductase, mitochondrial	3	6.70	3	6.70	3	6.70
Q9BV86	Alpha N-terminal protein methyltransferase 1A	2	3.14	0	0.00	0	0.00
Q9BVA1	Tubulin beta-2B chain	169	67.42	105	66.29	91	65.84
Q9BVC6	Transmembrane protein 109	5	9.05	2	4.94	3	4.94
Q9BVG4	UPF0368 protein Cxorf26	2	4.29	0	0.00	0	0.00
Q9BVI4	Nucleolar complex protein 4 homolog	3	5.62	0	0.00	0	0.00
Q9BVJ7	Dual specificity protein phosphatase 23	3	22.00	0	0.00	0	0.00
Q9BVK6	Transmembrane emp24 domain-containing protein 9	6	20.00	2	9.36	5	16.17
Q9BVK8	Transmembrane protein 147	1	7.59	0	0.00	1	7.59
Q9BVL4	Selenoprotein O	4	8.22	0	0.00	1	2.99
Q9BVP2	Guanine nucleotide-binding protein-like 3	2	2.73	4	9.11	3	4.92
Q9BW72	HIG1 domain family member 2A	2	23.58	1	23.58	0	0.00
Q9BW92	Threonyl-tRNA synthetase, mitochondrial	4	6.68	0	0.00	0	0.00
Q9BWD1	Acetyl-CoA acetyltransferase, cytosolic	6	16.62	2	9.57	3	14.61
Q9BWF3	RNA-binding protein 4	4	23.35	4	22.25	5	19.78
Q9BWM7	Sideroflexin-3	18	40.62	8	27.38	7	27.38
Q9BWS9	Chitinase domain-containing protein 1	6	19.34	1	3.56	6	15.78
Q9BX66	Sorbin and SH3 domain-containing protein 1	18	11.53	7	5.42	12	10.60
Q9BX68	Histidine triad nucleotide-binding protein 2, mitochondrial	8	31.90	6	31.90	4	31.90
Q9BX70	BTB/POZ domain-containing protein 2	1	2.67	0	0.00	0	0.00
Q9BXJ9	N-alpha-acetyltransferase 15, NatA auxiliary subunit	7	9.81	3	5.08	3	5.08
Q9BXK5	Bcl-2-like protein 13	26	39.59	12	24.54	14	25.36
Q9BXP2	Solute carrier family 12 member 9	6	10.83	1	1.09	0	0.00
Q9BXP5	Serrate RNA effector molecule homolog	4	5.48	0	0.00	0	0.00
Q9BXS5	AP-1 complex subunit mu-1	7	14.89	2	5.91	2	7.80
Q9BXV9	Uncharacterized protein C14orf142	2	18.00	0	0.00	2	18.00
Q9BXW6	Oxysterol-binding protein-related protein 1	3	3.89	0	0.00	1	1.68
Q9BXW7	Cat eye syndrome critical region protein 5	5	8.51	3	11.58	0	0.00
Q9BXY0	Protein MAK16 homolog	1	4.67	0	0.00	1	4.67
Q9BY32	Inosine triphosphate pyrophosphatase	3	14.95	0	0.00	1	8.76
Q9BY50	Signal peptidase complex catalytic subunit SEC11C	2	5.21	1	5.21	3	15.63
Q9BYD1	39S ribosomal protein L13, mitochondrial	5	22.47	5	28.65	2	8.43
Q9BYD2	39S ribosomal protein L9, mitochondrial	2	10.11	1	6.37	1	6.37
Q9BYD3	39S ribosomal protein L4, mitochondrial	7	28.30	1	5.14	2	11.25
Q9BYI3	Hyccin	2	6.33	2	3.07	1	2.11
Q9BYJ9	YTH domain family protein 1	1	1.61	0	0.00	0	0.00
Q9BYT8	Neurolysin, mitochondrial	6	9.66	2	4.54	5	5.82
Q9BZ67	FERM domain-containing protein 8	1	2.37	1	2.37	0	0.00
Q9BZE1	39S ribosomal protein L37, mitochondrial	3	7.56	2	5.44	0	0.00
Q9BZE9	Tether containing UBX domain for GLUT4	3	6.15	3	6.51	3	4.70
Q9BZF1	Oxysterol-binding protein-related protein 8	4	4.72	4	5.96	7	8.55

Q9BZF9	Uveal autoantigen with coiled-coil domains and ankyrin repeats	3	2.82	1	0.71	2	1.06
Q9BZH6	WD repeat-containing protein 11	4	4.57	3	3.43	2	2.78
Q9BZJ0	Crooked neck-like protein 1	2	2.83	0	0.00	0	0.00
Q9BZJ3	Tryptase delta	4	9.92	2	6.20	2	8.68
Q9BZL4	Protein phosphatase 1 regulatory subunit 12C	3	5.12	0	0.00	0	0.00
Q9BZQ8	Protein Niban	9	11.85	11	12.82	10	10.78
Q9BZZ5	Apoptosis inhibitor 5	11	18.13	4	9.35	3	3.44
Q9C005	Protein dpy-30 homolog	9	45.45	7	45.45	4	36.36
Q9C0C2	182 kDa tankyrase-1-binding protein	2	0.87	1	0.87	0	0.00
Q9C0E2	Exportin-4	5	4.52	2	2.35	2	1.48
Q9C0E8	Protein lunapark	6	19.39	0	0.00	0	0.00
Q9C0H2	Protein tweety homolog 3	2	4.97	0	0.00	0	0.00
Q9GIY3	HLA class II histocompatibility antigen, DRB1-14 beta chain	4	16.92	0	0.00	0	0.00
Q9GZM8	Nuclear distribution protein nudE-like 1	2	3.48	0	0.00	0	0.00
Q9GZR7	ATP-dependent RNA helicase DDX24	4	6.87	4	6.05	2	3.03
Q9GZS3	WD repeat-containing protein 61	1	5.57	0	0.00	0	0.00
Q9GZT3	SRA stem-loop-interacting RNA-binding protein, mitochondrial	4	22.02	2	12.84	1	12.84
Q9GZT8	NIF3-like protein 1	3	10.08	4	14.06	2	6.37
Q9GZY8	Mitochondrial fission factor	10	23.10	9	19.88	7	19.01
Q9H008	Phospholysine phosphohistidine inorganic pyrophosphate phosphatase	10	18.52	8	21.48	4	18.52
Q9H061	Transmembrane protein 126A	2	9.74	3	17.95	3	20.00
Q9H0A0	N-acetyltransferase 10	5	8.59	6	5.85	7	9.37
Q9H0A8	COMM domain-containing protein 4	2	17.09	0	0.00	2	20.10
Q9H0B6	Kinesin light chain 2	6	11.41	0	0.00	0	0.00
Q9H0C8	Integrin-linked kinase-associated serine/threonine phosphatase 2C	4	8.42	0	0.00	0	0.00
Q9H0D6	5'-3' exoribonuclease 2	7	12.32	5	8.63	6	10.00
Q9H0E2	Toll-interacting protein	7	15.33	3	10.58	3	9.85
Q9H0E9	Bromodomain-containing protein 8	1	1.05	1	1.05	0	0.00
Q9H0F6	Sharpin	1	3.88	0	0.00	0	0.00
Q9H0R4	Haloacid dehalogenase-like hydrolase domain-containing protein 2	10	27.41	9	27.80	1	11.20
Q9H0U3	Magnesium transporter protein 1	1	2.99	0	0.00	0	0.00
Q9H0W9	Ester hydrolase C11orf54	3	9.21	1	3.81	3	9.21
Q9H1A3	Methyltransferase-like protein 9	5	16.98	2	9.12	3	14.15
Q9H1A4	Anaphase-promoting complex subunit 1	2	1.80	0	0.00	0	0.00
Q9H1E3	Nuclear ubiquitous casein and cyclin-dependent kinases substrate	10	11.93	4	8.23	6	8.23
Q9H1E5	Thioredoxin-related transmembrane protein 4	2	7.74	2	4.30	1	4.30
Q9H1H9	Kinesin-like protein KIF13A	4	2.82	0	0.00	0	0.00
Q9H1I8	Activating signal cointegrator 1 complex subunit 2	1	1.72	0	0.00	0	0.00
Q9H1K0	Rabenosyn-5	1	1.53	0	0.00	0	0.00
Q9H1K1	Iron-sulfur cluster assembly enzyme ISCU, mitochondrial	1	5.39	1	5.39	0	0.00
Q9H1Z4	WD repeat-containing protein 13	4	8.25	3	5.36	0	0.00
Q9H1Z9	Tetraspanin-10	5	10.14	1	3.10	0	0.00
Q9H201	Epsin-3	2	1.58	1	1.58	1	1.58
Q9H223	EH domain-containing protein 4	18	24.21	9	14.42	11	16.45
Q9H246	Uncharacterized protein C1orf21	1	8.26	0	0.00	0	0.00
Q9H267	Vacuolar protein sorting-associated protein 33B	4	9.40	1	2.11	2	5.19
Q9H269	Vacuolar protein sorting-associated protein 16 homolog	7	5.01	6	5.01	3	2.26
Q9H270	Vacuolar protein sorting-associated protein 11 homolog	2	3.83	6	5.63	2	3.83
Q9H299	SH3 domain-binding glutamic acid-rich-like protein 3	3	26.88	2	26.88	3	16.13
Q9H2D6	TRIO and F-actin-binding protein	5	1.78	0	0.00	0	0.00
Q9H2G2	STE20-like serine/threonine-protein kinase	5	4.45	1	1.86	5	4.45
Q9H2I8	Leucine-rich repeat-containing protein C10orf11	1	11.62	0	0.00	1	11.62
Q9H2M9	Rab3 GTPase-activating protein non-catalytic subunit	8	5.03	3	2.15	1	1.15
Q9H2U1	Probable ATP-dependent RNA helicase DHX36	1	1.59	0	0.00	0	0.00
Q9H2U2	Inorganic pyrophosphatase 2, mitochondrial	19	44.91	8	22.46	5	14.07
Q9H2V7	Protein spinster homolog 1	3	5.87	0	0.00	0	0.00
Q9H307	Pinin	6	7.67	0	0.00	0	0.00
Q9H330	Transmembrane protein C9orf5	2	2.53	0	0.00	0	0.00
Q9H3G5	Probable serine carboxypeptidase CPVL	16	18.91	11	18.91	6	13.87
Q9H3K6	BolA-like protein 2	4	40.70	4	40.70	3	18.60
Q9H3N1	Thioredoxin-related transmembrane protein 1	5	12.14	2	6.79	0	0.00
Q9H3P7	Golgi resident protein GCP60	5	11.17	3	7.01	4	7.01
Q9H3Q1	Cdc42 effector protein 4	2	5.34	1	5.34	1	4.49
Q9H3S7	Tyrosine-protein phosphatase non-receptor type 23	8	5.75	5	3.67	4	3.91
Q9H446	RWD domain-containing protein 1	1	7.00	0	0.00	0	0.00
Q9H479	Fructosamine-3-kinase	4	16.83	0	0.00	0	0.00
Q9H490	Phosphatidylinositol glycan anchor biosynthesis class U protein	1	3.91	2	3.91	2	3.91
Q9H4A3	Serine/threonine-protein kinase WNK1	3	1.13	0	0.00	0	0.00
Q9H4A4	Aminopeptidase B	24	34.31	15	16.31	14	14.62
Q9H4A5	Golgi phosphoprotein 3-like	1	4.56	1	4.56	0	0.00
Q9H4A6	Golgi phosphoprotein 3	1	4.36	1	4.36	0	0.00
Q9H4B0	Probable tRNA threonylcarbamoyladenosine biosynthesis protein OSGEPL1	2	6.52	2	4.35	0	0.00
Q9H4G4	Golgi-associated plant pathogenesis-related protein 1	2	16.88	0	0.00	3	16.88
Q9H4M9	EH domain-containing protein 1	12	23.60	9	13.67	8	13.30
Q9H583	HEAT repeat-containing protein 1	3	2.01	1	0.75	2	1.40
Q9H5N1	Rab GTPase-binding effector protein 2	2	3.16	0	0.00	0	0.00
Q9H5X1	MIP18 family protein FAM96A	1	5.62	1	5.62	2	8.75
Q9H6F5	Coiled-coil domain-containing protein 86	1	3.06	0	0.00	0	0.00
Q9H6K4	Optic atrophy 3 protein	6	20.67	3	16.76	2	16.76
Q9H6R4	Nucleolar protein 6	6	5.41	5	5.41	4	5.06
Q9H6S3	Epidermal growth factor receptor kinase substrate 8-like protein 2	3	5.03	0	0.00	1	2.80
Q9H6V9	UPF0554 protein C2orf43	1	2.77	0	0.00	2	3.08
Q9H6Z4	Ran-binding protein 3	1	2.12	0	0.00	0	0.00

Q9H773	dCTP pyrophosphatase 1	5	26.47	0	0.00	0	0.00
Q9H7B2	Ribosome production factor 2 homolog	4	13.07	0	0.00	1	2.61
Q9H7C9	UPF0366 protein C11orf67	2	22.13	0	0.00	0	0.00
Q9H7D7	WD repeat-containing protein 26	5	5.60	4	7.87	3	7.87
Q9H7Z7	Prostaglandin E synthase 2	18	32.63	11	25.99	8	19.63
Q9H845	Acyl-CoA dehydrogenase family member 9, mitochondrial	2	3.54	3	4.51	3	5.96
Q9H871	Protein RMD5 homolog A	1	3.33	1	3.33	0	0.00
Q9H8H2	Probable ATP-dependent RNA helicase DDX31	2	2.00	1	2.00	1	2.00
Q9H8Y8	Golgi reassembly-stacking protein 2	3	10.84	0	0.00	4	14.82
Q9H910	Hematological and neurological expressed 1-like protein	4	22.11	1	7.37	0	0.00
Q9H936	Mitochondrial glutamate carrier 1	3	12.69	0	0.00	0	0.00
Q9H9B4	Sideroflexin-1	6	19.57	0	0.00	0	0.00
Q9H9C1	VPS33B-interacting protein	4	7.91	1	1.42	0	0.00
Q9H9J2	39S ribosomal protein L44, mitochondrial	1	5.12	1	5.12	0	0.00
Q9H9P8	L-2-hydroxyglutarate dehydrogenase, mitochondrial	4	7.13	0	0.00	1	2.59
Q9H9S3	Protein transport protein Sec61 subunit alpha isoform 2	3	5.25	0	0.00	0	0.00
Q9HA82	Ceramide synthase 4	3	5.58	0	0.00	0	0.00
Q9HAV7	GrpE protein homolog 1, mitochondrial	6	17.05	3	12.90	2	5.07
Q9HB07	UPF0160 protein MYG1, mitochondrial	8	15.43	3	9.04	0	0.00
Q9HB90	Ras-related GTP-binding protein C	2	5.76	1	2.26	0	0.00
Q9HBH5	Retinol dehydrogenase 14	3	9.82	0	0.00	0	0.00
Q9HBJ8	Collectrin	1	6.31	0	0.00	0	0.00
Q9HBL7	Transmembrane protein C9orf46	2	14.29	0	0.00	0	0.00
Q9HC35	Echinoderm microtubule-associated protein-like 4	2	2.85	0	0.00	0	0.00
Q9HC38	Glyoxalase domain-containing protein 4	13	33.23	6	23.64	5	23.00
Q9HCC0	Methylcrotonoyl-CoA carboxylase beta chain, mitochondrial	9	19.72	6	11.90	3	7.81
Q9HCD5	Nuclear receptor coactivator 5	2	3.11	3	3.11	2	3.11
Q9HCE1	Putative helicase MOV-10	7	9.67	0	0.00	0	0.00
Q9HCF4	Protein ALO17	4	3.03	1	0.77	1	0.77
Q9HCJ6	Synaptic vesicle membrane protein VAT-1 homolog-like	2	5.25	1	2.86	0	0.00
Q9HCN8	Stromal cell-derived factor 2-like protein 1	1	9.05	0	0.00	0	0.00
Q9HD20	Probable cation-transporting ATPase 13A1	13	9.80	5	4.48	8	6.81
Q9HD26	Golgi-associated PDZ and coiled-coil motif-containing protein	2	4.11	1	4.11	0	0.00
Q9HD33	39S ribosomal protein L47, mitochondrial	4	8.40	2	4.80	1	4.80
Q9HD45	Transmembrane 9 superfamily member 3	2	3.06	0	0.00	0	0.00
Q9HD67	Myosin-X	8	5.15	3	2.19	4	2.28
Q9HDC9	Adipocyte plasma membrane-associated protein	6	18.27	6	20.43	9	18.27
Q9NNW7	Thioredoxin reductase 2, mitochondrial	7	20.23	0	0.00	3	9.73
Q9NP66	High mobility group protein 20A	3	13.26	0	0.00	0	0.00
Q9NP72	Ras-related protein Rab-18	3	13.11	2	13.11	2	13.11
Q9NP81	Seryl-tRNA synthetase, mitochondrial	13	29.34	5	15.06	6	18.53
Q9NP97	Dynein light chain roadblock-type 1	3	29.17	4	29.17	4	29.17
Q9NPF4	Probable tRNA threonylcarbamoyladenosine biosynthesis protein OSGEP	4	13.73	4	14.03	2	7.46
Q9NPJ6	Mediator of RNA polymerase II transcription subunit 4	2	11.11	1	4.81	1	4.81
Q9NPL8	Translocase of inner mitochondrial membrane domain-containing protein 1	5	21.40	0	0.00	2	10.18
Q9NPQ8	Synembryn-A	4	11.49	3	8.66	5	12.43
Q9NQ50	39S ribosomal protein L40, mitochondrial	3	23.30	3	14.56	0	0.00
Q9NQ79	Cartilage acidic protein 1	5	10.59	5	8.02	4	6.50
Q9NQ88	Probable fructose-2,6-bisphosphatase TIGAR	3	12.96	1	4.07	2	12.96
Q9NQC3	Reticulon-4	8	5.96	7	5.96	11	8.98
Q9NQG5	Regulation of nuclear pre-mRNA domain-containing protein 1B	7	13.80	4	11.35	4	14.42
Q9NQL2	Ras-related GTP-binding protein D	2	5.75	1	2.25	0	0.00
Q9NQP4	Prefoldin subunit 4	6	36.57	3	20.15	6	20.15
Q9NQR4	Omega-amidase NIT2	13	32.61	11	26.45	11	38.04
Q9NQT8	Kinesin-like protein KIF13B	4	2.90	0	0.00	4	2.41
Q9NQU5	Serine/threonine-protein kinase PAK 6	1	1.61	0	0.00	0	0.00
Q9NQW7	Xaa-Pro aminopeptidase 1	12	17.82	6	13.64	9	17.01
Q9NQX3	Gephyrin	1	2.72	2	2.72	3	5.84
Q9NR28	Diablo homolog, mitochondrial	12	28.03	8	20.50	5	16.32
Q9NR30	Nucleolar RNA helicase 2	5	5.24	2	4.09	2	4.21
Q9NR31	GTP-binding protein SAR1a	18	54.55	10	34.85	8	23.23
Q9NR45	Sialic acid synthase	14	28.41	8	21.45	9	21.45
Q9NRF8	CTP synthase 2	8	12.80	0	0.00	4	6.83
Q9NRG7	Epimerase family protein SDR39U1	2	10.66	1	5.02	2	5.02
Q9NRH3	Tubulin gamma-2 chain	12	23.73	8	28.38	8	26.39
Q9NRP0	Oligosaccharyltransferase complex subunit OSTC	5	8.05	2	8.05	0	0.00
Q9NRV9	Heme-binding protein 1	17	64.02	5	19.58	7	44.97
Q9NRW7	Vacuolar protein sorting-associated protein 45	8	10.70	3	4.39	3	4.39
Q9NRX4	14 kDa phosphohistidine phosphatase	3	25.60	3	24.00	0	0.00
Q9NRZ7	1-acyl-sn-glycerol-3-phosphate acyltransferase gamma	3	5.58	0	0.00	0	0.00
Q9NS69	Mitochondrial import receptor subunit TOM22 homolog	7	33.80	3	25.35	2	17.61
Q9NS86	LanC-like protein 2	2	7.11	0	0.00	0	0.00
Q9NSB2	Keratin, type II cuticular Hb4	5	2.50	0	0.00	0	0.00
Q9NSD9	Phenylalanyl-tRNA synthetase beta chain	23	28.01	14	14.77	15	18.34
Q9NSE4	Isoleucyl-tRNA synthetase, mitochondrial	21	22.63	12	10.87	9	7.61
Q9NSK0	Kinesin light chain 4	8	12.92	0	0.00	0	0.00
Q9NT62	Ubiquitin-like-conjugating enzyme ATG3	2	7.33	2	7.33	2	7.33
Q9NTG7	NAD-dependent deacetylase sirtuin-3, mitochondrial	3	5.51	2	2.76	2	2.76
Q9NTI5	Sister chromatid cohesion protein PDS5 homolog B	3	1.59	0	0.00	2	1.93
Q9NTJ4	Alpha-mannosidase 2C1	2	2.50	2	2.50	3	3.46
Q9NTJ5	Phosphatidylinositide phosphatase SAC1	8	14.82	0	0.00	1	1.70
Q9NTK5	Obg-like ATPase 1	10	15.66	7	11.62	7	13.89
Q9NTX5	Enoyl-CoA hydratase domain-containing protein 1	4	10.10	1	3.91	2	9.77

Q9NTZ6	RNA-binding protein 12	4	3.65	3	2.58	2	2.58
Q9NUJ1	Abhydrolase domain-containing protein 10, mitochondrial	5	17.32	7	17.32	3	8.17
Q9NUL5	UPF0515 protein C19orf66	1	6.19	0	0.00	1	6.19
Q9NUN5	Probable lysosomal cobalamin transporter	1	3.33	0	0.00	0	0.00
Q9NUP1	Protein cappuccino homolog	2	14.29	0	0.00	0	0.00
Q9NUQ7	Ufm1-specific protease 2	2	6.82	0	0.00	2	3.62
Q9NUQ9	Protein FAM49B	12	30.25	6	17.90	6	17.90
Q9NV06	DDB1- and CUL4-associated factor 13	1	3.60	0	0.00	0	0.00
Q9NVA2	Septin-11	7	22.84	0	0.00	0	0.00
Q9NVD7	Alpha-parvin	3	7.53	3	8.60	3	11.29
Q9NVE7	Pantothenate kinase 4	2	3.88	1	1.81	1	1.81
Q9NVG8	TBC1 domain family member 13	4	13.00	3	11.00	0	0.00
Q9NVH1	DnaJ homolog subfamily C member 11	4	8.05	8	14.31	0	0.00
Q9NVI7	ATPase family AAA domain-containing protein 3A	13	20.50	10	14.83	8	12.62
Q9NVJ2	ADP-ribosylation factor-like protein 8B	3	12.37	0	0.00	0	0.00
Q9NVS9	Pyridoxine-5'-phosphate oxidase	3	16.09	2	12.64	0	0.00
Q9NVZ3	Adaptin ear-binding coat-associated protein 2	2	9.51	2	3.80	1	3.80
Q9NW81	ATP synthase subunit s-like protein	1	7.00	0	0.00	0	0.00
Q9NWQ8	Phosphoprotein associated with glycosphingolipid-enriched microdomains 1	1	2.55	0	0.00	0	0.00
Q9NWU2	Protein C20orf11	4	9.65	3	16.23	2	16.23
Q9NWV4	UPF0587 protein C1orf123	5	25.62	4	40.63	1	10.00
Q9NWV8	BRISC and BRCA1-A complex member 1	3	16.11	0	0.00	0	0.00
Q9NWW5	Ceroid-lipofuscinosis neuronal protein 6	1	6.75	2	10.29	2	6.75
Q9NX08	COMM domain-containing protein 8	1	6.56	0	0.00	1	6.56
Q9NX14	NADH dehydrogenase [ubiquinone] 1 beta subcomplex subunit 11, mitochondrial	2	22.22	0	0.00	0	0.00
Q9NX18	Succinate dehydrogenase assembly factor 2, mitochondrial	1	7.23	0	0.00	1	7.23
Q9NX24	H/ACA ribonucleoprotein complex subunit 2	2	23.53	0	0.00	1	12.42
Q9NX40	OCIA domain-containing protein 1	9	31.43	2	8.98	0	0.00
Q9NX46	Poly(ADP-ribose) glycohydrolase ARH3	6	20.11	3	11.85	3	11.85
Q9NX55	Huntingtin-interacting protein K	2	11.63	1	11.63	2	11.63
Q9NX58	Cell growth-regulating nucleolar protein	2	3.69	2	10.29	1	3.69
Q9NX62	Inositol monophosphatase 3	1	3.34	0	0.00	0	0.00
Q9NX63	Coiled-coil-helix-coiled-coil-helix domain-containing protein 3, mitochondrial	9	18.94	7	25.99	4	14.98
Q9NXA8	NAD-dependent deacetylase sirtuin-5	2	4.19	1	5.48	0	0.00
Q9NXD2	Myotubularin-related protein 10	1	2.57	0	0.00	1	1.67
Q9NXE4	Sphingomyelin phosphodiesterase 4	1	1.81	1	1.81	2	3.75
Q9NXF1	Testis-expressed sequence 10 protein	5	5.27	2	3.66	2	3.44
Q9NXR1	Nuclear distribution protein nudE homolog 1	2	3.47	0	0.00	0	0.00
Q9NXR7	BRCA1-A complex subunit BRE	2	6.27	1	3.66	0	0.00
Q9NY12	H/ACA ribonucleoprotein complex subunit 1	2	4.15	0	0.00	0	0.00
Q9NY15	Stabilin-1	2	1.28	5	2.76	0	0.00
Q9NY27	Serine/threonine-protein phosphatase 4 regulatory subunit 2	1	3.60	0	0.00	0	0.00
Q9NY33	Dipeptidyl peptidase 3	13	24.97	8	17.37	9	21.17
Q9NY65	Tubulin alpha-8 chain	88	48.55	70	41.43	64	44.10
Q9NYF8	Bcl-2-associated transcription factor 1	2	1.74	0	0.00	0	0.00
Q9NYK5	39S ribosomal protein L39, mitochondrial	2	7.69	2	7.69	1	4.44
Q9NYL4	Peptidyl-prolyl cis-trans isomerase FKBP11	6	24.88	0	0.00	0	0.00
Q9NYL9	Tropomodulin-3	2	9.09	0	0.00	0	0.00
Q9NYU2	UDP-glucose:glycoprotein glucosyltransferase 1	20	15.05	8	9.71	14	11.25
Q9NYY8	FAST kinase domain-containing protein 2	1	1.13	0	0.00	0	0.00
Q9NZ01	Trans-2,3-enoyl-CoA reductase	7	13.96	3	6.82	4	10.06
Q9NZ32	Actin-related protein 10	5	12.71	1	3.36	1	3.36
Q9NZ45	CDGSH iron-sulfur domain-containing protein 1	4	34.26	0	0.00	2	13.89
Q9NZ53	Podocalyxin-like protein 2	2	2.31	1	2.31	1	2.31
Q9NZB2	Constitutive coactivator of PPAR-gamma-like protein 1	12	11.54	1	1.70	2	3.76
Q9NZH0	G-protein coupled receptor family C group 5 member B	1	2.98	2	5.95	3	2.98
Q9NZJ7	Mitochondrial carrier homolog 1	3	11.31	0	0.00	0	0.00
Q9NZL9	Methionine adenosyltransferase 2 subunit beta	5	18.26	1	7.49	2	11.08
Q9NZM1	Myoferlin	6	4.27	0	0.00	0	0.00
Q9NZM5	Glioma tumor suppressor candidate region gene 2 protein	1	3.77	0	0.00	1	3.77
Q9NZN4	EH domain-containing protein 2	7	12.34	5	8.29	7	8.29
Q9NZT2	Opioid growth factor receptor	4	5.76	3	3.69	2	2.36
Q9NZZ3	Charged multivesicular body protein 5	1	7.31	1	7.31	2	7.31
Q9P000	COMM domain-containing protein 9	7	48.48	3	23.74	0	0.00
Q9P015	39S ribosomal protein L15, mitochondrial	2	8.45	2	8.45	2	8.45
Q9P032	NADH dehydrogenase [ubiquinone] 1 alpha subcomplex assembly factor 4	1	8.00	1	8.00	0	0.00
Q9P035	3-hydroxyacyl-CoA dehydratase 3	14	24.86	12	18.78	11	15.47
Q9P0J0	NADH dehydrogenase [ubiquinone] 1 alpha subcomplex subunit 13	11	44.44	5	26.39	5	18.06
Q9P0J7	E3 ubiquitin-protein ligase KCMF1	4	8.14	4	8.14	3	8.14
Q9P0K7	Ankycorbin	2	2.86	0	0.00	2	3.47
Q9P0L0	Vesicle-associated membrane protein-associated protein A	7	15.26	6	15.26	0	0.00
Q9P0M6	Core histone macro-H2A.2	13	16.40	0	0.00	11	16.40
Q9P0V9	Septin-10	5	8.15	0	0.00	2	6.83
Q9P1F3	Costars family protein C6orf115	5	35.80	4	35.80	0	0.00
Q9P253	Vacuolar protein sorting-associated protein 18 homolog	1	1.13	3	4.63	0	0.00
Q9P258	Protein RCC2	6	12.26	7	14.75	3	4.98
Q9P260	LisH domain and HEAT repeat-containing protein KIAA1468	6	5.43	2	0.99	0	0.00
Q9P265	Disco-interacting protein 2 homolog B	6	5.08	3	2.73	4	4.00
Q9P273	Teneurin-3	1	0.37	0	0.00	0	0.00
Q9P286	Serine/threonine-protein kinase PAK 7	1	1.53	0	0.00	0	0.00
Q9P2B2	Prostaglandin F2 receptor negative regulator	1	1.59	0	0.00	0	0.00
Q9P2E9	Ribosome-binding protein 1	44	37.66	17	13.33	21	15.32
Q9P2J5	Leucyl-tRNA synthetase, cytoplasmic	19	19.90	11	13.44	12	12.41

Q9P2R3	Ankyrin repeat and FYVE domain-containing protein 1	10	12.23	4	5.90	6	8.04
Q9P2R7	Succinyl-CoA ligase [ADP-forming] subunit beta, mitochondrial	14	28.94	6	12.10	4	9.50
Q9P2T1	GMP reductase 2	3	12.36	2	10.34	0	0.00
Q9P2X0	Dolichol-phosphate mannosyltransferase subunit 3	1	10.87	0	0.00	0	0.00
Q9P2X3	Protein IMPACT	3	13.12	1	6.25	4	13.12
Q9TQE0	HLA class II histocompatibility antigen, DRB1-9 beta chain	6	13.16	3	4.89	3	9.77
Q9UBB4	Ataxin-10	2	6.95	1	3.58	1	3.58
Q9UBB6	Neurochondrin	1	1.65	0	0.00	0	0.00
Q9UBB9	Tuftelin-interacting protein 11	1	2.75	0	0.00	0	0.00
Q9UBC2	Epidermal growth factor receptor substrate 15-like 1	6	8.68	1	1.62	2	1.62
Q9UBE0	SUMO-activating enzyme subunit 1	14	23.12	8	17.92	9	17.92
Q9UBF2	Coatomer subunit gamma-2	8	10.56	0	0.00	7	9.18
Q9UBI6	Guanine nucleotide-binding protein G(I)/G(S)/G(O) subunit gamma-12	10	66.67	8	56.94	9	66.67
Q9UBP0	Spastin	1	1.79	0	0.00	0	0.00
Q9UBQ0	Vacuolar protein sorting-associated protein 29	10	25.82	7	25.82	2	20.33
Q9UBQ5	Eukaryotic translation initiation factor 3 subunit K	4	17.89	3	11.47	0	0.00
Q9UBQ7	Glyoxylate reductase/hydroxypyruvate reductase	18	42.99	9	26.52	13	31.40
Q9UBR2	Cathepsin Z	8	12.54	4	7.26	3	7.26
Q9UBS4	DnaJ homolog subfamily B member 11	6	13.97	6	13.97	3	13.97
Q9UBS8	E3 ubiquitin-protein ligase RNF14	1	4.22	0	0.00	1	4.22
Q9UBT2	SUMO-activating enzyme subunit 2	10	20.31	8	8.75	11	17.50
Q9UBV2	Protein sel-1 homolog 1	2	4.91	1	2.39	0	0.00
Q9UBV8	Peflin	3	8.45	0	0.00	1	4.58
Q9UBW8	COP9 signalosome complex subunit 7a	5	20.73	5	17.09	6	21.45
Q9UDW1	Cytochrome b-c1 complex subunit 9	4	38.10	0	0.00	2	26.98
Q9UDY2	Tight junction protein ZO-2	3	3.02	6	4.03	2	1.77
Q9UEU0	Vesicle transport through interaction with t-SNAREs homolog 1B	6	24.57	2	10.34	0	0.00
Q9UEW8	STE20/SPS1-related proline-alanine-rich protein kinase	2	4.59	3	9.17	2	4.59
Q9UFG5	UPF0449 protein C19orf25	3	39.83	3	39.83	2	35.59
Q9UFN0	Protein NipSnap homolog 3A	9	36.84	5	24.29	4	16.19
Q9UG56	Phosphatidylserine decarboxylase proenzyme	2	6.85	2	6.85	0	0.00
Q9UG63	ATP-binding cassette sub-family F member 2	4	4.49	3	3.53	0	0.00
Q9UGT4	Sushi domain-containing protein 2	1	1.70	1	1.70	0	0.00
Q9UH65	Switch-associated protein 70	13	17.09	10	13.33	8	10.09
Q9UH99	SUN domain-containing protein 2	5	9.76	7	10.46	1	2.09
Q9UHA4	Ragulator complex protein LAMTOR3	5	43.55	4	43.55	5	20.97
Q9UHB6	LIM domain and actin-binding protein 1	4	5.53	0	0.00	0	0.00
Q9UHB9	Signal recognition particle 68 kDa protein	4	7.02	2	3.51	3	7.02
Q9UHD8	Septin-9	24	30.72	9	10.24	11	17.24
Q9UHG3	Prenylcysteine oxidase 1	6	12.08	4	11.09	3	8.32
Q9UHK6	Alpha-methylacyl-CoA racemase	3	10.73	0	0.00	0	0.00
Q9UHL4	Dipeptidyl peptidase 2	21	30.89	12	24.80	13	33.54
Q9UHQ9	NADH-cytochrome b5 reductase 1	15	28.52	9	34.75	10	26.23
Q9UHV9	Prefoldin subunit 2	3	29.22	2	9.09	3	21.43
Q9UHX1	Poly(U)-binding-splicing factor PUF60	13	17.17	5	14.13	6	14.31
Q9UHY1	Nuclear receptor-binding protein	4	10.47	1	2.80	1	2.80
Q9UHY7	Enolase-phosphatase E1	6	25.29	4	25.29	2	9.19
Q9UI09	NADH dehydrogenase [ubiquinone] 1 alpha subcomplex subunit 12	2	8.28	2	8.28	2	20.00
Q9UI12	V-type proton ATPase subunit H	12	14.08	14	14.49	7	15.11
Q9UI30	tRNA methyltransferase 112 homolog	3	32.80	2	21.60	2	11.20
Q9UIG0	Tyrosine-protein kinase BAZ1B	5	3.51	0	0.00	0	0.00
Q9UII2	ATPase inhibitor, mitochondrial	5	31.13	2	14.15	0	0.00
Q9UIJ7	GTP:AMP phosphotransferase, mitochondrial	15	48.90	4	26.43	6	24.67
Q9UIQ6	Leucyl-cystinyl aminopeptidase	7	6.83	3	4.29	6	6.93
Q9UIW2	Plexin-A1	3	1.63	1	0.79	0	0.00
Q9UJ70	N-acetyl-D-glucosamine kinase	9	22.97	4	15.41	7	20.06
Q9UJA5	tRNA (adenine(58)-N(1))-methyltransferase non-catalytic subunit TRM6	1	3.22	0	0.00	2	3.22
Q9UJS0	Calcium-binding mitochondrial carrier protein Aralar2	20	26.81	14	22.22	12	22.22
Q9UJU6	Drebrin-like protein	12	33.95	9	20.70	8	25.58
Q9UJV9	Probable ATP-dependent RNA helicase DDX41	1	3.22	0	0.00	0	0.00
Q9UJX5	Anaphase-promoting complex subunit 4	2	1.98	0	0.00	0	0.00
Q9UJY4	ADP-ribosylation factor-binding protein GGA2	2	6.20	0	0.00	0	0.00
Q9UJZ1	Stomatin-like protein 2	15	43.26	12	35.39	8	26.69
Q9UK45	U6 snRNA-associated Sm-like protein LSm7	2	17.48	2	25.24	2	17.48
Q9UKD2	mRNA turnover protein 4 homolog	2	9.62	0	0.00	0	0.00
Q9UKK3	Poly [ADP-ribose] polymerase 4	2	1.45	0	0.00	0	0.00
Q9UKK9	ADP-sugar pyrophosphatase	5	23.29	3	12.79	2	12.79
Q9UKS6	Protein kinase C and casein kinase substrate in neurons protein 3	6	12.97	3	7.55	3	7.55
Q9UKU0	Long-chain-fatty-acid--CoA ligase 6	1	1.43	0	0.00	0	0.00
Q9UKU7	Isobutyryl-CoA dehydrogenase, mitochondrial	5	11.57	1	3.37	0	0.00
Q9UKV3	Apoptotic chromatin condensation inducer in the nucleus	11	7.53	7	5.67	6	3.80
Q9UKY7	Protein CDV3 homolog	3	31.40	2	22.09	2	24.03
Q9UL12	Sarcosine dehydrogenase, mitochondrial	3	3.60	1	1.85	0	0.00
Q9UL15	BAG family molecular chaperone regulator 5	1	3.36	0	0.00	0	0.00
Q9UL25	Ras-related protein Rab-21	10	22.67	6	16.89	6	22.67
Q9UL41	Paraneoplastic antigen Ma3	4	10.37	0	0.00	0	0.00
Q9UL45	Pallidin	4	11.05	2	11.05	0	0.00
Q9UL46	Proteasome activator complex subunit 2	14	30.54	16	34.73	14	30.54
Q9ULA0	Aspartyl aminopeptidase	8	20.42	5	8.42	4	17.05
Q9ULE4	Protein FAM184B	1	0.94	0	0.00	1	0.94
Q9ULV4	Coronin-1C	10	18.35	2	3.38	4	6.12
Q9ULZ3	Apoptosis-associated speck-like protein containing a CARD	6	23.59	0	0.00	0	0.00
Q9UM00	Transmembrane and coiled-coil domain-containing protein 1	3	12.23	2	7.98	3	7.98

Q9UM54	Myosin-VI	4	4.10	0	0.00	3	3.40
Q9UMS0	NFU1 iron-sulfur cluster scaffold homolog, mitochondrial	3	14.57	0	0.00	0	0.00
Q9UMS4	Pre-mRNA-processing factor 19	10	21.83	11	21.83	6	21.63
Q9UMX0	Ubiquilin-1	9	13.07	12	13.92	9	11.04
Q9UMY4	Sorting nexin-12	2	13.37	3	14.53	1	8.14
Q9UN37	Vacuolar protein sorting-associated protein 4A	5	11.44	0	0.00	1	2.52
Q9UN86	Ras GTPase-activating protein-binding protein 2	5	8.71	2	5.19	2	3.53
Q9UNF0	Protein kinase C and casein kinase substrate in neurons protein 2	13	20.16	5	9.67	3	2.26
Q9UNF1	Melanoma-associated antigen D2	5	8.91	2	5.28	0	0.00
Q9UNH7	Sorting nexin-6	5	5.17	4	9.36	5	10.84
Q9UNK0	Syntaxin-8	2	12.29	0	0.00	0	0.00
Q9UNL2	Translocon-associated protein subunit gamma	3	7.57	3	7.57	3	7.57
Q9UNM6	26S proteasome non-ATPase regulatory subunit 13	15	23.94	10	25.00	7	13.56
Q9UNN5	FAS-associated factor 1	2	3.38	0	0.00	0	0.00
Q9UNX3	60S ribosomal protein L26-like 1	8	26.90	5	20.69	3	20.00
Q9UNX4	WD repeat-containing protein 3	1	1.80	2	2.76	2	2.76
Q9UNZ2	NSFL1 cofactor p47	11	31.08	11	23.78	12	21.89
Q9UP83	Conserved oligomeric Golgi complex subunit 5	4	6.44	0	0.00	0	0.00
Q9UPN3	Microtubule-actin cross-linking factor 1, isoforms 1/2/3/5	7	1.04	0	0.00	8	1.42
Q9UPQ0	LIM and calponin homology domains-containing protein 1	3	2.58	1	1.48	0	0.00
Q9UPT5	Exocyst complex component 7	5	7.35	0	0.00	0	0.00
Q9UPT8	Zinc finger CCCH domain-containing protein 4	2	2.53	0	0.00	0	0.00
Q9UQ80	Proliferation-associated protein 2G4	22	43.15	15	34.77	13	23.35
Q9UQ90	Paraplegin	7	10.94	0	0.00	0	0.00
Q9UQB3	Catenin delta-2	2	1.96	0	0.00	1	0.82
Q9UQE7	Structural maintenance of chromosomes protein 3	6	5.83	6	5.67	2	1.81
Q9Y224	UPF0568 protein C14orf166	14	33.20	11	27.05	11	29.92
Q9Y230	RuvB-like 2	8	18.79	7	18.14	3	5.83
Q9Y259	Choline/ethanolamine kinase	4	12.91	0	0.00	2	7.09
Q9Y262	Eukaryotic translation initiation factor 3 subunit L	15	18.62	8	15.43	12	21.28
Q9Y263	Phospholipase A-2-activating protein	3	6.16	2	3.65	2	3.65
Q9Y265	RuvB-like 1	20	35.09	18	28.29	10	24.56
Q9Y266	Nuclear migration protein nudC	4	7.25	1	4.53	0	0.00
Q9Y276	Mitochondrial chaperone BCS1	12	33.17	9	22.91	3	12.65
Q9Y277	Voltage-dependent anion-selective channel protein 3	10	23.32	8	16.25	5	8.13
Q9Y285	Phenylalanyl-tRNA synthetase alpha chain	14	24.21	6	16.34	8	16.34
Q9Y2A7	Nck-associated protein 1	9	8.78	4	3.72	0	0.00
Q9Y2B0	Protein canopy homolog 2	16	47.25	9	41.76	14	41.76
Q9Y2D0	Carbonic anhydrase 5B, mitochondrial	1	5.36	1	5.36	2	5.36
Q9Y2D4	Exocyst complex component 6B	6	9.86	0	0.00	1	1.60
Q9Y2E5	Epididymis-specific alpha-mannosidase	1	1.59	0	0.00	0	0.00
Q9Y2J2	Band 4.1-like protein 3	9	9.66	3	2.21	4	4.14
Q9Y2J4	Angiomotin-like protein 2	2	1.93	0	0.00	0	0.00
Q9Y2P8	RNA 3'-terminal phosphate cyclase-like protein	1	2.14	0	0.00	1	2.14
Q9Y2Q3	Glutathione S-transferase kappa 1	13	45.13	7	34.51	3	24.34
Q9Y2R0	Coiled-coil domain-containing protein 56	3	17.92	0	0.00	0	0.00
Q9Y2R9	28S ribosomal protein S7, mitochondrial	3	10.33	0	0.00	0	0.00
Q9Y2S2	Lambda-crystallin homolog	36	55.49	24	41.07	26	37.93
Q9Y2U8	Inner nuclear membrane protein Man1	3	3.84	1	1.43	1	1.43
Q9Y2V2	Calcium-regulated heat stable protein 1	1	10.88	4	10.88	3	10.88
Q9Y2W1	Thyroid hormone receptor-associated protein 3	11	10.16	4	4.08	3	3.66
Q9Y2W2	WW domain-binding protein 11	2	3.59	0	0.00	0	0.00
Q9Y2X3	Nucleolar protein 58	20	35.92	21	34.03	14	22.68
Q9Y2X7	ARF GTPase-activating protein GIT1	5	6.18	0	0.00	0	0.00
Q9Y2X8	Ubiquitin-conjugating enzyme E2 D4	4	12.24	3	12.24	2	12.24
Q9Y2Z0	Suppressor of G2 allele of SKP1 homolog	3	11.78	0	0.00	0	0.00
Q9Y2Z4	Tyrosyl-tRNA synthetase, mitochondrial	5	13.00	4	8.60	3	4.40
Q9Y303	Putative N-acetylglucosamine-6-phosphate deacetylase	12	30.56	13	30.56	10	24.94
Q9Y305	Acyl-coenzyme A thioesterase 9, mitochondrial	7	24.15	5	14.35	4	11.39
Q9Y315	Putative deoxyribose-phosphate aldolase	5	21.38	0	0.00	4	20.13
Q9Y320	Thioredoxin-related transmembrane protein 2	2	9.12	0	0.00	0	0.00
Q9Y333	U6 snRNA-associated Sm-like protein LSm2	3	40.00	2	27.37	1	20.00
Q9Y376	Calcium-binding protein 39	5	12.90	3	9.68	0	0.00
Q9Y383	Putative RNA-binding protein Luc7-like 2	6	11.73	6	12.50	7	11.99
Q9Y394	Dehydrogenase/reductase SDR family member 7	8	22.42	2	5.90	4	12.39
Q9Y3A5	Ribosome maturation protein SBDS	4	15.20	2	10.80	1	4.00
Q9Y3A6	Transmembrane emp24 domain-containing protein 5	2	5.24	1	5.24	1	5.24
Q9Y3B3	Transmembrane emp24 domain-containing protein 7	4	9.82	1	4.46	3	9.82
Q9Y3B7	39S ribosomal protein L11, mitochondrial	1	9.38	0	0.00	0	0.00
Q9Y3B8	Oligoribonuclease, mitochondrial	1	7.59	3	15.61	0	0.00
Q9Y3C4	TP53RK-binding protein	2	18.29	2	26.29	1	16.00
Q9Y3C8	Ubiquitin-fold modifier-conjugating enzyme 1	1	5.39	0	0.00	0	0.00
Q9Y3D6	Mitochondrial fission 1 protein	9	31.58	7	23.03	7	23.03
Q9Y3D9	28S ribosomal protein S23, mitochondrial	5	20.00	1	5.26	2	13.68
Q9Y3E0	Vesicle transport protein GOT1B	3	10.87	2	10.87	0	0.00
Q9Y3E1	Hepatoma-derived growth factor-related protein 3	3	16.26	0	0.00	0	0.00
Q9Y3E5	Peptidyl-tRNA hydrolase 2, mitochondrial	3	21.23	2	8.38	5	31.84
Q9Y3E7	Charged multivesicular body protein 3	1	5.40	0	0.00	0	0.00
Q9Y3I0	tRNA-splicing ligase RtcB homolog	10	19.80	5	13.47	4	12.48
Q9Y3Q8	TSC22 domain family protein 4	3	10.89	0	0.00	1	4.56
Q9Y3T9	Nucleolar complex protein 2 homolog	1	1.33	2	1.33	2	1.33
Q9Y3U8	60S ribosomal protein L36	6	29.52	2	20.00	2	20.00
Q9Y3X0	Coiled-coil domain-containing protein 9	1	2.26	0	0.00	0	0.00

Q9Y3Y2	Chromatin target of PRMT1 protein	4	17.34	0	0.00	1	8.07
Q9Y3Z3	SAM domain and HD domain-containing protein 1	21	33.07	19	27.16	11	22.04
Q9Y450	HBS1-like protein	1	2.34	0	0.00	0	0.00
Q9Y490	Talin-1	146	42.58	109	36.13	104	34.32
Q9Y4C8	Probable RNA-binding protein 19	1	1.67	0	0.00	0	0.00
Q9Y4F1	FERM, RhoGEF and pleckstrin domain-containing protein 1	7	7.08	4	4.79	4	6.12
Q9Y4G6	Talin-2	22	9.68	9	4.37	0	0.00
Q9Y4I1	Myosin-Va	40	18.22	28	16.17	20	13.96
Q9Y4L1	Hypoxia up-regulated protein 1	20	18.92	15	18.12	11	16.72
Q9Y4P3	Transducin beta-like protein 2	2	5.37	0	0.00	1	2.91
Q9Y4W2	Protein LAS1 homolog	1	1.91	1	1.23	1	1.91
Q9Y4W6	AFG3-like protein 2	26	24.59	11	12.80	10	8.78
Q9Y570	Protein phosphatase methylesterase 1	3	5.18	0	0.00	4	8.55
Q9Y580	RNA-binding protein 7	1	6.77	0	0.00	0	0.00
Q9Y5A9	YTH domain family protein 2	1	1.55	0	0.00	0	0.00
Q9Y5B0	RNA polymerase II subunit A C-terminal domain phosphatase	1	0.94	0	0.00	0	0.00
Q9Y5B9	FACT complex subunit SPT16	10	8.60	4	5.73	6	5.64
Q9Y5K5	Ubiquitin carboxyl-terminal hydrolase isozyme L5	4	14.59	2	8.21	2	8.51
Q9Y5K6	CD2-associated protein	6	11.11	1	3.91	2	6.42
Q9Y5K8	V-type proton ATPase subunit D	10	40.49	7	29.96	5	29.96
Q9Y5L0	Transportin-3	4	5.96	2	4.12	3	4.01
Q9Y5L4	Mitochondrial import inner membrane translocase subunit Tim13	5	36.84	1	14.74	2	14.74
Q9Y5M8	Signal recognition particle receptor subunit beta	7	21.77	2	9.59	2	9.59
Q9Y5P4	Collagen type IV alpha-3-binding protein	2	3.36	0	0.00	2	3.36
Q9Y5Q9	General transcription factor 3C polypeptide 3	1	1.69	1	1.69	3	3.16
Q9Y5S1	Transient receptor potential cation channel subfamily V member 2	5	7.46	0	0.00	5	7.46
Q9Y5S2	Serine/threonine-protein kinase MRCK beta	6	5.03	3	2.51	4	2.69
Q9Y5S9	RNA-binding protein 8A	9	32.18	7	47.70	1	6.32
Q9Y5X1	Sorting nexin-9	5	9.08	3	3.87	3	7.56
Q9Y5X2	Sorting nexin-8	8	12.04	6	11.40	6	13.12
Q9Y5X3	Sorting nexin-5	3	7.67	0	0.00	0	0.00
Q9Y5Y2	Cytosolic Fe-S cluster assembly factor NUBP2	4	25.09	3	25.09	2	19.56
Q9Y5Z4	Heme-binding protein 2	4	13.66	0	0.00	2	6.34
Q9Y606	tRNA pseudouridine synthase A, mitochondrial	5	12.88	0	0.00	1	2.81
Q9Y608	Leucine-rich repeat flightless-interacting protein 2	3	3.47	0	0.00	1	1.94
Q9Y617	Phosphoserine aminotransferase	4	11.89	3	9.19	0	0.00
Q9Y618	Nuclear receptor corepressor 2	2	1.27	0	0.00	0	0.00
Q9Y639	Neuroplastin	7	12.31	4	7.03	0	0.00
Q9Y646	Plasma glutamate carboxypeptidase	2	4.66	0	0.00	0	0.00
Q9Y653	G-protein coupled receptor 56	1	3.46	1	3.46	2	3.46
Q9Y672	Dolichyl pyrophosphate Man9GlcNAc2 alpha-1,3-glucosyltransferase	2	4.14	0	0.00	0	0.00
Q9Y678	Coatomer subunit gamma	21	25.97	9	11.33	12	18.19
Q9Y679	Ancient ubiquitous protein 1	7	10.29	2	6.30	2	6.30
Q9Y696	Chloride intracellular channel protein 4	12	43.08	9	20.95	3	9.49
Q9Y697	Cysteine desulfurase, mitochondrial	3	9.19	1	3.06	0	0.00
Q9Y6B6	GTP-binding protein SAR1b	9	36.87	4	34.34	2	17.17
Q9Y6C2	EMILIN-1	4	7.28	0	0.00	1	2.26
Q9Y6C9	Mitochondrial carrier homolog 2	9	12.21	6	17.49	4	12.21
Q9Y6D5	Brefeldin A-inhibited guanine nucleotide-exchange protein 2	7	6.55	2	1.23	4	3.14
Q9Y6D6	Brefeldin A-inhibited guanine nucleotide-exchange protein 1	4	2.76	0	0.00	5	3.62
Q9Y6E0	Serine/threonine-protein kinase 24	7	17.83	1	3.39	3	11.06
Q9Y6G9	Cytoplasmic dynein 1 light intermediate chain 1	3	8.99	1	3.63	3	8.60
Q9Y6K5	2'-5'-oligoadenylate synthase 3	7	7.54	0	0.00	0	0.00
Q9Y6K9	NF-kappa-B essential modulator	1	3.82	0	0.00	0	0.00
Q9Y6M1	Insulin-like growth factor 2 mRNA-binding protein 2	4	9.18	4	7.01	5	12.02
Q9Y6M9	NADH dehydrogenase [ubiquinone] 1 beta subcomplex subunit 9	6	21.79	2	13.97	2	12.85
Q9Y6N5	Sulfide:quinone oxidoreductase, mitochondrial	6	16.44	0	0.00	0	0.00
Q9Y6U3	Adseverin	16	21.12	0	0.00	0	0.00
Q9Y6Y8	SEC23-interacting protein	2	3.60	0	0.00	1	1.50
RRRRRA6NF79	REVERSED Zinc finger protein 734	1	2.86	0	0.00	0	0.00
RRRRRA6NHR9	REVERSED Structural maintenance of chromosomes flexible hinge domain-containing	2	0.65	0	0.00	0	0.00
RRRRRA6NK21	REVERSED Putative zinc finger protein LOC730110	1	2.92	0	0.00	0	0.00
RRRRRA6NK75	REVERSED Zinc finger protein 98	1	2.80	0	0.00	0	0.00
RRRRRA6NKZ1	REVERSED Zinc finger protein 733	1	3.06	0	0.00	0	0.00
RRRRRA6NN14	REVERSED Zinc finger protein 729	1	4.09	0	0.00	0	0.00
RRRRRA6NNF4	REVERSED Zinc finger protein 726	1	5.42	0	0.00	0	0.00
RRRRRA6NP11	REVERSED Zinc finger protein 716	1	1.66	0	0.00	0	0.00
RRRRRA8MTY0	REVERSED Putative zinc finger protein 724	1	3.88	0	0.00	0	0.00
RRRRRA8MUZ8	REVERSED Putative zinc finger protein 705G	1	2.67	0	0.00	0	0.00
RRRRRA8MWA4	REVERSED Putative zinc finger protein 705E	1	2.65	0	0.00	0	0.00
RRRRRA8MXY4	REVERSED Zinc finger protein 99	1	3.09	0	0.00	0	0.00
RRRRRB4DXR9	REVERSED Zinc finger protein 732	1	1.37	0	0.00	0	0.00
RRRRRO43309	REVERSED Zinc finger and SCAN domain-containing protein 12	2	2.15	0	0.00	0	0.00
RRRRRO43345	REVERSED Zinc finger protein 208	1	0.69	0	0.00	0	0.00
RRRRRO75373	REVERSED Zinc finger protein 737	1	1.49	0	0.00	0	0.00
RRRRRO75437	REVERSED Zinc finger protein 254	1	4.86	0	0.00	0	0.00
RRRRRP0C7V5	REVERSED Putative zinc finger protein 812	1	1.76	0	0.00	0	0.00
RRRRRP0CB33	REVERSED Putative zinc finger protein 735	1	3.88	0	0.00	0	0.00
RRRRRP17019	REVERSED Zinc finger protein 708	1	5.68	0	0.00	0	0.00
RRRRRP17029	REVERSED Zinc finger protein with KRAB and SCAN domains 1	1	1.42	0	0.00	0	0.00
RRRRRP17038	REVERSED Zinc finger protein 43	1	1.98	0	0.00	0	0.00
RRRRRP49959	REVERSED Double-strand break repair protein MRE11A	1	0.99	0	0.00	0	0.00
RRRRRP56381	REVERSED ATP synthase subunit epsilon, mitochondrial	1	15.69	0	0.00	0	0.00

RRRRRQ03923	REVERSED Zinc finger protein 85	1	8.07	0	0.00	0	0.00
RRRRRQ03924	REVERSED Zinc finger protein 117	1	1.66	0	0.00	0	0.00
RRRRRQ03936	REVERSED Zinc finger protein 92	1	6.83	0	0.00	0	0.00
RRRRRQ05481	REVERSED Zinc finger protein 91	1	4.03	0	0.00	0	0.00
RRRRRQ14593	REVERSED Zinc finger protein 273	1	1.41	0	0.00	0	0.00
RRRRRQ15928	REVERSED Zinc finger protein 141	1	1.69	0	0.00	0	0.00
RRRRRQ5JVG8	REVERSED Zinc finger protein 506	1	3.60	0	0.00	0	0.00
RRRRRQ5T0T0	REVERSED E3 ubiquitin-protein ligase MARCH8	1	2.06	0	0.00	0	0.00
RRRRRQ5VTU8	REVERSED ATP synthase subunit epsilon-like protein, mitochondrial	1	15.69	0	0.00	0	0.00
RRRRRQ68DY1	REVERSED Zinc finger protein 626	1	3.03	0	0.00	0	0.00
RRRRRQ6IPT2	REVERSED Protein FAM71E1	2	2.83	0	0.00	0	0.00
RRRRRQ6ZN08	REVERSED Putative zinc finger protein 66	1	5.39	0	0.00	0	0.00
RRRRRQ6ZN79	REVERSED Zinc finger protein 705A	1	2.67	0	0.00	0	0.00
RRRRRQ6ZNG1	REVERSED Zinc finger protein 600	1	1.11	0	0.00	0	0.00
RRRRRQ6ZR52	REVERSED Zinc finger protein 493	1	2.48	0	0.00	0	0.00
RRRRRQ70YC5	REVERSED Protein ZNF365	1	1.97	0	0.00	0	0.00
RRRRRQ8IYB9	REVERSED Zinc finger protein 595	1	1.24	0	0.00	0	0.00
RRRRRQ8IYN0	REVERSED Zinc finger protein 100	1	1.48	0	0.00	0	0.00
RRRRRQ8IYX0	REVERSED Zinc finger protein 679	1	1.95	0	0.00	0	0.00
RRRRRQ8N7Q3	REVERSED Zinc finger protein 676	1	5.44	0	0.00	0	0.00
RRRRRQ8TCQ1	REVERSED E3 ubiquitin-protein ligase MARCH1	1	2.08	0	0.00	0	0.00
RRRRRQ8TD23	REVERSED Zinc finger protein 675	1	2.82	0	0.00	0	0.00
RRRRRQ8TF32	REVERSED Zinc finger protein 431	1	6.94	0	0.00	0	0.00
RRRRRQ96GX1	REVERSED Tectonic-2	1	1.29	0	0.00	1	1.29
RRRRRQ96H40	REVERSED Zinc finger protein 486	1	1.73	0	0.00	0	0.00
RRRRRQ96JC4	REVERSED Zinc finger protein 479	1	3.05	0	0.00	0	0.00
RRRRRQ96N22	REVERSED Zinc finger protein 681	1	3.72	0	0.00	0	0.00
RRRRRQ96N38	REVERSED Zinc finger protein 714	1	2.88	0	0.00	0	0.00
RRRRRQ96N58	REVERSED Zinc finger protein 578	1	2.19	0	0.00	0	0.00
RRRRRQ9BV36	REVERSED Melanophilin	1	1.17	0	0.00	0	0.00
RRRRRQ9BX10	REVERSED GTP-binding protein 2	1	1.00	0	0.00	0	0.00
RRRRRQ9H8G1	REVERSED Zinc finger protein 430	1	5.61	0	0.00	0	0.00
RRRRRQ9NSC5	REVERSED Homer protein homolog 3	1	2.22	0	0.00	0	0.00
RRRRRQ9NZU7	REVERSED Calcium-binding protein 1	1	2.16	0	0.00	0	0.00
RRRRRQ9P241	REVERSED Probable phospholipid-transporting ATPase VD	1	0.49	0	0.00	0	0.00
RRRRRQ9P255	REVERSED Zinc finger protein 492	1	3.01	0	0.00	0	0.00
RRRRRQ9UII5	REVERSED Zinc finger protein 107	1	5.11	0	0.00	0	0.00
RRRRRQ9Y2Q1	REVERSED Zinc finger protein 257	1	5.68	0	0.00	0	0.00

Appendix 2. Semi-quantitative immunohistochemical validation of iTRAQ relative quantification

	Nesprin 2				S100 A6				PDCD4					
Sample	iTRAQ ratio	cyto int	cyto %	IHC tot	iTRAQ ratio	cyto int	cyto %	IHC tot	iTRAQ ratio	cyto int	cyto %	cyto tot	nucl %	IHC tot
S065-12 HR	4.365	2	3	6	1.138	2	2	4	2.399	2	3	6	0	6
S166-11 HR	5.546	3	1	3	2.355	3	3	9	1.888	1	3	3	3	6
S067-11 HR	1.572	2	2	4	1.282	3	2	6	1.393	1	3	3	2	5
S061-11 HR	0.643	2	1	2	0.063	0	0	0	2.63	2	2	4	2	6
S165-11 HR	1.803	N/A	N/A		0.445	N/A	N/A		1.528	N/A	N/A		N/A	
S228-11 HR	1.888	1	3	3	1.086	2	3	6	0.787	1	2	2	1	3
S116-12 HR	0.698	1	1	1	#N/A	0	0	0	4.831	2	3	6	2	8
S197-12 HR	0.832	2	1	2	#N/A	1	2	2	8.091	0	0	0	0	0
S216-12 HR	0.847	2	1	2	#N/A	2	1	2	0.832	0	0	0	0	0
S195-12 HR	0.661	1	1	1	#N/A	1	4	4	3.945	1	1	1	2	3
Mean	1.886			2.7	1.062			3.7	2.832			2.8	1.3	4.1
S159-11 LR	1.871	0	0	0	0.153	0	0	0	8.71	2	4	8	3	11
S196-11 LR	0.233	1	1	1	2.606	1	1	1	1.271	1	4	4	1	5
S042-11 LR	1.213	1	1	1	0.205	0	0	0	5.495	0	0	0	2	2
S124-12 LR	1.33	1	1	1	0.221	0	0	0	4.365	0	0	0	3	3
S070-12 LR	1.086	1	2	2	0.231	0	0	0	5.058	1	4	4	3	7
S147-12 LR	0.236	1	1	1	0.377	1	1	1	4.018	3	1	3	3	6
S194-12 LR	0.474	2	1	1	0.067	0	0	0	3.436	1	3	3	2	5
S113-12 LR	0.592	1	3	3	#N/A	0	0	0	6.792	1	4	4	2	6
S163-12 LR	0.394	1	1	1	#N/A	1	1	1	8.63	2	4	8	3	11
S204-12 LR	0.759	1	2	2	#N/A	1	1	1	7.87	3	3	9	1	10
Mean	0.819			1.3	0.551			0.4	5.565			4.3	2.3	6.6

HR: high risk, LR: low risk; cyto: cytoplasmic; nucl: nuclear; int: intensity; IHC tot: overall immunohistochemical scoring (details explained in Table 2.2); N/A: not available

Appendix 3. Optimisation of culture conditions and serum depletion for secretome production from primary UM cells in culture

Optimization of culture conditions for the analysis of the secretome of primary uveal melanoma cells

Martina Angi, Rosalind Jenkins, Bertil E Damato, Sarah E Coupland, Helen Kalirai

Liverpool Ocular Oncology Research Group

Department of Molecular and Clinical Cancer Medicine, University of Liverpool, Liverpool, UK

M.Angi@liverpool.ac.uk

Liverpool Ocular Oncology Research Group
www.loorg.org

Program Number: 3392

Purpose

Despite successful treatment of the primary uveal melanoma (UM), almost 50% of patients develop metastatic disease, which usually involves the liver, with a fatal outcome. Current screening for metastatic disease relies on 6-monthly imaging and liver function tests, with low sensitivity and specificity. A secreted biomarker that can be measured in blood samples would allow earlier detection of metastatic disease and aid monitoring of systemic adjuvant therapy in high risk UM patients.[1]

Analysis and characterisation of the cancer *secretome* (the complex set of molecules secreted or shed from the surface of living cells) using proteomics profiling is a relevant approach to biomarker discovery. In UM, analysis of biological fluids proximal to the tumor, e.g. subretinal fluid, is limited by their availability. It has been shown in other malignancies that proteins secreted by tumor cells *in vitro* are similar to those released by the same tumors *in vivo*. However, optimised procedures have to be followed for culture, collection and preparation of the samples.[2]

Aim

To identify the best culture conditions for the production and analysis of secretome from primary UM cells.

Methods: cell culture

- **Adherent vs non-adherent culture conditions**

Mel270 and Omm2.5 cell lines were grown in duplicate as adherent, clonogenic adherent and clonogenic suspension in a 75cm^2 flask for 5 days, then progressively adapted to serum depletion and incubated for 48 hours in serum free medium (SFM).

- **Adherent cultures with different media**

Mel270 and Omm2.5 cell lines, as well as cells from one high risk monosomy 3 (M3) and one low risk disomy 3 (D3) primary UM were grown as adherent cultures in three different media: RPMI-based, DMEM-based, αMEM-based. Cell proliferation was assessed at day 0, 2, 4, 5, 7 using the sulforhodamine B (SRB) method.

- **Different incubation times in SFM**

Primary UM cells where grown under adherent conditions in αMEM-based medium in eight identical 75cm^2 flask (1.5x10^6 cells/flask) until 70% confluence. Cells were then either washed 4x with PBS and incubated with serum free and phenol red free medium for 24 or 48 hours or they were progressively depleted of serum in phenol red free medium over 4 days prior to incubation for 24 or 48 hours as above. Viability of the cells under each condition was assessed by trypan blue.

- **Genetic and phenotypic characterization of cultured cells**

For each primary culture, cells were also grown in 2x8-well chamber slides, which were then fixed and examined by immunofluorescence. In all cases, DNA was extracted from cells at the end of the incubation in SFM and analised by multiplex ligation-dependent probe amplification.

Results

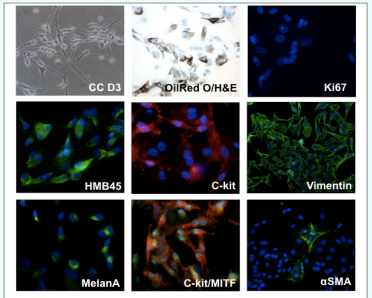

Figure 1A. Cultured cells (CC) from a D3 UM, showing low proliferative capacity in culture (Ki67), high expression of melanoma specific antigens (HMB45, MelanA, Vimentin, MITF), small number of cells positive for the myofibroblast marker αSMA, but no positive staining for Oil Red O.

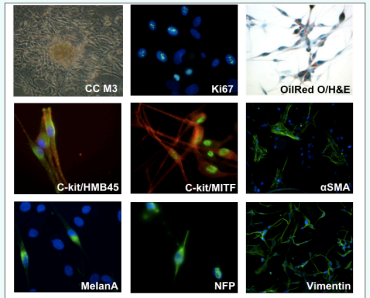

Figure 1B. Cultured cells (CC) from a M3 UM, showing high proliferative capacity in culture (Ki67), low expression of melanoma specific antigens (HMB45, MelanA, Vimentin, MITF), large number of cells positive for the myofibroblast marker αSMA and positive staining for Oil Red O and NFP.

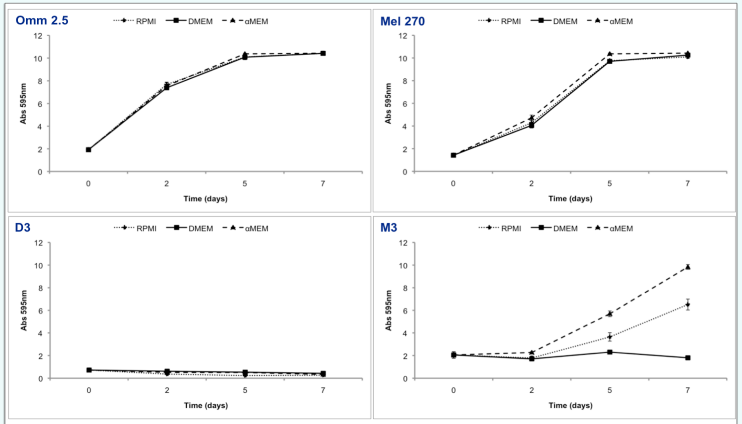

Figure 2. Assessment of cell number in different media using SRB. The growth of Mel270 and Omm2.5 cell lines (top) was not influenced by culture medium. Disomy 3 (D3, bottom left) primary UM cells did not grow in the short term culture, irrespective of the medium used. Monosomy 3 (M3, bottom right) primary UM cells showed the greatest increase in cell number in the αMEM-based medium.

Methods: mass spectrometry

- **Sample preparation**

Conditioned SFM was collected, centrifuged and filtered to remove cellular debris, concentrated on ultracentrifugation (Amicon Ultra 3KDa), desalted using a HPLC column, reduced/alkylated, trypsin digested and ZipTipped (C18).

- **Protein identification**

Proteins were analysed by nanoLC-MS/MS (ABSciex 5600) and identified using Protein Pilot (4.0) with a False Discovery Rate set to 5%. Secreted proteins were identified searching the SwissProt database and using the PANTHER Classification System.

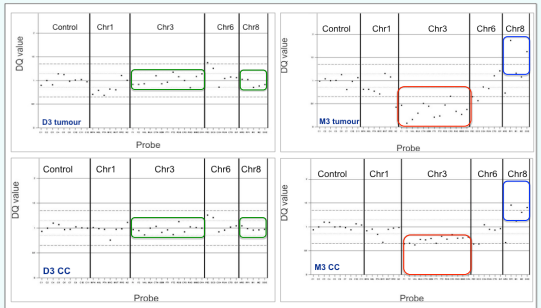

Figure 3. Multiplex Ligation-dependent Probe Amplification (MLPA) of UM cells before and after culture. Molecular genetic analysis of DNA extracted from the primary tumour and from the cultured cells at the time of secretome collection did not differ.
Left: normal chromosome 3 and chromosome 8 copy numbers in the less aggressive, slow growing D3 tumour and CC. **Right:** Loss of one copy of chromosome 3 and gains of chromosome arm 8q in the more aggressive, faster growing M3 tumour and CC.

- **Adherent vs non-adherent culture conditions**

An average of 320 proteins has been identified in conditioned SFM from adherent cells grown to 80% confluence, six folds more than in conditioned SFM from the other culture conditions.

- **Different incubation times in SFM**

At the end of the incubation time in SFM, trypan blue showed a greater number of non-viable cells in the progressively serum-depleted flasks (40% at 48 hours). The number of non-viable cells did not significantly differ after 24 (15%) and 48 (17%) incubation straight into 100%SFM.

- **Proteins of interest**

Putative secreted proteins, already identified as potential biomarkers in UM (cathepsin D, protein DJ-1)[3] or in other cancer types (galectin 3, galectin-3-binding protein, osteopontin, SPARC)[4] were identified with greater confidence in conditioned SFM after 48 hours of incubation. Proteins associated with cell leakage were present in all conditions.

Conclusions

Culture of primary UM cells in an αMEM-based medium under adherent conditions up to 80% confluence, followed by rinsing and incubation in serum-free and phenol red-free medium for 48 hour is optimal for *in vitro* UM secretome analysis.

Future work will validate the presence of candidate proteins in ocular fluids, such as subretinal fluid, extracted from the same patient as the cultured UM cells. In this way, we hypothesize that prognostic biomarkers of clinical relevance in UM will be identified.

References

1) Triozzi PL, Singh AD *Future Oncol* 2012;8:205-15. 2) Makridakis M, Vlahou A *J Proteomics* 2010;73:2291-305. 3) Pardo M et al. *J Proteome Res* 2007;6:2082-11. 4) Chen St et al. *J Proteome Res* 2008;7:1379-87.

Appendix 4. Details of the 18 proteins that discriminate between HR and LR secretome samples

Expression	Accession no.	Name	Gene	Function	GO biological process	GO cellular component
LR>HR	P04083	Annexin A1 (Lipocortin I)	ANXA1	Calcium/phospholipid-binding protein which promotes membrane fusion and is involved in exocytosis. This protein regulates phospholipase A2 activity. It seems to bind from two to four calcium ions with high affinity.	Cell surface receptor signaling pathway; hepatocyte differentiation negative regulation of apoptotic process; positive regulation of vesicle fusion	Cell membrane Cell projection Cilium Cytoplasm Membrane Nucleus
HR>LR	P13674	Prolyl 4-hydroxylase subunit alpha-1	P4HA1	Catalyzes the post-translational formation of 4-hydroxyproline in -Xaa-Pro-Gly- sequences in collagens and other proteins	Collagen fibril organization	Endoplasmic reticulum, mitochondrion
LR>HR	P02545	Prelamin-A/C	LMNA	Laminins are components of the nuclear lamina, a fibrous layer on the nucleoplasmic side of the inner nuclear membrane, which is thought to provide a framework for the nuclear envelope and may also interact with chromatin. Required for normal development of peripheral nervous system and skeletal muscle and for muscle satellite cell proliferation. Required for osteoblastogenesis and bone formation.	Apoptotic process; activation of signaling protein activity involved in unfolded protein response; cellular response to hypoxia	Nucleus. Nucleus envelope. Nucleus lamina. Perinuclear region of cytoplasm
LR>HR	B4DNM8	B4DNM8 (cDNA FLJ53395, highly similar to Prolyl 3-hydroxylase 1)	B4DNM8	L-ascorbic acid and iron binding	N/A	N/A

LR>HR	P17096	High mobility group protein HMG-I/HMG-Y	HMGA1	HMG-I/Y bind preferentially to the minor groove of A+T rich regions in double-stranded DNA. It is suggested that these proteins could function in nucleosome phasing and in the 3'-end processing of mRNA transcripts. They are also involved in the transcription regulation of genes containing, or in close proximity to A+T-rich regions.	Host-virus interaction (HIV-1 pre-integration complex) Transcription Transcription regulation	Chromosome Nucleus
HR>LR	G3V394	Unconventional myosin-Va	MYO5A	ATP biniding, motor activity	Nucleotide-binding	Myosin complex
LR>HR	F8VTQ5	Heterogeneous nuclear ribonucleoprotein A1	HNRNPA1	Involved in the packaging of pre-mRNA into hnRNP particles, transport of poly(A) mRNA from the nucleus to the cytoplasm and may modulate splice site selection.	Nucleic acid binding	Cytoplasm Nucleus Spliceosome
LR>HR	B4DN87	Serpin H1	SERPINH1	Binds specifically to collagen. Could be involved as a chaperone in the biosynthetic pathway of collagen.Stress response protein, induction by heat shock	Collagen biosynthetic process; collagen fibril organization; protein maturation	Endoplasmic reticulum, extracellular space
LR>HR	P21291	Cysteine and glycine-rich protein 1	CSRP1	May play a role in neuronal development.	RNA binding	Extracellular vesicular exosome, nucleous
HR>LR	O60486	Plexin-C1	PLXNC1	Receptor for SEMA7A, for smallpox semaphorin A39R, vaccinia virus semaphorin A39R and for herpesvirus Sema protein. Binding of semaphorins triggers cellular responses leading to the rearrangement of the cytoskeleton and to secretion of IL6 and IL8	Axon guidance cell adhesion signal transduction	Membrane; Single-pass type I membrane protein

HR>LR	F5H6I0	Beta-2-microglobulin	B2M	Component of the class I major histocompatibility complex (MHC). Involved in the presentation of peptide antigens to the immune system	Immunity	Secreted
LR>HR	B2RDM2	Thioredoxin domain-containing protein 5	TXNDC5	Endoplasmic reticulum resident protein, possesses thioredoxin activity. Has been shown to reduce insulin disulfide bonds.	Membrane organization; negative regulation of apoptotic process; post-Golgi vesicle-mediated transport	Endoplasmic reticulum, extracellular vesicular exosome, lysosomal lumen
LR>HR	H7C1J8	Heterogeneous nuclear ribonucleoprotein A3	HNRNPA3	Plays a role in cytoplasmic trafficking of RNA.	mRNA splicing, via spliceosome. Gene expression	Ribonucleoprotein complex, nucleoplasm
HR>LR	B4DDF9	Annexin	ANXA4	Calcium/phospholipid-binding protein which promotes membrane fusion and is involved in exocytosis	Negative regulation of coagulation	Cytoplasm, extracellular vesicular exosome
HR>LR	P14174	Macrophage migration inhibitory factor	MIF	Pro-inflammatory cytokine. Mediator in regulating the function of macrophages in host defense.	Innate immunity, negative regulation of apoptotic process, positive chemotaxis, positive regulation of MAP kinase activity, positive regulation of ERK1 and ERK2 cascade	Cytoplasm, secreted, extracellular vesicular exosome
HR>LR	H9KVA0	Thymidine phosphorylase	TYMP	Platelet-derived endothelial cell growth factor. Has growth promoting activity on endothelial cells, angiogenic activity in vivo and chemotactic activity on endothelial cells in vitro.	Angiogenesis Chemotaxis Differentiation	Cytosol
LR>HR	Q15393	Splicing factor 3B subunit 3	SF3B3	Subunit of the splicing factor SF3B required for pre-mRNA assembly	mRNA processing mRNA splicing	Nucleoplasm, spliceosomal complex
HR>LR	B5MCV4	Complement C1s sub-component	C1S	Component of complement (classical pathway), protease	Complement activation, classical pathway	Blood microparticle, extracellular region